Organ-specific heterogeneity in the endothelial cell hypoxia response

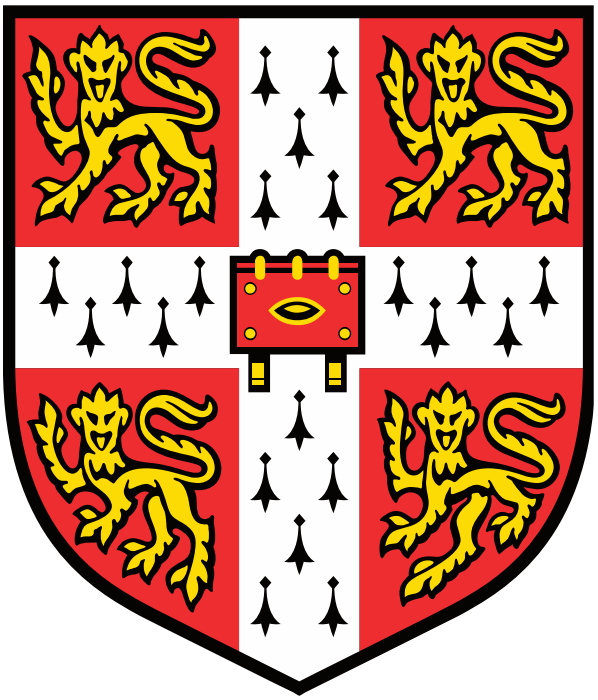

Moritz Reiterer

St John's College

University of Cambridge

Supervisor: Dr Cristina Branco

Dissertation submitted for the degree of Doctor of Philosophy

December 2019

Declaration

This thesis is the result of my own work and includes nothing which is the outcome of work done in collaboration, except as declared in the text and Acknowledgements. It is not substantially the same as any that I have submitted, or, is being concurrently submitted for a degree, diploma or other qualification at the University of Cambridge or any other University or similar institution, except as declared in the Preface and specified in the text. This dissertation contains fewer than 60,000 words.

Abstract: Organ-specific heterogeneity in the endothelial cell hypoxia response – Moritz Reiterer

The aim of this thesis is to study the hypoxia response pathways within microvascular endothelial cells. In the first results chapter I investigated the differential role of the two hypoxia inducible transcription factors HIF-1α and HIF-2α in the murine lung endothelium during cancer metastasis, and how the hypoxia response of the vascular endothelium remodels the lung pre-metastatic niche. Previous work had shown that lung endothelial-specific knockouts of HIF-1α and HIF-2α respectively inhibit and promote metastatic success. Thus, hypoxic stimuli of varying lengths were used to preferentially stabilise either HIF isoform prior to tumour cell injection. Acute hypoxia resulted in stabilisation of HIF1α, endothelial cell death, and increased vascular permeability, facilitating tumour cell extravasation. This was potentiated by the recruitment and retention of specific myeloid cells that further supported a pro-metastatic environment. Chronic hypoxia on the other hand reduced metastatic success, in conjunction with HIF-2α-mediated increases in endothelial cell viability and vascular integrity. These effects were reversed by the endothelial-specific deletion of each isoform.

Having investigated the role of the HIF pathway lung metastasis, the second results chapter aimed to broaden the scope to the vasculature of a different metastatic target of breast cancer, the brain. To achieve this, I cultured microvascular endothelial cells (MVECs) of both organs *in vitro* and exposed them to hypoxia (1% O_2). My initial observations suggested that brain MVECs fared much more poorly in hypoxia than their lung counterparts. This was puzzling, given that the brain microvasculature is exposed to much lower oxygen levels in vivo and should thus presumably be better equipped to deal with hypoxia. Crucially however, both tissues contain much less oxygen than the 18.5% O_2 found in standard tissue culture incubators, and thus the cellular responses seen in these conditions are unlikely to relevantly represent the adaptations seen in physiological conditions. To investigate this possibility, the subsequent experimental set-up included culturing each cell population also in physiological O_2 tensions. Indeed, this resulted in a much more pronounced hypoxia response, both in terms of viability and expression of key genes. Still, there were pronounced differences between the two cell types, most notably a differential stabilisation of HIF isoforms. Brain MVECs relied much more heavily on HIF-2α whereas lung MVECs contained considerably higher levels of HIF-1α.

The third results chapter further explored the effect of hyperoxia versus physioxia on brain and lung MVECs, with a specific focus on their metabolic response. I performed

metabolic stress tests to measure the cells' mitochondrial and glycolytic capacities if cultured at normoxia or physioxia, both at baseline and after subsequent exposure to hypoxia. Furthermore, I assessed the metabolic adaptation of each cell type to hypoxia in real time. Similar to what was observed in chapter 2, both cell types but particularly brain MVECs grown at ambient oxygen levels were less able to increase glycolysis in response to hypoxia. Furthermore, brain MVECs also displayed severely impaired mitochondrial metabolism, as evidenced by reduced maximal respiration and expression of respiratory complex proteins.

Overall, this thesis highlights the importance of hypoxia response pathways in endothelial cells in pathology, such as during cancer metastasis, as well as during normal cell physiology, shown by the detrimental effects of non-physiological oxygen levels.

Acknowledgments

I would like to thank my supervisor Cristina Branco for giving me the opportunity to work in her lab, and for her continuous support and guidance throughout this project.

I am very grateful to Randall Johnson for his valuable insights and ideas.

Thanks also to all the other members of the Branco and Johnson groups, in particular Amanda and Gloria for looking after my cells countless times.

Beyond the lab, I have appreciated the warm welcome of the Queen's University Mountaineering Club after my move to Belfast.

Thank you to my parents for their unwavering support and food shipments and my sister for always believing in me. And thank you Sarah for always being there.

This work was funded by a PhD studentship from the Cancer UK Cambridge Centre and by Breast Cancer Now.

Table of Contents

List of Figures

List of Tables

Abbreviations

2-DG	2-deoxy glucose
2-HG	2-hydroxyglutarate
αKG	α-ketoglutarate
ANGPT2	Angiopoietin 2
ARG2	Arginase 2
BBB	Blood brain barrier
bFGF	Basic fibroblast growth factor
CNS	Central nervous system
CTC	Circulating tumour cell
DF	Double floxed
EB	Evans Blue
EC	Endothelial cell
ECAR	Extracellular acidification rate
EndMT	Endothelial to mesenchymal transition
FIH	Factor inhibiting HIF
GLUT1	Glucose transporter 1
HB-EGF	Heparin-binding epidermal growth factor-like growth factor
HGF	Hepatocyte growth factor
HIF	Hypoxia-inducible factor
HOT	Hyperbaric oxygen treatment
HRE	Hypoxia response element
HRP	Horseradish peroxidase
HUVEC	Human umbilical vein endothelial cell
ICAM1	Intercellular adhesion molecule 1
IDH	Isocitrate dehydrogenase
IF	Immunofluorescence
IH	Intermittent hypoxia
iNOS	Inducible nitric oxide synthase
K_M	Michaelis Menten constant
LDHA	Lactate dehydrogenase A
MVEC	Microvascular endothelial cell
mCSF1	Macrophage colony-stimulating factor

NSC	Neural stem cell
OCR	Oxygen consumption rate
ODD	Oxygen-dependent degradation domain
OSA	Obstructive sleep apnoea
OXPHOS	Oxidative phosphorylation
PBS	Phosphate buffered saline
PDGF	Platelet-derived growth factor
PDH	Pyruvate dehydrogenase
PDK1	Pyruvate dehydrogenase kinase 1
PFK2	Phosphofructokinase 2
PHD	Prolyl hydroxylase
PIGF	Placental growth factor
PKM2	Pyruvate kinase M2
PGK	Phosphoglycerate kinase
ROS	Reactive oxygen species
RT	Room temperature
SD	Standard deviation
SE	Standard error
SDF1	Stromal-derived factor 1
STA	Standard tissue culture atmosphere
TECs	Tumour endothelial cells
TEM	Trans-endothelial migration
VEGF	Vascular endothelial growth factor
VHL	Von Hippel-Lindau protein

Chapter 1: Background and Introduction

1.1 The role of endothelial cells

The vascular system is arguably the largest organ in the human body, covering a surface area of 1000 to 7000 m^2, and only rivalled in mass by the liver and skin (Cines *et al.*, 1998). It is also likely the most heterogeneous (Augustin and Koh, 2017). What can be in basic terms defined a continuous single cell layer of endothelial cells (EC), for the most part is known for its importance as a vehicle for transport of substances, signals and other cells throughout the organism and between tissues. This essential function is at the heart of homeostasis (Michiels, 2003; Augustin and Koh, 2017), as it facilitates the adjustments needed to meet the demands of individual tissue types in specific circumstances. This includes normal physiological conditions, such as during exercise, and exposure to altitude or temperature oscillations (Kalsi *et al.*, 2017), or in pathologies such as inflammation (Clarenbach *et al.*, 2012; Gimbrone and García-Cardeña, 2016), cancer (Carmeliet and Jain, 2011a; Rohan *et al.*, 2014; Wenes *et al.*, 2016), ageing (Burnstock and Ralevic, 1994), degeneration (Wadley *et al.*, 2013; Janota *et al.*, 2016) or wound healing/tissue remodelling (Yu *et al.*, 2005; Barbacena *et al.*, 2016; Cowburn *et al.*, 2016; Watson *et al.*, 2017). Indeed, it has been claimed that the endothelium is involved in most if not all human disease states, either as a primary cause of the pathology or as a victim of collateral damage (Aird, 2012). Simply, this system keeps the organism connected and functioning as such.

1.1.1 Endothelial cell heterogeneity

Depending on their position in the vascular tree, endothelial cells can be broadly differentiated into three classes, that differ substantially in terms of morphology (Yamamoto *et al.*, 2016; Franco and Gerhardt, 2017), structure (Davies *et al.*, 2014) and function (Augustin and Koh, 2017): arterial, venous, and microvascular ECs. The main role of arterial ECs is the regulation of vascular tone, through the production of signalling molecules that cause the smooth muscle surrounding the vessel to constrict (e.g. endothelin) or relax (e.g. nitric oxide). Arterial ECs are also exposed to considerably more shear stress than any other EC, causing them to be longer and thinner. Venous ECs on the other hand are short and wide, and their main task is the regulation of leukocyte trafficking, in particular in post-capillary venules. These ECs are much less tightly connected than their arterial counterparts and are the main site of vascular leakage during inflammation, in response to factors such as histamine and serotonin (Dela Paz and D'Amore, 2009).

Capillary or microvascular ECs (MVECs) are by far the most heterogeneous class. It is in this section of the vasculature where most of fluid and solute exchange between blood and tissues occurs (Aird, 2012). Depending on the function of the underlying organ, different microvascular beds organise in highly distinct ways. Continuous capillaries are characterised by tightly connected endothelial cells, with few paracellular gaps, and a continuous basal membrane. Such a microvasculature can be found in the lung, the brain, and the retina. The liver, spleen, and to a large extent bone on the other hand possess a discontinuous endothelium, with large, irregular intercellular gaps and a poorly formed basement membrane; this allows cellular trafficking through the endothelium. Lastly, fenestrated endothelia are found in organs involved in filtration or secretion, such as exocrine and endocrine glands, gastric and intestinal mucosa, choroid plexus, glomeruli, and a subpopulation of renal tubules. This endothelium also possesses gaps, but they are regular in size and facilitate selective permeability (Ribatti *et al.*, 2002; Aird, 2007b).

Transport across the endothelium can occur either via a paracellular or via a transcellular route. The rate of paracellular transport is largely defined by the type of microvasculature and consequently the size of the gaps between endothelial cells, as well as the nature of endothelial cell-to-cell junctions. ECs are mainly connected by two different types of junction complexes, adherens junctions and tight junctions (Bazzoni and Dejana, 2004; Wallez and Huber, 2008). As their name suggests, tight junctions yield a closely connected endothelium, with little opportunity for paracellular gaps. This class of junctions is particularly abundant at the blood-brain-barrier (BBB), the microvascular bed with the lowest permeability (Daneman and Prat, 2015). Transcellular transport on the other hand occurs mainly through caveolae, large membrane-bound vesicles that shuttle between the luminal and abluminal sides of the endothelium. Most microvascular beds contain an abundance of caveolae, many more than are found in arterial or venous ECs (Bendayan, 2002). A notable exception is the BBB, which contains almost none, since the transport of molecules into the CNS is highly specific and controlled and does therefore not occur in bulk (Simionescu *et al.*, 2002).

These differences in structure and barrier function were the first indicators of microvascular organ heterogeneity. However, during the past decade new insights have shown that these features are only the tip of the iceberg. In fact, MVECs have emerged as essential gatekeepers of organ function; due to their position between the vasculature and the underlying tissue, they are uniquely situated to respond to both local and systemic stimuli. As such, they actively control organ development, homeostasis, and regeneration following injury (Rafii *et al.*, 2016; Augustin and Koh, 2017). For example, liver regeneration following a partial

hepatectomy is stimulated by angiocrine signals from liver sinusoidal ECs, such as hepatocyte growth factor (HGF) or Wnt2, which induce rapid proliferation of hepatocytes (Ding *et al.*, 2010; Kostallari and Shah, 2016). Similarly, during foetal lung development, progenitor differentiation into lung epithelial cells is governed by angiocrine factors from primitive lung capillaries (Herriges and Morrisey, 2014; Woik and Kroll, 2015).

Endothelial heterogeneity is a highly conserved feature and present even in the oldest extant vertebrates, such as the hagfish (Feng *et al.*, 2007; Yano *et al.*, 2007), highlighting it as a core property of a vascular system, rather than a secondary feature evolved only in more complex organisms. However, it remains to be determined how much of this heterogeneity is intrinsic to ECs from different vascular beds and how much is induced by signals from nearby tissue-specific cell types such as neurons or astrocytes at the blood-brain-barrier or hepatocytes and Kupffer cells in the liver (Abbott, 2002; Sakamoto *et al.*, 2002). Furthermore, different capillary beds also provide a distinct physical environment to ECs, with parameters such as tissue stiffness, blood flow rate, oxygen levels, as well as metabolic rate and metabolite availability (Fig. 1-1) (Aird, 2007b, 2007a; Marcu *et al.*, 2018). Properties resulting from such cues are likely lost during *in vitro* cell culture. Indeed, the gene expression profile of ECs has been shown to change drastically *in vitro*. Some of these properties may be re-acquired when the relevant stimulus is re-established, for example venous EC exposed to artery-like flow develop properties of arterial ECs *in vitro* (Tsukurov *et al.*, 2000; Dai *et al.*, 2004), whereas generic ECs derived from stem cells *in vitro* develop organotypic features when engrafted into a regenerating tissue (Nolan *et al.*, 2013). Other organ-specific differences may be more permanent, for example if maintained by epigenetics. DNA microarray studies found that about half of all organotypic genes are maintained in culture (Chi *et al.*, 2003; Lacorre *et al.*, 2004).

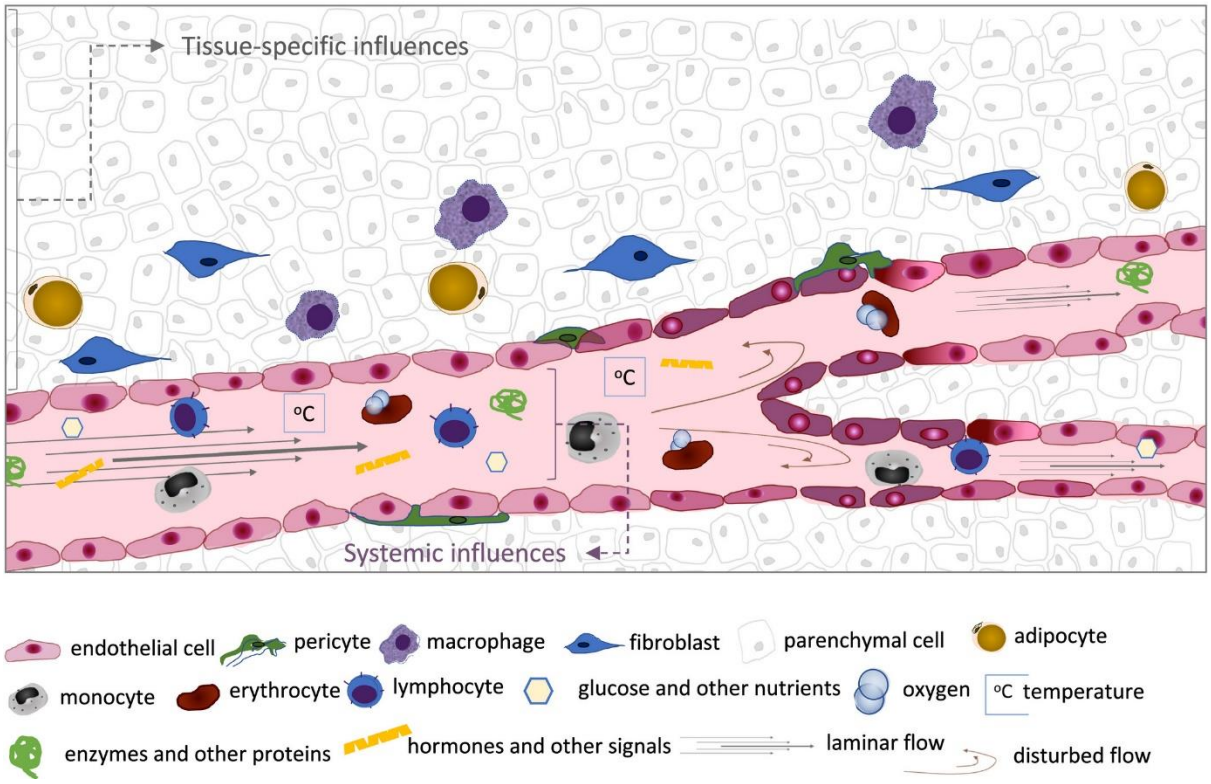

Figure 1-1: Overview of biological, chemical and physical influences on EC behaviour. Endothelial cells in capillary networks are exposed to tissue-specific cues, which include signals from resident parenchymal and other stromal cells, the composition and stiffness of the ECM and the metabolic activity of the organ at any given time, which in turn affects the metabolite and gas composition, and extracellular pH. From the luminal side, EC perceive and respond to compounds and cells transported in circulation, such as nutrient status, circulating cells and oxygen levels (systemic influences); tissue-specific influences include temperature and shear stress, which is altered as a function of vessel diameter, flow and branching; additionally, resident cells and metabolic, physiological and pathological status of specific organs in specific circumstances will provide the endothelium cues with very localized (tissue-specific) relevance, but which can, too, provide systemic signals (e.g. angiocrine/endocrine). The activation status of the EC dictates its permeability, angiogenic potential, surface receptors and transporters, secretory profile and metabolism, and thus organ function. (Reiterer and Branco, 2019)

1.1.2 Metabolic shifts as mediators of EC form and function

In recent years, the interest in EC metabolism has grown. Pioneering studies in the unique tumour microenvironment demonstrated that metabolic switches are not mere bystanders but play active roles in shaping EC behaviours, such as angiogenic sprouting (Theodorou and Boon, 2018). A crucial feature of EC metabolism is their reliance on aerobic glycolysis in favour of mitochondrial respiration. EC display markedly higher glycolytic rates than other cell types (De Bock *et al.*, 2013), while containing fewer mitochondria (Blouin *et al.*, 1977). Indeed at least 75% of the ATP generated by porcine aortic EC derives from glycolysis (Culic *et al.*, 1997). It has been postulated that this allows more oxygen to diffuse into tissues, while limiting the exposure of EC to potentially harmful reactive oxygen species (Verdegem *et al.*, 2014). Furthermore, glucose supply to EC is generally abundant due to their direct exposure to blood. Therefore, glycolysis actually provides a faster means of energy production than oxidative phosphorylation. In conditions of increased or decreased glucose availability, EC can accordingly modulate the rate of mitochondrial respiration versus glycolysis (Krützfeldt *et al.*, 1990; Koziel *et al.*, 2012).

Although these paradigms hold generally true, comparative studies between EC from different regions of the vascular tree, as well as between EC from different organs, have found substantial divergences in their metabolic phenotypes. For example, pulmonary venous EC rely more on aerobic glycolysis than their arterial counterparts *in vitro* (Lee *et al.*, 2017). Heart microvascular EC show higher metabolic rates than those found in lung, liver and kidney, both in glycolysis and mitochondrial respiration (Marcu *et al.*, 2018) whereas brain EC have a higher mitochondrial volume than other EC (Oldendorf *et al.*, 1977). In all cases, there has been little effort to investigate the underlying reasons or functional consequences of these differences *in vivo*, although it has been shown that mitochondrial inhibitors increase the permeability of the blood-brain barrier (Doll *et al.*, 2015). It is tempting to speculate that these various metabolic phenotypes represent an adaptation of EC to their individual niche, reflecting the specific needs of the underlying organ. For example, brain microvascular EC form part of the BBB, transport across which is highly regulated through a host of influx and efflux pumps. It has been hypothesized that the higher mitochondrial density in brain microvascular EC is required to supply sufficient energy to fuel these transporters (Theodorou and Boon, 2018). Furthermore, glucose is the main source of energy for the brain (Mergenthaler *et al.*, 2013). Thus, increased reliance on oxidative phosphorylation over glycolysis within EC allows more glucose to pass through the BBB. Similarly, heart microvascular EC express higher levels of fatty acid transporters than other vascular beds, to account for the metabolic needs of cardiomyocytes.

This feature is mediated by the transcriptional regulator Meox2/Tcf15, uniquely expressed in cardiac EC (Coppiello *et al.*, 2015).

The close link between endothelial metabolism and overall physiology is highlighted by the fact that during many pathologies, EC dysfunction coincides with maladapted or perturbed metabolism. For example, pulmonary hypertension is a disease characterised by increased vascular resistance within the lung arteries and arterioles, caused in part the excessive proliferation of apoptosis-resistant endothelial cells (Farber and Loscalzo, 2004). It has been proposed that the initial driver of this pathology is a suppression of mitochondria in pulmonary ECs, resulting in dysfunction and increased apoptosis (Paulin and Michelakis, 2014; Sutendra and Michelakis, 2014). This metabolic disturbance then gives rise to numerous other abnormalities that shape pulmonary hypertension, such as promoting a proliferative and glycolytic state in the remaining ECs, to compensate for the lost cells, which leads to the aberrant accumulation of ECs described above (Sakao *et al.*, 2005).

1.2 HIF as a regulator of endothelial cells

Oxygen is an essential prerequisite for all animal life; it is the final acceptor in the mitochondrial electron transport chain, allowing our cells to obtain considerably more energy from nutrients than through anaerobic means. Yet, oxygen availability can be variable. Environmental oxygen supply may be diminished, such as at high altitude, or demand may increase, such as during exercise. Oxygen levels may also decrease locally within an organism, for example following vascular injury. It is therefore unsurprising that evolution has enabled organisms to adjust to changes in oxygen supply. The underlying mechanisms range from large-scale physiological changes down to modifications at the cellular level. Endothelial cells form the boundary between the circulation and the underlying tissues. As such, they are the first cells to perceive changes in oxygen tension within the blood, making them a crucial player in both the global and local response to hypoxia.

1.2.1 The HIF system

At the heart of oxygen sensing lies a family of transcription factors aptly named Hypoxia-inducible factors (HIFs). The first member of this family, HIF-1α, was identified for its role in regulating the production of the hormone erythropoietin (EPO) in human liver and kidneys during reduced oxygen availability, such as at high altitude (Semenza and Wang, 1992; Wang and Semenza, 1995). EPO leads to increased production of red blood cells, increasing the oxygen carrying capacity of blood and thus counteracting the effects of reduced oxygen

availability (Reissmann, 2016). During hypoxia, HIF-1α binds to hypoxia response elements (HREs) within the 3' region of hypoxia-induced genes such as EPO, leading to their transcriptional upregulation (Beck *et al.*, 1991; Pugh *et al.*, 1991; Semenza and Wang, 1992). HIF-1α acts as a heterodimer, together with the Aryl Hydrocarbon Receptor Nuclear Translocator (ARNT), also called HIF-1β (Wang *et al.*, 1995). Since ARNT is constitutively expressed and known to heterodimerize with several other transcription factors, the control of HIF activity lies entirely upon the α-isoform.

Soon after the discovery of HIF-1α, a closely related protein was identified and cloned by several independent research groups (Ema *et al.*, 1997; Flamme *et al.*, 1997; Hogenesch *et al.*, 1997; Tian *et al.*, 1997). Its gene was termed EPAS1 while the protein itself is nowadays more commonly referred to as HIF-2α. Like its paralog HIF-1α, HIF-2α is stabilised during hypoxia and forms a transcription factor complex together with ARNT. Indeed, the transcriptional targets of the two HIF isoforms are highly overlapping, albeit not completely (Carroll and Ashcroft, 2006; Koh and Powis, 2012). HIF-1α is expressed ubiquitously in all mammalian tissues, while HIF-2α is restricted to specific cell types, such as endothelial cells (Ema *et al.*, 1997; Tian *et al.*, 1997). The distinct roles of HIF-1α and HIF-2α in endothelial cells will be discussed in more detail below (section 1.3).

A third HIFα isoform, HIF-3α, has also been discovered (Gu *et al.*, 1998) but it remains much less studied than its two prominent relatives. This is in part due to the existence of over 10 distinct HIF-3α splice variants, containing different combinations of the protein domains found in HIF-1α and HIF-2α (Duan, 2016). Some variants even lack the domain responsible for oxygen-dependent degradation (see section 1.2.1.1). HIF-3α can dimerise with HIF-1α and HIF-2α, and thus one of its main roles is to negatively regulate the activity of the other two isoforms, by preventing their dimerization with ARNT (Makino *et al.*, 2001; Maynard *et al.*, 2007). Similarly, HIF-3α can also bind ARNT and thus sequester it away from the other two HIFα isoforms (Maynard *et al.*, 2005). In endothelial cells, HIF-3α has been shown to promote a pro-angiogenic phenotype by reducing the HIF-2a mediated transcription of VE-Cadherin (Kobayashi *et al.*, 2015). There is still debate about the role of the HIF-3α/ARNT dimer in transcriptional regulation, as effects are usually only seen in overexpression models (Hara *et al.*, 2001; Scharf *et al.*, 2005; Huang *et al.*, 2013). However, some recent *in vivo* experiments in zebrafish suggest that HIF-3α may indeed act as a transcription factor in its own right (Zhang

et al., 2014). This thesis, however, will exclusively discuss the roles of HIF-1α and HIF-2α in EC.

1.2.1.1 Oxygen-dependent control of HIF activity

HIF activity is predominantly controlled through degradation of its α-subunit. In the presence of oxygen, prolyl hydroxylase domain proteins (PHDs) hydroxylate two proline residues within HIF's oxygen-dependent degradation domain (ODD) (Bruick and McKnight, 2001; Epstein *et al.*, 2001). This induces a conformational change which allows the Von-Hippel-Lindau (VHL) protein to bind to HIF-α (Maxwell *et al.*, 1999; Ivan *et al.*, 2001; Jaakkola *et al.*, 2001). VHL is part of an ubiquitin E3 ligase complex which targets HIF-α for proteasomal degradation (Cockman *et al.*, 2000). Crucially, the initial hydroxylation reaction relies on oxygen as a substrate. Therefore, HIF stability is directly tied to oxygen availability (Figure 1-1).

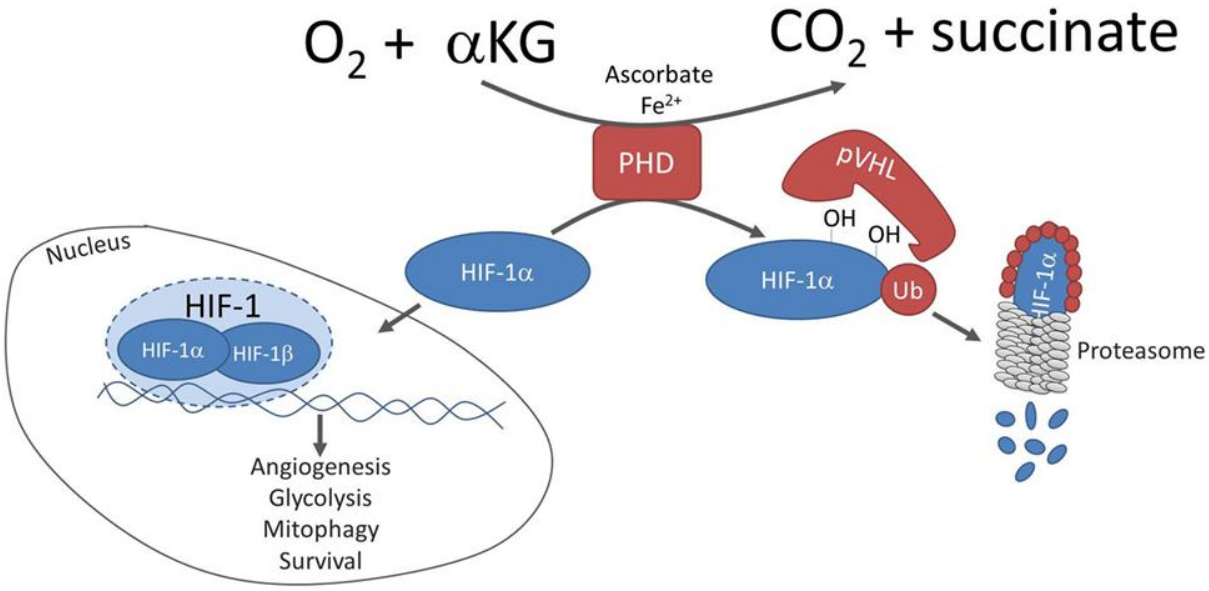

Figure 1-2: Regulation of HIF-α protein abundance by prolyl hydroxylases
HIF-1α and HIF-2α protein levels are post-translationally controlled; the figure shows HIF-1a as an example but the mechanism applies to both isoforms. In the presence of oxygen and α-ketoglutarate (αKG), prolyl hydroxylases of the PHD family target HIF-α. Hydroxylated HIF-a is recognised by the Von-Hippel-Lindau (VHL) protein and ubiquitylated, which targets it for proteasomal degradation. In the absence of oxygen, degradation does not occur and HIF-α can translocate to the nucleus, and carry out its function as a transcription factor together with the constitutively expressed HIF-β. (adapted from Iommarini *et al.*, 2017)

Before the discovery of the HIF regulatory mechanism, a different family of prolyl hydroxylases had been known to hydroxylate collagen, facilitating its triple helix formation (Pihlajaniemi *et al.*, 1991). The main difference between these two classes of enzymes is their affinity for oxygen. The Michaelis-Menten constant (K_M) for oxygen of collagen prolyl-hydroxylases is 40 μM, whereas it is 230-250 μM for the three different HIF-PHDs (Hirsilä *et al.*, 2003). Ambient air contains about 200 μM oxygen, well above the K_M of collagen prolyl-hydroxylases, so substrate availability is usually not rate-limiting for these enzymes. The rate of HIF hydroxylation on the other hand is sensitive to oxygen concentration across the entire available range, which substantiates the role of PHDs as the oxygen sensor of the HIF system.

In addition to the degradation by PHDs and VHL, HIF-1α and HIF-2α are subjected to a second layer of oxygen-dependent regulation. This mechanism is mediated by the Factor Inhibiting HIF (FIH) and similarly relies on oxygen-dependent hydroxylation (Mahon *et al.*, 2001). Unlike the PHDs, FIH hydroxylates an asparagine residue in the C-terminal activation domain of HIF-1α and HIF-2α. This activation domain is not present in any HIF-3α variant, likely excluding it from regulation by FIH (Duan, 2016). Asparagine hydroxylation does not target HIF for degradation; instead, HIF is left unable to bind its co-activator CBP/p300 and thus cannot trigger a transcriptional response (Lando, Peet, Gorman, *et al.*, 2002; Lando, Peet, Whelan, *et al.*, 2002). FIH has a lower K_M for oxygen than the PHDs (90 μM) and is therefore able to inhibit HIF activity at lower oxygen concentrations (Koivunen *et al.*, 2004; Ehrismann *et al.*, 2007; Tarhonskaya *et al.*, 2015). The relative roles of PHDs and FIH in shaping the hypoxia response are still being investigated. While it was initially proposed that their functions may be redundant, recent evidence suggests that they are fundamentally different (Sim *et al.*, 2018). Indeed, loss of VHL and FIH lead to distinct phenotypes, such as a decrease in aerobic metabolism in VHL null cells but an increase in FIH null. The authors of this study proposed that the role of FIH is to delay the hypoxic response as long as possible and then rapidly induce it.

1.2.1.2 Oxygen-independent control of HIF activity

Hydroxylation through PHDs is only one of many cellular processes relying on oxygen as a substrate; this includes oxidative phosphorylation (OXPHOS) in the mitochondria. Therefore, inhibiting mitochondrial respiration leads to an increase in local O_2 availability for PHDs and thus HIF degradation even if external oxygen supply is unchanged (Hagen *et al.*, 2003). In addition to oxygen, HIF activity is regulated by a wide variety of other signals. The hydroxylation reaction catalysed by PHDs, and thus the degradation of HIF, is dependent on

Fe^{2+} and ascorbate as co-factors (Fig. 1-1) (Hirsilä *et al.*, 2003). Consequently, mice fed iron deficient diets display increased *in vivo* HIF stabilisation, even in normoxia (Peyssonnaux *et al.*, 2007; Shah *et al.*, 2009). In turn, genes regulating iron uptake are positively regulated by HIF-2α, providing an elegant feedback mechanism. Ascorbate on the other hand appears dispensable for HIF degradation *in vivo*, as other reductive compounds such as glutathione compensate for its absence (Nytko *et al.*, 2011).

In addition to these co-factors, HIF hydroxylation by PHDs also requires α-ketoglutarate (αKG) as a co-substrate. αKG is produced by the Krebs cycle enzyme isocitrate dehydrogenase I (IDH1). Alternatively, isocitrate can be converted into 2-hydroxyglutarate (2-HG) by a different isoform of this enzyme, IDH2. Due to their close structural similarity, 2-HG acts as a competitive inhibitor of PHDs (Xu *et al.*, 2011). Therefore, HIF stability is regulated by the ratio of IDH1 to IDH2 activity. In glioma, both IDH1 loss of function and IDH2 gain of function mutations are common, leading to an accumulation of 2-HG over αKG and thus inhibition of PHDs (Yan *et al.*, 2009). Similarly, accumulation of succinate inhibits PHDs through product-inhibition (Selak *et al.*, 2005), and the enzyme responsible for its degradation, succinate dehydrogenase, has been identified as a tumour suppressor gene (Baysal *et al.*, 2000; Niemann and Muller, 2000; Astuti *et al.*, 2001).

Other ways in which cancer cells can increase HIF levels is by inhibiting VHL. This can occur either through outright loss of function mutations, as frequently seen in renal cell carcinoma (Atkins *et al.*, 2007). Alternatively, VHL itself can be targeted for proteasomal degradation, for example by increased expression of WSB1 (Kim *et al.*, 2015). Phosphorylation of VHL by the protein kinase CK2 similarly reduces its stability (Ampofo *et al.*, 2010). c-myc on the other hand has been shown to disrupt the binding of HIF-1α to VHL in breast cancer (Doe *et al.*, 2012). Association of HIF with cancer will be further described in subsequent sections (1.3 and Chapter 2).

Several control mechanisms of HIF are entirely independent of the PHD-VHL system. Signalling through the PI3K/Akt/mTOR pathway for example increases HIF translation by promoting the activity of the translation initiation factor 4E (Laughner *et al.*, 2001). MAPK/ERK signalling on the other hand leads to the phosphorylation of HIF-1α and HIF-2α within their c-terminal activation domain, as well as phosphorylation of the cofactor CBP/p300. Phosphorylation at either site strengthens the binding between HIF and its cofactor, thus leading to improved transcriptional control of its targets (Richard *et al.*, 1999; Hur *et al.*, 2001; Lee *et al.*, 2002; Sang *et al.*, 2003).

Reactive oxygen species (ROS) have also been connected to HIF activity in a multitude of ways, although some dispute persists about the correct mechanism. Theories include direct inhibition of PHDs (Metzen *et al.*, 2003), posttranslational modifications of HIF-α (Sumbayev *et al.*, 2003), as well as indirect activation of HIF either through the MAPK/PI3K pathways (Koshikawa *et al.*, 2009) or via miRNAs (Puisségur *et al.*, 2011; Kim *et al.*, 2013).

1.2.2 The role of HIF in endothelial cells

1.2.2.1 Cell autonomous effects of HIF on metabolism

The HIF system is highly conserved across all metazoan species and its primordial role appears to be the balance of anaerobic and aerobic metabolism within a cell according to oxygen supply (Prabhakar and Semenza, 2012); this is exemplified by the fate of glucose. After being broken down into pyruvate, this molecule can either be shuttled into the mitochondria where it serves as a substrate for the Krebs cycle, or it can be converted into lactate, which is usually excreted by the cell. Conversion into lactate does not yield any further ATP and is therefore less desirable from an energetic point of view. Mitochondrial respiration on the other hand requires oxygen as the final acceptor for its electron transport chain. Continued OXPHOS without sufficient oxygen supply leads to the production of harmful reactive oxygen species (ROS) which can damage the cell and even lead to cell death (Zhang *et al.*, 2008). To counteract this, HIF-1α coordinates a transcriptional response aimed at curbing mitochondrial respiration while simultaneously increasing glycolytic flux. This involves the upregulation of several enzymes involved in the glycolytic pathway, such as glucose uptake transporters, hexokinase, phosphofructokinase-2 (PFK2), and pyruvate kinase M2 (PKM2). It also upregulates lactate dehydrogenase (LDHA), responsible for the conversion of pyruvate into lactate, and lactate efflux transporters such as MCT4 (Ullah *et al.*, 2006). Furthermore, it upregulates pyruvate dehydrogenase kinase 1 (PDK1), which inactivates pyruvate dehydrogenase (PDH), the enzyme responsible for conversion of pyruvate into the Krebs cycle substrate acetyl-CoA. To further reduce ROS production by OXPHOS, HIF-1α induces a reduction in overall mitochondrial mass through increased autophagy via BNIP3 (Bellot *et al.*, 2009)

1.2.2.2 Local hypoxia: HIF and angiogenesis

Local hypoxia within the body can result from inadequate perfusion. If O_2 is lacking, the affected cells stabilise HIF, which triggers the production of a series of pro-angiogenic factors such as vascular endothelial growth factor (VEGF), platelet-derived growth factor (PDGF), stromal-derived factor 1 (SDF1), and angiopoietin 2 (ANGPT2). These signals diffuse

to nearby vessels, where they induce a shift within the quiescent ECs composing the vessel (Krock *et al.*, 2011). The EC closest to the source of the signal starts migrating towards it; the cells in the immediate vicinity of this leading tip cell become proliferative and form the elongating neovessel (Draoui *et al.*, 2017). Eventually, this results in the formation of new vasculature within the previously poorly perfused region, increased O_2 delivery and HIF degradation until a steady state is reached. For example, cardiac hypertrophy leads to increased O_2 consumption within the heart muscle, causing a local drop in O_2 availability and thus HIF-1α stabilisation. This persists until new vessels formed through angiogenesis supply enough oxygen to compensate for the increased demand.

1.2.2.3 Endothelial HIF

Vascular cells thus play a key role in shaping the response to both local and global hypoxia. As in all mammalian cells, the EC hypoxia response is mainly mediated by HIF-1α and HIF-2α. In EC however, these are not only stress response factors, but act primarily, as physiological regulators (Kapitsinou *et al.*, 2014; Gong *et al.*, 2015; Cowburn *et al.*, 2016).

HIF-2α is thought to be constitutively expressed in EC, and essential for the maintenance of monolayer stability and barrier function (Le Bras *et al.*, 2007; Kapitsinou *et al.*, 2014), through the regulation of Vascular Endothelial (VE)-cadherin expression and localization at the cell surface. VE-cadherin, the adhesion molecule found in adherens junctions and essential for reversible vascular permeability (Montero-Balaguer *et al.*, 2009; Le Guelte and Gavard, 2011), is an important regulator of cytoskeleton structure and cell architecture, intracellular signalling via initiation of transduction cascades, and is thought to be determinant in the establishment of EC polarity (Giannotta *et al.*, 2013; Gong *et al.*, 2015). Even though HIF-2α in EC is vital for vascular integrity, stability and recovery (Kapitsinou *et al.*, 2014; Gong *et al.*, 2015; Reiterer *et al.*, 2019), it is also required for the onset and exacerbation of pulmonary hypertension (Cowburn *et al.*, 2016; Tang *et al.*, 2018), and deletion of lung EC HIF-2α resulted in ameliorated hypertension phenotypes in mice (Cowburn *et al.*, 2016). In general, HIF-2α is seen as the gatekeeper of EC quiescence, but depending on the tissue or the combined parameters within certain conditions, stabilization of endothelial HIF-2α is not advantageous.

HIF-1α can be seen as the disruptor of EC quiescence. This isoform is more ubiquitously expressed in mammalian cells (Weidemann and Johnson, 2008), and its role in EC function, like in most other cells, is usually of a transient nature, occurring as a result of demand, change or insult (Bartoszewski *et al.*, 2019). HIF-1α causes EC activation, which is a

pro-coagulant (Evans *et al.*, 2016), pro-inflammatory (Gras *et al.*, 2016; Wu *et al.*, 2017; Reiterer *et al.*, 2019) and pro-angiogenic state (Michiels, 2003; Schönenberger and Kovacs, 2015). This function is essential for new vessel formation to accompany growth and development, as well as for EC reshaping and migration, metabolic reprogramming (Wong *et al.*, 2017; Wu *et al.*, 2017; Li and Carmeliet, 2018) and recruitment of other cells to sites of injury and inflammation (Schönenberger and Kovacs, 2015; Gras *et al.*, 2016; Reiterer *et al.*, 2019). Activated EC are pro-thrombotic (Wang *et al.*, 2018), due to the surface expression of intercellular adhesion molecules that promote platelet interaction and binding of circulating myeloid cells (Michiels, 2003; Yau *et al.*, 2015). Essential as this function is for control of blood flow and tissue remodelling, it needs to be reversible. As such, activation of the coagulation cascade also and concomitantly stimulates fibrinolytic function, in an intricately choreographed and critically timed series of events (Michiels, 2003). Constitutively high levels of endothelial HIF-1α are known to potentiate a number of pathologies, including hypertension (Nanduri *et al.*, 2015; Wu *et al.*, 2017) and cancer, when HIF-1α permanence as a result of hypoxia incurs a vicious cycle of angiogenesis and inflammation, with consequences in tumour cell migration and aggressiveness (Augustin and Koh, 2017; Li and Carmeliet, 2018).

Many HIF-derived functions are implemented via accumulation of vascular endothelial growth factor (VEGF) and downstream receptors and effectors (Rahimi, 2006; Semenza, 2012; Schönenberger and Kovacs, 2015; Yamamoto *et al.*, 2016; Gerri *et al.*, 2018). The levels and source of VEGF, as well as what isoforms are present, dictate the behaviour of both EC and their relation to the surrounding tissue.

However essential the HIF-regulated pathways are in adequate adaptation to oscillations in oxygen levels, it has become increasingly evident that their stabilization and activity in EC is graded, complementary, and occur in response to a myriad of other parameters, frequently independent of oxygen levels. HIF and VEGF signalling are also involved in the regulation and the responses to signals affecting EC function, including reactive oxygen and nitrogen species, cell proliferation, cell death, and shear stress resulting from oscillations in laminar flow.

1.3 Endothelial effects in cancer and metastasis

1.3.1 The tumour microenvironment

In the first stages of tumour development, genetic and epigenetic modifications lead to a proliferating and thus constantly expanding cell mass, removing the centre of the tumour

further and further from oxygen and nutrient supply. This leads to severe hypoxia, or even anoxia, with O_2 levels commonly below 1% (McKeown, 2014), resulting in the stabilisation of HIF, the secretion of VEGF and other similar factors, and an angiogenic response from nearby vessels (section 1.2.2.2). VEGF in particular plays a crucial role in tumour angiogenesis, as shown by the reduced growth of VEGF -/- tumours compared to WT controls (Tsuzuki *et al.*, 2000). However, attempts to target VEGF for therapeutic purposes have not been successful; anti-angiogenic treatment does initially reduce tumour volume but it also leads to exacerbated hypoxia, which increases tumour aggressiveness and metastatic dissemination (Carmeliet and Jain, 2011b).

The resulting tumour vessels are structurally and functionally abnormal, with the endothelial cells themselves being irregular in shape and size, leading to poor perfusion and gaps in the vessel wall (Carmeliet and Jain, 2000). Pericyte coverage is inconsistent and they are less tightly connected to the endothelial cells than in normal vessels. This is partly because, unlike during physiological angiogenesis, tumours continue to produce angiogenic factors even when vessels have been established. Indeed, most tumours consistently overexpress HIF-1α and HIF-2α (Zhong *et al.*, 1999; Talks *et al.*, 2000), independently of their oxygenation status. Often, this is achieved through loss of function mutations in one or multiple components of the HIF system, such as VHL (Atkins *et al.*, 2007). Tumour cells also frequently possess constitutively active growth signalling through the MAPK or PI3K-Akt pathways, which also leads to HIF stabilisation. Furthermore, cells within the tumour microenvironment frequently secrete molecules that can stabilise HIF even in the presence of oxygen, such as NO or ROS (see section 1.2.1.2).

As a result of this constitutive HIF-1α expression, tumour cells are predominantly glycolytic, even under normoxia (Warburg *et al.*, 1927). While it has become clear that aerobic glycolysis is a necessary part of tumour development, the selective advantage it confers is not entirely clear. It has been proposed that high rates of glycolysis allow cancer cells to maintain steady ATP levels but also generate macromolecules necessary for cell growth and division, by siphoning off some glycolytic flux into side branches, such as serine biosynthesis and the pentose phosphate pathway (Heiden *et al.*, 2009; Ward and Thompson, 2012). However, the large majority of carbon derived from glucose is excreted as lactate and therefore not used in anabolic processes. This lactate secretion results in the acidification of the tumour microenvironment, which has been shown to increase tumour cell invasiveness, aiding cancer progression (Estrella *et al.*, 2013). The lactate could also be used by less hypoxic and thus more

oxidative parts of the tumour, by re-converting it into pyruvate and entering it into the Krebs cycle (Nakajima and Van Houten, 2013). The high glycolytic flux of tumour cells may also divert glucose and glutamine away from other cells in their vicinity, such as tumour-infiltrating lymphocytes, promoting immune suppression (Chang *et al.*, 2015).

HIF expression in cancer cells also promotes invasion and metastatic success through several mechanisms, such as promoting a more mesenchymal state through the downregulation of E-Cadherin and increased production of matrix-metalloproteases (MMPs) (Krishnamachary *et al.*, 2006; Muñoz-Nájar *et al.*, 2006; Jing *et al.*, 2012), remodelling of collagen fibres in the extracellular matrix to facilitate cell motility (Gilkes, Bajpai, Chaturvedi, *et al.*, 2013; Gilkes, Bajpai, Wong, *et al.*, 2013; Gilkes, Chaturvedi, *et al.*, 2013), and increased expression of adhesion factors that facilitate attachment to the endothelium of the metastatic target organ (Zhang *et al.*, 2012).

The roles of HIF in the tumour vasculature are complex and can vary considerably depending on the experimental model. Due to their aberrant nature, tumour vessels are usually poorly perfused and thus hypoxic, leading to persistent HIF activation within ECs. This keeps them in an active and proliferative state, displaying even higher rates of glycolysis than other ECs and secreting large amounts of VEGF, which further prevents vessel normalisation. Tumour cells have been shown to actively promote this aberrant EC state. For example, media from glioblastoma cells leads to normoxic stabilisation of HIF-1α in nearby ECs, through competitive inhibtion of VHL by profilin-1. This causes ECs to secrete a host of angiocrine factors which act as a pro-proliferative signal towards tumour cells (Fan *et al.*, 2014).

Following this rationale, deleting HIF-1α in ECs should decrease tumour vessel formation, leading to tumour necrosis and reduced growth, and this has indeed been shown (Tang *et al.*, 2004). Similarly, a HIF-2α global EC knockout has been shown to display reduced tumour angiogenesis and increased tumour apoptosis (Skuli *et al.*, 2009). However, reducing tumour angiogenesis further exacerbates hypoxia, which can promote tumour mobility and metastasis (Giatromanolaki *et al.*, 2003; Helczynska *et al.*, 2008; Wang *et al.*, 2010; Hao, 2015). Additionally, it reduces accessibility for chemotherapeutic agents and susceptibility to radiotherapy. Therefore, vessel normalisation through stimulation of HIF-2α can actually be beneficial. This can also be achieved by targeting glycolysis in TECs directly, such as through inhibition of PFKFB3; this leads to vessel normalisation, improved chemotherapy and reduced metastasis (Cantelmo *et al.*, 2016).

In line with the angiocrine role of ECs described in section 1.1.1, delivering oxygen and nutrients to tumour cells is not the only role of TECs. Angiocrine signalling molecules that are usually responsible for orchestrating tissue development and regeneration can promote a chemoresistent cancer stem cell phenotype (Butler *et al.*, 2010). FGF4 from tumour cells induces IGF-1 production in TECs which promotes cancer stem cell formation and consequently leads to increased mortality. Importantly, chemotherapy treatment further strengthened this pathway, leading to the development of a resistant population of cancer cells (Cao *et al.*, 2017).

1.3.2 Endothelial cells in metastasis

Importantly, tumour vasculature not only provides a source of nutrients and growth signals, but it also provides a route for tumour cells to enter the vasculature and metastasise to different organs. This involves the crossing of two endothelial barriers, once during intravasation and once during extravasation. Hence both tumour ECs and ECs of the metastatic target organ play a key role in metastatic progression.

Intravasation is reliant on close proximity between vessels and the tumour, therefore intravasation rates often correlate with vascular density within the tumour (Tien *et al.*, 2001; Yamamura *et al.*, 2001). Indeed, most intravasation takes place within the core of the tumour, rather than at its proliferative, invading front (Deryugina and Kiosses, 2017). Anti-angiogenic therapies have therefore been proposed as a method to reduce intravasation, but the results have been mixed. Similarly to what was described above with regards to the primary tumour, anti-angiogenic therapy can indeed reduce intravasation (Conn *et al.*, 2009; Harney *et al.*, 2015) but this has the secondary effect of making the tumour more hypoxic, which increases HIF stabilisation, tumour cell motility and vascular leakage (Carmeliet *et al.*, 1998). As a result, it has been suggested that tumour vessel normalisation may actually be more effective in combatting intravasation, since it improves EC barrier function (Cantelmo *et al.*, 2016).

Once in circulation, tumour cells are vulnerable and usually short-lived, less than 0.1% remain viable after 24 h in circulation (Fidler, 1970). Thus, a rapid and efficient way for tumour cells to cross the endothelial barrier is required for metastasis to occur. Transendothelial migration (TEM) of tumour cells usually occurs in the microvasculature, since circulating tumour cells (CTCs) are frequently larger than small capillaries and thus become arrested there (Chambers *et al.*, 2002). Extravasation is a multi-step process, involving tumour cell adhesion to the endothelium, modulation of the endothelial barrier, and eventually TEM (Strilic and Offermanns, 2017). It has been hypothesised that endothelial-to-mesenchymal transition

(EndMT) is a crucial component. EndMT involves a series of changes in gene expression and protein localisation that result in endothelial cells losing their specific markers and intercellular junction proteins (e.g. VE-Cadherin). Instead, they start expressing mesenchymal and fibroblast-specific proteins and become motile and migratory. This results in paracellular gaps which tumour cells can use to extravasate. TGF-b plays a major role in this transition, as it induces the expression of mesenchymal transcription factors such as SNAIL within EC. It is expressed by CTCs, as well as platelets, which are often bound to clumps of CTCs. Indeed, a series of other cell types, such as neutrophils and monocytes/macrophages, are required for efficient tumour extravasation to take place (Coupland *et al.*, 2012; Reymond *et al.*, 2013; Kitamura, Qian and Pollard, 2015).

1.3.3 Pre-conditioning the endothelial cells of metastatic target sites

First proposed in 1889 and now widely recognised, the "seed and soil" theory stipulates that cancer cell extravasation does not commence when the CTC gets arrested in a particular vascular bed (Paget, 1889). Rather, this is preceded by a series of signals from the primary tumour that prepare the eventual metastatic site for the arrival of the CTC. The formation of this so-called pre-metastatic niche involves alterations in endothelial cells, as well as the recruitment and/or education of additional cell types such as fibroblasts and bone-marrow derived cells (Peinado *et al.*, 2017). In melanoma model, signals from the primary tumour led to the upregulation of MMP3, MMP10 and ANGPT2 in the lung vasculature, causing increased permeability and immune cell infiltration (Huang *et al.*, 2009). Similarly, mice bearing mammary adenocarcinoma showed increased levels of myeloid progenitor cells in the lung, which resulted in increased secretion of pro-inflammatory cytokines and MMP9. Importantly, a pre-metastatic niche can also be created through signals that are independent of the primary tumour, such as surgery, infection, and ageing (Smith and Kang, 2013; Peinado *et al.*, 2017; Pasquier *et al.*, 2018).

1.4 The role of oxygen in endothelial cell priming – Aims of this thesis

This chapter highlights the role of endothelial cells as sensors of a diverse array of stimuli, both from the systemic vasculature, as well as their underlying organ. Adapting and responding to these stimuli is one of EC's main physiological functions. However, due to their plastic nature, EC responses are also easily corrupted, as shown by the countless pathologies in which they are either directly involved or contribute to co-morbidity. Amongst this array of stimuli, oxygen is of particular importance; in response to hypoxia endothelial cells undergo a

vast remodelling process, governed by HIF, that allows our body to adjust to both local and global lack of oxygen. On the other hand, the same responses that mediate homeostasis can become dysregulated and result in pathology, such as during pulmonary hypertension (Cowburn *et al.*, 2016) or ocular neovascularisation (Campochiaro, 2013). Furthermore, it has been previously established that endothelial HIF levels modulate metastasis to the lung (Branco-Price *et al.*, 2012). This led to the first question of this thesis: Does HIF-activation through hypoxic pre-conditioning affect the role of endothelial cells in metastasis? If so, what is the mechanism behind this?

This question was answered with respect to lung metastasis, since this vascular bed had been investigated previously by the group and it is also the first vascular bed that is encountered by CTCs originating from the systemic circulation. It was found that hypoxic stimuli of differing length could preferentially stabilise HIF-1α or HIF-2α within the lung endothelium. Exposing these pre-conditioned vascular beds to tumour cells resulted in differential metastatic success to the lung.

As described in section 1.1.1, microvascular beds from different organs are often highly specialised to their role. With regards to their oxygen response this is particularly true for the lung, since it is a net oxygen source rather than a sink. Indeed, in response to global hypoxia, the lung microvasculature constricts whereas all other vascular beds dilate (Weir and Anand, 1995). Therefore, this raised the question whether the observed effects of oxygen-preconditioning were unique to the lung endothelium or if similar effects occurred in other microvascular beds.

The next step was thus to compare the hypoxia response and the role of HIF in lung capillaries to those of another metastatic target organ. The brain was chosen since its microvasculature is continuous, like the lung's, while also being highly specialised as a part of the BBB. The two organotypic microvasculatures were compared using primary murine microvascular endothelial cells (MVECs) *in vitro*.

At first, these cells were cultured under standard cell culture conditions, with ambient oxygen levels, before being exposed to hypoxia. However, it soon became clear that culturing MVECs at ambient oxygen levels already represented a priming step, since ambient air is hyperoxic compared to the *in vivo* setting of these cells. As a result of this hyperoxic pre-conditioning, both MVEC populations cultured in hyperoxia performed poorly in response to a subsequent exposure hypoxia. To mitigate this, MVECs were cultured at two additional

oxygen levels: 10% and 5% O_2, which represent physiological levels in the lung and brain microvasculature, respectively.

This led to a series of new questions: How does each oxygen level shape MVEC function? Does it affect their ability to react to a subsequent stimulus such as hypoxia? Are these effects organ-specific? The last question in particular connects to a very fundamental discussion about EC heterogeneity: is it intrinsic or acquired? As mentioned in section 1.1.1, endothelial cells are shaped considerably by their local environment, be it through signalling from nearby cells or by the physical features of the organ they inhabit. Priming MVECs for several weeks *in vitro* in the same culture medium should remove a significant amount of this induced heterogeneity. Thus, culturing these two populations of MVECs at different oxygen levels will show whether their oxygen sensing machineries are set intrinsically differently, or whether some of the differences observed *in vivo* are caused by physiological differences in oxygen supply.

This data will provide crucial insights into the effects of changes in oxygen exposure on endothelial physiology and plasticity, which will help us understand how organ-specific ECs behave in the myriad of instances in which they are exposed to altered oxygen levels such as during surgery or exercise, at high altitude, or during a series of pathologies.

Acknowledgment

Parts of this chapter were published as a viewpoint article written and edited by me and Cristina Branco (Reiterer and Branco, 2019).

Chapter 2: Acute and chronic hypoxia differentially predispose lungs for metastases

2.1 Introduction

Extravasation efficiency is a critical rate-limiting step of the metastatic cascade (Labelle and Hynes, 2012) and vascular endothelial cells (EC) constitute the main barrier, affecting both blood flow and cell penetration to surrounding tissues (Weis *et al.*, 2004; Gupta *et al.*, 2007; Labelle and Hynes, 2012). Microvessels are typically the site of arrest of circulating tumour cells (CTC), often present from the onset of cancer, and these micro-occlusions impair tissue perfusion and reduce oxygen availability - transiently or long term - leading to altered EC behaviour and microvascular integrity (Le Bras *et al.*, 2007; Gong *et al.*, 2015). The hypoxia-sensitive family of Hypoxia Inducible factors (HIF) are key regulators of EC physiology and of the metabolic shifts underlying their responses to oxygenation and organ demand (Michiels, 2003; Cowburn *et al.*, 2016; Rankin *et al.*, 2016; Wong *et al.*, 2017). Endothelial HIF can be stabilized as a result of transient ischemic events (Barteczek *et al.*, 2017), such as the arrest of CTC in small capillaries (Evans *et al.*, 2017) but also in response to cytokine and tumour-derived signals, and indirectly via pharmacological agents or radiotherapy (Harrison and Blackwell, 2004; Qi *et al.*, 2013; Trollmann *et al.*, 2014).

Previous work from our group has shown that deletion of endothelial HIF-1α inhibits growth of lung metastasis in spontaneous breast cancer, implanted mammary gland tumours, or models of experimental metastasis, whereas deletion of HIF-2α increases metastatic frequency in all of these models (Branco-Price *et al.*, 2012, 2013). The lungs are frequent hosts of metastatic tumours, and are often the first microvascular network encountered by CTC; additionally, the pulmonary vasculature is particularly responsive to changes in oxygenation. Most pulmonary hypoxic challenges are intermittent (Prabhakar and Semenza, 2012), and can result from a myriad of pathologies or environmental challenges (Kumar and Choi, 2015), ranging from hypertension (Shimoda and Semenza, 2011; Bryant *et al.*, 2016), smoke exposure, cardiovascular and hepatic disease (Daijo *et al.*, 2016), to sleep apnoea (Skuli *et al.*, 2009; Almendros *et al.*, 2014; Gras *et al.*, 2016). Importantly, it has been shown that intermittent hypoxia can lead to the stabilization of HIF-1α and decreases in HIF-2α levels in lung tissue (Nanduri *et al.*, 2009; Prabhakar *et al.*, 2010), with detrimental effects on cancer progression (Prabhakar and Semenza, 2012; Almendros *et al.*, 2014). A number of groups have shown that each HIF isoform has downstream physiological consequences that are cell-type

specific (Yu and Hales, 2011; Almendros *et al.*, 2013, 2014), and the stabilization of either in different contexts can determine disease outcome.

We hypothesised that the stabilization of either of these HIF factors will have a role in modulating the lung microenvironment and affect its vulnerability to metastatic colonization depending on the relative abundance of HIF-1α and HIF-2α. In this work, one or the other isoform of HIF transcription factors was selectively induced in the lung microenvironment using acute (for highest HIF-1α stabilization) and chronic (for highest HIF-2α stabilization) environmental hypoxia exposure. The efficiency of lung tumour seeding in the different pre-conditioning settings was characterized. Additionally, animals with lung endothelium-specific (Park *et al.*, 2008) deletion of HIF isoforms were used to investigate which components of organ remodelling were mediated by EC-derived signals, and to establish the role of endothelial HIF in lung vulnerability to metastatic colonization.

The endothelial response to hypoxia is shown to remodel the lung microenvironment in a time-dependent manner: acute environmental hypoxia, driving stabilization of pulmonary HIF-1α results in a pro-metastatic environment, while chronic environmental hypoxia, and concomitantly higher levels of HIF-2α, reduces endothelium-mediated metastatic cell penetrance.

2.2 Results

2.2.1 EC response to hypoxia results in staggered and dynamic activation of HIF transcription factors

Primary lung EC were transferred to 1% O_2 and HIF-α isoform activation was assessed over time. HIF-1α activation was seen at the shorter exposure time-points, peaking at 4 h and starting to decline after 8 h, when increased stabilization of HIF-2α became more evident (Fig. 2-1A), consistent with what has recently been reported for microvascular cells of human lung and other organs (Bartoszewski *et al.*, 2019). To investigate whether this pattern of HIF isoform expression is also seen *in vivo*, animals were exposed to environmental hypoxia (10% O_2). After 24 h and 10 d exposures, HIF activation was assessed in whole lung tissue by western blotting (Fig. 2-1B), and levels of both isoforms were increased in hypoxic lungs, irrespective of exposure length; however HIF-1α was preferentially activated after 24 h of hypoxia, and hardly detectable in lungs of mice exposed to normoxia or prolonged hypoxia; HIF-2α protein was seen in all time points, but highest after prolonged (10 d) exposure to hypoxia (Fig. 2-1B). Total lung HIF signal was also investigated by immunofluorescence (Fig. 2-1C), and frozen tissue was stained for both HIF (green signal) and endothelial cells (Podocalyxin, red). In the

panels to the right, average total HIF signal is shown for each isoform (grey line, left y-axis), as well as endothelial-derived HIF, quantified by co-localization of podocalyxin and HIF signal (green line, right y-axis). Even though HIF is expected to be stabilised in multiple cell types in response to hypoxia, the activation pattern of endothelial HIF follows that seen in whole lung tissue, and confirms the trend seen in Fig. 1B.

The time-points and activation patterns seen *in vivo* do not fully overlap with the ones seen *ex vivo*. This is likely a result of the fact that atmospheric O_2 levels used to trigger a hypoxic response in the lung endothelium are different from those necessary to trigger the same response in EC in the tissue culture environment. The *in vivo* model was used to reflect the effect of endothelial HIF in modulating metastatic success, independently of tumour-derived signals. Thus, acute and chronic hypoxia were defined as the treatments yielding the highest activation of HIF-1α or HIF-2α, respectively, and these conditions were subsequently used to test differential organ susceptibility to metastatic tumour colonization, as a function of EC activation status.

2.2.2 Hypoxia pre-conditioning affects metastatic tumour burden in a time-dependent manner

To assess the effect on organ susceptibility to colonization by CTC after hypoxia, animals in each pre-treated group received tumour cells intravenously, as illustrated in Fig. 2-2A,B. Lung tumours were counted by H&E staining of paraffin-embedded sections obtained 14 d post injection, during which animals were maintained in normal room air. Mice exposed to acute hypoxia, showing the highest lung HIF-1α levels (Fig. 2-1B,C), had more tumours than the controls breathing room air, whereas mice exposed to chronic hypoxia developed lung tumours in numbers similar to those found in normoxic controls (Fig. 2-1D).

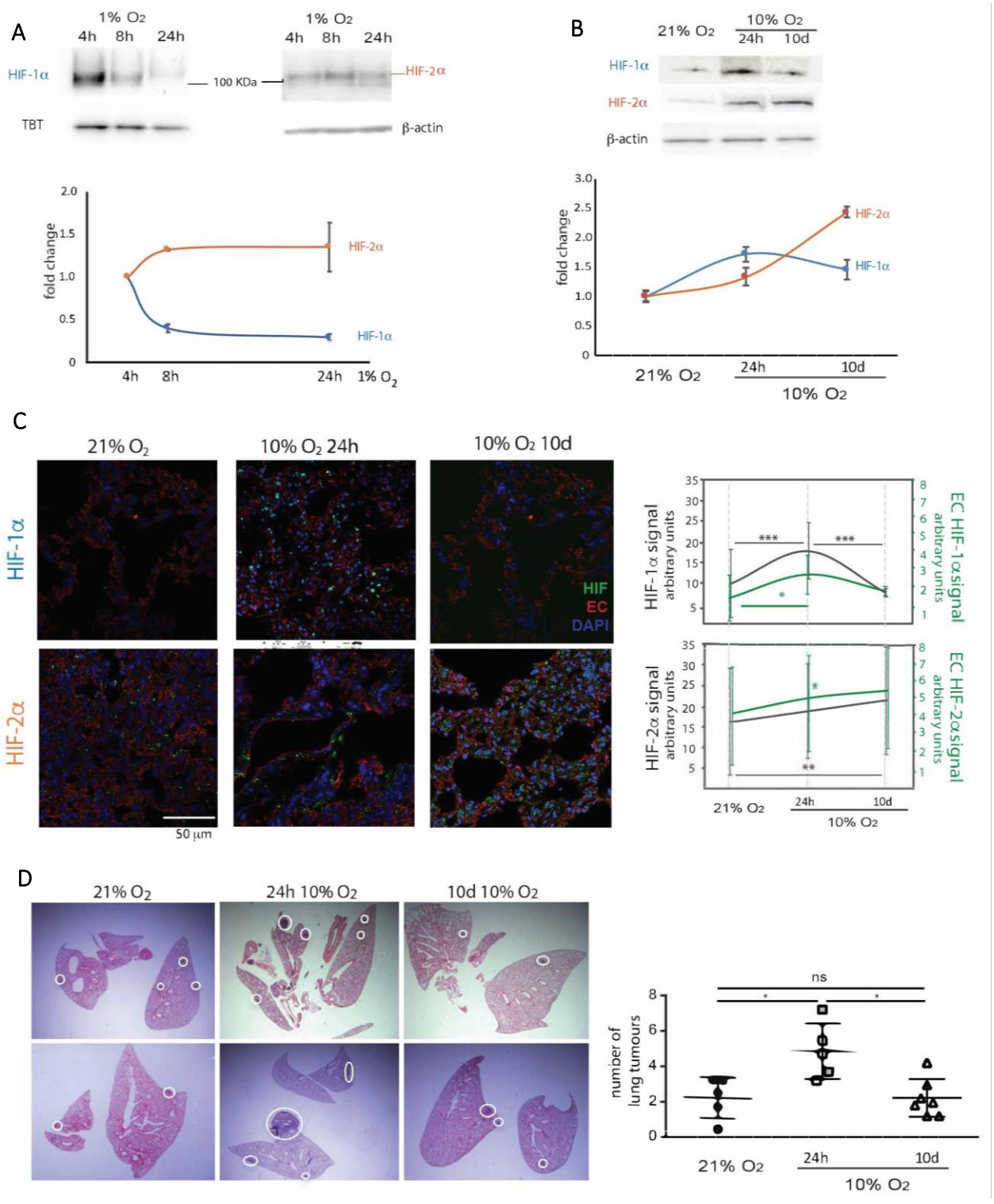
A
1% O2
4h 8h 24h
1% O2
4h 8h 24h
HIF-1α
100 KDa
HIF-2α
TBT
β-actin
fold change
HIF-2α
HIF-1α
4h 8h 24h 1% O2
B
21% O2
10% O2
24h 10d
HIF-1α
HIF-2α
β-actin
fold change
HIF-2α
HIF-1α
21% O2 24h 10d
10% O2
C
21% O2
10% O2 24h
10% O2 10d
HIF-1α
HIF-2α
HIF
EC
DAPI
50 μm
HIF-1α signal arbitrary units
EC HIF-1α signal arbitrary units
HIF-2α signal arbitrary units
EC HIF-2α signal arbitrary units
21% O2 24h 10d
10% O2
D
21% O2
24h 10% O2
10d 10% O2
number of lung tumours
ns
21% O2 24h 10d
10% O2

Figure 2-1

Figure 2-1: Distinct temporal patterns of activation of HIF-1 and HIF-2 primary lung endothelial cells and whole lung tissue, and impact on metastatic seeding.

(**A**) Representative western blot of HIF-1α, HIF-2α and loading control (TBP- tata binding protein, or β-actin), from nuclear extracts of primary mouse lung EC exposed to a hypoxic (1% O_2) or normal atmosphere (21% O_2) over time. Graph below shows quantification of signal intensity of HIF signal for each time point, normalised to respective loading control (n=3)

(**B**) Whole lung HIF-1α and HIF-2α western blot (quantification underneath), from mice in normal atmosphere or housed in hypoxic chambers (10% O_2) for a short exposure (24 h) or prolonged exposure (10d). HIF signal was normalized to β-actin. Data are Avg. fold change (hypoxia/normoxia) ± SD, $n \geq 3$ per treatment;

(**C**) Immunofluorescent detection of HIF-1α (top) and HIF-2α (bottom) signal in frozen lungs of mice maintained at 21% O_2 (normoxia), or exposed to oxygen-deprived atmosphere (10% O_2, hypoxia) for 24 h or 10d. Charts on the right represent the Avg. signal ± SD, obtained from a minimum of 10 evenly spaced lung sections from ≥ 5 mice per treatment, 5 images acquired per section; left y-axis represents total HIF intensity (grey line on the chart); endothelial HIF signal was calculated from co-localized signal between HIF and podocalyxin, and is shown on the right y-axis (green line on the chart). Significance assessed by student's *t*-tests; $*p < 0.05$, $***p < 0.001$ refers to comparisons between time-points;

(**D**) Average number of lung tumours ± SD counted from a minimum of 20 evenly spaced paraffin sections of lungs harvested 14d post tumour cell injection, $n \geq 5$ animals per group. Significance was assessed by students *t*-test with Welch's correction, $*p < 0.05$. Illustrative

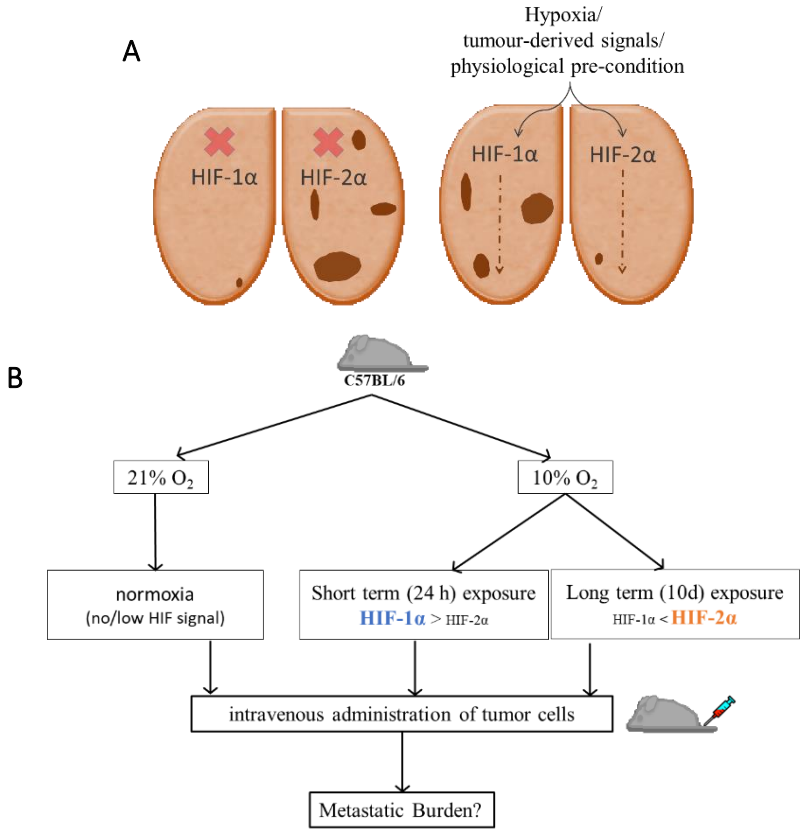

Figure 2-2: Hypothesis and experimental approach

(A) Upon the initial observation that deletion of HIF-1α resulted in less metastasis, and deletion of HIF-2α resulted in increased metastatic burden (Branco-Price *et al*., 2012, left), it was hypothesised that the stabilization of HIF-1α or HIF-2α would result in the opposite phenotype (right panel);

(B) Using WT animals, mouse lungs were pre-conditioned using short and long hypoxia exposure to selectively stabilize HIF-1α or HIF-2α, respectively, prior to intravenous injection of tumour cells (5 x 10^5 LLC via tail vein), assess tumour burden; time points for optimal preferential proportion of specific isoforms were determined in prior pilot experiments;

2.2.3 Microvascular permeability transiently increases during adaptation to hypoxia

Lung microvascular permeability was quantified using intravenous administration of Evans Blue (EB) to investigate if the higher tumour incidence was the result of improved extravasation efficiency, caused by increased vascular leakage. EB leaked from the lung microvasculature was quantified by spectrometry of the bronchoalveolar lavage of a minimum of 5 animals per group, collected 20 min post EB injection. An increase in permeability was seen after 24 h of hypoxia (Fig. 2-3A), correlating with the increased number of lung tumours seen in Fig 2-1D. When hypoxic exposure was prolonged to 10 days, permeability returned to the levels seen in animals maintained in room air.

Transcripts of genes that regulate vascular permeability were surveyed by qPCR from whole lung extracts. Inducible nitric oxide synthase (iNOS) and vascular endothelial growth factor A (VEGF) were expressed at the highest levels after acute hypoxia, when permeability and metastatic incidence were also increased, whereas levels of VE-cadherin transcript dropped in acute hypoxia (Fig. 2-3B). Arginase II expression, a HIF-2α target (Cowburn *et al.*, 2016), increased only after prolonged hypoxia. These differences were not statistically significant, illustrating the diverse contribution of different cell types to whole-lung transcript levels, likely responding in different ways to the same hypoxic challenge, and underscoring that only a subset will effectively contribute to the observed trends.

iNOS protein was shown to be visibly elevated by acute hypoxia in frozen lung sections (Fig. 2-3C,D) and also in primary EC (Fig. 2-3E); iNOS activity is transcriptionally regulated by HIF-1α, but not HIF-2α, and therefore its accumulation corroborates HIF-1α activation; it also suggests that the increased permeability may have occurred due to NO production by iNOS (Branco-Price *et al.*, 2012).

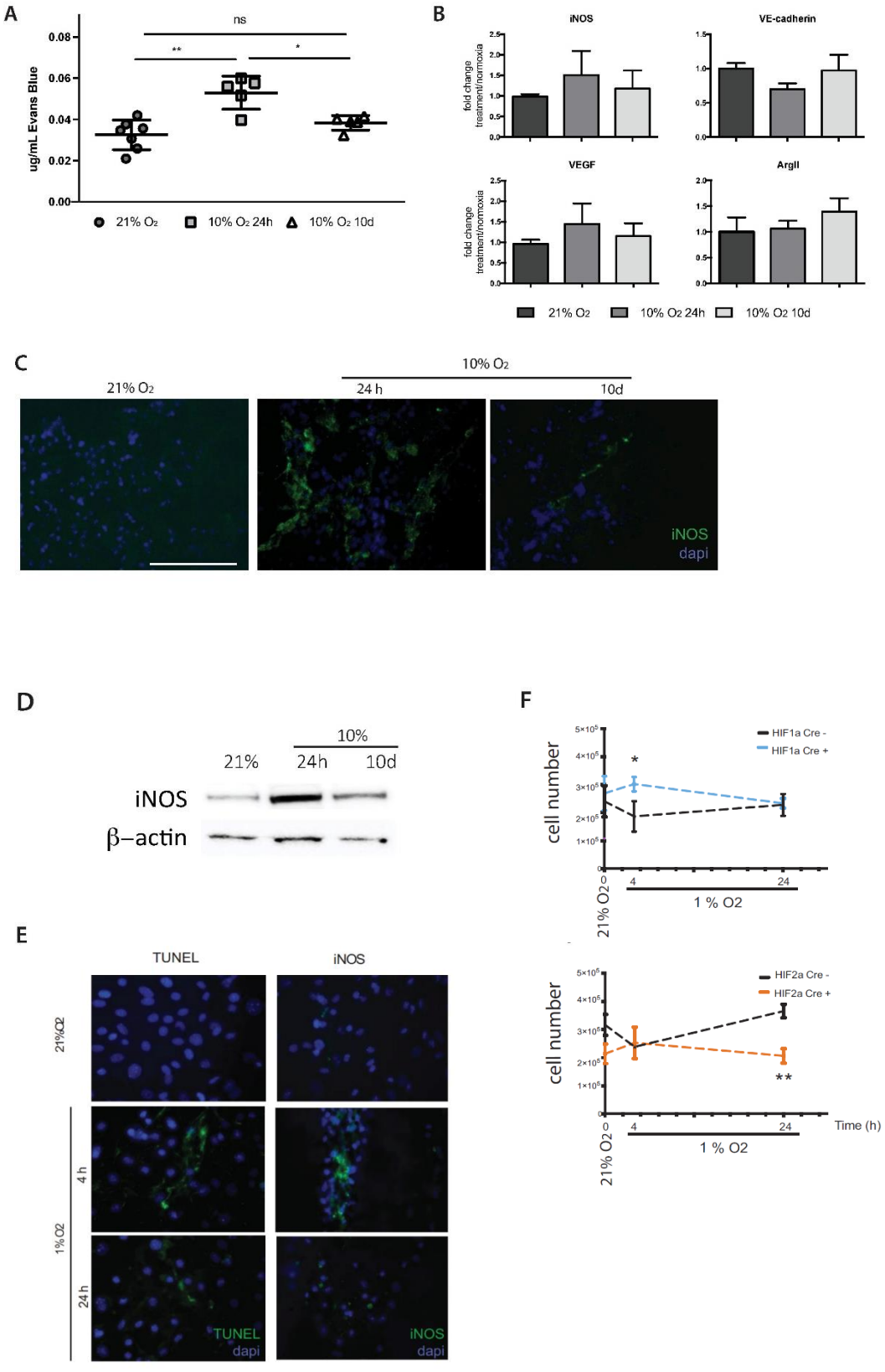
A
ns
**
*
ug/mL Evans Blue
0.08
0.06
0.04
0.02
0.00
21% O2
10% O2 24h
10% O2 10d
B
iNOS
VE-cadherin
VEGF
ArgII
fold change treatment/normoxia
21% O2
10% O2 24h
10% O2 10d
C
10% O2
21% O2
24 h
10d
iNOS
dapi
D
10%
21%
24h
10d
iNOS
β–actin
E
TUNEL
iNOS
21%O2
1%O2
4 h
24 h
TUNEL
dapi
iNOS
dapi
F
cell number
HIF1a Cre -
HIF1a Cre +
*
4
24
21% O2
1 % O2
HIF2a Cre -
HIF2a Cre +
**
Time (h)

Figure 2-3

Figure 2-3: Hypoxia transiently induces vascular permeability, correlating with transient accumulation of iNOS mRNA and protein

(A) Lung vascular permeability was assessed by quantification of Evans Blue in Bronchoalveolar Lavage (average +/- SD, n > 5 animals per group)

(B) qPCR of whole lun tissue for transcripts encoding proteins involved in modulation of vascular permeability: iNOS, VEGF, and VE-Cadherin, and ArgII as a surrogate marker for HIF-2α activation (average fold change of signal of treatment to control, normalised to β-actin, +/- SE)

(C) iNOS signal was detected by IF in frozen lung sections or animals exposed to acute or prolonged hypoxia as a qualitative representation of protein levels (scale bar 100 μm)

(D) Western blot of whole lung portein extracts of animals exposed to normoxic or hypoxic atmospheres, probed for iNOS protein

(E) TUNEL staining and immunofluorescent detection of iNOS levels in primary EC fixed after acute or prolonged hypoxia

(F) Viability in HIF-1α null (left) and HIF-2α null (right) EC and their respective double-floxed control in normoxia and after 4 h and 24 h of hypoxia

Statistical significance was assessed by student's t-test, *$p<0.05$, **$p<0.01$

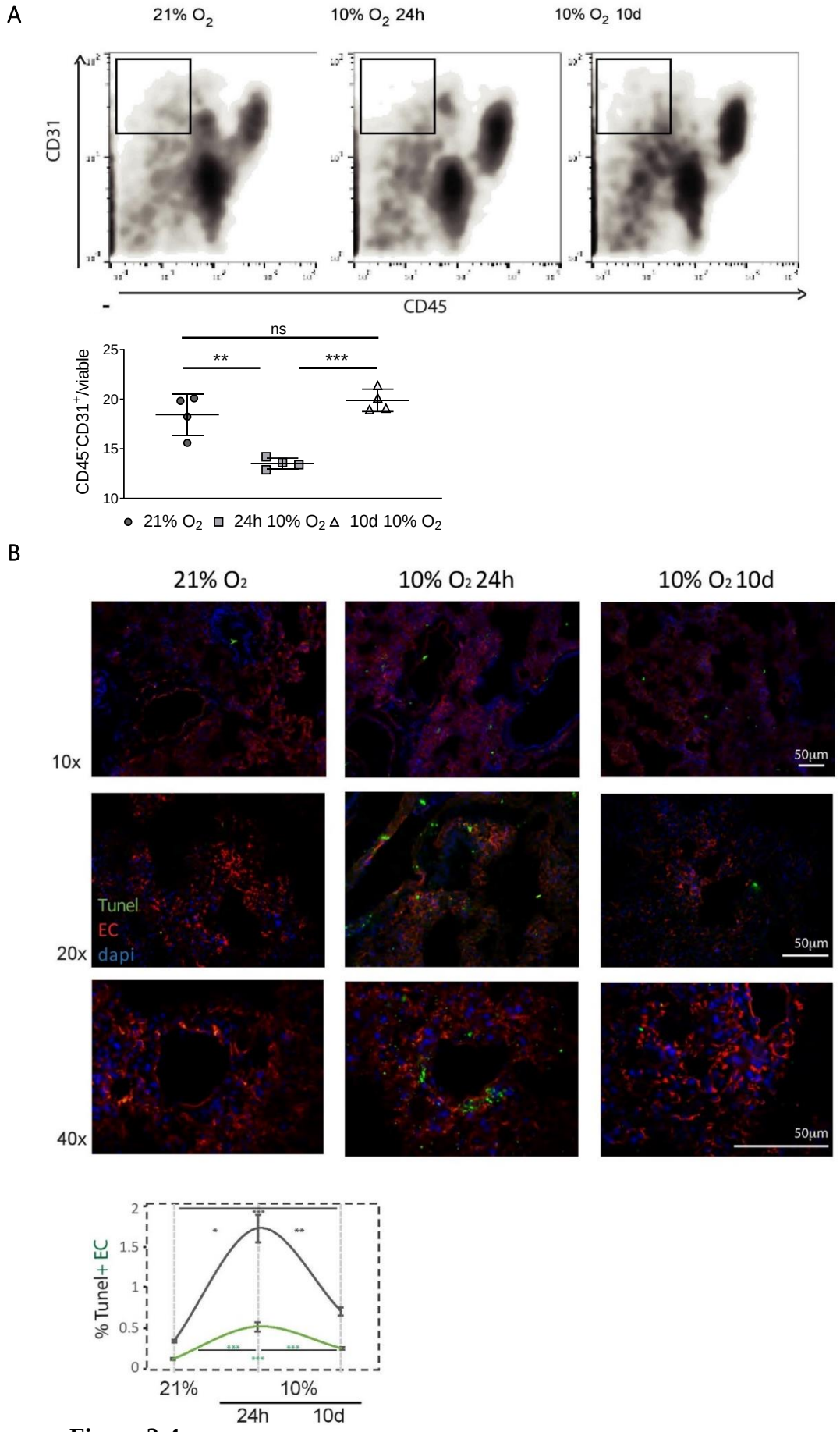
A
21% O2
10% O2 24h
10% O2 10d
CD31
CD45
ns
**
***
CD45-CD31+/viable
25
20
15
10
21% O2
24h 10% O2
10d 10% O2
B
21% O2
10% O2 24h
10% O2 10d
10x
20x
40x
Tunel
EC
dapi
50µm
% Tunel+ EC
2
1.5
1
0.5
0
21%
10%
24h
10d

Figure 2-4

Figure 2-4: Endothelial cell population decreases with acute hypoxia exposure
(A) Representative flow cytometry plots sorted for EC marker CD31+CD45− viable cells are shown for each treatment and control; lung tissue was sorted immediately after hypoxia treatment (no tumour injection); graph below represents average % of viable EC (CD31+CD45−);
(B) Representative images of TUNEL staining of frozen lung sections from mice exposed to normoxia and hypoxia, and counter-stained with vasculature marker Podocalyxin; scale bar = 50 μm; Quantification of total TUNEL staining in each group (grey line) and EC + TUNEL (green line) obtained by co-localization of TUNEL and Podocalyxin signals; values represent Avg. ± SE number of TUNEL-positive cells; images were obtained from randomly selected individual sections of a minimum of 4 mice in each treatment, at least 8 sections per animal, 3 images per section. *$p < 0.05$, **$p < 0.005$, ***$p < 0.001$, by Student's t-test with Welch's correction.

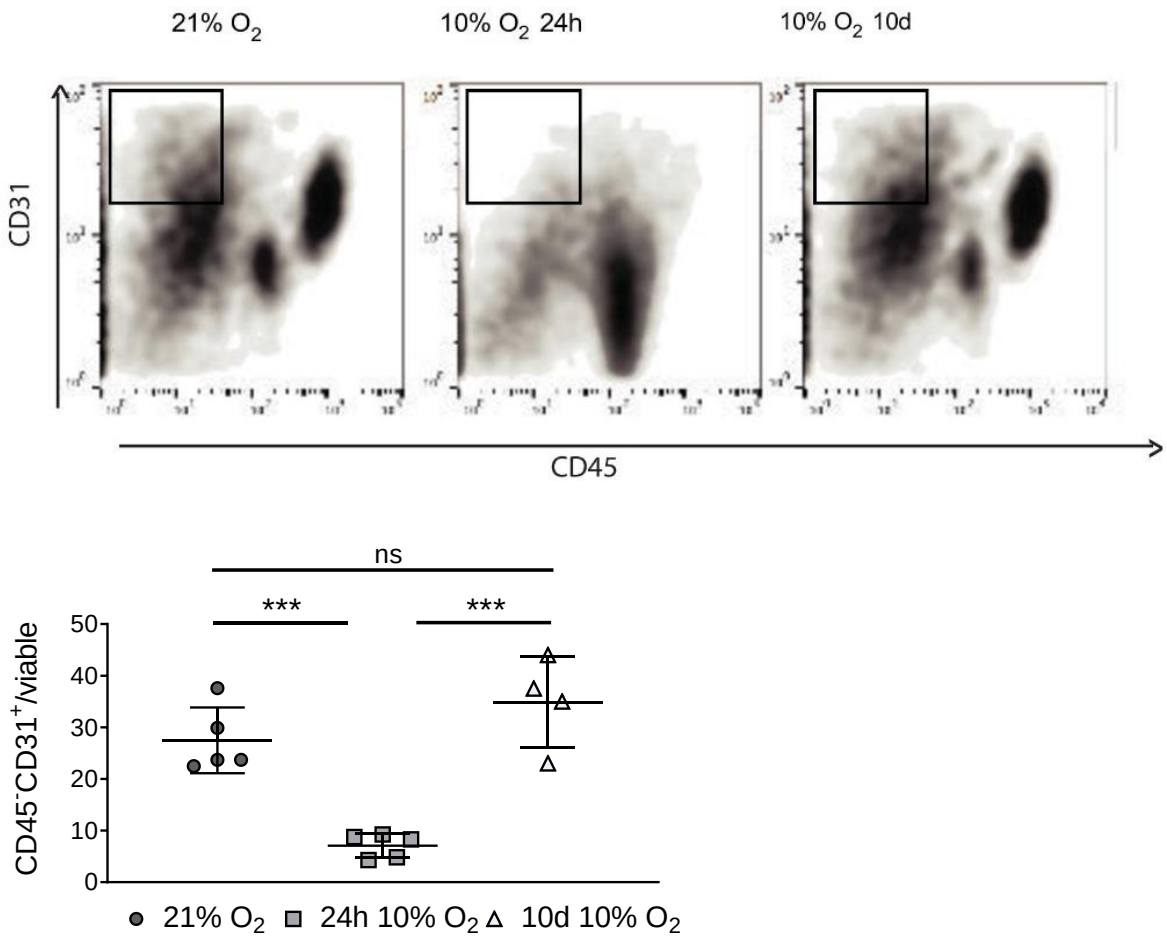

Figure 2-5: Viable endothelial cell numbers transiently decrease upon acute hypoxia exposure

Representative flow cytometry plots for identification and quantification of EC (CD31+CD45-) in whole lung tissue exposed to normoxia or hypoxia followed by tumour cell injection (via tail vein). Upon tumour cell injection, animals were removed from hypoxia chambers and lung tissue was harvested 24 h later. Viable cells are shown for each treatment and control; graph below represents average % of viable EC

Error bars show SD, $n \geq 4$. $^{**}p < 0.005$, $^{***}p < 0.001$, by Student's t-test with Welch's correction.

To evaluate potential differences in the lung microenvironment during hypoxia, different cell populations were quantified by flow cytometry of lungs harvested immediately after each treatment. A significant decrease in the relative number of EC (CD31+CD45−) was seen after acute hypoxia (Fig. 2-4A). An additional group of animals instead received intravenous tumour cell injections after each hypoxia pre-treatment and were subsequently removed from the hypoxic chambers; lungs were analysed by flow cytometry 24 h later. The decrease in CD31+CD45− cells in this experimental group was strikingly exacerbated (Fig. 2-5), suggesting a suppression in EC proliferation, or increased cell death as part of the remodelling process (Watson *et al.*, 2017) which was only seen in the acute hypoxia pre-condition, but not in the chronically treated animals.

To investigate this possibility, cell death was visualised by TUNEL signal, which was increased after acute hypoxia. Fig. 2-4B shows representative images of TUNEL-stained frozen sections at different magnifications, to illustrate changes in overall rates of cell death as well as tissue distribution of TUNEL-positive cells. Signal per section (percent TUNEL+ cells per field), is shown in the chart below (gray line), and EC-specific TUNEL (TUNEL + Podocalyxin, green line), shows that the pattern of cell death for EC was similar to that seen for whole lung, and correlates with the increased vascular permeability seen at this time point (Fig. 2-3A).

2.2.4 Selective macrophage recruitment after short and prolonged hypoxia

Because myeloid cell infiltration is implicated in vascular remodelling and extravasation (Harney *et al.*, 2015; Wenes *et al.*, 2016), an antigen-presenting cell population was identified by Mac2 (Galectin-3) staining (Tan and Krasnow, 2016), in paraffin-embedded tissue of lungs from mice exposed to different treatments (Fig. 2-6A). Mac2-positive cells represent a heterogeneous group of myeloid cells that can perform multiple functions. Their density appeared higher in acutely hypoxic lungs and was maintained in lungs exposed to chronic hypoxia (Fig. 2-6B, left). Association of Mac2-positive cells (green) with the endothelium (red), known to be a key parameter in tumour cell transendothelial migration (Laoui *et al.*, 2014; Harney *et al.*, 2015; Lewis *et al.*, 2016), was also equivalent between acute and chronic hypoxia, although in both cases it was higher than in animals maintained in normoxic room air (Fig. 2-6B, right). Finally, whole lung mRNA levels of intercellular adhesion molecule 1 (ICAM1), involved in mediating endothelium-macrophage adhesion (Lorenzo *et al.*, 2011; Liu *et al.*, 2015), were also higher in both hypoxia treatments relative to levels seen in lungs from control animals (Fig. 2-6C). These data suggest an overall increase

in myeloid cell infiltration in hypoxic lungs, irrespective of length of hypoxia exposure, which does not correlate with the different metastatic burden seen in each condition.

This result was validated by flow cytometry, where myeloid cells (CD45+CD11b+) were gated directly from the viable cell population, after hypoxia pre-treatment (Fig. 2-6D, top row), and a similar result was obtained, showing an increased rate of myeloid cell infiltration in response to both acute and chronic hypoxia. Intriguingly, when lungs were harvested 24 h after tumour cell injection, there was a striking increase in CD45+CD11b+ cells in the lungs of mice pre-exposed to acute hypoxia (Fig. 2-6D, bottom row). This suggests the presence of a recruitment signal stimulated by acute hypoxia, which is activated or increased in the presence of a second insult, in this case tumour cells.

CCL2 is a known mediator of EC interaction with macrophages, and essential for metastatic success in breast cancer (Qian *et al.*, 2011; Kitamura, Qian, Soong, *et al.*, 2015; Lewis *et al.*, 2016; Sun *et al.*, 2017), and therefore the next step was to investigate whether this was the signal promoting the increase in general myeloid cell population (CD45+CD11+ cells) in that group of animals. CCL2 mRNA levels were dramatically elevated in lungs of animals exposed to acute hypoxia, but not prolonged hypoxia (Fig. 2-6E); this increased expression coincided with the transient increase in myeloid cell retention seen in Fig. 2-6D (bottom panel). CCL2 levels were increased in primary lung EC-conditioned medium (Fig. 2-6F), as were levels of mCSF1 (also a mediator of EC-myeloid cell communication). Levels of EC-secreted CCL2 were further verified by ELISA in the same conditioned media samples (Fig. 2-6G). These results suggest that CCL2, produced by EC after acute hypoxia, potentiates lung vulnerability to CTC by remodelling the pulmonary tissue microenvironment.

To confirm this, the infiltration of CCR2+ macrophages into the lung by flow cytometry was assessed; they were seen to increase only in animals exposed to acute hypoxia (Fig. 2-6H). These data show that the myeloid cells identified as Mac2+ (Fig. 2-6A) or CD45+CD11b+ (Fig. 2-6D), represent a heterogeneous myeloid cell population, and that EC-derived CCL2 (a HIF-1α transcriptional target (Wacker *et al.*, 2012; Li *et al.*, 2016)) selects for the arrest of pro-metastatic CCR2+ myeloid cells (Kitamura, Qian, Soong, *et al.*, 2015) in the lung during acute hypoxia. Mice were given tumour cell injections while still in the hypoxic chamber but were returned to room air for either 24 h (to evaluate changes during early extravasation events) or 14 d (to assess overt metastasis). They were returned to normoxia to circumvent the effect that continuous hypoxia would have in the movement of tumour cells themselves, or in tumour progression. This allowed observations to be attributed only to the effect of the pre-existing hypoxic microenvironment. In either acute or prolonged hypoxia, the removal of the animals

from the chamber post-tumour cell injection resulted in a period of reoxygenation, which likely affected the vasculature. Nevertheless, and irrespective of the oxidative consequences derived from the experimental approach, lungs of mice exposed to prolonged hypoxia did not show selective retainment of CD45+CD11+ cells.

2.2.5 EC viability and pulmonary vascular permeability are mediated by HIF

EC viability in hypoxia is compromised relative to viability at normoxia, but Cre-mediated deletion of HIF-1α appeared to protect cells from hypoxia-induced death, especially in the acute phase (4 h at 1% O_2), as seen in Fig. 2-3F. As previously shown (Branco-Price *et al.*, 2012), cells lacking HIF-1α failed to accumulate iNOS mRNA after 4 h in hypoxia (Fig. 2-7A), although this is not seen after 24 h, suggesting an alternative and HIF-1α-independent iNOS activation. An analogous trend, albeit less marked, was seen for BNIP3 transcript in HIF-1αCre+ cells. iNOS and BNIP3 are known HIF-1α transcriptional targets (Keith *et al.*, 2011), and interestingly, both were increased in cells lacking HIF-2α after acute, but not prolonged, hypoxia.

BNIP3 drives a unique pro-apoptotic pathway, which bypasses the canonical leakage of mitochondrial cytochrome c45, and has been proposed to be activated downstream of NO (Zamora *et al.*, 2001; An *et al.*, 2006). To better understand how hypoxia/HIF-1α-induced NO accumulation might affect apoptosis, EC were harvested from animals with a conditionally targeted NOS2 (iNOS) gene (Cowburn *et al.*, 2017), which was subsequently excised *ex vivo* by Cre-mediated recombination. The resulting NOS2-null EC had impaired BNIP3 accumulation in acute, but not chronic hypoxia (Fig. 2-7A). Furthermore, iNOS protein levels were lower in animals lacking pulmonary EC HIF-1α (Park *et al.*, 2008; Cowburn *et al.*, 2016), and highest in animals lacking lung endothelial HIF-2α (Fig. 2-7B).

To assess endothelial integrity, EC monolayers of different genotypes were cultured on Fluoroblock inserts, assembled in a Boyden chamber-like setting. A FITC-labelled dextran solution was loaded in the upper chamber, and the fluorescence in the lower chamber, representing the amount of dextran able to cross the endothelial barrier, was quantified in real time using an Omega plate reader (BMG Labtech). HIF-1α null endothelium (blue) was significantly less permeable than control cells (Cre− double-floxed, black), whereas HIF-2α null (orange) monolayers exhibited much higher permeability (Fig. 2-7C), suggesting HIF-mediated intercellular junction stability. The values reflect the different arbitrary fluorescent unit ranges within each plate relative to WT controls.

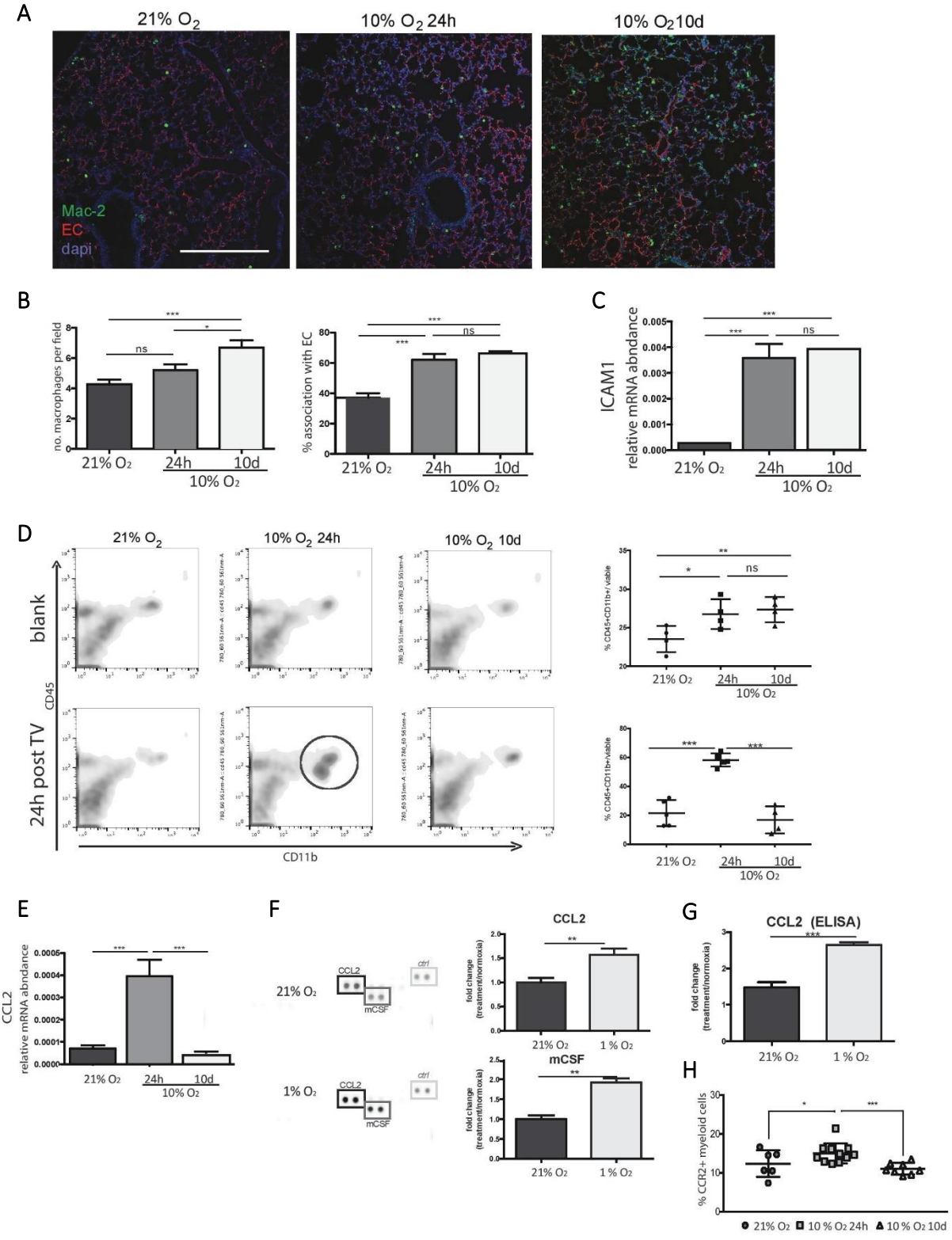
A
21% O2
10% O2 24h
10% O2 10d
Mac-2
EC
dapi
B
no. macrophages per field
% association with EC
21% O2
24h
10d
10% O2
C
ICAM1
relative mRNA abndance
D
blank
24h post TV
CD45
CD11b
% CD45+CD11b+/ viable
E
CCL2
relative mRNA abndance
F
CCL2
mCSF
ctrl
1% O2
fold change (treatment/normoxia)
G
CCL2 (ELISA)
H
% CCR2+ myeloid cells
21% O2
10 % O2 24h
10 % O2 10d

Figure 2-6

Figure 2-6: Inflammatory landscape during hypoxia exposure is distinct after short and long treatments and correlates with metastatic pre-disposition

(A) Representative IF images from paraffin-embedded lung sections probed for vasculature (Podocalyxin) and myeloid cells (Mac-2); scale bar = 100 μm

(B) left, no. of Mac-2^+ cells per field; right, % Mac-2^+ cells associated with EC; Shown Avg ± SD, n ≥ 4 mice per treatment, 10 sections/animal

(C) relative mRNA levels for intercellular adhesion molecule (ICAM1) in whole lung tissue (same animals as in A and B), shown Avg ± SD

(D) Representative flow cytometry scatter plots of $CD45^+CD11b^+$ cells from samples obtained immediately after each treatment (blank, no tumour cell injection, top panel) or 24 h post tail vein injection of tumour cells (bottom panel). Animals are transferred to normal room air after tumour cell injection to avoid hypoxia effect on tumour cell motility; quantification is shown on the right, n ≥ 4 mice per group;

(E) CCL2 mRNA levels in whole lung; Avg. ± SD, n ≥ 4;

(F) Cytokine array of normoxic and hypoxic primary lung EC-conditioned medium; representative blots showing CCL2 and mCSF signal (left), quantification by densitometry, normalized to internal array controls (light grey box) on the right; Avg. ± SD, n = 3

(G) ELISA of CCL2 in conditioned media (same as in F)

(H) %$CCR2^+$ cells in myeloid population obtained by FACS of whole lung tissue after each treatment, Avg. SEM, n ≥ 6. Significance in all cases was assessed by students *t*-test with Welch's correction, and $*p < 0.05$, $**p < 0.005$, $***p < 0.001$.

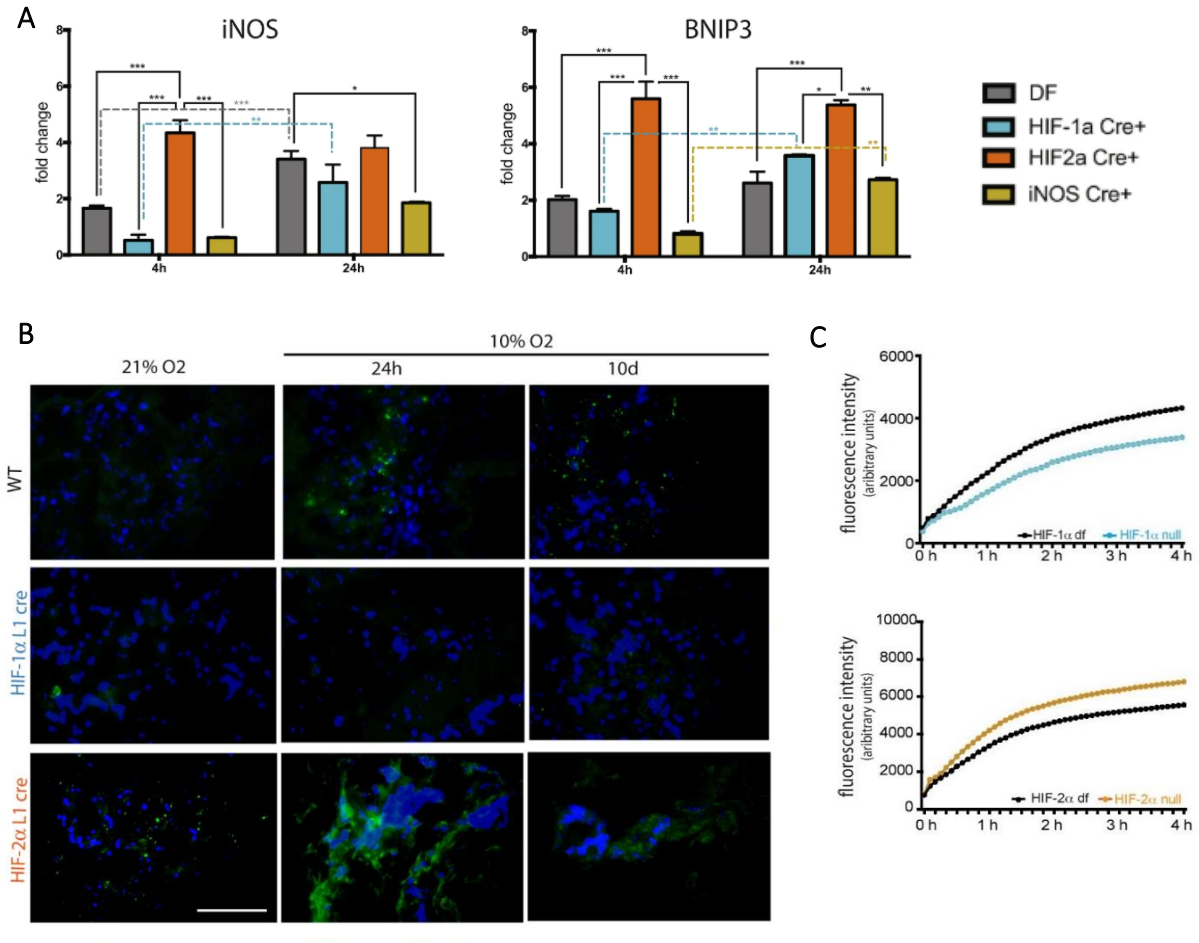

Figure 2-7: Hypoxia effects on iNOS and BNIP3 expression is HIF-α dependent.
(A) qPCR of iNOS and BNIP3 in primary lung EC exposed to hypoxia; samples include double-floxed controls, HIF-1α Cre+, HIF-2α Cre+ and iNOS Cre+ (infected *ex vivo*), and data represents average fold change ± SEM, from combined results from two independent experiments, 3 replicates each; statistical significance was assessed by two-way ANOVA with Holm-Sidak's multiple comparisons test;
(B) Qualitative assessment of iNOS signal in frozen lung sections from mice from different genotypes after different time-points; scale bar = 100 μm;
(C) EC permeability was measured in vitro using freshly prepared FITC dextran (70 kDa)-containing media over primary lung EC monolayers cultured in fluoroblock inserts. Each monolayer of HIF-1α null (Cre+) or HIF-2α null (Cre+) was assessed with their respective WT controls (double-floxed, Cre−). Measurements are arbitrary fluorescence units that represent the amount of FITC dextran (70 kDa) that crossed the EC monolayer over time. Three biological replicates were

2.2.6 Hypoxia-driven predisposition for metastasis is mediated by endothelial HIF

Animals carrying deletion of lung EC HIF-1α or HIF-2α were used to investigate *in vivo* hypoxia-induced metastasis. HIF-1αL1 and HIF-2αL1 animals, generated with specific Cre recombinase expression in the pulmonary endothelium (Park *et al.*, 2008), and Cre− controls were exposed to hypoxia treatments prior to tumour cell injections, as before. Metastatic burden was again assessed 14 days post intravenous injection of tumour cells.

In normoxic conditions, deletion of HIF-1α (blue) resulted in fewer lung tumours, whereas deletion of HIF-2α (orange) lead to increased tumour burden (Fig. 2-8A, left). Acute hypoxia exposure did not cause increased lung tumour frequency in the HIF-1αL1 mice (blue symbols in left and middle panels), whereas control mice (black symbols) showed more tumours when subjected to this same treatment (Fig. 2-1D). The difference in metastatic burden between WT and HIF-1α pulmonary EC deletion mice pre-exposed to acute hypoxia was thus significantly exacerbated. Interestingly, acute hypoxia did not further increase metastasis in HIF-2α pulmonary EC deletion animals compared to normoxic controls (orange symbols, left and middle panels), and as such there was no significant difference in tumour burden between those and WT controls. However, HIF-2αL1 animals pre-exposed to chronic hypoxia showed more lung tumours when compared to the other genotypes in the same pre-treatment, and at this time-point there was no difference between the metastatic burden found in HIF-1αL1 and WT.

All genotypes had more TUNEL+ cells after acute hypoxia, and in all cases these decreased after chronic hypoxia exposure. Additionally, HIF-2αL1 mice had consistently higher percentages of TUNEL+ cells (Fig. 2-8B) than the other genotypes, consistent with viability the patterns seen in cultured EC (Fig. 2-3F). However, unlike what was seen in isolated EC, HIF-1αL1 lungs appeared to have slightly higher rates of EC cell death than WT (Fig. 2-8B).

Co-localization of TUNEL and Podocalyxin signals is shown in Table 2-1. This table summarises the proportion of EC found within the total TUNEL+ cells, not the absolute number of TUNEL+EC. In the group treated for acute hypoxia (24 h), HIF-1αL1 lungs had an average 15.5% TUNEL+ EC; this was considerably, albeit not significantly lower than the rates of EC cell death seen in wild-type animals (27.9%, $p=0.08$). HIF2α-L1 animals after the same treatment showed a much higher rate of EC cell death, with an average 49.4% of TUNEL+ EC co-staining ($p<0.0001$). This discrepancy was not seen in either of the other treatments (all $p>0.75$), corroborating a HIF-1α-driven cell death that occurs only during an acute response to hypoxia. HIF-2αL1 mice had constitutively higher TUNEL+ EC than other genotypes under

all conditions, and thus the slightly lower proportion of dead EC in the 10d hypoxia group in fact represents overall more TUNEL+ EC, because there is higher TUNEL signal overall (approximately 2-fold higher than seen HIF-1αL1 animals, Fig. 5B).

Table 2-1: Average co-localization of TUNEL and Podocalyxin signal in frozen lung tissue following hypoxia pre-conditioning (n ≥10). Statistical significance as referred to in the text was calculated using two-way ANOVA with Holm-Sidak's multiple comparisons test.

Treatment	WT		HIF-1αL1		HIF-2αL1	
	Avg co-localization	*SEM*	Avg co-localization	*SEM*	Avg co-localization	*SEM*
21% O_2	0.311	*0.031*	0.367	*0.072*	0.378	*0.093*
10% O_2 24 h	0.279	*0.042*	0.155	*0.031*	0.494	*0.044*
10% O_2 10 d	0.388	*0.037*	0.446	*0.054*	0.409	*0.072*

Figure 2-8: Physiological pre-disposition for metastatic colonization is dependent on lung endothelium HIF-α in isoform- and time-dependent manner.
(A) Lung tumours per mouse were counted in H&E-stained, evenly spaced lung sections of WT animals (combined double-flox littermates, Cre^-, black symbols), and animals lacking lung endothelium HIF-1α (L1 Cre^+, blue symbols) or HIF-2α (L1 Cre^+, orange symbols); n ≥ 5 animals per group, 10 paraffin- embedded sections per mouse, lungs harvested 14 days post tumour cell injection
(B) TUNEL staining of frozen sections of WT, HIF-1α L1Cre or HIF-2α L1Cre lung tissue after each hypoxia treatment (no tumour cell injection), right panel shows mean ± SEM for each genotype over time; Scale bar = 50 μm
(C) Representative plots of interstitial macrophage population quantified by flow cytometry (after selective subtraction of non-macrophage $CD45^+$ cells) in all genotypes, after each hypoxia treatment; average percent macrophages shown on the right (Avg ± SEM, n ≥ 5).
(D) Relative proportion of $CCR2^+$ macrophages in pre-conditioned lungs, obtained by flow cytometry sorting of total lung tissue from mice exposed to different hypoxia challenges and normoxic controls; WT animals (combined double-flox littermates, Cre^-, black symbols), and animals lacking lung endothelium HIF-1α ($L1Cre^+$, blue symbols) or HIF-2α ($L1Cre^+$, orange symbols) were used; n ≥ 5; average SEM are shown
Statistical significance was assessed by student's *t*-tests, *p < 0.05, ***p < 0.001.

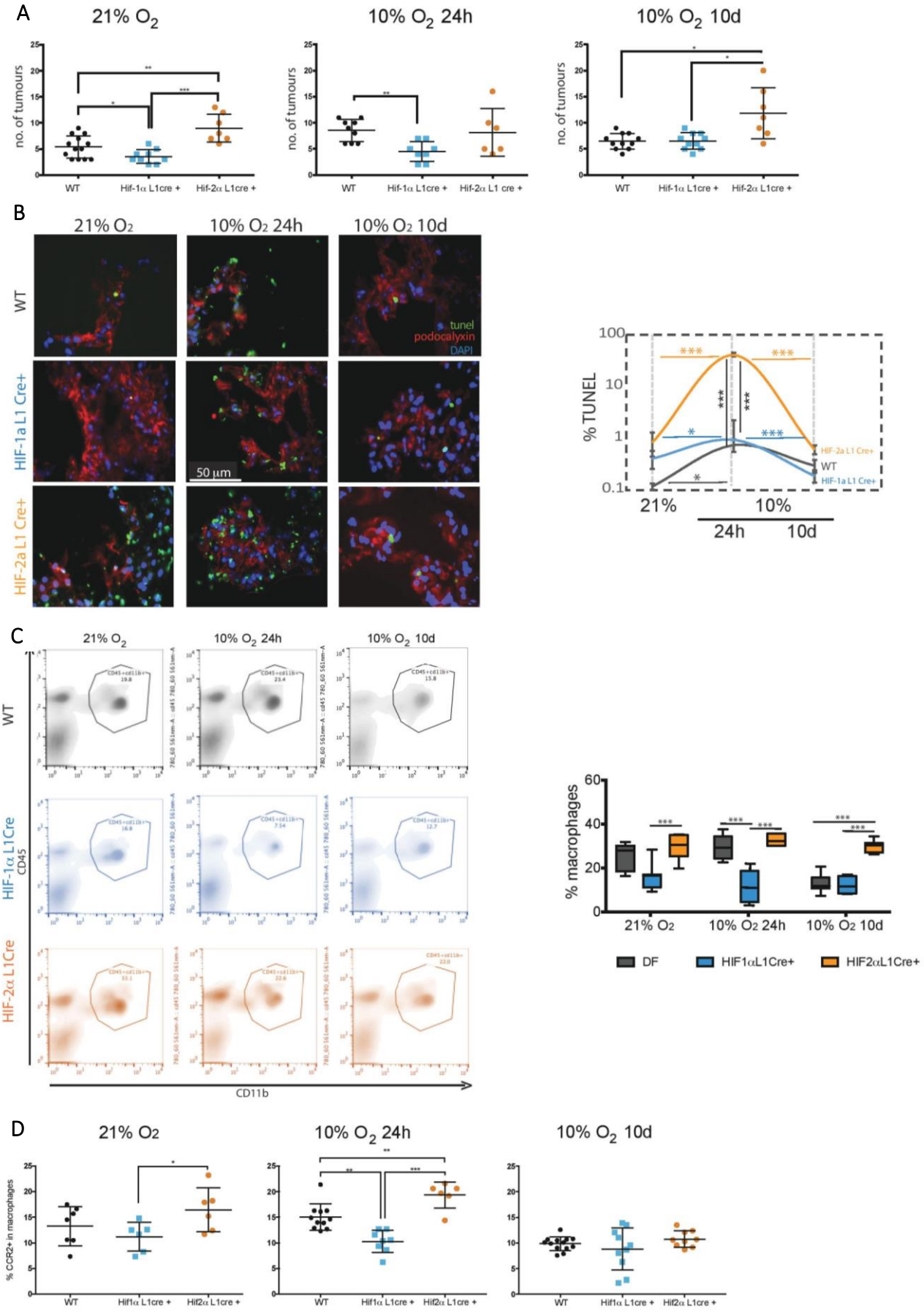
A
21% O2
10% O2 24h
10% O2 10d
no. of tumours
WT
Hif-1α L1cre +
Hif-2α L1cre +
B
21% O2
10% O2 24h
10% O2 10d
WT
HIF-1a L1 Cre+
HIF-2a L1 Cre+
tunel
podocalyxin
DAPI
50 µm
% TUNEL
21%
10%
24h
10d
C
21% O2
10% O2 24h
10% O2 10d
HIF-1α L1Cre
HIF-2α L1Cre
CD45
CD11b
% macrophages
DF
HIF1αL1Cre+
HIF2αL1Cre+
D
21% O2
10% O2 24h
10% O2 10d
% CCR2+ in macrophages
Hif1α L1cre +
Hif2α L1cre +

Figure 2-8

2.2.7 Endothelial response to hypoxia affects the lung inflammatory milieu

Numerous studies have reported the role of macrophages in tumour cell extravasation (Hamm *et al.*, 2013; Harney *et al.*, 2015; Kitamura and Pollard, 2015; Qian *et al.*, 2015), as well as in vascular remodelling (Hamm *et al.*, 2013). Thus, it was essential to understand if the rates of inflammation in response to acute and chronic hypoxia in mutant lungs were different from those seen in WT controls; this was analysed by observing the CD45+CD11b+ cell population. Unlike in Fig. 2-6D, the gate was applied after selective subtraction of other cells from the myeloid lineage (CD45+) to more accurately quantify macrophage infiltration (Rose *et al.*, 2012).

In WT animals, a higher number of macrophages was found in lungs after 24 h of hypoxia (Fig. 2-8C, grey panels), correlating with increased metastatic incidence (Fig. 2-1D). HIF-1αL1 mice (blue) showed a constitutively lower proportion of these cells, whereas HIF-2αL1 (orange) have consistently higher numbers of lung macrophages: HIF-2αL1 animals exhibit constitutive inflammation. The proportion of CCR2+ cells within this macrophage population is lower in HIF-1αL1 mice exposed to acute hypoxia (24 h) (Fig. 2-8D), in correlation with the lower level of metastatic events observed in this genotype (Fig. 2-8A). Following chronic hypoxia, there are no differences in the levels of CCR2+ macrophages between genotypes, consistent with CCL2 induction forming part of an acute and HIF-1α-mediated response.

2.3 Discussion

Exposure to hypoxia involves adaptive responses that evolve over time. The remodelling processes that occur in lungs when exposed to transient or persistent changes in oxygen availability cause changes in immediate and long-term organ physiology and adaptive strategies to subsequent stimuli (Cowburn *et al.*, 2016). These rely initially on a shift to glycolytic metabolism (Kim *et al.*, 2006; Barteczek *et al.*, 2017), which is mediated by HIF-1α. HIF-1α also regulates cell fate via transcriptional activation of apoptotic mediators including BNIP3 and p53 (Greijer and Van Der Wall, 2004). Here, the transient increase of HIF-1α seen in whole lung tissue following acute hypoxia correlated with increased tumour numbers, as well as transient increases in pulmonary microvessel permeability and iNOS expression (Fig. 2-8 and Fig. 2-3B–E). Deletion of HIF-1α resulted in decreased iNOS and BNIP3 transcript levels in cultured EC, less paracellular permeability (Fig. 2-7), and fewer apoptotic EC in lungs after exposure to acute hypoxia (Fig. 2-8B combined with Table 2-1). Even though HIF activation occurred in multiple cell types within the lung, the experiments performed using conditional deletion of HIF in pulmonary endothelium indicated a substantial role of these transcription factors specifically in the microvasculature, in the metastatic process.

Lungs lacking endothelial HIF-2α, on the other hand, showed more TUNEL+ EC, and higher iNOS and BNIP3 mRNA expression (Fig. 2-7A), in line with previous reports of NO-potentiation of BNIP3 signalling (An *et al.*, 2006). HIF-2α is an essential regulator of endothelial barrier function, as shown in brain microvascular EC exposed to chronic hypoxia (Mata-Greenwood *et al.*, 2017). Deletion of endothelial HIF-2α has also been shown to prevent recovery from kidney injury and inflammation (Kapitsinou *et al.*, 2014; Gong *et al.*, 2015), and has been proposed to be a transcriptional co-activator of VE-cadherin in a hypoxia-independent fashion (Le Bras *et al.*, 2007). EC are especially vulnerable to anoikis when compared to other cell types (Gilmore, 2005), and the increased cell death seen in cultured pulmonary HIF-2α null EC is likely a result of deficient EC-EC cell adhesion; this hypothesis is supported by the higher paracellular permeability seen in these monolayers (Fig. 4C). iNOS accumulation and subsequent NO production are critical factors in mediating endothelial permeability and cell death, which can, to a large extent, explain the increased metastatic burden in conditions where HIF-1α activity is highest: HIF-1αL1 animals had lower levels of iNOS, as expected (Keith *et al.*, 2011) , whereas the opposite was seen in those lacking lung endothelium HIF-2α (HIF-2αL1). This trend was most pronounced at earlier hypoxia time-points.

Fig. 2-9 shows a model to incorporate the findings of this chapter with previously reported data: differential proportion of HIF isoforms in lung endothelium were seen depending on the oxygen levels and duration of hypoxia. The increased permeability of lung endothelium, seen after acute hypoxia, resulted from an increase in HIF-1α-mediated cell death; WT lungs recovered after prolonged hypoxia exposure, likely via incremental activation of HIF-2α, but in the absence of this isoform endothelial integrity was compromised and appeared unable to recover. This suggests that EC viability (Li *et al.*, 1999; Wahl *et al.*, 2002) was compromised in HIF-2αL1 lungs as a result of deficient monolayer stability (possibly disruption of adherens junctions (Le Bras *et al.*, 2007; Gong *et al.*, 2015)) and increased anoikis (Lee *et al.*, 2009). Consequently, the interrupted microvessel barrier facilitated extravasation events and lead to the higher metastatic burden seen in the absence of endothelial HIF-2α. This hypothesis could be validated through a series of further experiments, analysing the levels and localisation of VE-Cadherin in WT and mutant EC after acute and prolonged hypoxia. This could include whole-tissue qPCR and western blots, as well as IHC staining of tissue sections and ICC staining of cultured ECs. Assessing VE-Cadherin localisation may be of particular importance since its availability is frequently regulated by internalisation into clathrin-coated vesicles (Gavard, 2014).

Fig. 2-9 also illustrates that increased HIF-1α levels in hypoxic lungs correlated with macrophage infiltration; this has been shown to promote tumour growth and metastasis (Almendros *et al.*, 2013, 2014). The results presented here suggest that prolonged exposure to hypoxia allows vascular regeneration, in agreement with previous reports that this is a process dependent on HIF-2α activation (Yu and Hales, 2011; Gong *et al.*, 2015; Cowburn *et al.*, 2016; Zhang *et al.*, 2017). This chapter also shows that the endocrine function of lung EC changed throughout the duration of the hypoxic stimulus, in turn affecting the recruitment and arrest of myeloid cells to the lung (Figs 2-6 and 2-8). Upon exposure to acute hypoxia, there was a striking increase in CCL2, likely downstream of HIF-1α activation (Wacker *et al.*, 2012; Li *et al.*, 2016), and an effective recruitment and arrest of CCR2+ macrophages from an already exacerbated myeloid cell population (Fig. 2-6). CCR2+ macrophage infiltration was not seen in HIF-1αL1 animals, and was conversely seen at much higher levels in HIF-2αL1 animals only after acute hypoxia; this correlated with highest CCL2 (and HIF-1α) signals (Figs 2-1 and 2-8). Presumably, the recruitment of CCR2+ macrophages, as well as increased EC permeability and cell death both contribute to the rise in cancer metastasis seen after acute hypoxia exposure. To characterise this effect in more detail, an endothelial-specific knockout

of CCL2 could be employed, as this would hamper the ability of EC to recruit CCR2+ macrophages but maintain the effects of HIF on cell-intrinsic effects such as iNOS-induced permeability and cell death.

Multiple factors affect extravasation and tumour cell survival post extravasation, including macrophage assistance during transendothelial migration, matrix remodelling and post-extravasation vascularization of the incipient tumour. This study demonstrates that EC mediate a tissue's predisposition for metastatic colonization, including the selective recruitment of myeloid cells. This effect is seen specifically in changes in endothelial viability, integrity and endocrine function, downstream of activation of specific branches in the HIF pathway. Multiple cells may respond to the HIF-stabilizing stimulus, also in a time-dependent manner (Fig. 2-1C). The observations presented here validate the contribution of the endothelium-derived HIF, both in constitutive and adaptive responses, to the metastatic potential of the lung. Importantly, similarly EC-dependent remodelling phenomena are likely to occur in other pre-metastatic organs (Augustin and Koh, 2017).

The experimental approach in this chapter used hypoxia as a driver for differential HIF-isoform stabilization, and as a model to understand the role of HIF in the pre-metastatic microenvironment. This study does not include the effects of hypoxia in other cell types within the lung, nor the systemic effects of atmospheric hypoxia in cancer progression and dissemination. Additionally, this model does not account for the fact that HIF isoform stabilization is initiated by signals other than hypoxia (Prabhakar and Semenza, 2012; Gras *et al.*, 2016), especially in the context of cancer (Haddad and Harb, 2005) and therapy (Trollmann *et al.*, 2014; Gandhi and Chandna, 2017), and those limitations should be addressed in the future. However, with the use of lung EC-specific deletion of HIF-1α and HIF-2α, the data presented here has demonstrated and substantiated the non-redundancy of these transcription factors in endothelial barrier function, and the relevance of the endothelium in mediating pre-metastatic organ remodelling. The understanding of the molecular events downstream of cell type- and organ-specific HIF-α activation has powerful implications in the ability to pre-empt distant organ vulnerability to metastatic disease, and potentiate the development of improved diagnostic and therapeutic approaches for aggressive cancer types.

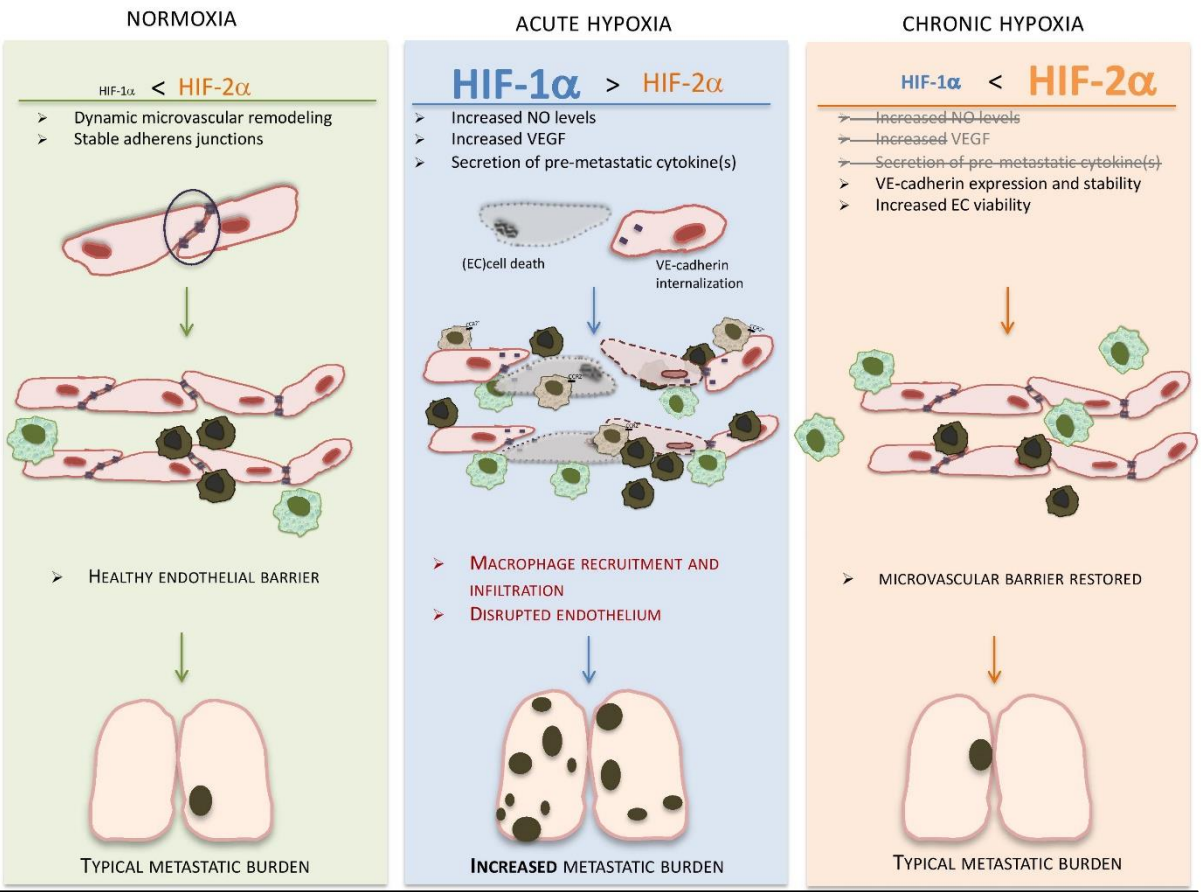

Figure 2-9: Effect of hypoxia in HIF-α isoform activation and endothelial barrier remodeling.

In this model, the findings of this chapter were integrated with previously reported and/or hypothesised processes in EC stability and metastasis. Endothelial HIF-1α levels are negligible in normoxic lung environment (left), whereas HIF-2α is constitutively present; this is essential for vessel stability (Gong *et al.*, 2015), microvascular perfusion (Kapitsinou *et al.*, 2014) and endothelial barrier function (as shown by Branco-Price *et al.*, 2012 and Fig. 2-7). During the initial stages of hypoxia response (middle panel), and as part of the vascular remodelling process (Gras *et al*., 2016; Guo *et al*., 2001), HIF-1α levels increase dramatically in EC, largely surpassing those of HIF-2α, and predictably results in increased NO production (Branco Price *et al*., 2012; Cowburn *et al*, 2016), VEGF levels, apoptotic and endocrine signals (Figs. 2-6 and 2-7), promoting infiltration and retention of inflammatory cells (Figs. 2-6 and 2-8), specifically pro-metastatic $CCR2^{+}$ macrophages (Kitamura *et al.,* 2015; Qian *et al.,* 2011 and Fig. 2-8). The combined effects of acute hypoxia result in compromised endothelial integrity and inflammation, which should facilitate extravasation, and promote metastasis. With prolonged exposure to hypoxia (right panel), levels of HIF-2α increase to higher than those of HIF-1α, reinstating the balance observed in normoxia. Increased levels of HIF-2α should restore adherens junctions (Gong *et al.*, 2015) and monolayer stability, and the absence of HIF-1α results in less cell death and removal of CCL2 recruitment signal. Deletion of endothelial HIF-2α results in compromised integrity and likely the microvasculature's ability to regenerate, leading to increased metastatic incidence (Fig. 2-8).

2.4 Materials and Methods

2.4.1 Animal models

Deletion of HIF-1α or HIF-2α in lung EC was obtained by crossing female animals homozygous for the floxed alleles of HIF-1α (Ryan *et al.*, 1998) or HIF-2α (Gruber *et al.*, 2007) (double-floxed, DF) to HIF-1α df/L1Cre+ or HIF-2α df/L1Cre+ males (Park *et al.*, 2008). Experimental cohorts including L1Cre+ were perfomed using Cre- littermate controls (DF animals with no deletion, physiologically wildtype, as previously shown (Ryan *et al.*, 1998; Gruber *et al.*, 2007)). It was previously shown that L1-driven Cre expression is confined to the pulmonary endothelium (Cowburn *et al.*, 2016). C57Bl/6 WT mice were purchased from the Charles River laboratories (UK).

2.4.2 *In vivo* Hypoxia treatments

Eight-week old male animals were exposed to 10% O_2 for either 24 h (acute exposure, optimised for preferential activation of HIF-1α in lung tissue) or 10 d (chronic exposure, optimised for preferential activation of HIF-2α in lung tissue), in chambers with controlled humidity and CO_2 (Biospherix). Control animals were maintained in normal atmosphere. Tissues were collected immediately after hypoxia exposure and either fast frozen for protein or RNA extraction, processed for flow cytometry or placed in OCT compound (Tissue-Tek, Cat # 4583) for histological analyses. Lung tissue hypoxia upon exposure to 10% O_2 was confirmed by pimonidazole (Hypoxyprobe, HP1-1000 kit), according to manufacturer's instructions; briefly, pimonidazole was administered at 30 mg/Kg in sterile saline via tail vein injection, and allowed to penetrate tissues for 90 min. Animals were sacrificed by cervical dislocation and lung tissue immediately collected into OCT medium for cryosectioning. 20 PM sections were fixed in acetone for 8 min and then stained with MAB1 antibody (included, 1:50 in PBS, at 4^{o}C, O/N) and detected with anti-mouse AF647 conjugated antibody (Abcam, ref. ab150127, 1:100 in PBS, 2 h at RT).

2.4.3 Metastasis Assay

A total of $5x10^5$ LLC cells in 200 µl sterile PBS were injected into tail veins of animals pre-conditioned in hypoxia or normal air controls. Injections were performed inside the hypoxia chamber for the hypoxic pre-conditioned animals, and animals were subsequently placed in room air until tissue collection. Treatments were set-up such that all animals were exactly the same age at the time of injection (hypoxia treatments started at day -10 for chronic treatments and at day -1 for acute treatments; at day 0 all animals received tumour cells from the same culture batch). Animals were transferred to normal air after tumour cell injection.

Lung tissue was collected either 24 h (to monitor immediate responses) or 14 days post-injection (to quantify metastatic take). Lung tissue was collected directly into OCT, immediately processed for flow cytometry, snap frozen in liquid N_2 (for protein and RNA extractions), or perfused with 10 mg/mL heparin in PBS, and fixed in 4% PFA for paraffin embedding and H&E staining. Lung tumors were counted in H&E-stained 10 μm evenly spaced sections across whole lungs (≥ 20 sections per animal). Tumor area was quantified using ImageJ software (Schindelin *et al.*, 2012).

2.4.4 Pulmonary vascular permeability

50 mg/Kg of Evans Blue (Sigma, Cat. # E2129) dye in PBS were injected into the tail vein of each animal, and bronchoalveolar lavage was collected 20 minutes later in 1 mL of PBS. Evans Blue concentration in the lavage, an indication of leaked dye from the lung microvascular network, was quantified against a standard curve by spectrophotometry at 540 nm.

2.4.5 Flow cytometry

Lung tissue was digested for 20 min in Collagenase D (Roche, 500 μg / ml) / DNAse I (Roche, 50 μg/ml) at 37ºC, and neutralized with EDTA. The digested tissue was strained through a 70 μm filter and the filtrate was treated for 2 min with ACK lysing buffer (ThermoFisher). Cells were stained with fluorophore-conjugated antibodies for 20 minutes at 4 ºC, and data was acquired on Fortessa (BD Biosciences). The fluorophore-conjugated antibodies used were: CD11b (eBioscience, M1/70, Alexa Fluor 700), NK-1.1 (Biolegend, PK136, PE), CCR2 (R&D systems, 475301, APC), Ly-6G (Biolegend, 1A8, PerCP/Cy5.5), CD11c (BD Bioscience, HL3, FITC), CD45.2 (Biolegend, 104, PE/Cy7), Ly-6C (BD Bioscience, AL-21,APC-Cy7), CD16/CD32 (BD Bioscience,2.4G2), Zombie Yellow (viability dye, Biolegend). Data analysis and gating was performed on FlowJo. Endothelial cells were identified as CD45- CD31+ gated directly from the viable cell population (Figure 2-4A). Macrophages (Figure 2-6D) were initially identified as CD45+CD11b+ from the viable cell pool, and these markers generally identify perivascular and activated macrophages. A “true macrophage” population (Figure 2-8C) was further identified by sequential subtractive gating of non-macrophage cells: CD45+ viable cell population was gated to exclude NK1.1 and B220 (Natural Killer cells) and subsequently CD11b+CD11c+ cells (Dendritic cells), followed by removal of the neutrophil (Ly6G+) and monocyte populations (Ly6C+), finally isolating a classic “true” macrophage population (modified from Rose et al., 2012).

2.4.6 Immunochemistry/Immunofluorescence

Deparaffinised or frozen-fixed sections were blocked with Universal Protein Blocking Reagent (GeneTex), followed by an incubation with 0.1% Sudan Black (Sun *et al.*, 2011; Jenvey and Stabel, 2017) in 70% Ethanol (10 min, RT) and Mouse-on-Mouse Blocking Reagent (Vector) when appropriate, and according to the supplier's instructions. Primary antibody incubations occurred O/N at 4 ºC (HIF-1α (NB100-105) or HIF2α (NB100-132), Podocalyxin (R&D Systems AF1556), iNOS (NB300-605), VE-cadherin (Novus Biologicals, AF1002)). Secondary antibodies conjugated with either Alexa Fluor 488 (Thermofisher Scientific) or Alexa Fluor 647 (Abcam) were used (1 hour at RT, in the dark). Slides were mounted with ProLong Diamond antifade with DAPI (P36962, ThermoFisher Scientific) and imaged the following day. For primary EC staining, cells were plated and cultured in gelatine-coated glass slides and fixed immediately after hypoxia treatments in cold 4% PFA in PBS, for 20 min at 4 ºC. Fixed cells were permeabilized with 0.4% Triton-X in PBS for 5 min, blocked with Universal Protein Blocking Reagent (as above), and protein targets were detected by overnight, 4 ºC incubations with primary antibodies, and 1 h room temperature incubation with fluoro-conjugated secondary antibodies. Slides were mounted with Vectashield hardset antifade medium with DAPI (Vector, H-1500). Images were collected in a Leica fluorescent microscope and analysed in Image J5

2.4.7 TUNEL Assay Protocol

This was performed using a slightly modified version of manufacturer's instructions (Thermofisher- Click-iT® TUNEL Alexa Fluor® 488 Imaging Assay, #C10245); Slides containing frozen tissue sections were fixed in pre-cooled acetone for 10 minutes; slides with primary endothelial cells were instead fixed with cold 4% PFA for 20 min at 4 ºC. Following washes, all samples were treated with 3% H_2O_2 in MeOH for 10 min, sections were blocked and permeabilized with 0.4% Triton-X in PBS for 5 min, and lung tissue sections were further incubated with Sudan Black B (Sigma, Cat # 199664) for 10 min to reduce autofluorescence. Equilibration with TdT for 10 min at RT preceded a 1 h incubation with TdT reaction cocktail (TdT reaction buffer, EdUTP, TdT*), at 37 ºC in a humidified chamber. Slides were washed with 3% BSA in PBS for 5 min. Signal was generated with Click-iT reaction buffer and additive, according to manufacturer's protocol. Secondary immunostaining, when performed, was done after this step. All slides were mounted in Vectashield anti-fade mounting medium with DAPI (Vector) and imaged the following day.

2.4.8 Microscopy and image analysis

Images were taken with Leica fluorescence microscope using a x20, x40 or x63 (oil immersion) objective. Gain and offset were set to negative controls and used to standardize image acquisition for each experiment (tissue: three images per section, a ≥ 8 randomly chosen sections from each animal; cells: ≥ 4 images per slide chamber, three slides per treatment). Quantification of fluorescence was done using ImageJ. After setting the threshold to a duplicate image, stained areas were identified and selected. "Dark background" was selected for fluorescence. "Analyze-Analyze particles" was used for measurement of various parameters; background values were acquired by selecting three random areas in gray-scale image using the circle tool and "AnalyzeMeasure" function. Quantification in tissue samples was performed as follows

$$\text{Mean cell/background fluorescence} = \frac{\text{Integrated density}}{\text{area}}$$

To correct for uneven fluorescence the following formula was used:

$$\text{Correction factor} = \text{Mean cell fluorescence} - \text{Mean background fluorescence}$$

The number of TUNEL+ cells was identified by DAPI co-staining.

2.4.9 Confocal Imaging and co-localization:

Images were acquired in a Leica SP5 confocal microscope using x20, x40 or x63 (Oil Immersion) objective. Images were acquired through LAS (Leica) and analysed using ImageJ. Pearson's correlation was calculated to assess co-localization through the Coloc 2 plugin.

2.4.10 qPCR:

For quantification of steady-state mRNA levels, total RNA was extracted from fast-frozen lung tissue or cells, using RNeasy columns (QIAGEN) with DNaseI in-column treatment (QIAGEN). cDNA was synthesized using Superscript III (Invitrogen) according to the manufacturer's instructions. Relative abundance of transcripts of interest was assessed by quantitative real-time PCR and normalised to β-ACTIN transcript levels. Primer pair and primer/probe sets are listed in Table 2-2. Data are presented as average fold-change (ratio) ± SD (or SEM, as stated in each figure), between each sample and the respective control.

Table 2-2: Primer sequences used in qPCR, SYBR Green was used as a probe

b-ACTIN	FWD	AGGCCCAGAGCAAGAGAGG
	REV	TACATGGCTGGGGTGTTGAA
	Probe	SYBR Green
iNOS	FWD	TaqMan Gene Expression Assay Mm00440488_m1 (Applied Biosystems)
	REV	
	Probe	
BNIP3	FWD	GACGAAGTAGCTCCAAGAGTTCTCA
	REV	CTATTTCAGCTCTGTTGGTATCTTGTG
	Probe	SYBR Green
VEGF	FWD	ATCCGCATGATCTGCATGG
	REV	AGTCCCATGAAGTGATCAAGTTCA
	Probe	[6~FAM]-TGCCCACGTCAGAGAGCAACATCAC-[BHQ1a-Q]
ARG2	FWD	AACACGGCAGTGGCTTTAACC
	REV	GGTTTTCATGTGGCGCATTC
	Probe	SYBR Green
VE-Cadherin	FWD	Qiagen (Cat. No. QT000110467)
	REV	
	Probe	

2.4.11 Cell culture and hypoxia treatments:

Primary EC were isolated and cultured from lungs of HIF-1αdf, HIF-2αdf, or iNOSdf male animals between 6 and 8 weeks of age as described previously (Branco-Price *et al.*, 2012) with slight modifications. The lungs of 4-6 mice were excised and stored in DMEM on ice. The tissue was minced and digested for 90 min at 37 ˚C with collagenase A (Roche) in HBSS supplemented with 2 mM $CaCl_2$, 2 mM $MgSO_4$, and 20 mM HEPES. The digested tissue was then filtered through a 70 µM nylon mesh, in order to retain large vessel fragments, and washed once in HBSS. The resulting pellet was resuspended in PBS containing 0.1% BSA and incubated with dynabeads coated with sheep anti-rat IgG (Invitrogen) bound to rat anti-mouse CD31 antibody (553370, BD Pharmingen) for 90 min at 4 ˚C. The beads were washed three times with 0.1% BSA in PBS, resuspended in MVEC growth medium and plated onto cell culture plates. Cre recombinase-mediated gene deletion was performed *ex vivo* by overnight incubation with Cre Recombinase Gesicles (Clontech, cat. No. 631449), or with Adenovirus Cre, in which case control double-floxed cells were infected with E-galactosidase expressing

Adenovirus; Cells were allowed to recover for 24 h post-gene deletion before experiments were performed. Hypoxia (1% O_2) treatments were performed in cultures no later than Passage 3.

2.4.12 *Ex vivo* endothelial monolayer permeability:

Primary cells were plated onto Fluroblok 8Pm inserts (light-blocking PET, Corning), placed in 24-well companion plates (Falcon, Cat # 353504), in Boyden chamber-like set up. Cells were maintained with 200 PL media on the upper compartment. When confluent, the basal media inside the insert was replaced by 150 PL media containing 1mg/mL FITC Dextran 70 KDa, and 250 PL FITC Dextran-free media was placed in the lower chamber, all pre-equilibrated at 1% O_2. Plates with inserts were placed inside plate reader at 1% O_2, and fluorescence was measured in the lower compartment, as an indication of FITC leaked through the endothelial monolayer to the lower chamber. Readings were taken every 5 minutes for 4 hours.

2.4.13 Western blotting:

Equal amounts of protein (15 μg) were obtained from either cells or whole lung tissue lysed in RIPA buffer, resolved in 3–8% acrylamide Tris-Acetate gels (Life Sciences, EA0375BOX) and transferred to a PVDF membrane using the BioRad Transblot Turbo Transfer System. Primary antibodies were used at 1:1,000 (iNOS, sc-651; HIF-1α, NB-100-149) or 1:500 dilutions (HIF-2α, R&D AF2997). Membranes were cut at 75 kDa band and targets were probed on the upper half of the membrane, whereas β-actin (Sigma, A1978, running at ~50 kDa), used as normalization control, was probed on the bottom half of the membrane. Membranes were not re-probed for multiple antibodies. Protein signals were detected following secondary incubation with HRP-conjugated antibodies for 1 h at room temperature, and ECL Plus chemiluminescence detection kit (Amersham, Cat. # RPN2232), according to manufacturer's protocol. Image capture and quantification were performed using FusionFX (Vilber), using default exposure for optimal signal detection.

Acknowledgement

This chapter is the result of collaborative work and was published (Reiterer *et al.*, 2019). The manuscript was written, revised, and edited by Cristina Branco and me. I assisted with animal work, purified and maintained primary EC cultures, and measured RNA and protein expression; Cristina Branco performed animal experiments, tissue processing and staining, immunofluorescence assays, and ELISA; Renato Colaço performed the flow cytometry; Pardis Emrouznejad performed immunofluorescence, microscopy and image analyses.

Chapter 3: Comparing the hypoxia response in brain and lung microvascular endothelial cells

3.1 Introduction

Having investigated the role of the HIF pathway in cancer metastasis to the lung, it was relevant to diversify our focus to another metastatic site, especially considering the unique nature of the lung microvasculature. The most prevalent targets of breast cancer are bone (51%), lung (17%), brain (16%), and liver (6%) (Patanaphan *et al.*, 1988). The microvasculature of the liver and bone is sinusoidal and thus characterised by large, irregular gaps and a discontinuous or entirely absent basal lamina (Braet and Wisse, 2002; Ramasamy, 2017). Consequently, transcellular permeability in these vascular beds is high by design, and less limited by endothelial cell adhesion. Any role of the endothelium in the establishment of a metastatic site is therefore likely very different form the effects observed in the lung in the previous chapter. Indeed, it has already been established that inhibition of endothelial Notch signalling promotes melanoma metastasis to the liver but inhibits metastasis to the lung (Banerjee *et al.*, 2015; Wieland *et al.*, 2017; Wohlfeil *et al.*, 2019).

Lung and brain microvasculature on the other hand are both continuous; individual ECs are attached by junction proteins to form a tight mesh with no major gaps, supported by a complete basement membrane. In fact, the brain microvasculature is even more close-fitting than the one found in the lung, as it forms part of the blood-brain-barrier (BBB), a highly restrictive assembly of multiple cell types, tasked with controlling nutrient supply to the central nervous system (CNS) and protecting it from toxins and pathogens (Daneman and Prat, 2015). The integrity of brain and lung microvasculature is mainly mediated by two different types endothelial junctions: the vasculature of the BBB relies mostly on tight junctions, which, as their name suggests, closely link neighbouring ECs to each other, minimising paracellular permeability (Nitta *et al.*, 2003); lung microvasculature on the other hand is maintained predominantly by adherens junctions (Corada *et al.*, 1999). Furthermore, brain microvascular endothelial cells (MVECs) express lower levels of leukocyte adhesion molecules, which results in reduced immunosurveillance within the CNS (Dos Santos *et al.*, 1996). Therefore, brain and lung microvasculatures are relatively similar in their overall structure, yet highly specialised for their individual roles. Thus, they presented an appealing target for a comparative study.

The aim of this chapter is to compare and contrast the hypoxia response pathways in these two endothelial cell types in isolation, by using primary murine MVECs. Previous research on HIF-signalling in brain MVECs has shown that stabilisation of HIF-1α increases paracellular permeability by disrupting tight junctions (Schoch, 2002; Yan *et al.*, 2012; Engelhardt *et al.*, 2014), similar to its role in lung MVEC described in the previous chapter. HIF-1α was also described as a necessary factor for glucose uptake into brain MVECs as well as the brain as a whole (Huang *et al.*, 2012; Varela *et al.*, 2017). The role of HIF-2α in brain MVECs has not been investigated, although it has been established that it is stabilised within brain capillaries upon CO-induced hypoxia (Wiesener *et al.*, 2003). Furthermore, endothelial-specific HIF-2α knockout mice showed increased chronic vascular permeability in organs with continuous endothelium (lung and adipose tissue) but not in the kidney (fenestrated endothelium) or the liver (discontinuous endothelium) (Skuli *et al.*, 2009), and while the effects on the brain were not assessed in that study, the authors pointed to it as a subject for further investigation.

3.2 Results

3.2.1 Development of a protocol for the simultaneous isolation of brain and lung microvascular endothelial cells

In order to compare the hypoxia response of primary lung microvascular endothelial cells to those of the brain, it was necessary to develop a protocol that would enable the simultaneous isolation of endothelial cells from both tissues efficiently from the same animal donors. To achieve this, several published protocols for the isolation of brain MVECs (Coisne *et al.*, 2005; Watson *et al.*, 2013a; Ruck *et al.*, 2014; Welser-Alves *et al.*, 2014) were combined and modified, such that the final optimised procedure would able to fit within the gaps of the previously established protocol for obtaining lung MVECs (Branco-Price *et al.*, 2012); the resulting workflow is displayed in Fig. 3-1A and described in detail under Materials and Methods. The main purification steps are a density centrifugation in 20% BSA to remove the myelin, and treatment with the protein synthesis inhibitor puromycin. Brain MVECs express drug efflux transporters to pump potentially harmful substances out of the CNS into the bloodstream, which grant them resistance to puromycin, making this treatment an effective selection step (Cordon-Cardo *et al.*, 1989; Thiebaut *et al.*, 1989). The thus obtained brain and

lung MVECs formed densely packed, highly pure monolayers, as shown by the staining for the endothelial-specific marker VE-Cadherin (Fig. 3-1B,C).

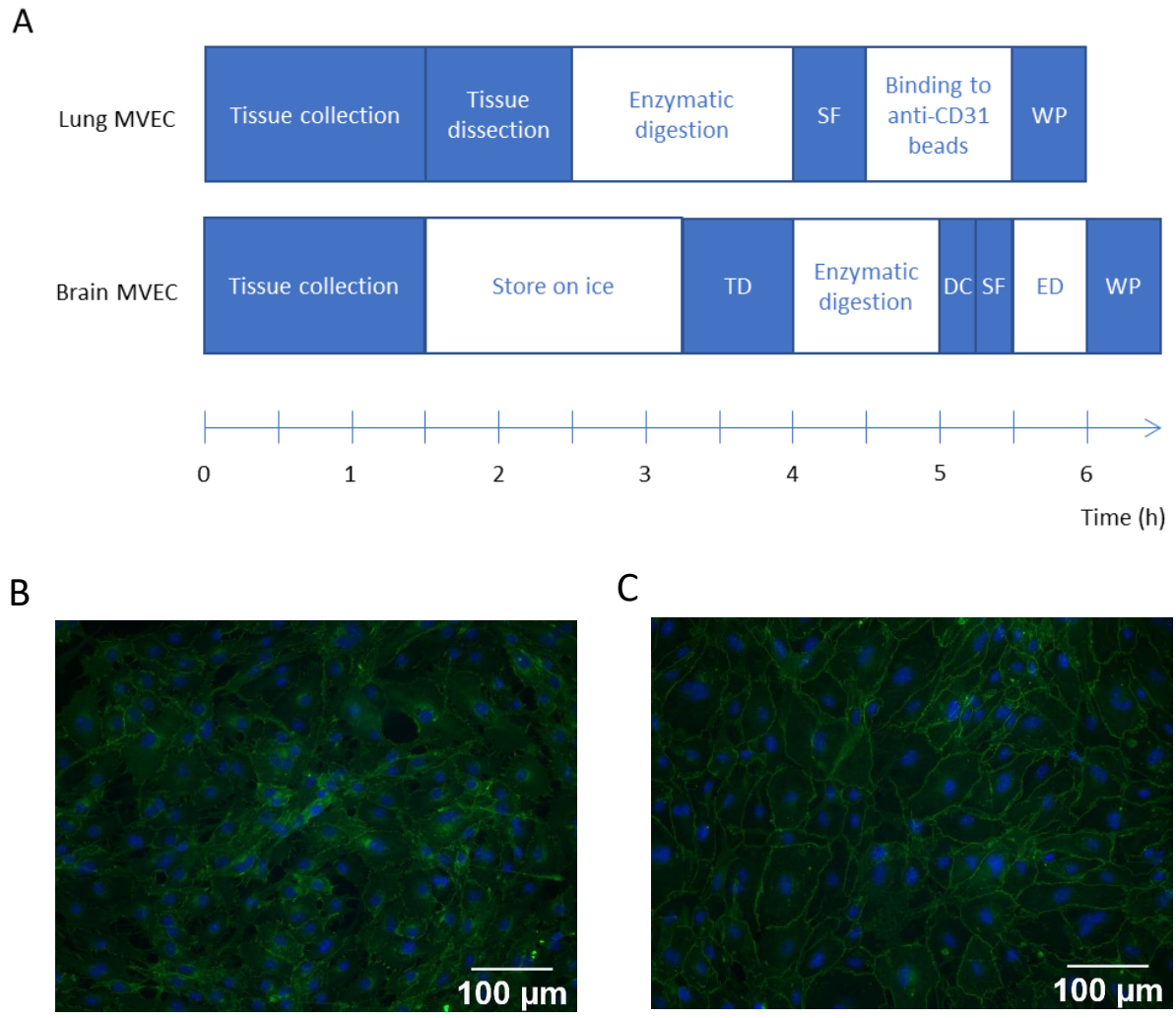

Figure 3-1: Development of a combined protocol for brain and lung MVEC isolation. (A) Schematic of the combined pulldown of brain and lung microvascular endothelial cells. White background indicates incubation steps, blue background indicates steps requiring active involvement. DC: density centrifugation, ED: enzymatic digestion, P: plate, SF: size filtration, TD: tissue dissection, WP: wash and plate.
(B,C) Lung (B) and brain (C) MVECs stained for VE-Cadherin (green) and DAPI (blue) indicating a pure culture

3.2.2 Brain and lung microvascular endothelial cells respond differentially to hypoxic stress

After isolation, both lung and brain MVECs were cultured in standard tissue culture atmosphere (STA; 5% CO_2, no O_2 control) for no more than 3 passages, and subsequently exposed to hypoxia (1% O_2) for up to 48h. The first parameter assessed was cell viability, using propidium iodide staining (Fig. 3-2A). Both MVEC populations lost viability over time, but the effect was visibly faster and more pronounced in brain MVECs. This was validated using a real-time viability assay (Mata-Greenwood *et al.*, 2017), which relies on the reductive potential of live cells to produce a luminescent signal (Fig. 3-2B); in both cell types, the slope of the growth curve decreased consistently over time, but the effect was again more severe in brain MVECs.

In order to characterise the hypoxia response in these two cell types, the stabilisation of the two predominant HIF-isoforms over time after exposure to 1% O_2 was measured. HIF-1α expression displayed the canonical trend of upregulation during acute hypoxia, followed by a decrease at later time points (Uchida *et al.*, 2004; Bartoszewski *et al.*, 2019; Reiterer *et al.*, 2019). Although HIF-1α was detected in both cell populations, lung MVECs accumulated much higher levels of this isoform at all time points (Fig. 3-2C). HIF-2α on the other hand showed more persistent expression that decreased at later time points. Strikingly, the signal intensity of the HIF-α isoforms was reversed between the MVEC populations, with brain MVECs showing much higher levels of HIF-2α protein throughout the hypoxia time course (Fig. 3-2D).

Transcriptional activation of HIF-1α target genes was quantified by qPCR. The targets were selected based on their relevance to shift to glycolytic metabolism (GLUT1, PGK, and LDH1), endothelial physiological response to hypoxia (VEGF), as well as the putative HIF-2α target ARG-2 (Fig 3-2E). The HIF-1α target and autophagy marker BNIP3 (Zhang *et al.*, 2008) was assessed to infer a possible correlation with the differential effects seen on cell survival to hypoxia. As expected, hypoxia lead to the transcriptional upregulation of the glycolytic genes PGK, LDH, and GLUT1 in both brain and lung MVECs. Yet, the relative pattern of upregulation differed for each target. PGK was significantly more upregulated in lung MVECs at all time points, whereas GLUT1 expression increased equally in brain and lung MVECs at early time points but lung MVECs eventually showed a greater upregulation at 24 h and 48 h. Brain MVECs displayed a more pronounced upregulation of LDH at 4 h and 8 h but no difference was observed at later time points. Lung MVECs exhibited an upregulation of VEGF

transcript, which was not seen in their brain counterparts. Similarly, lung MVECs also upregulated ARG2 throughout the hypoxia time course whereas brain MVECs actually downregulated this gene.

This was especially surprising, given that ARG2 has been described as a preferential target of HIF-2α (Krotova *et al.*, 2010), the HIF isoform which was found to be more highly expressed in brain MVECs. Lastly, the autophagy marker BNIP3 was indeed upregulated more strongly in brain than lung MVECs, correlating with the differential rates of hypoxia-induced cell death displayed by the two cell populations.

In the previous chapter, changes in inflammatory and pro-metastatic cytokines were shown to be produced by hypoxic MVECs. Here, the same panel was used to compare media conditioned by brain and lung MVECs, both at baseline and after 24 h at 1% O_2 (Fig. 3-2F). CCL2 and M-CSF were secreted by both MVECs at comparable levels, in normoxia as well as after hypoxia. Furthermore, both cell populations also expressed CXCL12 and TIMP-1. A series of cytokines, most notably CCL5, were specifically expressed by brain but not lung MVECs, but interestingly no lung MVEC-specific cytokine signature was detected. Further replicates would be needed to assess whether the differences between conditions are statistically significant.

These data show that MVECs from brain and lung display markedly distinct responses to hypoxia, including survival, HIF isoform stabilization and downstream transcription, as well as cytokine production. However, brain MVECs were more adversely affected and unable to mount a suitable adaptive transcriptional response when transferred to low oxygen tensions – as displayed by their reduced viability and inability to upregulate VEGF. This was surprising, given that brain physiological oxygen *in vivo* is considerably lower (~5%; Dings et al., 1998) than that found in the lung (~10%; Miller et al., 2009; Wild et al., 2005), which would presumably render brain MVEC better equipped to survive the hypoxic challenge. Crucially however, both tissues contain much less oxygen than the 18.5% O_2 found in standard tissue culture incubators (Wenger *et al.*, 2015), and thus the cellular responses seen in these conditions are unlikely to relevantly represent the adaptations seen in physiological conditions. To investigate this possibility, the subsequent experimental set-up included culturing each cell population also in physiological O_2 tensions.

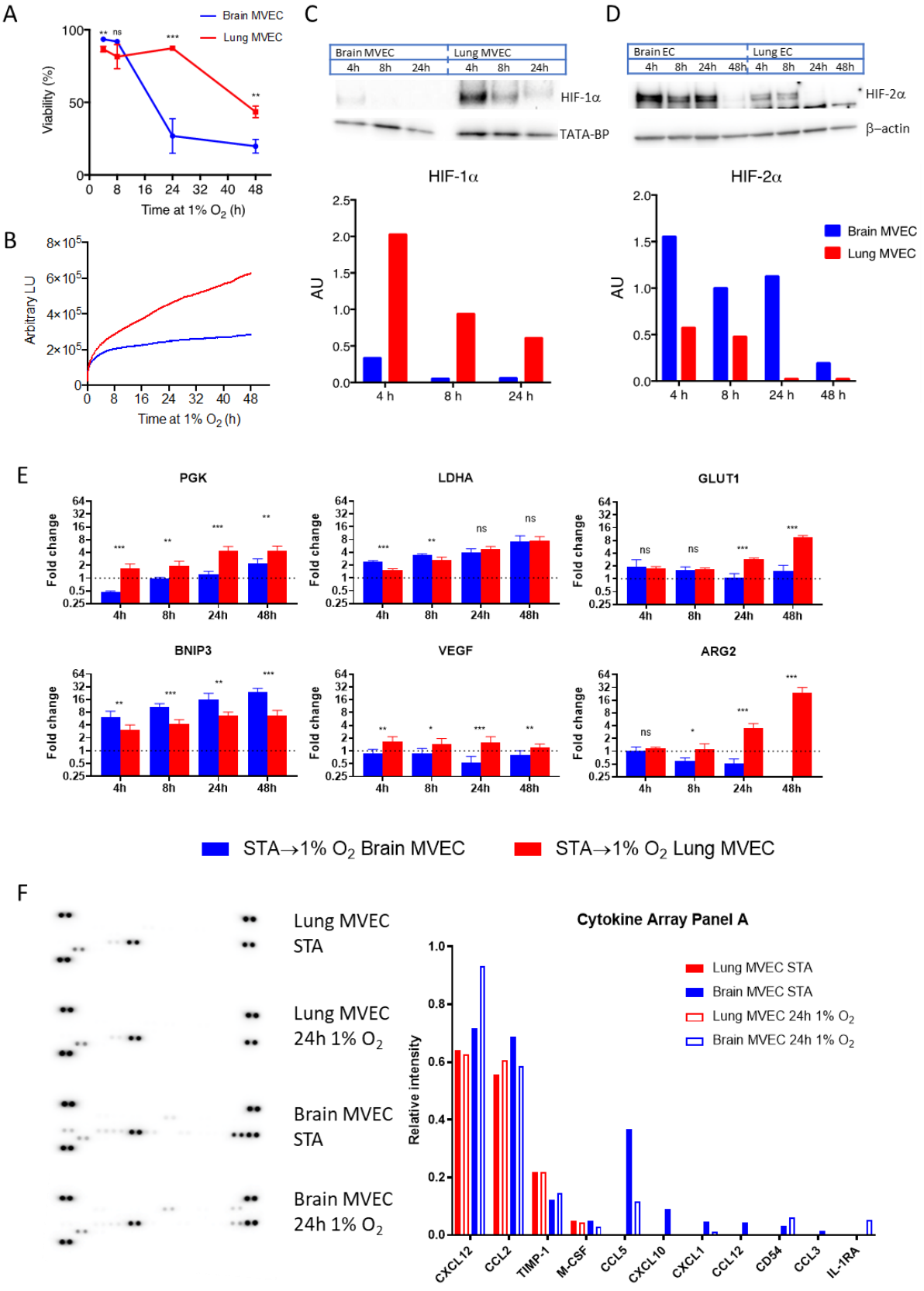
A
Brain MVEC
Lung MVEC
Viability (%)
Time at 1% O2 (h)
B
Arbitrary LU
Time at 1% O2 (h)
C
Brain MVEC
Lung MVEC
HIF-1α
TATA-BP
HIF-1α
AU
D
Brain EC
Lung EC
HIF-2α
β–actin
HIF-2α
AU
Brain MVEC
Lung MVEC
E
PGK
LDHA
GLUT1
BNIP3
VEGF
ARG2
Fold change
STA→1% O2 Brain MVEC
STA→1% O2 Lung MVEC
F
Lung MVEC STA
Lung MVEC 24h 1% O2
Brain MVEC STA
Brain MVEC 24h 1% O2
Cytokine Array Panel A
Relative intensity
CXCL12
CCL2
TIMP-1
M-CSF
CCL5
CXCL10
CXCL1
CCL12
CD54
CCL3
IL-1RA

Figure 3-2

Figure 3-2: Lung and brain MVECs show differential responses to hypoxia
(A) Viability of brain and lung MVECs exposed to 1% O_2 at t=0, measured by propidium iodide staining (n=3)
(B) Real-time viability of brain and lung MVECs exposed to 1% O_2 at t=0, measured using the Real-Time Glo assay (Promega) (n=3)
(C,D) Western blot of HIF-1α and HIF-2α using nuclear extracts from brain and lung MVECs exposed to 1% O_2 for the indicated amount of time. The quantification was normalized to the loading control.
(E) qPCR of PGK, LDHA, GLUT1, BNIP3, VEGF, and ARG2 in lung and brain MVECs exposed to 1% O_2 for the indicated time, displayed as fold-change from the normoxic control (n=3)
(F) Cytokine array using brain and lung MVEC growth medium at baseline or after 24 h at 1% O_2, with quantification of the blots. A schematic showing the label for each signal spot is shown in Appendix A
Error bars represent SD, t-tests corrected for multiple comparisons (Holm-Sidak)*p<0.05, **p<0.01, ***p<0.001)

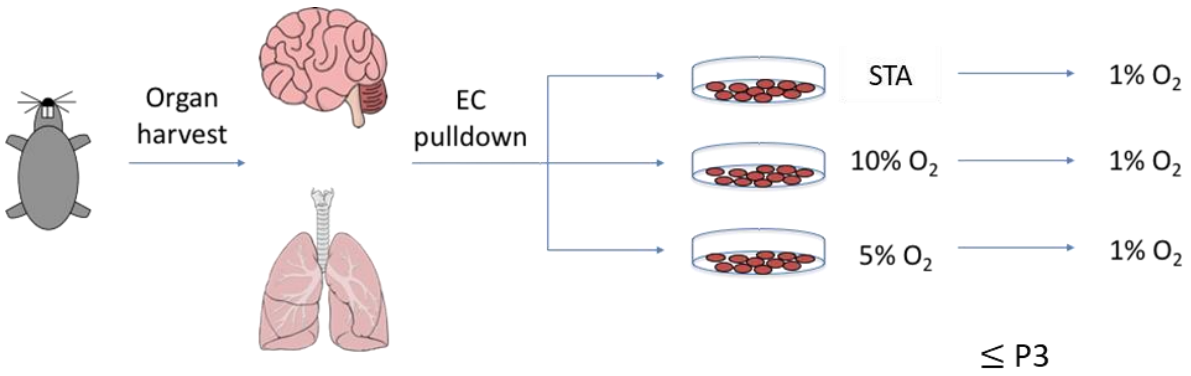

Figure 3-3 Experimental setup for MVEC isolation and physioxic culture
MVECs were isolated from brains and lungs of WT mice as outlined in Fig. 3-1; immediately after the end of the pulldown cells were placed in tissue culture incubators with ambient O_2 (standard tissue culture atmosphere – STA), 10% O_2 and 5% O_2. After at most three passages, the cells were used in experiments.

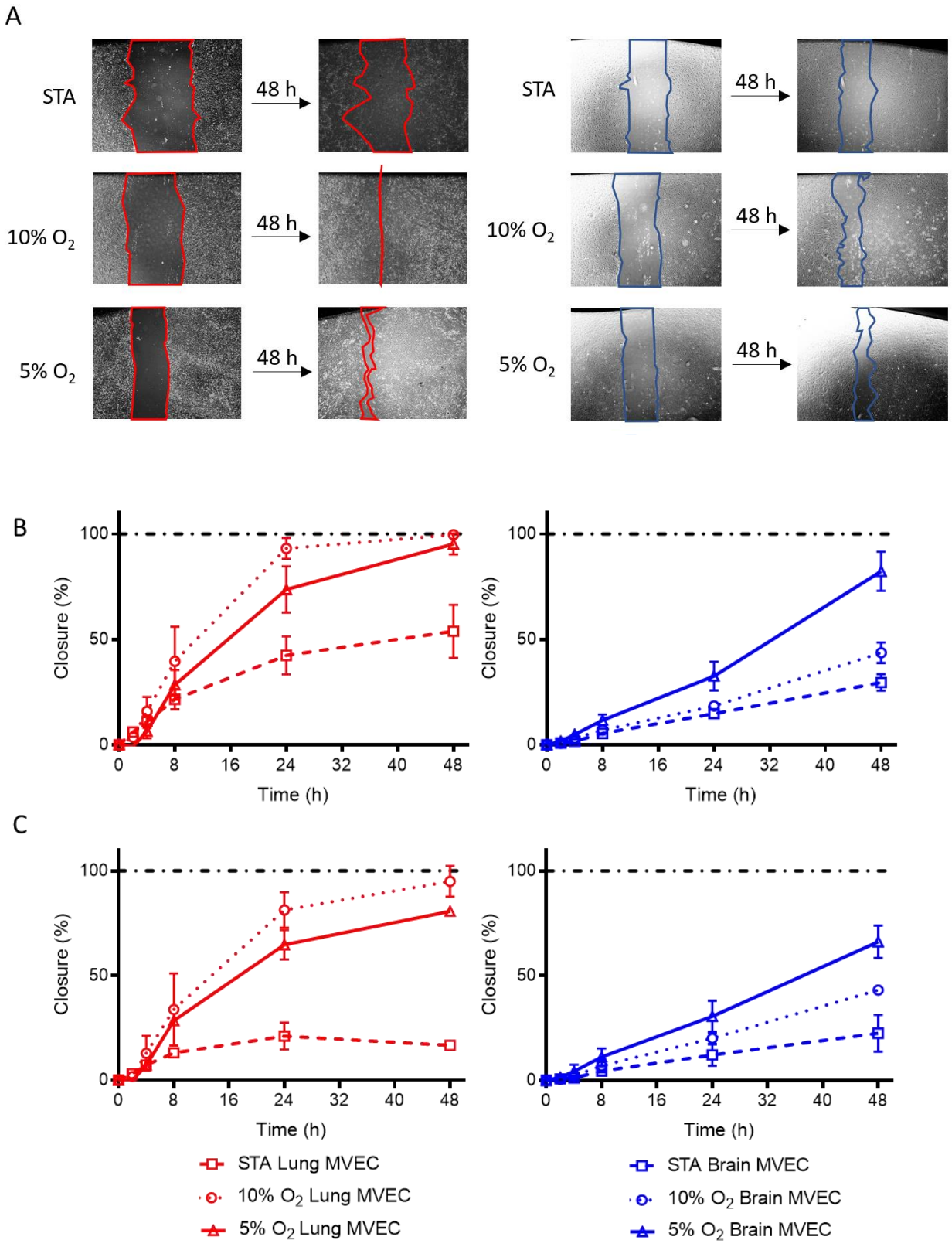
A
STA
48 h
10% O2
5% O2
B
Closure (%)
Time (h)
C
STA Lung MVEC
10% O2 Lung MVEC
5% O2 Lung MVEC
STA Brain MVEC
10% O2 Brain MVEC
5% O2 Brain MVEC

Figure 3-4

Figure 3-4: Physioxic MVECs close wounds faster
(A) Representative picture of wound closure assays using brain and lung MVECs cultured at different oxygen levels. Wounds were applied using a P1000 tip at t=0 and wound closure was measured as % relative to the area of the original scratch
(B,C) Quantification of wound closure over time. Cells were treated with DMSO (B) or 10 mM Mitomycin C (C) for 2 h before the scratch was applied (n=4) to measure wound closure with or without cell proliferation, respectively

3.2.3 The hypoxia response of brain and lung MVECs is shaped by O_2 levels during cell culture

To evaluate the influence of a hyperoxic-driven effect on EC behaviour, the cells were provided with conditions that more closely reflect their physiological environment, MVECs were cultured at either 10% or 5% O_2 – physioxia for lung and brain MVECs respectively – immediately following their isolation, in addition to standard tissue culture atmosphere (Fig. 3-3). First, it was assessed how growth and motility of these cells was affected under these three different baseline culture conditions (Fig. 3-4). To distinguish between proliferation- and motility-based wound closure, the cells were treated with the proliferation inhibitor mitomycin C (Chen *et al.*, 2013) before applying the scratch. Not surprisingly, mitomycin C reduced the closure rate under all conditions compared to the vehicle control, but the relative patterns remained unchanged. In both cell populations, MVECs cultured under physioxic conditions closed the scratch more quickly than their counterparts grown at ambient O_2. Lung MVECs grown at 10% O_2 showed the overall faster closure rate, with the same cell type at 5% O_2 in close second. Both promoted faster closure than STA. Brain MVECs were generally less motile than those from lung, and the effect of changing oxygen levels was less pronounced. In these cells, the fastest closure rate was achieved when grown at 5% O_2. Each population showed the fastest wound closure rate at the oxygen level that most closely reflects their *in vivo* environment.

Next, it was assessed how changing the baseline oxygen conditions affected the expression of the hypoxia target genes investigated in Fig. 3-2E, as this could have an impact on the hypoxia-induced fold-change and is informative as to the steady state profile of the cells in culture. Perhaps unsurprisingly, there were considerable differences in the relative abundance of these genes at baseline, both between different oxygen levels within the same MVEC population, but even more strikingly between brain and lung MVECs (Fig. 3-5). Amongst the glycolytic genes, PGK showed the least variation; only in lung MVECs grown at

10% O_2 its expression was slightly lower than in the other samples. LDHA showed similarly little variation across oxygen levels but it was consistently higher expressed in lung MVECs. GLUT1 mRNA on the other hand was lower in cells grown in 5% O_2 than STA, and at both oxygen levels there was no difference between lung and brain MVECs.

This was not the case in cells grown at 10% O_2; in lung MVECs GLUT1 transcript levels were equivalent to the normoxic level, whereas in brain MVECs it was comparable to 5% O_2. Conversely, BNIP3 was higher in cells maintained at lower O_2. Again, the transcript levels of BNIP3 between lung and brain MVECs only differed if grown at 10% O_2. ARG2 expression was consistent across all conditions except for lung MVECs grown at STA, where it was surprisingly elevated. All the differences described until this point were relatively small in magnitude, no more than 5-fold. Strikingly, however, VEGF transcript was expressed almost 100-fold higher in lung MVECs compared to brain ones, across all oxygen levels. Generally, no consistent trend was observed; even the three glycolytic had different steady-state levels depending on atmospheric oxygen availability.

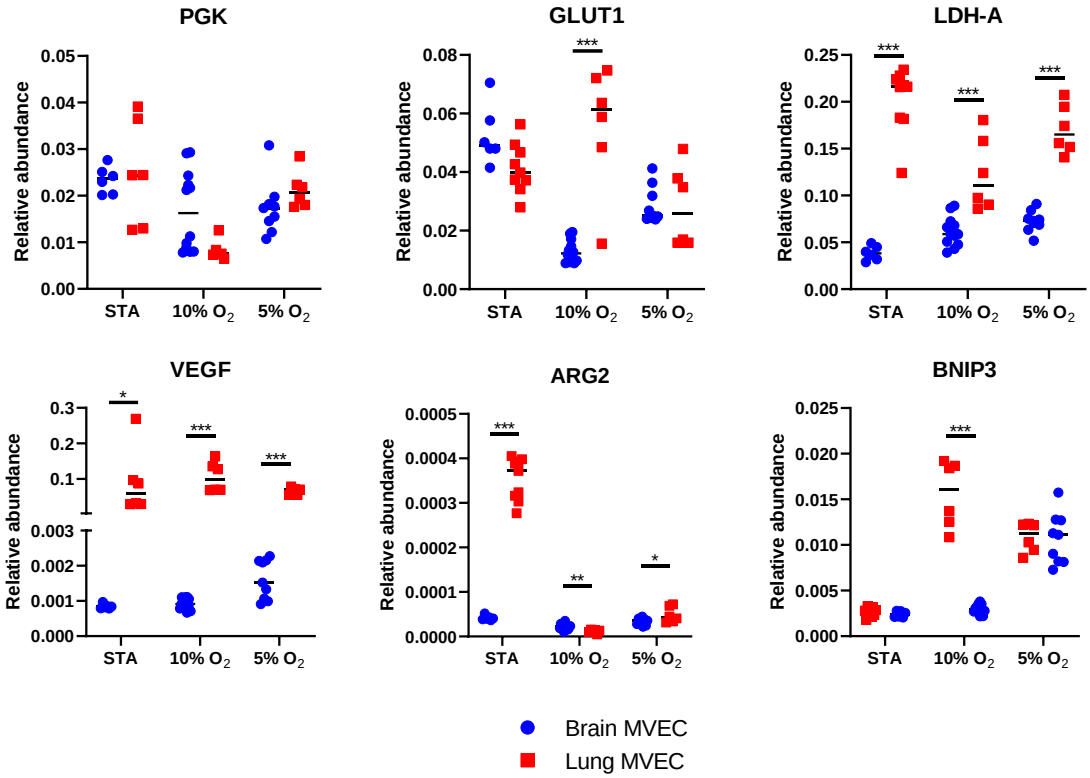

Figure 3-5: Relative mRNA abundance of hypoxia response genes under different baseline O_2 conditions

RNA was isolated from brain (blue) and lung (red) MVECs cultured at different oxygen levels. Transcript levels were measured by RT-qPCR and displayed as relative abundance compared to the b-actin housekeeping gene

Statistics were done using t-tests corrected for multiple comparisons (Holm-Sidak) *p<0.05, **p<0.01, ***p<0.001)

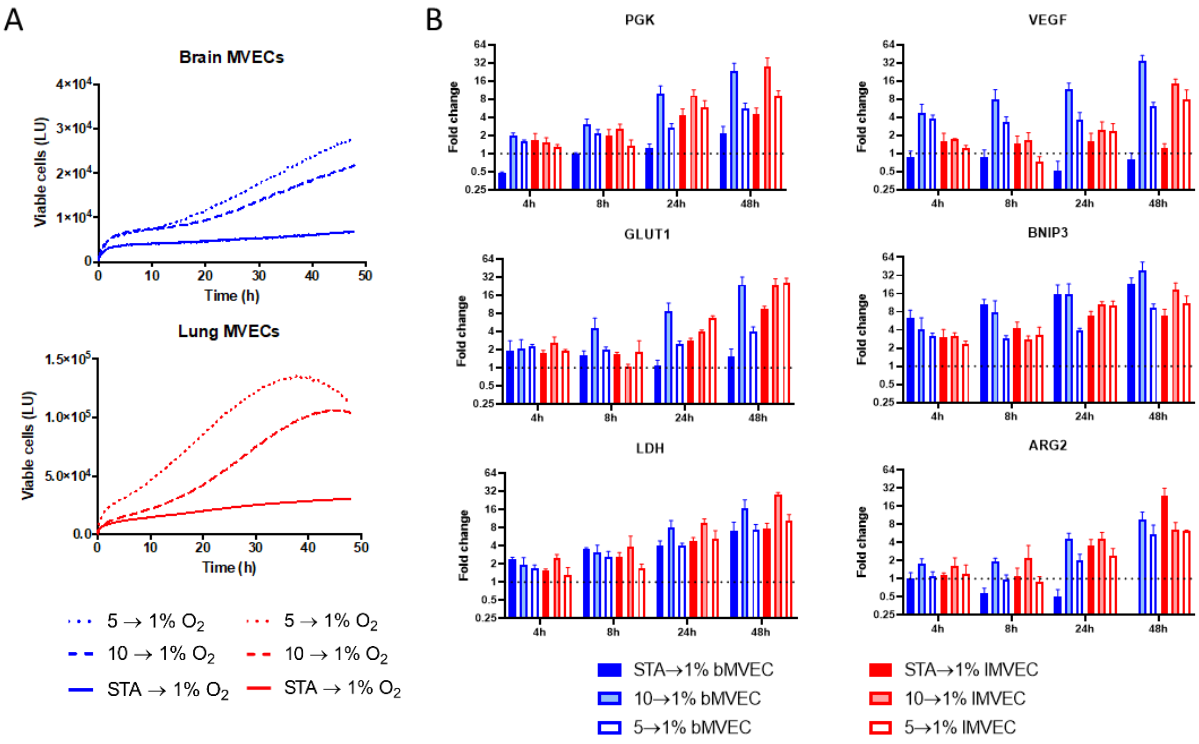

Figure 3-6: The hypoxia response of brain and lung MVECs is shaped by O_2 levels during cell culture
(A) Real-time viability of brain and lung MVECs cultured at STA, 10%, or 5% O_2 and exposed to 1% O_2 at t=0, measured using a Real-Time Glo assay (Promega) (n=3)
(B) RT-qPCR of PGK, VEGF, GLUT1, BNIP3, LDH-A, and ARG2 mRNA in brain and lung MVECs cultured at STA, 10%, or 5% O_2 and exposed to 1% O_2 for the indicated time, displayed as fold-change from the normoxic control (not shown) (n=3)

After two weeks in culture, the cells were exposed to hypoxia (1% O_2) to compare viability as well as induction of HIF and hypoxia-response genes following adaptation to low O_2. In both MVEC populations, culture in a lower O_2 atmosphere correlated with increased viability during adaptation to hypoxia (Fig. 3-6A). Both lung and brain MVECs cultured at STA fared strikingly worse than the same cells grown at 10% or 5% O_2, suggesting that exposure to high oxygen levels (physiological hyperoxia) compromised their ability to adjust and survive to oxygen shortage, even though 1% O_2 can still be considered physiological in many tissues, including the brain (Cater *et al.*, 1961; Smith *et al.*, 1977). Similarly, the expression of hypoxia response genes in these cells was also significantly lower (Fig. 3-6B). In brain MVEC, all four metabolic genes as well as VEGF were upregulated most strongly by cells grown at 10% O_2, followed by cells grown at 5% O_2. Most strikingly, VEGF and ARG2 were induced by hypoxia only if the cells had been cultured at 10% or 5% O_2. The exception

to this pattern was the autophagy marker BNIP3, which was induced most strongly in brain MVEC cultured at STA, correlating with their reduced viability. Lung MVECs displayed similar patterns of upregulation; the largest increases in gene expression of targets involved in the canonical hypoxia response were generally seen in cells grown at 10% O_2, although the differences to cells grown in STA were less pronounced than in brain MVECs.

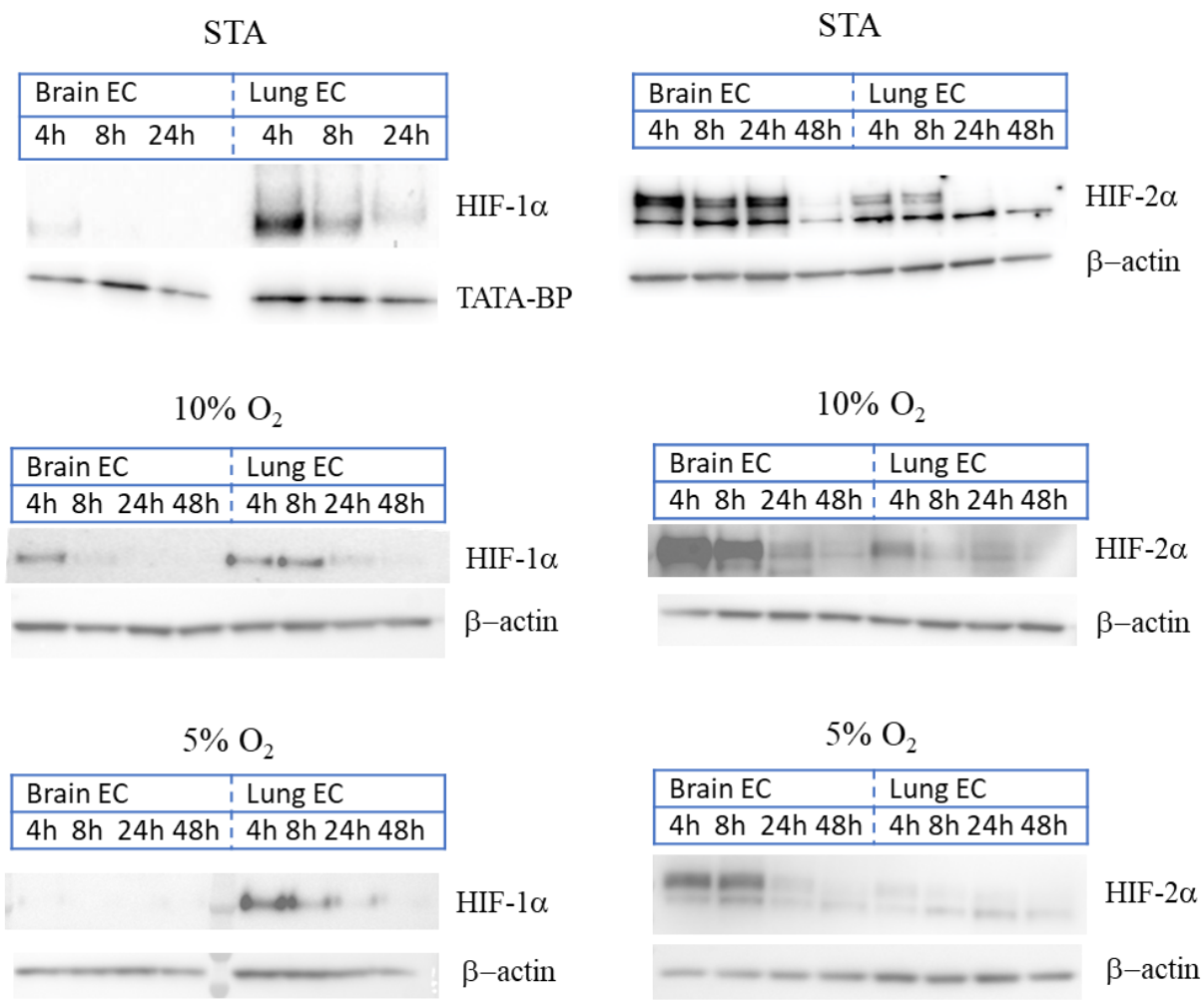

Figure 3-7: HIF levels in hypoxia over time
Western blot for HIF-1α and HIF-2α using nuclear extracts from brain and lung MVECs cultured at STA, 10%, or 5% O_2 and exposed to 1% O_2 for the indicated amount of time

These patterns were also reflected in the stabilisation of HIF. To assess HIF-stabilisation in hypoxia over time, time course experiments with lung and brain MVECs grown at 10% and 5% O_2 were performed, and the kinetics observed were the same as with cells grown at STA (Fig. 3-7). Of note, HIF-2α protein levels here decreased at earlier time points compared to the data presented in the previous chapter, a result from a slight modification of the hypoxia protocol, whereby medium was equilibrated before the start of the experiment. Both HIF-isoforms showed maximal expression after 4h in 1% O_2; therefore this time point for each condition was blotted onto the same membrane (Fig. 3-8).

After 4 h of hypoxia, the highest levels of HIF-1α were displayed by lung and brain MVECs cultured at 10% O_2. Lung MVECs originally grown at 5% O_2 or STA displayed equal levels of HIF-1α whereas brain MVECs grown at STA stabilised HIF-1α to an even smaller degree than cells grown at 5% O_2. Although consistent across replicates, these differences were too variable in magnitude to be statistically significant. In each condition, lung MVECs expressed higher levels of HIF-1α than brain cells, and HIF-2α on the other hand was present at higher levels in brain MVECs. In both cell types, culturing at 5% O_2 resulted in the highest levels of HIF-2α after 4 h in hypoxia.

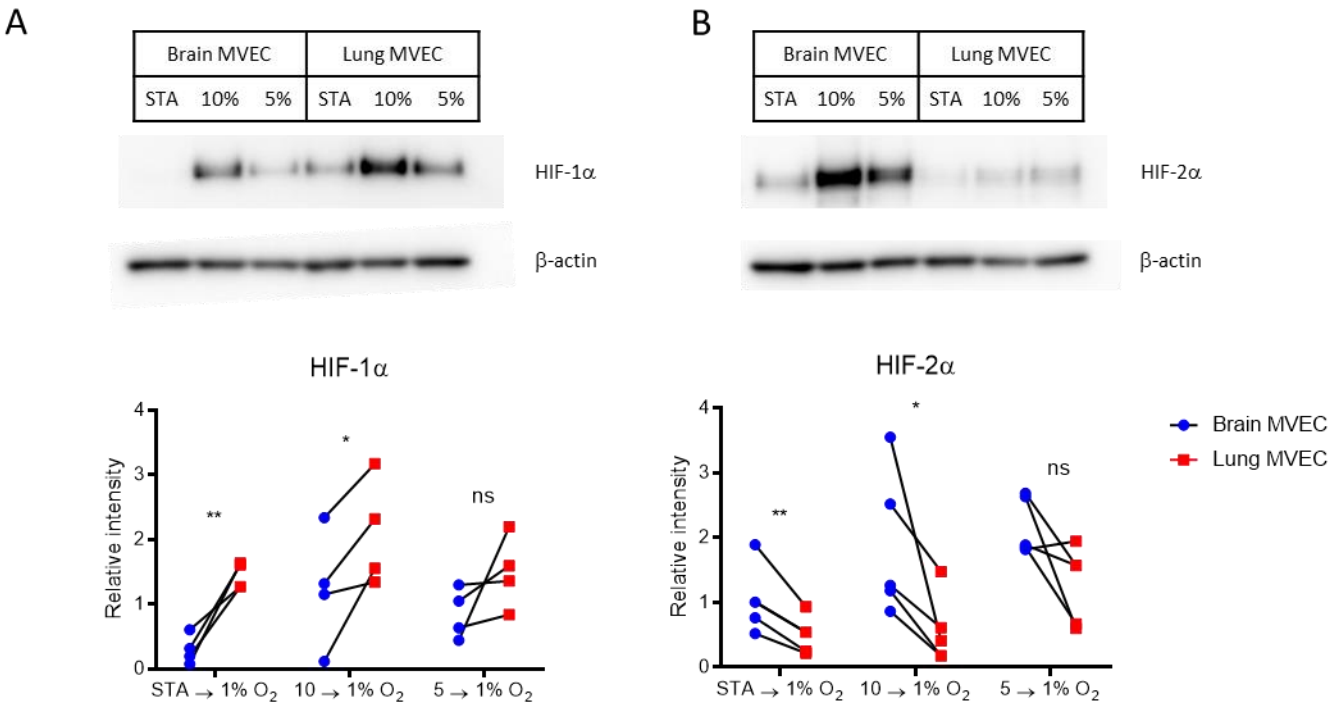

Figure 3-8 HIF levels in hypoxia are shaped by baseline oxygen levels
(A,B) Western blot of HIF-1α and HIF-2α using nuclear extracts from brain and lung MVECs cultured at STA, 10%, or 5% O_2 and exposed to 1% O_2 for 4h. The quantification was normalized to the loading control (n=4; paired t-test, *p<0.05, **p<0.01)

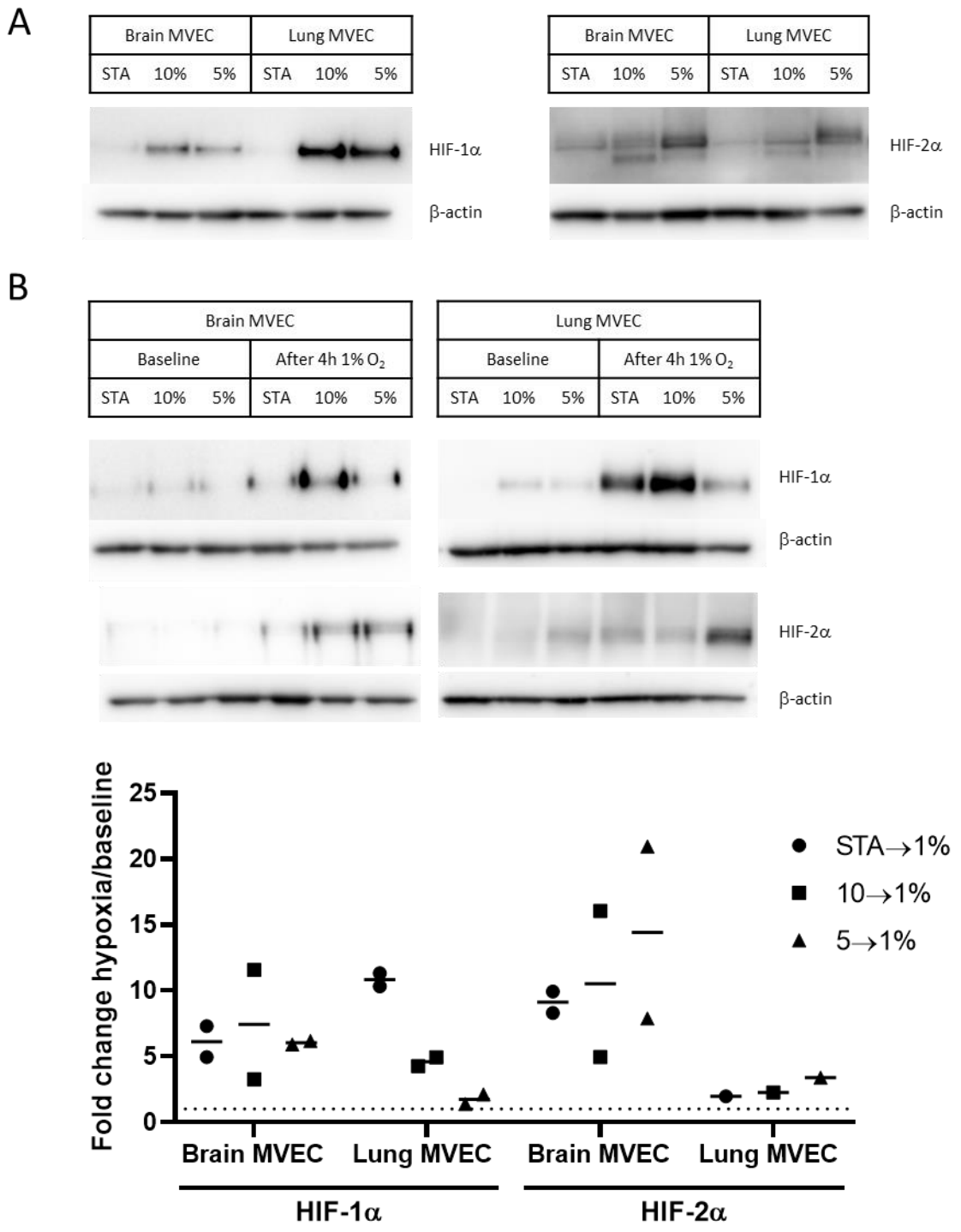

Figure 3-9: HIF levels at baseline

(A) Western blot with nuclear protein comparing the baseline levels of HIF-1α and HIF-2α in brain and lung cells grown at different oxygen levels, before hypoxia treatment

(B) Western blot showing the hypoxia-induced increase in HIF-1α and HIF-2α protein levels in brain and lung MVECs grown at different oxygen levels with quantification (normalised to loading control, dotted line showing no fold change, n=2 except for Lung MVEC HIF-2α where n=1)

The data above shows that, brain and lung MVECs clearly rely on different HIF isoforms independently of the baseline oxygen level. Indeed, MVECs grown at 10% or 5% O_2 displayed much higher levels of HIF-1α even without being exposed to hypoxia (Fig. 3-9A), underscoring the role of this transcription factor in cell function in physiological and not only hypoxic environments. Again, lung MVECs showed a much more pronounced signal than the brain cells. Exposure to 1% O_2 for 4 h increased the expression of HIF-1α under all conditions (Fig. 3-9B). The fold increase between hypoxia and baseline was a consistent 6-fold for brain MVECs in all three conditions. Lung MVECs showed a similar induction (~5 fold) if cultured at 10% O_2 but this was increased considerably in cells grown at STA (~ 11-fold); lung MVECs grown at 5% O_2 on the other hand barely showed any induction of HIF-1α after 4 h at 1% O_2. This suggests that 5% O_2 is already significantly below the *in vivo* oxygen setpoint of a lung MVEC, and thus likely perceived as hypoxia for these cells.

HIF-2α was significantly more stabilised in all MVECs grown at 5% O_2, when compared to 10% or STA (Fig. 3-9A). Unlike after hypoxia exposure, there was no difference in HIF-2α expression between brain and lung MVECs at baseline, and exposure to 1% O_2 lead to an increase in HIF-2α levels under all conditions, with the fold-change being considerably more pronounced in brain MVECs (Fig. 3-9B).

To further explore the cause of these differences in HIF abundance, the levels of HIF-1α and HIF-2α mRNA were measured. Surprisingly, the protein levels previously assessed were almost entirely reflected by the abundance of mRNA (Fig. 3-10A), in spite of the traditional assumption that HIF is mostly post-translationally regulated. Brain MVECs expressed more HIF-2α mRNA than lung MVECs in all conditions. Conversely, the levels of HIF-1α mRNA for the same cells were lower when cultured at 10% and 5% O_2. However, lung MVECs grown at STA displayed much lower levels of HIF-1α mRNA than any other sample, a trend not reflected at the protein level.

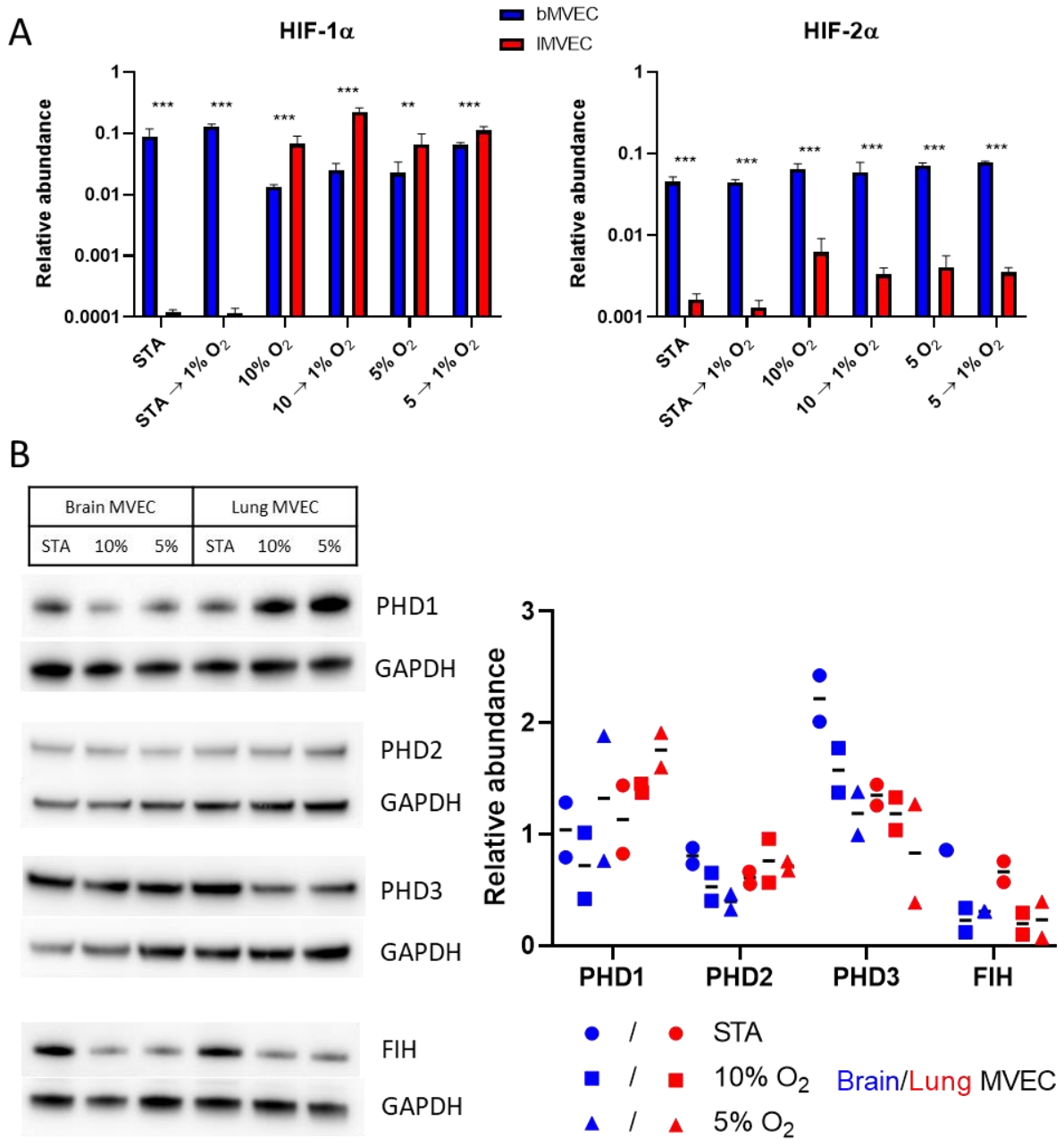

Figure 3-10: Analysis of upstream regulators of HIF protein and activity
(A) Comparing the mRNA levels of HIF-1α and HIF-2α in brain and lung MVECs grown at different oxygen levels, before hypoxia treatment and after 4h at 1% O_2. Transcript levels were quantified by RT-PCR and are displayed as relative abundance compared to the β-actin housekeeping gene (n=3)
(B) Western blot of enzymes responsible for the post-translational control of HIF: prolyl hydroxylase (PHD) 1-3 and factor inhibiting HIF (FIH) using whole-cell protein lysate (quantification normalised to loading control, n=2)

To investigate upstream regulation of HIF stabilisation and activity, the expression levels of the canonical regulators of HIF abundance, the prolyl hydroxylases PHD1-3 and FIH were also assessed (Fig. 3-10B).

PHD1 was slightly higher expressed in lung ECs whereas the opposite was seen for PHD3; furthermore, PHD3 levels in both tissues decreased at lower oxygen levels. PHD2 showed the fewest tissue-specific differences but its levels were slightly reduced in brain MVECs at 10% and 5% O_2. FIH-mediated hydroxylation does not lead to HIF degradation but affects its transcriptional activity by preventing binding to its cofactor (Mahon *et al.*, 2001; Lando, Peet, Gorman, *et al.*, 2002). FIH expression was found to be comparable between brain and lung MVECs cultured at the same oxygen level but it was significantly elevated in MVECs grown in STA compared to physioxia. While this does not explain the differential levels of HIF isoforms, it may contribute to the dampened hypoxia response displayed by MVECs cultured in STA.

Combined, these data demonstrate that the ability of MVECs to respond to hypoxia is compromised in hyperoxia, specifically in brain MVEC, and that the environmental priming of endothelial cells affects their ability to respond and endure hypoxic challenges.

3.3 Discussion

3.3.1 Traditional i*n vitro* culture conditions do not reflect the *in vivo* physioxic setpoint

Increasing numbers of studies are showing that oxygen levels shape the *in vitro* behaviour of cells, including but not limited to endothelial cells (Timpano and Uniacke, 2016; Chen *et al.*, 2018; Ferguson *et al.*, 2018; Henn *et al.*, 2019). This work contributes to the growing concerns regarding the effect of hyperoxia and physioxia on EC behaviour. For example, Jiang et al. (2013) cultured human vein endothelial cells (HUVECs) at STA or 3% O_2 and observed large scale changes in gene expression at the mRNA and protein level. In this thesis hyperoxia was not only avoided but complemented with priming conditions to reflect the precise physioxic needs of the organ that the specific ECs supply, which is different for brain and lung MVECs. This is underscored by the fact that brain MVECs cultured at STA fare worse than the ones from lung, likely because brain MVECs underwent a more severe hyperoxic challenge relative to their physioxic setpoint. Consequently, their ability to adapt to a subsequent hypoxic challenge is likely lost, as evidenced by reduced viability, reduced HIF expression and reduced upregulation of hypoxia response genes, compared to the same cells cultured under physioxic conditions. While a similar effect can be seen in lung MVECs, it is

much less severe. This could actually indicate that lung MVECs are inherently more suited to adapting to changes in oxygen level, since they consistently undergo exposure to wider oscillations due to their close proximity to environmental air.

Apart from their implications on endothelial plasticity, these data also raise an important technical issue within the field of EC biology. The vast majority of *in vitro* EC studies rely on commercially available cells, which are usually cultured in normoxia before shipping, often for several passages. Jiang et al. (2013) show that the effects of hyperoxia are not entirely reversible, even after prolonged culture in physioxia. According to the data presented in this chapter, this would have a differentially detrimental effect on endothelial cells from different organs, depending on their *in vivo* oxygen setpoint, thus introducing a confounding variable into any subsequent experiments. However, it is frequently impossible to obtain human cells directly from donors. In house pulldowns, such as shown here, and in spite of inherent inter-species variation, actually minimise and normalise the time exposed to normoxia during the isolation process.

3.3.2 Brain MVECs at STA secrete a broader range of cytokines than lung MVECs

The role of capillary endothelial cells reaches beyond control of blood flow and perfusion. MVECs have been found to interact with neighbouring cells through a series of signalling molecules collectively termed angiocrine factors. In the brain, capillary endothelial cells regulate the regeneration and homeostasis of neural stem cells (NSCs), through direct cell-to-cell interaction as well as paracrine signalling molecules. These EC-derived signals usually induce NSC quiescence, which aids in the maintenance of a healthy stem cell pool (Delgado *et al.*, 2014; Ottone *et al.*, 2014). Following injury however, a different set of angiocrine factors triggers a regenerative process composed of NSC proliferation and differentiation (Andreu-Agulló *et al.*, 2009; Gómez-Gaviro *et al.*, 2012; Crouch *et al.*, 2015; Han *et al.*, 2015). Similarly, angiocrine signals by lung MVECs play a major role in coordinating the regenerative response to lung injury (Ding *et al.*, 2011, 2015; Rafii *et al.*, 2015). While some of the underlying mechanisms seem to be common to all MVECs, and indeed even HUVEC (Leventhal *et al.*, 1999), many are tissue-specific. This could either be a result of the presence of different target cells in different organs, such as the proximity of brain MVECs to neurons, or due to intrinsic differences among organotypic MVECs.

Amongst the cytokines assessed in this panel (Fig. 3-2F), no lung MVEC specific signal was detected; CXCL12, CCL2, TIMP-1 and M-CSF were all expressed by both populations of

endothelial cells at comparable levels. Brain MVECs on the other hand secreted a further series of cytokines, of which CCL5 and CXCL10 were most highly expressed. CCL2, CCL5 and CXCL10 have all been implicated in regulating leukocyte trafficking into the CNS (Huang *et al.*, 2001; Biernacki *et al.*, 2004; Dos Santos *et al.*, 2005). In multiple sclerosis patients, CCL5 and CXL10 are increasingly secreted by brain MVECs in proximity to demyelinated plaques (Subileau *et al.*, 2009). Interestingly, the data presented here shows a considerable reduction in the secretion of both these cytokines in hypoxic brain MVECs.

Therefore, brain and lung MVECs maintain intrinsic differences in their cytokine secretome even after several weeks in culture. Further experiments in this area could include exposing the MVECs to a pro-inflammatory stimulus such as TNF-α and IFN-γ. Considering the data presented in this chapter, subsequent further experiments should be performed at physiological O_2 levels.

3.3.3 Brain and lung MVECs differentially express HIF isoforms

Irrespective of the oxygen level during cell culture, lung MVECs exposed to hypoxia express more HIF-1α than those isolated from brain (Fig. 3-8). In fact, this pattern holds true even at baseline under physioxic conditions, while in normoxia HIF-1α protein is absent (Fig. 3-9A). The opposite was shown for HIF-2α protein, which is seen at higher levels in brain MVECs after hypoxia exposure; at baseline, brain and lung MVECs express comparable amounts of this isoform.

As outlined in the introduction, HIF-1α and HIF-2α share many of their transcriptional targets but also perform several non-overlapping functions. Most notably, HIF-2α is implicated in EC monolayer stability and cell-to-cell adhesion, whereas HIF-1α acts as the responder to acute insults. Maintaining a functional barrier is of paramount importance to brain MVECs, which guard the CNS as part of the BBB. In the lung this is less critical, and an opening of the microvasculature coupled with the recruitment of leukocytes may be advantageous when dealing with a noxious stimulus. Therefore, the increased reliance on either HIF isoform by brain and lung MVECs may reflect the demand of their underlying organ.

The canonical control of HIF occurs posttranslationally, through hydroxylation by PHDs. Amongst the three PHD isoforms, only PHD3 was consistently elevated in brain compared to lung MVECs at every oxygen level (Fig. 3-10B). PHD1 showed the opposite trend, especially at physiological oxygen levels but further replicates are needed to draw a firm conclusion. Similarly, PHD2 was slightly elevated in lung MVECs at 10% and 5% O_2.

While all PHD isoforms contribute to the regulation of both HIF-1α and HIF-2α, some isoform selectivity has been reported (Appelhoffl *et al.*, 2004). PHD2 was found to preferentially regulate HIF-1α whereas PHD3 preferentially selects HIF-2α for degradation. This is the exact opposite to the trend observed here, where brain MVECs expressed higher levels of PHD3 and slightly less PHD2 but more HIF-2α and less HIF-1α than lung MVECs. This suggests that the differences in HIF isoform expression between lung and brain MVECs are unlikely due to isoform-specific PHD activity. To fully confirm this hypothesis, knockout or knockdown studies targeting one or multiple PHD isoforms could be performed. Further experiments may also include measuring the levels of the PHDs during hypoxia, as it is well established that HIFs upregulate PHD expression (Aprelikova *et al.*, 2004). This would aid dissecting the mechanism by which HIF-2α levels in brain cells after 4 h at 1% O_2 are higher, when no differences are seen at baseline between lung and brain.

Although HIF expression is traditionally seen as being controlled primarily posttranslationally, there are some reports that mRNA levels may also play a role. Several signalling pathways such as JAK/STAT (Niu *et al.*, 2008) and PI3K/Akt/mTOR (Pagé *et al.*, 2002; Yuan *et al.*, 2008) as well as heat shock proteins (Chen *et al.*, 2011) have been shown to modulate HIF protein levels through transcriptional regulation. In fact, isoform-specific regulation of HIF at the transcriptional level has been demonstrated in macrophages where stimulation with Th1 or Th2 cytokines increased transcript levels of HIF-1α or HIF-2α mRNA, respectively. This results in differential HIF expression at the protein level and distinct downstream signalling cascades (Takeda *et al.*, 2010). Indeed, in both lung and brain MVECs there is a clear correlation between HIF-1α and HIF-2α abundance at the mRNA and protein level, both at baseline and after 4 h at 1% O_2 (Fig. 3-10A). The only exception are lung MVECs grown at STA which show a more than 100-fold less HIF-1α mRNA compared to any of the other conditions, both at baseline and after hypoxia; this difference is not, however, reflected in the HIF-1α protein level. Thus, while mRNA levels may play some role in explaining the differential abundance of HIF isoforms in the two MVEC populations, it is clearly only part of a larger puzzle. mRNA stability, localisation, and translation all contribute to and affect protein levels.

In fact, and as described before, hypoxia is only one of many factors regulating the activity of HIF, some of which are isoform-specific. For example, the ubiquitin ligases CHIP and HAF bind HIF-1α but not HIF-2α, leading to isoform-specific ubiquitination and proteasomal degradation (Koh *et al.*, 2008; Luo *et al.*, 2010). mTOR on the other hand can

promote the expression of HIF even in the absence of hypoxia. In this context, HIF-1α is regulated by both mTOR complexes, mTORC1 and mTORC2, while HIF-2α only relies on mTORC2 (Toschi *et al.*, 2008). This hypothesis could be further explored by measuring the activity of each pathway in the two MVEC populations, for example by western blot analysis of the phosphorylated form their targets S6K (mTORC1) and Akt S473 (mTORC2). Selective inhibition of each complex could then reveal their effect on HIF abundance in MVECs; this could be achieved for example by siRNA targeting of Raptor and Rictor, two mTOR components exclusive to mTORC1 and mTORC2, respectively.

3.3.4 Brain and lung MVECs show considerable differences in baseline gene expression

Differences in the expression of hypoxia-response in brain and lung MVECs precede the hypoxia treatment and are affected both by the cell origin, as well as the baseline oxygen level in which they were cultured (Fig. 3-5). The initial hypothesis was that the expression of these genes should mirror the HIF levels at baseline; however, this was not the case. As shown in Fig. 3-6B, although HIF is present under physioxic conditions, it is expressed at much lower levels than in hypoxia. Therefore, its effects may be overridden by other transcription factors. This hypothesis could be validated through knockout or knockdown studies targeting HIF. Of the six assessed genes only BNIP3 and GLUT1 showed a pronounced change across oxygen levels, albeit in opposite directions. In both cases however, the two cell populations behaved similarly at the extremes (5% O_2, STA) but differently at 10% O_2 (Fig. 3-5). Curiously, this reflects the physiological *in vivo* O_2 levels of the two tissues, where 10% O_2 is hyperoxic for a brain but not a lung MVEC.

There was variation in all targets between the tissue-specific MVECs, but only LDHA and VEGF showed consistent differences across all oxygen levels and both were more highly expressed in lung MVECs. The difference was at most 5-fold for LDHA but more than 100-fold for VEGF. This is highly intriguing, since VEGF is a key regulator of EC development and function, affecting a diverse array of processes such as cell proliferation, migration, vessel sprouting, and permeability (Ferrara *et al.*, 2003). If confirmed, one could speculate that this difference may be part of the BBB role. It is a well-established role of VEGF to increase vascular permeability and leakage (Senger *et al.*, 1983). Indeed, this has been specifically shown to be the case within brain MVECs (Schoch, 2002). The BBB is the most tightly controlled, least permeable vascular bed; therefore, reduced expression of VEGF may be necessary to maintain proper barrier function.

However, these data need to be further validated, for example by measuring protein levels of VEGF within the MVECs as well as in the culture medium. Importantly, cell purity is critical for this and should be confirmed at the time of the experiment, for example by staining a fraction of the cells for an endothelial-specific marker such as VE-Cadherin. Lung MVEC in particular are prone to contamination by fibroblasts, since they may adhere to EC during the bead-based purification step. Throughout this thesis, all experimental wells were visually inspected for such contamination, since fibroblasts are morphologically easily distinguishable from ECs; if fibroblasts were found, the cells were discarded. However, since fibroblasts express very high levels of VEGF, even a small contamination could have led to the difference in VEGF abundance seen in these experiments. Yet, the persistence across biological replicates and O_2 conditions makes this somewhat unlikely.

These data highlight the importance of oxygen availability for endothelial cell physiology and plasticity. Baseline gene expression as well as the hypoxia response of both brain and lung MVEC were considerably altered by O_2 availability during expansion. This shows that ECs are to a large extent reprogrammable by environmental priming. On the other hand, brain and lung MVEC maintained differences even after several weeks of *in vitro* culturing under the same conditions, confirming that these two vascular beds are indeed intrinsically different and not simply a product of their *in vivo* environment. This chapter also suggests several new avenues of research, such as the differential expression of HIF isoforms and VEGF in brain and lung MVECs.

Table 3-1: Summary of previously published protocols for the isolation of brain MVECs and the resulting protocol used in this thesis

	Coisne et al., 2005	**Ruck et al., 2014**	**Watson et al., 2013**	**Welser-Alves et al., 2014**	**Final protocol**
Model organism	Mouse	Mouse	Rat	Mouse	Mouse
Brain parts removed by dissection	cerebellum, striatum, optic nerves and brain white matter	brain stem, cerebellum and thalamus	brain stem, cerebellum, mid-brain white matter and choroid plexus	n/a	Brain stem, olfactory bulb, cerebellum, brain white matter
Removal of meninges	Cotton swabs	Rolling on Whatman paper	Rolling on Whatman paper	n/a	Rolling on Whatman paper
First digestion	n/a	Collagenase CLS2, DNase I (1 h)	Collagenase/ dispase, DNase I (30 min)	Papain, DNase I (70 min)	Collagenase A, DNase I (1 h)
First density centrifugation	30% Dextran, 3000x *g*, 25 min	20% BSA, 1000x *g*, 20 min	22% BSA, 1000x g, 15 min	22% BSA, 1360x *g*, 10 min	20% BSA, 1000x *g*, 10 min
Size filtration	60 μM mesh	n/a	n/a	n/a	70 μM mesh
Second digestion	Collagenase/ dispase, DNase I (30 min)	Collagenase/ dispase, DNase I (1 h)	Collagenase/ dispase, DNase I (15 min)	n/a	Collagenase/ dispase, DNase I (30 min)
Second density centrifugation	n/a	Percoll, 700x g, 10 min	n/a	n/a	n/a
Puromycin selection	n/a	8.5 μM for 2 days	3 μM for 7 days	8.5 μM for 2.5 days	8.5 μM for 3 days

3.4 Materials and methods

3.4.1 MVEC growth medium

The growth medium for both lung and brain MVECs is composed of a 1:1 mixture of low-glucose DMEM (Gibco) and F12 HAM nutrient mixture (Sigma), buffered with 20 mM HEPES (Gibco), and supplemented with 1% nonessential amino acids (Sigma), 2 mM sodium pyruvate (Gibco), 20% FBS (Gibco), 75 µg/mL endothelial cell growth supplement (Sigma), and 100 µg/mL heparin (Sigma).

3.4.2 Collagen coating of cell culture plates

Collagen, type I, solution from bovine skin (3 mg/mL, Sigma) was diluted 1:10 in H_2O and added to cell culture wells (1 mL/well of a 6-well plate, 400 µL/well of a 12-well plate, 30 µL/well of a 96 well plate). The plates were placed at 37 ˚C for 2 h. Then, the remaining solution was removed, and the wells were washed twice with PBS. All plates were coated immediately before use.

3.4.3 Isolation of brain MVECs

Brain MVECs were isolated as described previously (Coisne *et al.*, 2005; Watson *et al.*, 2013b; Ruck *et al.*, 2014; Welser-Alves *et al.*, 2014), with modifications (Table 3-1). The brains of 4-6 male C57BL6/J mice, aged 6-8 weeks, were excised and stored in DMEM on ice. The olfactory bulbs, cerebellum, and mid-brain white matter were surgically removed. The remaining cortical tissue was rolled on sterile filter paper to remove outer vessels and meninges. The tissue was then transferred to a digestion solution composed of 2 mg/mL collagenase A (Roche) and 10 µg/mL DNase I (Roche) in DMEM and incubated on a shaker at 37 ˚C for 1 h. The digested tissue was pelleted at 290 *x g* and resuspended in 20% BSA (w/v) in DMEM. The suspension was centrifuged for 10 min at 1000 *x g* to separate the vessel pellet from the buoyant myelin fraction. The pellet was resuspended in DMEM and filtered through a 70 µM nylon mesh, to remove large vessel fragments. The filtrate was then pelleted at 290 *x g* and resuspended in a digestion mix containing 2 mg/mL collagenase/dispase (Roche) and 10 µg/mL DNase I in DMEM and incubated on a shaker at 37 ˚C for 30 min. The microvessel fragments were pelleted at 290 *x g*, washed once in DMEM, resuspended in MVEC growth medium supplemented with 4 µg/mL puromycin (Sigma) and plated on cell culture plates precoated with collagen I. Puromycin was maintained in the culture medium for the first 4 days to inhibit growth of non-endothelial cells.

3.4.4 Verification of brain MVEC identity by immunocytochemistry

Brain MVECs were plated on sterile glass chamber slides precoated with collagen I and grown to confluence. The cells were then fixed with 4% paraformaldehyde in PBS for 20 min at 4 ˚C and permeabilised with 0.5% Triton-X100 in PBS for 5 min at room temperature. Blocking was carried out for 1 h at room temperature using GeneTex protein blocking reagent. Primary antibody incubation occurred over night at 4 ˚C, secondary antibody at room temperature for 1 h (Table 3-2). Slides were mounted using ProLong Diamond Antifade with DAPI (ThermoFisher).

Table 3-2: Antibodies used for Immunocytochemistry

Antibody target (host)	**Supplier**	**Catalog number**	**Dilution**
Mouse VE-Cadherin (goat)	R&D Systems	AF1002	1:50
Goat IgG (donkey), conjugated with Alexa Fluor 488	Invitrogen	A-11055	1:100

3.4.5 Isolation of lung MVECs

Lung MVECs were isolated from male C57BL6/J mice as described in section 2.4.11 The cells were plated on cell culture plates precoated with collagen I.

3.4.6 Cell culture and hypoxia treatment

Brain and lung MVECs were grown in atmospheres containing 5% CO_2 and either ambient, 10% or 5% O_2 – corresponding to *in vivo* levels in lung and brain microvasculature, respectively (Dings *et al.*, 1998; Wild *et al.*, 2005; Miller *et al.*, 2010). The O_2 levels in the ambient tissue culture incubator were not controlled but are estimated to be approximately 18.5% (Wenger *et al.*, 2015). All media changes were carried out using medium that had been pre-equilibrated with the appropriate oxygen concentration for 12 h. All hypoxia experiments were carried out in an atmosphere containing 5% CO_2 and 1% O_2 at 37 ˚C, with controlled humidity, using either a Ruskinn Sci-Tive or a Whitley H35 HEPA hypoxystation. Cells received fresh medium at the start of the hypoxia treatment, which had been pre-equilibrated for 24 h. All pre-incubation times corresponded to the reported diffusion time of oxygen out of a stationary solution (Newby *et al.*, 2005).

3.4.6 Viability time course using Propidium Iodide

Brain and lung MVECs were grown to 90% confluence before being transferred to 1% O_2. At each timepoint, cells were washed once in PBS, detached using 0.25% trypsin, and resuspended in fresh media. All reagents used had been pre-equilibrated to 1% O_2. Cell viability was assessed using an Adam-MC automated cell counter (NanoEnTek) according to manufacturer's instructions. Cells were incubated with either a total cell stain, containing PI and a lysis agent, or with a non-viable cell stain, containing only PI. Viability was measured as a percentage of non-viable cells compared to total cell number.

3.4.7 Real time viability assay

Real time viability was assessed using the RealTime-Glo^{TM} MT Cell Viability Assay (Promega) according to manufacturer's instructions. 3000 cells were plated one day before the start of the assay on white 96-well plates coated with collagen I. Immediately before the start of the assay, MT Cell Viability Substrate and NanoLuc enzyme were added to growth medium pre-equilibrated to the appropriate oxygen level. The growth medium in the assay plate was replaced with this medium containing the assay components. Luminescence was read every 10 min over 48 h, using a FLUOstar Omega plate reader set to 37 ˚C, 5% CO_2, and the appropriate oxygen level using an Atmospheric Control Unit (BMG Labtech).

3.4.8 RT-qPCR

Brain and lung MVECs were grown to 90% confluence. The cells were then either transferred into a hypoxia chamber containing 1% O_2 or maintained at the same oxygen concentration. RNA was isolated using the RNeasy isolation kit (Qiagen) according to manufacturer's instructions. cDNA was synthesised from 1 μg of RNA using SuperScript III reverse transcriptase (Invitrogen) according to manufacturer's instructions. All transcript levels were measured in triplicates and normalised to b–ACTIN; fold-changes were calculated in relation to the 4 h baseline reading. Primer and probe sequences are shown in Table 3-3. Negative controls without RNA and without reverse transcriptase were run with every plate.

Table 3-3: Primer and probe sequences used in qPCR

b-ACTIN	FWD	AGA GGG AAA TCG TGC GTG AC
	REV	CAA TAG TGA TGA CCT GGC CGT
	Probe	[`FAM] CACTGCCGCATCCTCTTCCTCCC [TAMRA]
PGK	FWD	CAA ATT TGA TGA GAA TGC CAA GAC T
	REV	TTC TTG CTG CTC TCA GTA CCA CA
	Probe	[~FAM] TAGCTCGACCCACAGCCTCGGCATAT/BHQ_/

GLUT1	FWD	GGG CAT GTG CTT CCA GTA TGT
	REV	ACG AGG AGC ACC GTG AAG AT
	Probe	[~FAM] CAACTGTGCGGCCCCTACGTCTTC [BHQ]
BNIP3	FWD	GCA GGG CTC CTG GGT AGA A
	REV	GAC GGA GGC TGG AAC GCT
	Probe	[~FAM] TGCACTTCAGCAATGGCAATGGGA [BHQa-Q]
VEGF-A	FWD	TGA AGC CCT GGA GTG CGT
	REV	AGG TTT GAT CCG CAT GAT CTG
	Probe	[~FAM] CCCACGTCAGAGAGCAACATCACCA [BHQa-Q]
LDH-A	FWD	TGT CTC CAG CAA AGA CTA CTG T
	REV	GAC TGT ACT TGA CAA TGT TGG GA
	Probe	SYBR Green
ARG2	FWD	ACC AGG AAC TGG CTG AAG TG
	REV	TGA GCA TCA ACC CAG ATG AC
	Probe	SYBR Green
HIF-1a	FWD	GGTGCTGGTGTCCAAAATGTAG
	REV	ATGGGTCTAGAGAGATAGCTCCACA
	Probe	[~FAM] CCTGTTGGTTGCGCAGCAAGCATT [36-TAMSp]
HIF-2a	FWD	GTCCGAAGGAAGCTGATGG
	REV	TCTATGAGTTGGCTCATGAGTTG
	Probe	[~FAM] CCACCTGGACAAAGCCTCCATCAT [36-TAMSp]

3.4.9 Western blot analysis

Brain and lung MVECs were grown to 90% confluence. The cells were then either transferred into a hypoxia chamber containing 1% O_2 or maintained at the same oxygen concentration in which they were cultured since isolation. In both cases, a media change was carried out at t = 0 using oxygen-equilibrated growth medium. This represents a slight change in methodology compared to chapter 2, necessitated by the inclusion of physioxic baseline conditions. In chapter 2, the growth medium given to the cells at the start of the hypoxia time course was not pre-equilibrated to 1% O_2, leading to a gradual decrease of oxygen in the well until equilibration with the surrounding air. The duration of this equilibration depends on the amount of O_2 initially present in the well and would have therefore been different for each of the three baseline conditions, effectively changing the timing of the hypoxia treatment. To avoid this, all media was pre-equilibrated to 1% O_2, leading to a quicker but simultaneous induction of hypoxia.

Cytoplasmic and nuclear protein was collected after the indicated times using NE-PER Nuclear and Cytoplasmic Extraction Reagents (Thermo-Scientific) according to manufacturer's instructions. Total protein was collected with RIPA buffer (Table 3-6). Protein

concentration was measured using a Pierce™ BCA Protein Assay Kit (Thermo Scientific). Unless specified otherwise, the amount of protein used per lane was 3 µg for nuclear protein and 20 µg for cytoplasmic and total protein; this was combined with 10x reducing agent (Invitrogen) and 4x sample buffer (Invitrogen). Samples were heated to 70 ˚C for 10 min proteins, separated on 3-8% tris-acetate gels (Invitrogen) or 4-12% Bis-Tris gels (Invitrogen) and subsequently transferred to PVDF membranes using semi-dry blotting cassettes (Power Blotter XL, ThermoFisher Scientific or Trans-Blot Turbo, Bio-Rad). The membranes were blocked in 5% milk in PBS-Tween 0.05% (PBST) for 1 h, probed with primary antibodies for 16 h at 4 ˚C (Table 3-4), washed 3x 5 min in PBST, probed with secondary antibodies for 1 h at room temperature (Table 3-5), and washed 3x 5 min in PBST. All antibodies were diluted in 2% milk in PBST. All secondary antibodies were HRP-conjugated and bands were visualised with Pierce ECL western blot substrate (Thermo Scientific). Quantification was performed with ImageJ.

Table 3-4: Primary antibodies used in western blots

Antibody target	**Supplier**	**Catalog number**	**Dilution**
HIF-1α	Novus Biologicals	NB100-449	1:1000
HIF-2α	R&D Systems	AF2997	1:500
FIH	Cell Signaling Technology	D19B3	1:1000
PHD1	Abcam	AB113077	1:1000
PHD2	Novus Biologicals	NB100-2219	1:500
PHD3	Novus Biologicals	NB100-303	1:1000
α-tubulin	Santa Cruz Biotechnology	sc-23948	1:2500
β-actin	Sigma-Aldrich	A1978	1:5000
GAPDH	Santa Cruz Biotechnology	sc-365062	1:5000
TATA-BP	Abcam	AB63766	1:1000
Vinculin	Cell Signaling Technology	E1E9V	1:2500
OXPHOS Rodent WB Antibody Cocktail	Abcam	110413	1:250

Table 3-5: Secondary antibodies used in western blots (all conjugated to HRP)

Antibody target (host)	**Supplier**	**Catalog number**	**Dilution**
Mouse IgG (donkey)	Santa Cruz Biotechnology	sc-2314	1:2000
Rabbit IgG (goat)	R&D Systems	HAF008	1:2000
Goat IgG (donkey)	Santa Cruz Biotechnology	Sc-2304	1:2000

Table 3-6: RIPA buffer recipe

Ingredient	**Stock**	**Final concentration**	**Vol. for 10 mL**
NaCl	5 M	150 mM	300 μL
Tris-HCl (pH 8.0)	1 M	10 mM	100 μL
EDTA	0.5 M	5 mM	100 μL
Sodium Deoxycholate	10%	0.5%	500 μL
Sodium Dodecyl Sulfate	20%	0.1%	50 μL
Triton X-100	/	1%	100 μL
H_2O			8.35 mL
Add to the appropriate volume immediately before using:			
PMSF	0.1 M	1 mM	100x
cOmplete protease inhibitor (Roche)	1 tablet/mL in H_2O		50x

3.4.10 Comparison of cytokines in MVEC media

Cytokine expression in MVEC media was analysed using the Mouse Cytokine Antibody Array, Panel A (R&D Systems), according to manufacturer's instructions. 500 μL of culture media were incubated for 1 h at room temperature with Mouse Cytokine Array Panel A Detection Antibody Cocktail. The anti-cytokine coated membranes were then incubated with media-antibody mix for 12 h at 4 ˚C, and subsequently with streptavidin-HRP for 30 min at room temperature. The signal was visualized with a Fusion FX imager (Vilber Lourmat) and quantified using ImageJ.

3.4.11 Scratch assays

MVECs were grown to 100% confluence in a 12-well plate. The cells were then treated for 2 h with Mitomycin (10 μM) or DMSO vehicle control in oxygen-equilibrated, serum-free growth medium to stop proliferation. A vertical scratch was applied to the plate using a P1000

tip to create a gap in the cell monolayer. The wells were washed twice with PBS to remove detached cells and incubated with fresh oxygen-equilibrated growth medium. A picture of each scratch was taken after 0, 2, 4, 8, 24, and 48 h. The area of the scratch was measured using ImageJ and normalised to the area at t = 0.

Acknowledgement

The qPCR data in this chapter is the result of collaborative work. I performed all the cell culture and hypoxia treatments, as well as RNA purification, cDNA synthesis and qPCR for all samples grown at STA and for the first replicate of cells grown at 5% and 10% O_2. Amanda Eakin performed RNA purification, cDNA synthesis, and qPCR for the second and third replicate of cells grown at 5% and 10% O_2.

Chapter 4: Metabolic effects of physioxia and hypoxia on brain and lung microvascular endothelial cells

4.1 Introduction

In the previous chapter, pre-conditioning microvascular endothelial cells (MVECs), at non-physiological oxygen levels was shown to have profound consequences on their physiology and on their ability to respond to hypoxia; this coincided with altered levels of the transcriptional master regulator HIF, both at baseline and following hypoxic challenge. One of the best described functions of HIF, in particular HIF-1α, is to initiate a metabolic rewiring, away from oxidative phosphorylation (OXPHOS) in favour of glycolysis (Semenza, 2011). This allows cells to maintain ATP homeostasis, while avoiding excessive production of reactive oxygen species (ROS), which would lead to large scale DNA and protein damage, and eventually cell death (Zhang *et al.*, 2008). Therefore, it is very likely that changes in oxygen availability over time will reprogram MVEC metabolism. As described previously, endothelial cells of all vessel types are generally described as being primarily glycolytic, rivalled in their metabolic preference only by cancer cells (Theodorou and Boon, 2018). A hyperoxia-induced decrease in HIF protein levels and thus glycolytic capacity, is likely to be particularly damaging to endothelial cells and may explain the lack of physiological plasticity exhibited by MVECs grown at STA (Chapter 3). Furthermore, endothelial metabolism is being increasingly recognised as a driver rather than a bystander of EC function (De Bock *et al.*, 2013; Rohlenova *et al.*, 2018; Theodorou and Boon, 2018). Therefore, this chapter explores the hypothesis that the effects of oxygen priming on MVEC survival and behaviour described in the previous chapter occurred as the result of metabolic reprogramming.

Catabolic cellular metabolism can be divided into two main categories, glycolysis and oxidative phosphorylation, and a number of techniques have been employed to measure the flux through these pathways. This includes the use of radioactive substrates (Neely *et al.*, 1972; Metallo *et al.*, 2009), measuring the flux through rate-limiting enzymes (Christofk *et al.*, 2008; Yi *et al.*, 2012), as well as measuring changes in the concentration of the substrates or products involved in these pathways (Lambert *et al.*, 2010; Sim *et al.*, 2018; Yang *et al.*, 2018); this chapter will rely heavily on the latter approach. The final product of glycolysis is lactate, which is excreted into the medium, causing a change in pH. Thus, extracellular acidification rate (ECAR) can be used as a measurement of glycolytic flux (Teslaa and Teitell, 2014). OXPHOS

on the other hand relies on oxygen as the final substrate of the mitochondrial electron transport chain (ETC). Therefore, the oxygen consumption rate (OCR) can be used to infer the flux through this pathway. Here, these parameters will be assessed with an Agilent Seahorse metabolic analyser, a system which simultaneously assesses ECAR and OCR in real time on a multi-well plate.

4.1.1 Metabolic stress tests

The Seahorse system uses metabolic stress tests to assess both basal and maximal metabolic rates for each pathway. It does so by injecting metabolic inhibitors into the assay medium and measuring the resulting changes to OCR and ECAR.

The glycolytic stress test consists of a series of three injections, which allow the measurement of non-glycolytic acidification, basal glycolytic rate and maximal glycolytic capacity (Fig. 4-1A,C). At the start of the assay, cells are starved of pyruvate and glucose, to minimise glycolytic activity, such that any acidification seen under these conditions is due to sources other than glycolysis. Glucose is then injected, allowing glycolysis to commence and leading to an increase in ECAR; the measurements following the addition of glucose thus represent the basal glycolytic rate. Oligomycin, an inhibitor of the mitochondrial ATP synthase, is injected after stabilisation of glycolytic activity. This stimulus shifts the energetic needs of the cell entirely onto glycolysis, since it prevents ATP formation via OXPHOS. Therefore, glycolysis is driven to full capacity. Finally, injecting 2-deoxy glucose (2-DG), a glucose analogue, stalls glycolytic activity by competitively inhibiting the first enzyme in the glycolytic pathway, hexokinase; ECAR then returns to the non-glycolytic levels measured at the beginning of the assay.

The mitochondrial stress test also consists of three successive injections of selective inhibitors to measure basal respiration rate, maximal respiration rate, proton leak, and non-mitochondrial oxygen consumption (Fig. 4-1B,C). Basal respiration rates are measured at the start of the assay and once these are determined, mitochondrial ATP production is blocked through the injection of Oligomycin. This stops ATP production in the mitochondria but does not prevent oxygen consumption *per se*, since the mitochondrial electron transport chain (ETC) is still active. The protons that are pumped into the intermembrane space may move back into the matrix through a route other than the ATP synthase, allowing oxygen to be consumed. The remaining OCR is therefore not coupled to ATP production and is termed proton leak. FCCP is added next and acts as a molecular shuttle for protons across the mitochondrial membrane, collapsing the proton gradient. As a result, electron flow through the ETC and thus oxygen

consumption is maximised, and we can quantify maximal respiratory capacity. Finally, two inhibitors of the electron transport chain, rotenone (complex I) and antimycin A (complex III) are injected into the assay wells, shutting down mitochondrial oxygen consumption by stopping electron transport and shuttling through the ETC. Any residual OCR observed is due to non-mitochondrial sources.

4.2 Results

4.2.1 Optimising the Seahorse Metabolic Stress Test

Seahorse metabolic stress tests require optimisation of the cell number. According to the manufacturer, the assay well should not be more than 90% confluent (Agilent Learning Center, 2019). This was empirically determined to lie at $3.0x10^4$ for XFe24 assay plates and $1.2x10^4$ cells for XFe96 assay plates.

OCR readings are only valid if the wells do not experience anoxia during the assay, as this would yield a lower apparent oxygen consumption rate (Fig. 4-2A). Therefore, the cell number needed to be further refined for mitochondrial stress tests in hypoxia. Anoxia was determined by analysis of the raw oxygen levels within in each well, as recommended by the manufacturer (agilent.com). Thus, all hypoxia assays were carried out with 3 different seeding densities: $1x10^4$, $8x10^3$, $5x10^3$. For assays at 10% and 5% O_2, reducing the cell number to $8x10^3$ was sufficient, whereas for assays at 1% O_2, $5x10^3$ cells were used. This lower number also accounted for further proliferation during the 24h hypoxia incubation period, shown previously (Figure 3-5A)

The assay was further validated by performing single drug control experiments, to determine the toxicity of the inhibitors. OCR and ECAR measurements stayed constant for the remainder of the assay, indicating a healthy and metabolically active cell population following each drug injection (Fig. 4-2B). Furthermore, after assay completion, the total protein content in blank, single drug control, and assay wells were comparable, showing that no significant amount of cells detached or died due to the treatments (not shown).

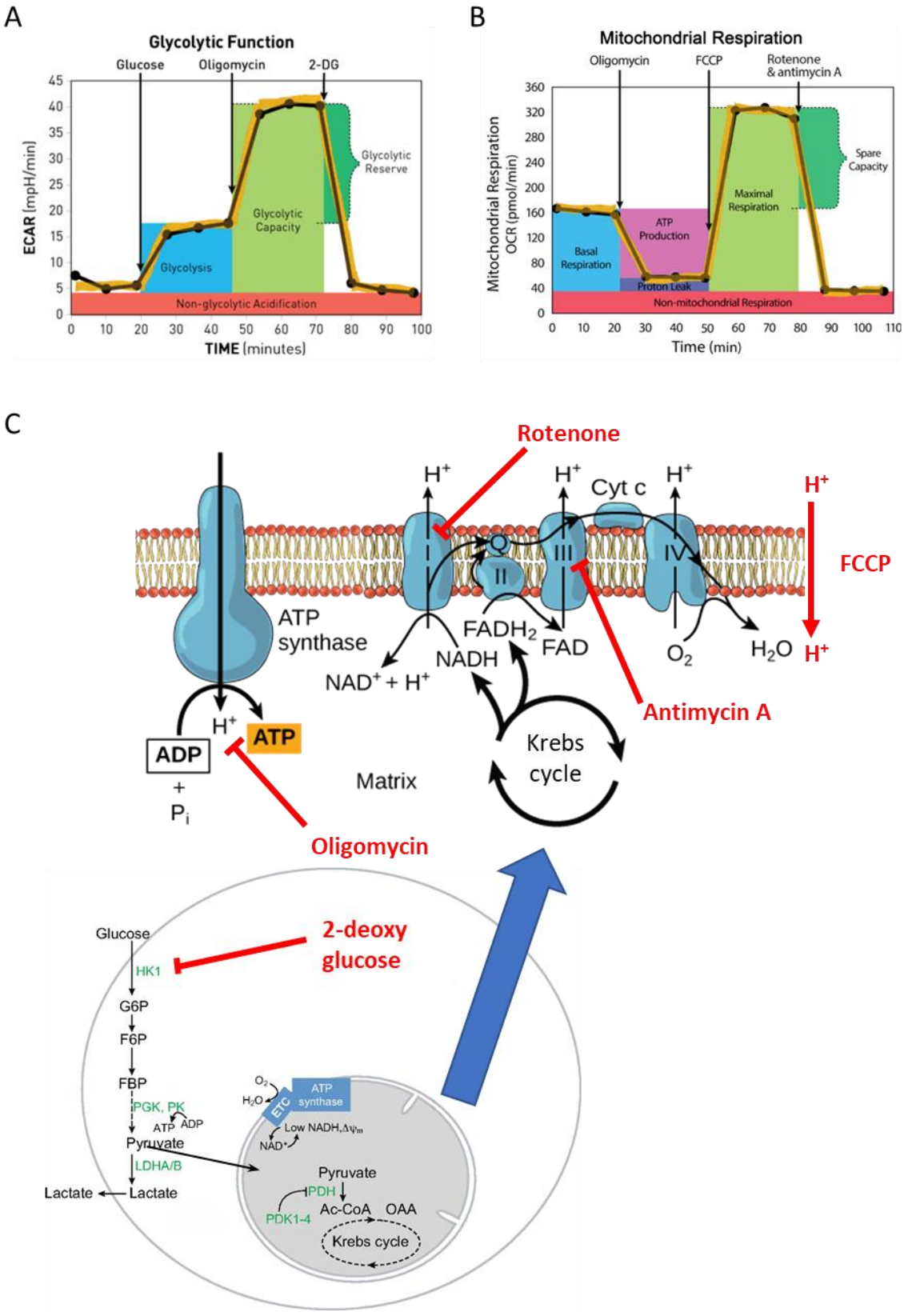
A
Glycolytic Function
Glucose
Oligomycin
2-DG
ECAR (mpH/min)
Glycolysis
Glycolytic Capacity
Glycolytic Reserve
Non-glycolytic Acidification
TIME (minutes)
B
Mitochondrial Respiration
Oligomycin
FCCP
Rotenone & antimycin A
Mitochondrial Respiration OCR (pmol/min)
Basal Respiration
ATP Production
Proton Leak
Maximal Respiration
Spare Capacity
Non-mitochondrial Respiration
Time (min)
C
Rotenone
ATP synthase
NADH
NAD+ + H+
FADH2
FAD
Cyt c
FCCP
Antimycin A
ADP
+
Pi
ATP
Matrix
Krebs cycle
Oligomycin
2-deoxy glucose
Glucose
HK1
G6P
F6P
FBP
PGK, PK
Pyruvate
LDHA/B
Lactate
ETC
ATP synthase
Low NADH, Δψm
Pyruvate
PDH
PDK1-4
Ac-CoA
OAA
Krebs cycle

Figure 4-1

Figure 4-1: Seahorse metabolic stress tests
(A,B) Schematic of Seahorse glycolytic (A) and mitochondrial (B) stress tests, displaying the injections that are used to measure basal and maximal activation of each pathway (Schematics from agilent.com)
(B) Schematic displaying the targets of the inhibitors used in the stress tests displayed in (A) and (B). 2-deoxy glucose inhibits the first enzyme of the glycolytic pathway, hexokinase. Oligomycin inhibits the mitochondrial ATP synthase, thus also preventing O_2 consumption due to a buildup of protons in the intermembrane space which stalls the ETC. FCCP disperses the proton gradient across the inner mitochondrial membrane, uncoupling O_2 consumption from ATP production. Rotenone and Antimycin A block ETC complexes I and III, respectively, leading to the shutdown of the chain.
Figure adapted from Shyh-Chang *et al.* (2013) and OpenStax, Biology (2015)

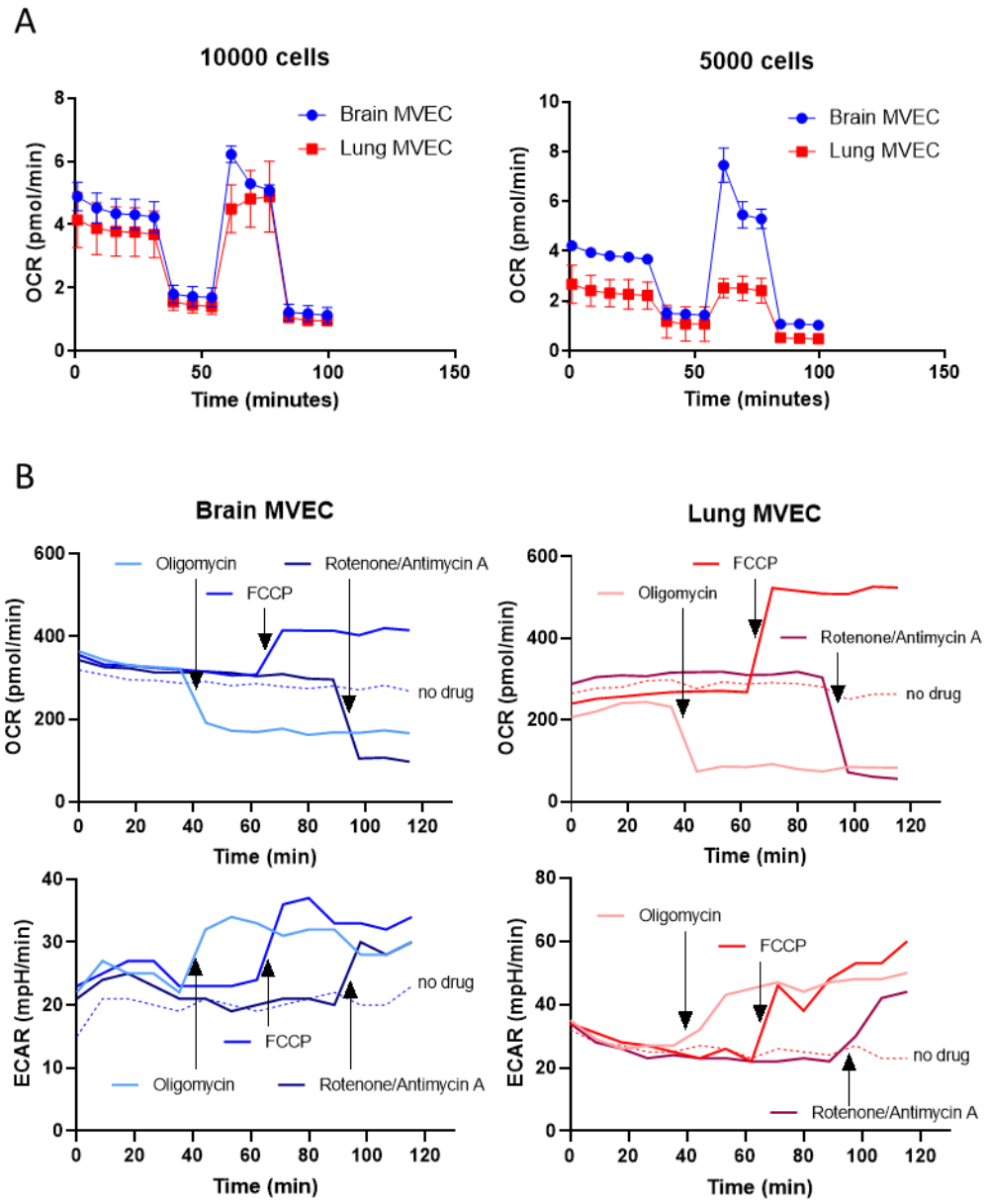

Figure 4-2: Optimisation steps for reliable use of Seahorse metabolic stress tests
(A) Mitochondrial stress tests in hypoxia require optimisation of cell number to avoid anoxia. The two panels show the same experiment carried out at 1% O_2 with 10,000 and 5,000 cells per well. The higher cell number leads to anoxia in brain MVEC, artificially limiting the OCR readings and abolishing the difference between the two cell lines.
(B) Single inhibitor controls to test for cell death during the assay; none of the drugs lead to a consistent decrease in OCR or ECAR in either cell type

4.2.3 Oxygen levels in culture determine the metabolic phenotype of MVECs

Lung and brain MVECs alike displayed the highest basal glycolytic rates if cultured at 5% O_2 (Fig. 4-3A, right panel, and Fig. 4-3C) while the same parameter was considerably lower in cells exposed to STA. Lung MVECs grown in their physioxic 10% O_2 already displayed some increase in basal glycolysis compared to STA, while brain MVECs did not. This may be reflective of their respective *in vivo* oxygen levels, since 10% O_2 is likely hyperoxic for the brain. In fact, the basal glycolytic rates of brain and lung MVECs cultured at their respective physiological oxygen level, 5% and 10% O_2 respectively, were equal. The maximal glycolytic rates showed a similar pattern, higher in cells grown at lower oxygen, but they were not significantly different between brain and lung MVECs grown at the same oxygen level (Fig. 4-3C). This observation further substantiates the premise that hyperoxygenation reduces the ability to upregulate glycolysis, even in the absence of mitochondrial respiration. Therefore, MVECs grown at lower O_2 levels yield both increased maximal glycolytic rates as well as increased viability during hypoxia (Fig. 3-5A); indeed, the differences in glycolytic potential may be the cause behind the differences in viability. Interestingly, glycolytic spare capacities were higher in brain MVECs compared to lung MVECs for each condition, however the differences were not statistically significant.

Conversely, mitochondrial basal and maximal respiration rates in both cell populations were directly correlated with oxygen levels (Fig. 4-3B,D); cells grown at STA displayed the highest OCR, followed by 10% O_2, and 5% O_2. Thus, unsurprisingly, with decreasing O_2 availability MVECs shifted their metabolic preference from mitochondrial respiration to glycolysis. Crucially, the decrease in maximal mitochondrial respiration at lower oxygen levels was considerably more pronounced in lung MVECs. As a result, the maximal OCR of lung MVECs grown at STA was higher than that of brain MVECs under those conditions, whereas at 10% O_2 there was no difference between the two populations, and, most interestingly, at 5% O_2 the trend was reversed (Fig 4-3B, right panel). This shows that brain MVECs are less glycolytic than lung MVECs at physiological O_2, and also maintain more of their mitochondrial spare capacity.

Having assessed the metabolic phenotype of both MVECs at baseline, changes in these parameters following adaptation to hypoxia were assessed. To achieve this, cells were exposed to 1% O_2 for 24h prior to the assay, to allow metabolic reprogramming to be established. Brain MVEC displayed similar basal and maximal glycolytic rates irrespective of O_2 priming conditions (Fig 4-4C).

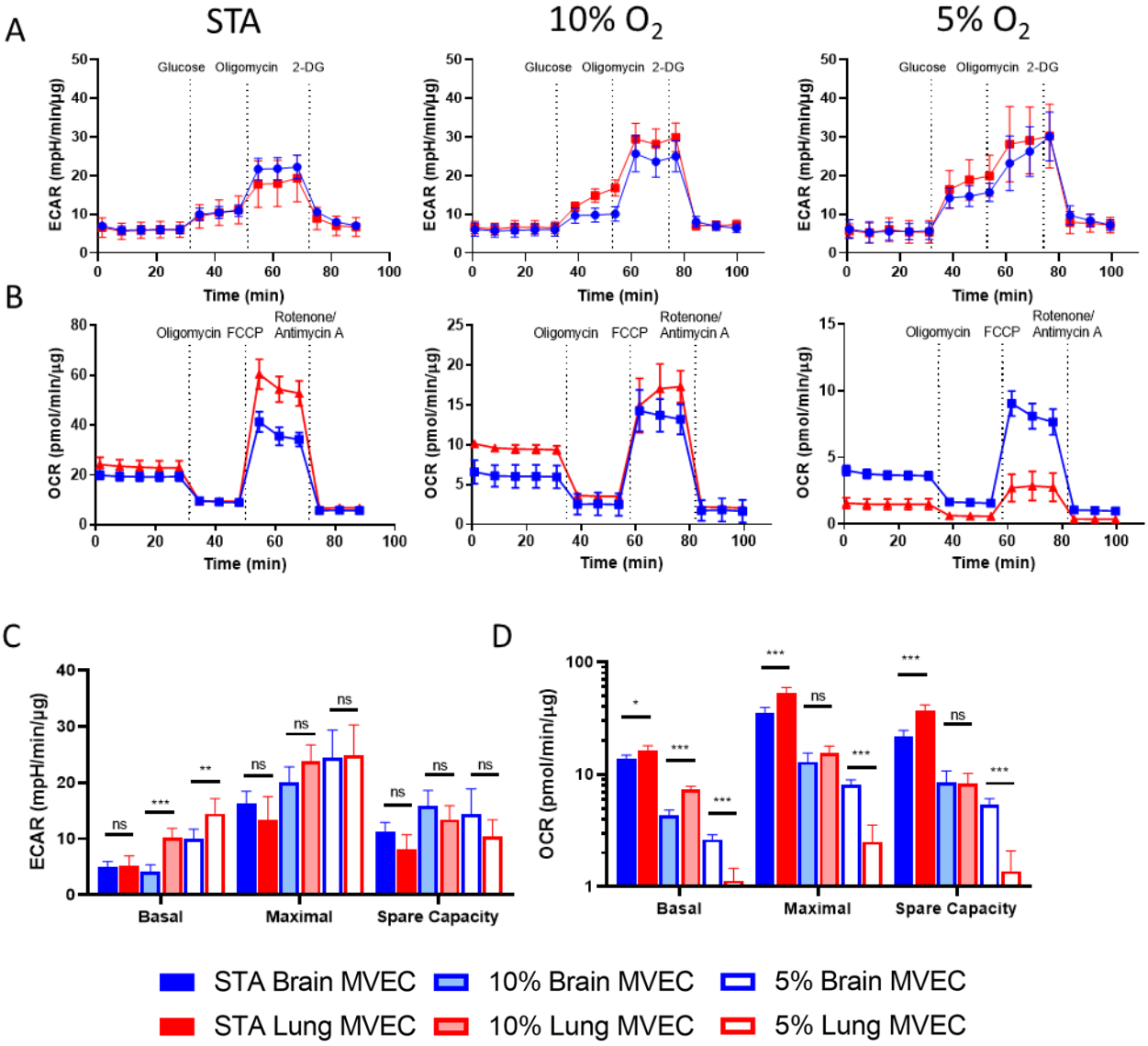

Figure 4-3: Baseline metabolic profile of brain and lung MVECs is dependent on oxygen availability

(A,B) Glycolytic (A) and mitochondrial (B) stress tests of brain and lung MVECs, cultured at STA, 10% O_2, or 5% O_2. ($n \geq 6$)

(C,D) Summaries of the stress tests displayed in A and B, using the parameters defined in Fig. 4-1A

Error bars show SD, statistical analysis using 2-way ANOVA (C) or multiple t-tests (D) with Holm-Sidak's multiple comparison test (*$p<0.05$, **$p<0.01$, ***<0.001)

Lung MVECs on the other hand maintained the inverse correlation between oxygen level and glycolytic rates seen at baseline, i.e. prior to the hypoxia challenge. Indeed, the basal glycolytic rate of lung MVECs was lower than that of the brain if the cells had been grown at STA, equal if the cells had been grown at 10% O_2, and higher if the cells had been grown at 5% O_2 (Fig. 4-4C). Furthermore, hypoxic lung MVECs displayed a much smaller glycolytic spare capacity following 24 h of hypoxia than brain MVEC, irrespective of the original culture conditions. This suggests that 1% O_2 represents a more severe hypoxic challenge to lung MVEC, causing them to use glycolysis almost to its full potential, whereas brain MVEC retain more glycolytic spare capacity. Indeed, brain MVEC are much more likely to encounter such low levels of oxygen *in vivo*.

Mitochondrial basal and maximal respiration rates in MVECs from all three culture conditions were similarly reduced to comparable levels after 24 h in hypoxia (Fig. 4-4D). The decrease in maximal respiration was in all cases more severe in lung than in brain MVECs. Brain MVECs previously cultured at 5% O_2 maintained their higher maximal respiration rate compared to lung MVECs (Fig. 4-3B and Fig 4-4B, left panels following FCCP injection).

A similar trend was observed in MVECs originally grown at 10% O_2 (Fig. 4-3B and Fig. 4-4B, middle panels following FCCP injection); while there was no difference in maximal respiration between the two cell populations at baseline, after 24 h at 1% O_2 brain MVECs maintained a higher maximal OCR than those from lung. These differences in maximal respiration emerged since hypoxic lung MVECs originally cultured at 5% or 10% O_2 maintained essentially no mitochondrial spare capacity after 24 h at 1% O_2 (Fig. 4-4D, right group), while brain MVECs did.

Lung and brain MVECs previously cultured at STA on the other hand showed no differences in maximal respiration after 24 h at 1% O_2; at baseline lung MVECs had displayed a higher value (Fig 4-3B and Fig 4-4B, left panels following FCCP injection). Therefore, lung MVECs from all three baseline conditions showed a more pronounced decrease in maximal respiration after 24 h at 1% O_2 than brain MVEC. Intriguingly however, lung MVECs grown at STA did maintain some respiratory spare capacity after being exposed to hypoxia, in contrast to the same cells cultured at 10% or 5% O_2 (Fig 4-4D, right group, red columns). Of note, in the experiment using cells originally cultured at 5% O_2, the maximal OCR of brain MVECs was actually somewhat underestimated, since it proved impossible to measure without exhausting the oxygen in the well.

Overall, these data suggest that brain MVEC mitochondria are more active at lower oxygen levels than their lung counterparts. However, this plasticity is lost when cells are

continuously exposed to high oxygen levels, since no difference in maximal respiration was observed between MVECs previously grown at STA.

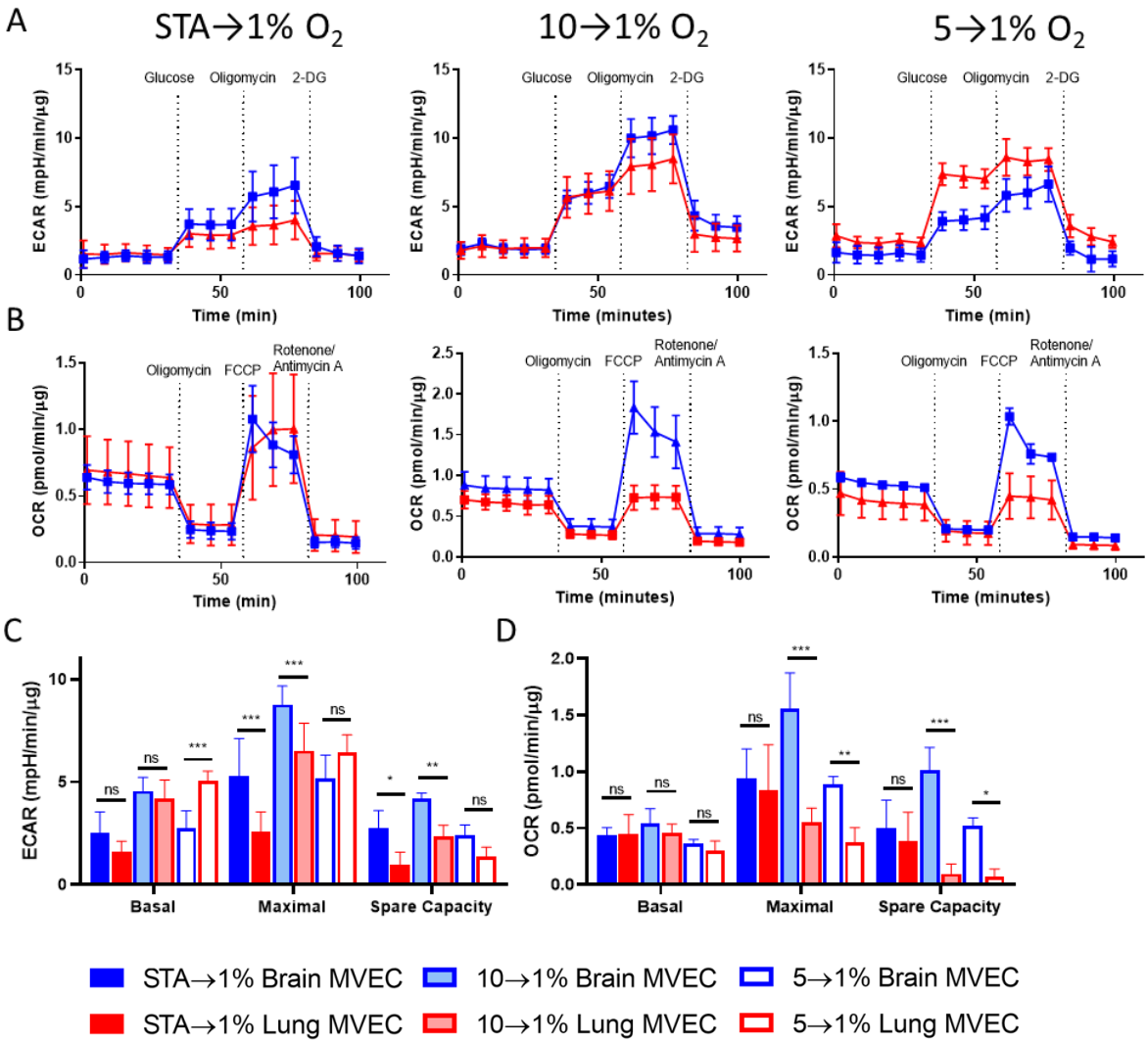

Figure 4-4: Hypoxia-induced metabolic shift of MVEC is dependent on oxygen priming
(A,B) Glycolytic (A) and mitochondrial (B) stress tests of brain and lung MVECs, cultured at STA, 10% O_2, or 5% O_2 and transferred to 1% O_2 for 24 h before the assay; assays were carried out at 1% O_2 ($n \geq 4$)
(C,D) Summaries of the stress tests displayed in A and B, using the parameters defined in Fig. 4-1A
Error bars show SD, statistical analysis using 2-way ANOVA with Holm-Sidak's multiple comparison test (*$p<0.05$,**$p<0.01$, ***<0.001)

4.2.4 Upregulation of glycolysis during hypoxia is shaped by environmental O_2

Following the characterization of the metabolic profiles of each MVEC population at baseline and after 24 h at 1% O_2, the real-time metabolic shift underlying the adaptation to hypoxia was assessed. This was necessary to capture the effect of HIFs on metabolism, since their induction during hypoxia is rapid but transient, and after 24h at 1% O_2 HIF protein expression is largely lost (Fig. 3-7). To achieve this, cells were plated in Seahorse assay plates and left to attach under baseline conditions while the metabolic analyser and assay medium were equilibrated to 1% O_2. ECAR measurements were started immediately following the change to assay medium and were carried out every 10 minutes over a period of 24 h, without any injections, giving a real-time measurement of the cells' metabolic shift to glycolysis.

Brain MVECs grown at ambient O_2 displayed an increase in ECAR upon hypoxia exposure, but the rate of ECAR increase was faster in lung MVECs, leading to an earlier and larger peak, indicative of increased ability to upregulate glycolysis (Fig. 4-5A, left panel). A similar response pattern was seen in cells grown at 10% O_2, albeit to substantially higher levels than those seen when cells were primed in STA (middle panel). It is noteworthy that the ECAR of lung MVECs at the start of this time course was already considerably higher than if cultured at STA, confirming the correlation between low oxygen and higher glycolytic rates shown in Fig. 4-3.

MVECs grown at 5% O_2, on the other hand, displayed a radically different pattern: the ECAR of both lung and brain MVECs at the start of the time course were again elevated compared to 10% O_2 and STA, but in this pre-condition (physiological for brain tissue), brain MVECs showed a sharp and quick increase in ECAR, more than three-fold the value obtained with cells grown at 10% O_2 (Fig. 4-5A, right panel). When cultured in 5% O_2, brain MVEC triggered glycolysis faster and to a strikingly higher level than those obtained from lung, in which no further increase was observed, suggesting that lung MVEC are operating at their maximal glycolytic potential when cultured at 5% O_2 and thus can increase it no further when moved to 1% O_2.

These observations are partially consistent with the HIF data presented in Fig. 3-9B. Brain MVECs showed a consistent fold-change in HIF-1α across all three conditions, whereas HIF-2α induction was higher at lower O_2. Therefore, the overall HIF change was the highest in brain MVECs pre-conditioned at 5% O_2 and lowest at STA, which is also reflected in Fig. 4-3.

In lung MVEC, hypoxia-induced increase in HIF-1α protein levels was smaller in cells preconditioned at lower O_2, whereas HIF-2α stabilisation was not very pronounced under any condition. This is also reflected by the lack of ECAR increase in lung MVECs moved from 5% to 1% O_2 (Fig. 4-5A, right panel). However, lung MVECs grown at STA only displayed a small increase in ECAR upon transfer to hypoxia (left panel), despite showing the greatest fold-change in HIF abundance (Fig. 3-9B). This may be explained by the presence of higher levels of FIH in these cells (Fig. 3-10B), since this hydroxylase only affects HIF activity but not its abundance. FIH also has a higher affinity for O_2 than PHDs, perhaps allowing it to maintain some activity even at 1% O_2 (Ehrismann *et al.*, 2007).

To further investigate the dependence of the two different MVEC populations on glucose metabolism, and how this may differ as a result of their external environment, glucose uptake in MVECs grown under each culture condition was quantified, at baseline as well as over time after transfer to hypoxia.

Unlike what was seen for ECAR, lung MVEC glucose uptake rate was not significantly altered by expansion in different oxygen levels (Fig. 4-5B). However, the basal glucose uptake rate in brain MVEC grown at 5% O_2 was significantly higher compared to cells grown in higher oxygen concentrations (Fig. 4-5C). When exposed to hypoxia, brain MVEC maintained in physiological oxygen levels (10% or 5% O_2) showed a swift and pronounced upregulation of glucose uptake, seen as early as 2 h, and further increased after 4 h, before reaching a plateau level, seen at 8 h. Lung MVECs grown at 5% or 10% O_2 similarly upregulated glucose uptake at 2 h, reaching a plateau quickly and maintaining this rate throughout the duration of the experiment with no further increase. Overall, the change in glucose uptake rate was larger in brain compared to lung MVECs in both conditions.

As pre-empted by the observations made thus far, both MVEC populations cultured at STA were less responsive to hypoxia in terms of increasing glucose uptake: MVEC obtained from lung significantly increased glucose uptake only after 4 h of exposure to hypoxia, whereas in MVEC from brain the effect was even further delayed and less pronounced, with a marginal increase seen only after 8 h (Fig. 4-5B, left panel). Interestingly, brain MVEC cultured at all oxygen conditions displayed significantly higher baseline rates of glucose uptake than their lung counterparts. This may reflect the physiological role of brain microvasculature to actively shuttle glucose from the blood and to neural tissue (Duelli and Kuschinsky, 2001).

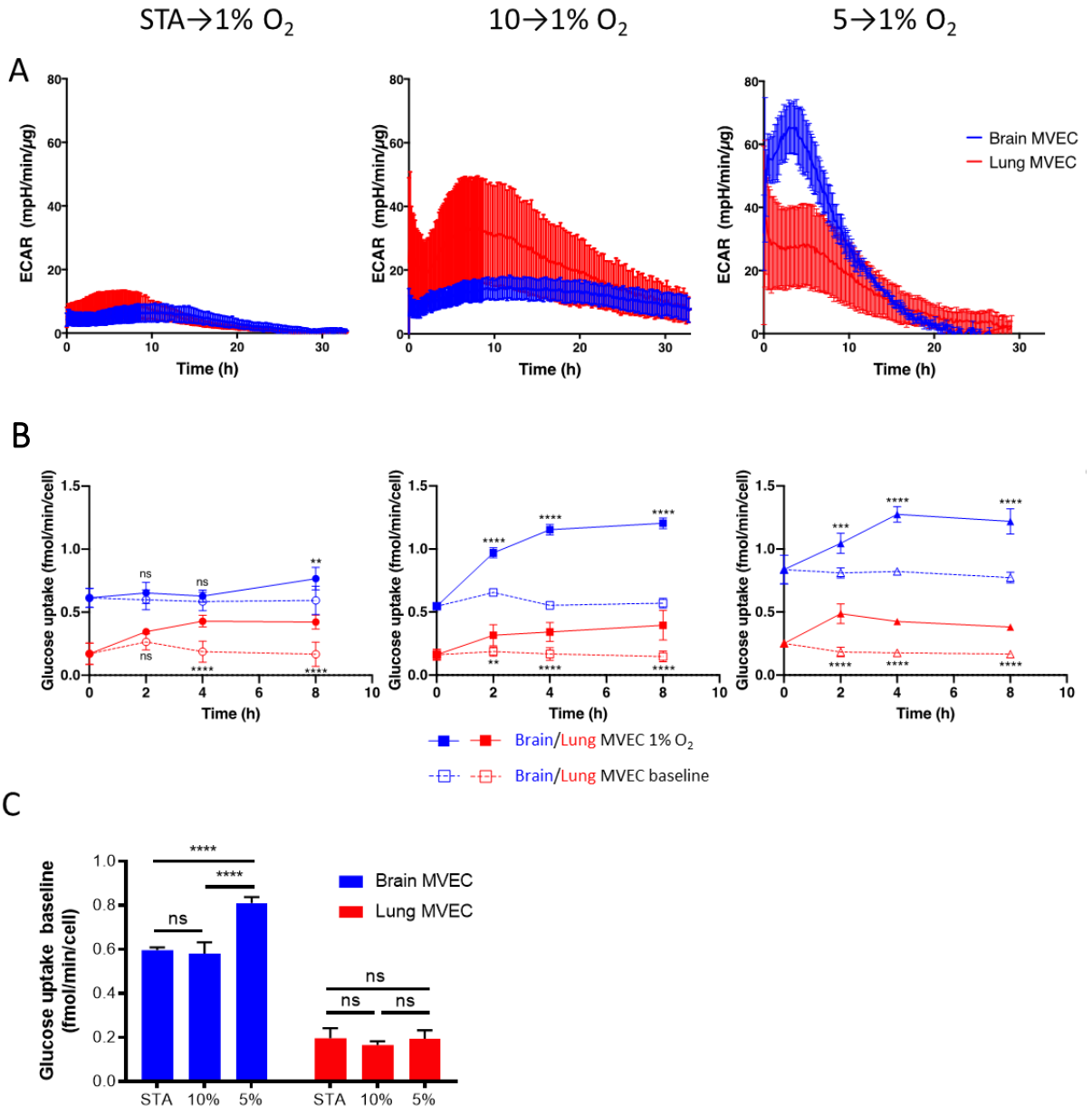

Figure 4-5: Real-time metabolic shift upon exposure to hypoxia

(A) MVECs primed at different atmospheres were transferred to 1% O_2 at t=0 and the hypoxia-induced increase in ECAR was measured in real time; the cells had been grown at either STA (left), 10% O_2 (middle), or 5% O_2 (right). (n≥4)

(B) Brain and lung MVECs were grown under different oxygen levels and either maintained under the same conditions (dashed line) or exposed to hypoxia (solid line). Glucose uptake was measured at the indicated times using the Glucose Uptake-Glo assay (Promega) (n≥3)

(C) Baseline glucose uptake rate of brain and lung MVECs grown at different O_2 tensions (n≥3)

Error bars show SD, statistical analysis using 2-way ANOVA with Holm-Sidak's multiple comparison test (**p<0.01, ***<0.001, ****p<0.0001)

To confirm that the increased hypoxic viability of MVECs grown at lower oxygen levels shown in the previous chapter was indeed due to increased glycolytic potential, the same viability assays shown in Fig. 3-5A were performed in the presence of 10 mM 2-DG, a competitive inhibitor of glycolysis (Fig. 4-6). Treatment with 2-DG reduced the viability of both brain and lung MVEC in hypoxia, for all conditions, eliminating the advantage derived from lower baseline oxygen levels; in other words, and not surprisingly, removal of the ability to use glucose for cellular energetic demands under oxygen deprivation resulted in arrest of proliferation, irrespective of the glycolytic reserve of each cell type or culture condition.

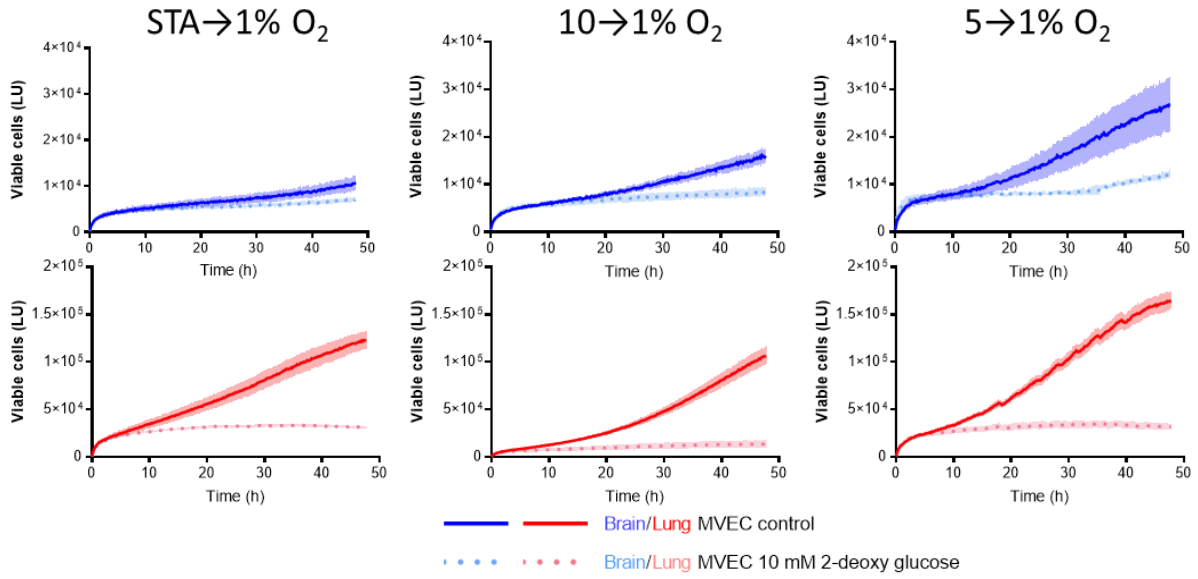

Figure 4-6: Glycolysis is essential for physioxia-induced viability advantage during hypoxia
Real-time viability of brain (top) and lung (bottom) MVECs grown at STA (left), 10% O_2 (middle), or 5% O_2 (right); at t=0 cells were transferred to 1% O_2 and treated with 10 mM 2-deoxy glucose or PBS vehicle control. Viability was assessed every 10 min using a Real-Time Glo assay (Promega). (Error bars show SD, n=6 for each condition)

4.2.4 Environment oxygen levels during cell expansion change the relative proportion of components of the mitochondrial electron transport chain

Having investigated the effects of varying oxygen levels on glycolytic and mitochondrial metabolism, the impact on the mitochondria was further analysed, by investigating if and how oxygen levels affect the composition of the mitochondrial electron transport chain (ETC) protein complexes. This was done using a commercially available antibody cocktail targeting a component of each of the five ETC complexes (Sim *et al.*, 2018). Protein was collected from brain and lung MVECs at each baseline priming condition and also following 24 h of adaptation to hypoxia.

In lung MVECs, lower baseline oxygen levels consistently reduced the expression of all ETC complexes, although not to a statistically significant extent (Fig. 4-7B,D). This reduction was further exacerbated after 24 h at 1% O_2.

Brain MVECs on the other hand showed increased levels of complex II if cultured at 10% or 5% O_2 compared to STA (Fig. 4-7A,C). This increase was exacerbated following exposure to 1% O_2 for 24 h; the same hypoxic treatment in cells grown at STA did not elicit any increase in complex II expression. In fact, cells preconditioned at STA actually showed a significant decrease in complex III after 24 h at 1% O_2. Complex I showed expression changes in several experimental repeats, but its levels were much lower than complex II, making it difficult to accurately quantify. In fact, the replicates for each experimental group contained both increased and decreased complex I expression compared to STA; thus, the data was highly variable and not statistically significant.

In summary, brain MVECs grown at lower oxygen levels showed a higher expression of complex II which was further exacerbated after hypoxia, whereas lung MVECs displayed the opposite trend, with cells grown at lower oxygen levels showing a lower expression of several components of the ETC; again, this was exacerbated after 24 h in hypoxia.

These opposing oxygen-induced changes in ETC composition in brain and lung MVECs are consistent with the measurements of maximal mitochondrial respiration (Fig. 4-3D and Fig. 4-4D), which showed a relatively higher maximal OCR in brain compared to lung MVEC at lower baseline oxygen levels. This difference was increased after 24 h in hypoxia, with lung MVECs grown at 10% or 5% O_2 losing their mitochondrial spare capacity almost entirely (Fig. 4-4D, right group).

Mitochondrial activity was further assessed by staining with MitoTracker Red-CMXRos (Fig. 4-8). This probe is a cationic fluorophore which accumulates in active mitochondria due to their negative membrane potential (Chazotte, 2011). Surprisingly, both

brain and lung MVECs grown at 5% or 10% O_2 showed increased mitochondrial staining compared to the same cells grown at STA. Indeed, even the fold changes in each MVEC population compared to STA were comparable (Fig. 4-8C). This result does not mirror either the mitochondrial stress tests or the ETC western blot, where lung and brain MVECs showed opposing trends.

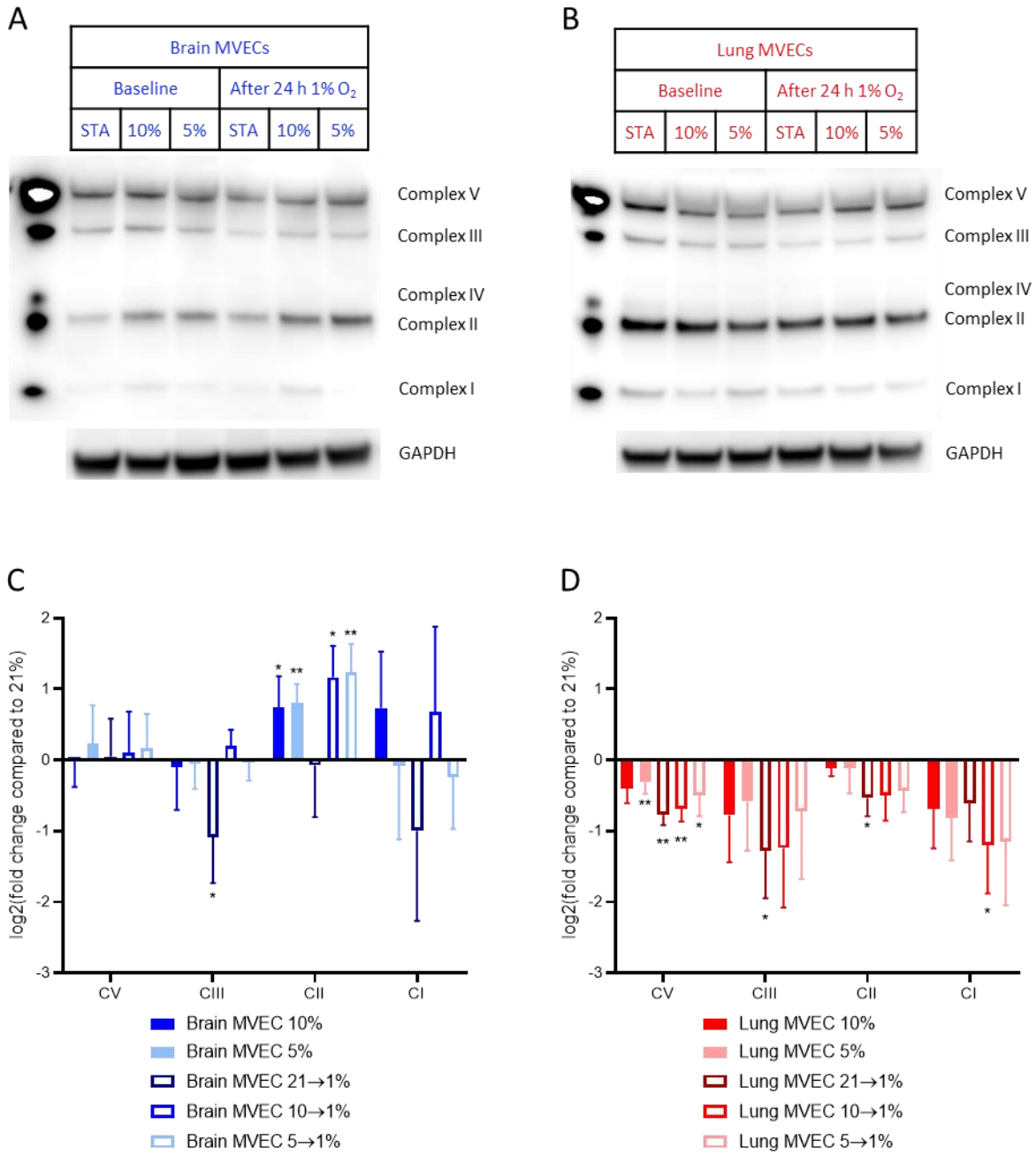

Figure 4-7

Figure 4-7: The effect of oxygen levels on the relative abundance of the mitochondrial ETC protein complexes

(A,B) Whole protein extracts were collected from brain (A) and lung (B) MVECs grown at the three baseline conditions (STA/10% O_2/5% O_2) and after exposure of each to 1% O_2 for 24 h. The lysates were probed with a mitochondrial antibody cocktail using western blot. Representative images are shown for each MVEC population.

(C,D) Quantification of the western blots shown in A and B. All values are normalized to the loading control and expressed as $\log_2$(fold change) compared to levels seen in cells grown at STA. (n = 4, error bars show SD, *p<0.05, **p<0.01 using one-sample t-test)

NB: The Complex IV band could not be quantified as it was overshadowed by the nearby Complex II band. Complex I was detected at very low levels and as such the signal was noisier

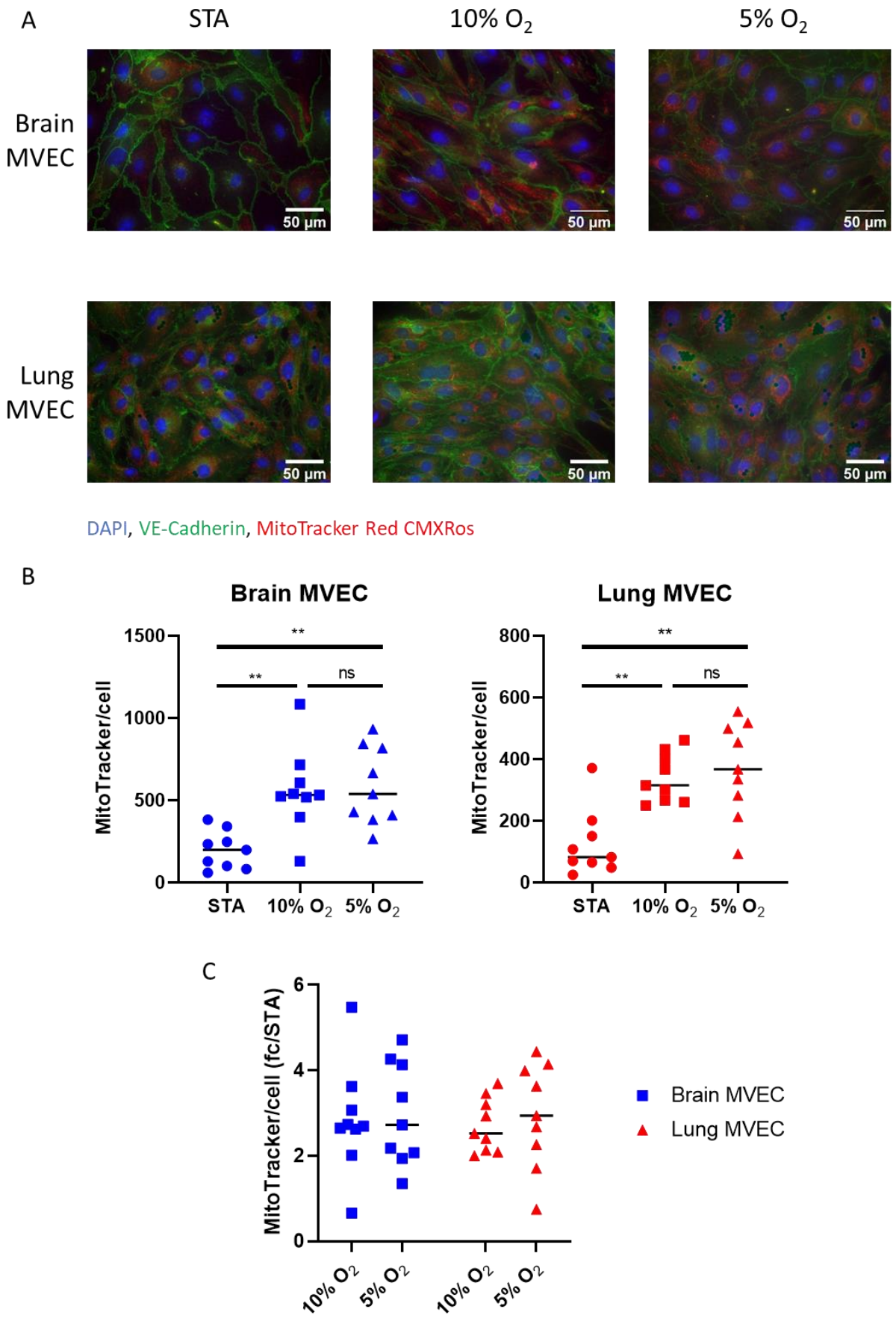
A
STA
10% O2
5% O2
Brain MVEC
Lung MVEC
50 µm
DAPI, VE-Cadherin, MitoTracker Red CMXRos
B
Brain MVEC
Lung MVEC
MitoTracker/cell
1500
1000
500
0
800
600
400
200
**
ns
STA
10% O2
5% O2
C
MitoTracker/cell (fc/STA)
6
4
2
0
Brain MVEC
Lung MVEC

Figure 4-8

Figure 4-8: Brain and lung MVEC at lower O_2 have a higher mitochondrial membrane potential

(A) Brain and lung MVECs stained for an endothelial cell marker (VE-Cadherin, green), for mitochondrial potential (MitoTracker Red CMXRos, red) and with a nuclear stain (DAPI, blue)

(B) Quantification of the MitoTracker stain shown in (A); different thresholds were used for the two cell populations

(C) Fold change compared to STA for each MVEC population

Error bars show SD, statistical analysis using multiple t-tests with Holm-Sidak's multiple comparison test (n=10 pictures from a single biological control **$p<0.01$)

4.3 Discussion

4.3.1 Brain and lung MVECs differ in their oxygen-induced metabolic shift

As expected, both brain and lung MVECs exhibited a shift away from mitochondrial respiration towards glycolysis concomitant with expansion in lower oxygen levels. Importantly however, these two cell populations differed in the timing and magnitude of the switch as well as in the oxygen level at which it was triggered.

At STA, lung and brain MVECs displayed broadly similar glycolytic activity and spare capacity, with only a slightly lower maximal glycolytic rate displayed by the lung cells (Fig. 4-3A, left panel). Conversely, maximal mitochondrial respiration in the lung MVECs was elevated compared to their brain counterparts (Fig 4-3B, left panel). Previous reports of these cells *in vivo*, where electron microscopy studies on vessels of different tissues were used, showed that brain MVECs contained an unusually high density of mitochondria compared to other microvascular beds (Oldendorf *et al.*, 1977). As such, brain MVECs were expected to display higher rates of mitochondrial respiration, which the data with cells grown at STA did not corroborate. At 10% O_2 this was still not observed, although there was no longer any difference in maximal respiration between the two cell populations. Only at 5% O_2, which represents physioxia for brain MVECs, did these cells display higher baseline and maximal mitochondrial respiration rates than their lung counterparts (Fig. 4-3B, right panel). These data were further corroborated by western blot quantification of ETC complexes, which showed that brain MVECs grown at 10% and 5% O_2 had higher levels of complex II when compared to those maintained in STA (Fig. 4-7C). This suggests that brain MVECs can only use their mitochondria to their full potential if grown at their physiological O_2 level (5%). Severe hyperoxia in STA is particularly damaging to these cells, as evidenced by the decreased maximal respiration relative to lung MVECs and the reduced complex II expression. Lung MVECs on the other hand showed a slight decrease in the abundance of all ETC complexes at either physioxic O_2 level, compared to STA (Fig. 4-7D). This suggests that 5% O_2 is already hypoxic for lung MVECs, which results in them losing their mitochondrial spare capacity, as well as their ability to induce HIF (Fig. 3-9B) and glycolysis (Fig. 4-5A) during a more severe hypoxic stimulus of 1% O_2.

Curiously, this difference between brain and lung MVECs was not observed when staining for mitochondrial potential (Fig. 4-8), where both cell populations behaved in a very similar manner. Brain and lung MVECs grown at 10% O_2 showed a stronger signal than the same cells grown at STA; no difference was seen between the same cells grown at 10% and

5% O_2 in either cell population. This was puzzling since the mitochondrial potential, which drives the localisation of the Mitotracker stain, is formed by the ETC and should thus reflect basal mitochondrial oxygen consumption. Furthermore, the Mitotracker stain is in direct opposition to the BNIP3 mRNA abundance, which was increased at lower O_2 levels (Fig. 3-5); BNIP3 triggers mitochondrial autophagy (Zhang and Ney, 2009) and therefore one might expect its levels to correlate with mitochondrial potential. This is especially likely given that BNIP3 is predominantly transcriptionally regulated, although some post-translational control through phosphorylation has also been reported (Liu and Frazier, 2015). Importantly, the MitoTracker stain was carried out using a single batch of MVECs. Therefore, this result needs to be confirmed. If it can be replicated, it may be the case that MVECs at STA have more but less active mitochondria, potentially due to oxidative damage caused by hyperoxia. Further evidence in this regard may be provided by measuring mitochondrial abundance more directly, for example by quantifying mitochondrial DNA, or by visualising mitochondria using electron microscopy.

Additionally, the validity of the MitoTracker stain in brain MVECs may be limited, since these cells express the multidrug efflux pump P-glycoprotein, which has been shown to target MitoTracker CMXRos, actively removing it from the cells (Zhitomirsky *et al.*, 2018). The expression of P-glycoprotein is severely reduced during *in vitro* culture of brain MVECs (Gaillard *et al.*, 2000; Welser-Alves *et al.*, 2014) but not entirely abolished. Those studies only considered brain MVECs cultured at STA; given the variations in gene expression shown in Fig. 4-4, it is possible that the level of P-glycoprotein in brain MVECs is also oxygen-dependent, which could skew the efficiency of the MitoTracker stain. Indeed, brain MVECs at each oxygen level showed considerably less MitoTracker stain than the respective lung MVECs, such that a different signal threshold had to be employed (see section 4.4.7). This effect may be difficult to circumvent since other common mitochondrial stains such as tetramethylrosamine, JC-1, or MitoTracker Green are similarly substrates of P-glycoprotein (Eytan *et al.*, 1997; Marques-Santos *et al.*, 2003; Elefantova *et al.*, 2018).

4.3.2 Hypoxic lung MVECs operate closer to their maximum OCR than brain MVEC

Metabolic shifts after hypoxia exposure were investigated in MVECs following priming at different oxygen levels. As a result, the mitochondrial metabolism of both brain and lung MVECs changed considerably from the baseline conditions shown in Fig. 4-3, irrespective of environmental preconditioning. The differences in basal respiration observed between

baseline O_2 levels largely disappeared and instead, both cell types, under all three conditions, displayed comparable basal respiration rates (Fig. 4-4D, left group).

The maximal respiration rates, however, varied substantially. Lung MVECs under both physioxic conditions (10% and 5% O_2) essentially lost all spare respiratory capacity while brain MVECs maintained it at the same relative level (~2-fold above baseline, Fig. 4-4D, right group). This was not observed in cells grown at STA, where both lung and brain MVECs maintained a comparable level of respiratory spare capacity. These data are to some extent mirrored by the quantification of ETC complexes (Fig. 4-7), where brain MVECs grown under 10% or 5% O_2 displayed an increase in complex II protein levels after 24 h in hypoxia, while lung MVECs under the same conditions reduced the expression of complexes II and V; this may explain the differences in maximal respiration. Indeed, complex II was recently reported as the main source of mitochondrial spare capacity in cardiac myocytes (Pfleger *et al.*, 2015; Wüst *et al.*, 2015). Intriguingly, brain MVECs cultured at STA failed to increase complex II and actually decreased the expression of complex III; the same was observed for their lung counterparts in addition to a reduction in complexes II and V. As a result, their maximal respiration did not differ (Fig. 4-4B, left panel).

Metabolic spare capacity *in vivo* is necessary to provide cells the ability to respond to stress with bursts of activity, and its loss is correlated with pathologies such as heart disease (Sansbury *et al.*, 2011) or glutamate excitotoxicity (Yadava and Nicholls, 2007). In ECs, spare oxidative capacity may be needed to deal with potentially noxious stimuli such as NO or ROS (Dranka *et al.*, 2010). In that study, the authors show that exposing EC to non-toxic levels of NO temporarily reduces their mitochondrial spare capacity, while maintaining basal respiration at a constant level. While mitochondrial spare capacity is reduced in this way, the EC are unable to cope with exposure to ROS, leading to irreversible inhibition of OCR and cell death. The data presented in this thesis thus suggests that lung MVEC at 1% O_2 are less plastic than brain MVEC and should deal less well with noxious stimuli such as ROS, as long as the brain MVEC are grown under physioxic conditions (5% or 10% O_2).

4.3.3 Glycolytic rate in hypoxia decreases over time

This study demonstrates that lower oxygen levels during cell culture lead MVECs to upregulate glycolysis in favour of OXPHOS, which in turn enables them to better respond to hypoxia. However, it appears that these high glycolytic rates are not maintained upon prolonged hypoxia exposure. The real-time hypoxia adaptation assays show an increase in glycolysis upon exposure to 1% O_2, followed by a decline (Fig. 4-5B). This is corroborated by

the post-hypoxia stress tests, which show lower levels of ECAR than any of the baseline assays (Fig. 4-3A and 4-4A). This could be caused by the general reduction of protein translation which is observed during chronic (>16 h) hypoxia (Thomas *et al.*, 2008). Additionally, the burst of glycolysis seen in the real-time adaptation assay may have led to exhaustion of glucose or excess lactate in the growth media. This hypothesis could be further investigated by measuring changes in the glucose/lactate levels within the growth medium after hypoxia exposure. An over-abundance of lactate is perhaps the most likely cause, since its export relies on facilitated diffusion, and thus requires a gradient between the cytosol and the medium. Additionally, the Seahorse analyser is incompatible with serum (aglient.com). While the effect of this is most likely insignificant for the time frame of a stress test, it inevitably affected the behaviour of MVECs during the 24h real time hypoxia adaptation, possibly contributing to the decline in ECAR observed after the initial peak (Fig. 4-5A).

4.3.4 ECAR as a measurement of glycolysis

The Seahorse metabolic analyser uses ECAR as a measurement to infer glycolysis. This seems to be widely accepted as a valid approximation, since Seahorse stress tests and similar approaches using ECAR are published frequently (Doddaballapur *et al.*, 2015; Marcu *et al.*, 2018; Sim *et al.*, 2018; Yetkin-Arik *et al.*, 2019). However, the connection between ECAR and glycolysis is by no means a straightforward one (Mookerjee *et al.*, 2017). To our knowledge, the data presented here is the first time that the effects of oxygen priming on MVEC metabolism and hypoxia response have been analysed. Therefore, it is difficult to validate the results against existing literature. Yet, the data presented here is in line with what is expected physiologically, since the cells display increased glycolytic rates if grown at lower O_2, and even more so when they are moved into hypoxia, thus correlating with HIF levels. This suggests that ECAR is indeed a valid approximation for glycolysis.

Nevertheless, the methodology still carries some inherent flaws which need to be kept in mind. For example, an increase in ECAR may be caused by molecules other than lactate. Importantly, this includes CO_2, one of the end products of OXPHOS. During glycolytic stress tests, OXPHOS is blocked by Oligomycin and as a result, ECAR increases, presumably due to an increased glycolytic flux. Notably, this very same injection also severely reduces the mitochondrial conversion of O_2 into CO_2, which could presumably decrease ECAR. Clearly, a net increase is still observed but this may not accurately reflect the true change in glycolytic flux. Conversely, glycolysis does not necessarily yield lactate: pyruvate may be converted into lactate or shuttled into the mitochondrion to be converted into acetyl-CoA and used in the Krebs

cycle. Correlating ECAR with glycolysis assumes that in both cell populations a constant fraction of pyruvate is converted into lactate. Furthermore, the enzyme responsible for the conversion of pyruvate into lactate, LDH-A, is expressed at different levels in brain and lung MVECs (Fig.4-4A). However, this step was not found to be rate-limiting in a flux analysis of glycolysis and is thus unlikely to affect ECAR (Tanner *et al.*, 2018). The same study however did find that the export of lactate into the extracellular medium is a rate-limiting step. This occurs via facilitated diffusion through the MCT4 shuttle (Draoui and Feron, 2011) and it depends both on the expression of the transporter protein as well as the pH gradient between the cytosol and the medium; differences in the expression level of this transporter may thus also influence ECAR readings.

Overall, in the present study, the inherent assumptions of these assays were mitigated by varying the experimental approaches with the Seahorse analyser (mitochondrial and glycolytic stress tests, as well as real-time adaptation) and by confirming the findings with other methods (glucose uptake assay, real-time viability with glycolysis inhibition, mitochondrial staining and ETC complex quantification). However, further experiments could be conducted to specifically address the weaknesses of the Seahorse system. For example, using ^{13}C-labeled glucose followed by mass spectrometry analysis of metabolites could show what fraction of glycolytic flux actually produces lactate.

4.3.5 Brain MVECs exhibit higher rates of glucose uptake

Brain MVECs consistently displayed higher rates of glucose uptake than their lung counterparts, irrespective of the oxygen level they were expanded in; even after hypoxic upregulation, lung MVECs were unable to match the baseline uptake rate of brain MVECs. Intriguingly, this observation does not correlate with the GLUT1 expression data shown before (Figs. 3-4 and 3-5). Instead, the baseline mRNA levels were actually directly correlated with oxygen availability, with both brain and lung MVECs grown at 5% O_2 expressing the least GLUT1. Furthermore, there was no difference in hypoxia-induced mRNA upregulation of GLUT1 at 4 h or 8h between the MVECs purified from the two organs. GLUT1 has long been recognised as the predominant glucose uptake transporter within vascular endothelial cells (Takata *et al.*, 1990, 1997; Olson and Pessin, 1996); it is therefore unlikely, albeit possible, that the observed discrepancy is due to a different transporter. Instead, it may be caused by post-transcriptional regulation, such as control of protein translation or subcellular localisation; many such mechanisms have already been described. For example, prolonged treatment of adipocytes with insulin enhances the association of GLUT1 mRNA with polyribosomes,

increasing its translation rate (Taha *et al.*, 1999). GLUT1 translocation to the plasma membrane has been described in a wide variety of cell lines following stimuli such as insulin treatment and hypoxia (Zhang *et al.*, 1999) and a similar effect was observed in retinal endothelial cells after VEGF treatment (Sone *et al.*, 2000). To investigate this question further, total GLUT1 protein could be assessed by western blot or flow cytometry, whereas immunocytochemistry could be used to determine its intracellular location, and thus discern the underlying reason for this apparent discrepancy.

This work shows that oxygen levels prime MVEC metabolism in an organ-specific fashion. Overall, lung MVECs are more glycolytic at physioxic levels whereas brain MVECs maintain a higher mitochondrial activity. Furthermore, each MVEC population is at their most plastic if cultured at their respective physioxia: 10% O_2 for lung MVECs and 5% O_2 for brain MVECs.

As shown in the previous chapter, MVECs are shaped by oxygen priming but still maintain intrinsic tissue-specific properties, that make the cell fit for purpose. For example, it has been postulated that the higher mitochondrial activity in brain MVECs compared to other microvascular beds is used to provide energy for the vast amounts of efflux pumps specifically expressed by this endothelium to prevent the entry of noxious substances into the CNS (Cucullo *et al.*, 2011; Theodorou and Boon, 2018).

The metabolic response to hypoxia is similarly shaped by oxygen pre-conditioning. Hyperoxia in particular has a significant effect and impairs the ability of MVECs to mount a adequate hypoxia response, which compromises their viability. This effect is particularly pronounced for brain MVECs. This may be reflective of the fact that standard tissue culture air is less hyperoxic for lung MVECs than their brain counterparts, relative to their *in vivo* setpoint. Conversely, 5% O_2 is hypoxic to lung MVECs but still physiologic in the brain.

4.4 Materials and methods

4.4.1 Glycolytic and mitochondrial stress tests

Local pH and O_2 changes in media were measured using a XF24-3 or XFe96 Analyzer (Agilent). MVECs of the appropriate density were plated on Seahorse microplates precoated with collagen I (Table 4-7). Mitochondrial stress tests required a lower cell number to avoid anoxia in the well after FCCP treatment. Cells were left to adhere for 12 h and assayed immediately (baseline readings) or transferred to 1% O_2 for 24 h before being assayed. Upon transfer to hypoxia, all wells received fresh growth medium which had been pre-equilibrated to 1% O_2. Before measuring, all wells were washed twice with Seahorse XF base medium supplemented with glucose, glutamine, and pyruvate, as shown in Table 4-2. The pH of the medium had been adjusted to 7.4 using 1 M NaOH. The cells were then equilibrated with assay medium for 45 min at 37 ˚C in a CO_2-free atmosphere containing the appropriate oxygen level. After recording baseline measurements, inhibitors were successively injected into the wells (Table 4-9) and changes in pH and oxygen consumption were tracked in real time. The inhibitor concentrations were selected as suggested by the manufacturer and as previously used on lung and brain endothelial cells (Diebold *et al.*, 2015; Nguyen *et al.*, 2016; Marcu *et al.*, 2018; Sure *et al.*, 2018). Each measurement was composed of a mix-wait-measure cycle which lasted 5 min – 1 min – 2min (XF24 in hypoxia and normoxia), 5 min – 0 min – 2 min (XFe96 in hypoxia), or 3 min – 0 min – 3min (XFe96 in normoxia), as recommended by the manufacturer. After all assays, protein concentration in each well was measured using Pierce™ BCA Protein Assay Kit (ThermoFisher) and extracellular acidification rates (ECAR) and oxygen consumption rates (OCR) were then normalised to µg of total protein. Basal and maximal rates, as well as spare capacity of glycolysis and oxidative phosphorylation were calculated as defined by the manufacturer (Table 4-4).

Table 4-7: Cell numbers seeded for metabolic assays using the XF24-3 and XFe96 Analyzers (Agilent)

	XF24	XFe96
Mitochondrial stress test - baseline	30’000	8’000
Mitochondrial stress test - 1% O_2	n/a	5’000
Glycolytic stress test	30’000	10’000

Table 4-10: Medium composition for metabolic assays using the XF24-3 and XFe96 Analyzers (Agilent)

	Glucose	Glutamine	Pyruvate
Mitochondrial stress test	7.8 mM	2.5 mM	3.5 mM
Glycolytic stress test	/	2.5 mM	/
Hypoxia response curve	7.8 mM	2.5 mM	3.5 mM

Table 4-9: Compounds injected during metabolic stress tests

	Compound 1	Compund 2	Compound 3
Mitochondrial stress test	Oligomycin (1 µM)	FCCP (1 µM)	Antimycin A (0.5 µM) Rotenone (0.5 µM)
Glycolytic stress test	Glucose (10 mM)	Oligomycin (1 µM)	2-deoxy glucose (50 mM)

Table 4-12: Definitions of metabolic parameters

	Mitochondrial stress test	Glycolytic stress test
Basal rate	Last measurement before Oligomycin injection – minimum measurement after Rotenone/Antimycin A injection	Maximum measurement before Oligomycin injection – last measurement before glucose injection
Maximal rate	Maximal measurement after FCCP injection – minimum measurement after Rotenone/Antimycin A injection	Maximum measurement after Oligomycin injection – last measurement before glucose injection
Spare Capacity	Maximal – basal rate	Maximal – basal rate

4.4.2 Real time hypoxia response curves

Real time hypoxia response curves were measured using a Seahorse XF24-3 analyser. 30’000 MVECs per well were plated the day before the assay on Seahorse microplates

precoated with collagen I. At the start of the assay, MVEC growth medium was replaced with Seahorse XF base medium supplemented with glucose (7.8 mM), pyruvate (3.5 mM), and glutamine (2.5 mM), corresponding to the concentrations found in the MVEC growth medium. The Seahorse medium had been equilibrated to 1% O_2 for 24 h. ECAR was then measured every 20 min for 24 h. Each measurement was composed of a mix-wait-measure cycle which lasted 5 min – 1 min – 2min, followed by a time delay of 12 min. After the assay, protein concentration in each well was measured using Pierce™ BCA Protein Assay Kit (ThermoFisher) and ECAR were then normalised to µg of total protein.

4.4.3 Hypoxia chambers for Seahorse analysers

For experiments carried out at non-atmospheric oxygen conditions, the XF24-3 Analyzer was placed within a gas flow-controlled Perspex hermetic chamber. The atmosphere was CO_2-free and O_2 levels were set to either 10%, 5%, or 1%. During the assay, there was no humidity control and temperature was controlled within the Seahorse analyser but not the chamber; internal air circulation was maintained by a fan.

The XFe96 Analyzer was placed in a Ruskinn hypoxia chamber, set to either 10%, 5%, or 1% O_2 and 0.1% CO_2, as the machine could not be set to 0% CO_2. The chamber was humidity and temperature controlled; internal air circulation was maintained by a fan.

In both cases, the instruments as well as all media and calibrant were equilibrated to the hypoxic atmosphere for 12 h prior to the assay. To avoid reoxygenation, the cell culture plates were transported from their incubators to the instrument chamber in a sealed box; all washes were carried out within the chamber.

4.4.4 Glucose uptake assays

30,000 MVECs per well were seeded in a 96-well plate 12 h before the start of the assay. The plates were then either transferred into a hypoxia chamber containing 1% O_2 or maintained at the same oxygen concentration. The start of each hypoxia incubation was staggered such that 2-DG treatment could be carried out at the same time for all conditions. The cells were washed once with PBS and incubated with 0.1 mM 2-DG in PBS for 10 min; glucose uptake was measured using the Glucose Uptake-Glo™ Assay (Promega) according to manufacturer's instructions. All reagents used had been pre-equilibrated to the appropriate oxygen concentration. Samples were incubated with detection reagent for 2 h and luminescence was measured with a FLUOstar Omega plate reader. A standard curve of 2-deoxy-glucose-6-phosphate was used to calculate glucose uptake rates. Replicate wells plated at the same time were used to determine the cell number at the time of 2-DG treatment.

4.4.5 Western blot for mitochondrial electron transfer chain complexes

Brain and lung MVECs were grown to 90% confluence. The cells were then either transferred into a hypoxia chamber containing 1% O_2 or maintained at the same oxygen concentration for 24 h. Cells from both treatments received fresh, oxygen-equilibrated medium at t=0. Protein was collected with ice-cold RIPA buffer and quantified using the Pierce™ BCA Protein Assay Kit (ThermoFisher) according to manufacturer's instructions. 35 µg of protein was loaded per well. Samples were not heated prior to gel-separation to prevent damage to mitochondrial complex I, which is unstable at temperatures above 50 ˚C, as advised by the manufacturer. Proteins were separated on 4-12% Bis-Tris gels and transferred to PVDF membranes. The primary antibody, Total OXPHOS Rodent WB Antibody Cocktail (Abcam 110413) was diluted with 1:250 in 1% milk in PBST. Blocking and probing with primary and secondary antibodies was carried out as described in section 3.4.9. Bands were visualized using Amersham ECL Western Blotting Detection Reagent (GE Healthcare). Rat heart mitochondrial extract was used as a positive control.

4.4.6 MitoTracker and VE-Cadherin stain

MVECs were seeded on sterile glass chamber slides precoated with collagen I and grown to confluence. The growth media was then replaced with fresh O_2-equilibrated media containing 200 nM MitoTracker Red CMXRos (ThermoFisher), or DMSO as a negative control. After 30 min, the media was removed and the wells were washed twice with PBS. The cells were fixed with cold acetone (-20 ˚C) for 10 min and permeabilised with 0.5% Triton-X100 in PBS for 5 min at room temperature. Blocking was done using 10% donkey serum in PBS for 1 h at room temperature. Primary antibody incubation occurred over night at 4 ˚C, secondary antibody at room temperature for 1 h. Antibody catalogue numbers and dilutions are listed in Tables 3-2. Secondary-only control wells were kept in blocking solution instead of primary antibody over night and then received the same dose of secondary antibody. Slides were mounted using ProLong Diamond Antifade with DAPI (ThermoFisher).

4.4.7 Quantification of the MitoTracker stain

The MitoTracker CMXRos stain was quantified in a multi-step process using ImageJ. First, a minimum threshold was applied to the MitoTracker images. This threshold was chosen such that no signal remained in the unstained control, and such that the resulting image was not oversaturated (Method 1, Fig. 4-9A). Then, the area of the resulting image was measured. Of note, the MitoTracker signal in all lung MVEC images was significantly brighter than for brain MVECs. Thus, different thresholds were chosen to allow for distinction between oxygen

treatments. However, this means that signal intensities cannot be compared between two EC populations. An alternative method was also attempted; here, instead of applying a threshold, the white signal in the original picture was measured and the value of the unstained control images was subtracted (Method 2, Fig. 4-9A). The results using these two methods was not significantly different (Fig. 4-9C) but method 1 yielded better differentiation between the experimental groups, hence this method was chosen for the main figure. The raw MitoTracker signal was normalised to the number of nuclei present in each picture. The workflow for this is shown in Fig. 4-9B. First, a threshold was applied, followed by a watershed, to separate touching nuclei. Then the number of nuclei was counted using a minimum size cutoff to prevent the counting of small artifacts.

For lung MVEC, an additional step had to be introduced before the MitoTracker stain could be quantified. As described in section 3.4.5, the isolation of lung MVECs relied on anti-CD31-coated dynabeads. Most of these beads were lost during passaging but some remained attached to the cells. Unfortunately, they proved to fluoresce at the same wavelength as MitoTracker CMXRos, appearing as bright red spheres in the images. In order to quantify only true signal, the area covered by beads was manually removed from the images, using a round, cookie-cutter approach (Fig 4-9D). The resulting image was then quantified as described above.

4.4.8 Real time viability assay with 2-DG

Real time viability assays were performed as described in section 3.4.7. 2-DG (10 mM) or vehicle control (PBS) was added to the growth medium containing MT Cell Viability Substrate and NanoLuc enzyme before replacing the growth medium in the assay plate.

Figure 4-9: Quantification strategy for MitoTracker Red CMXRos
(A) MitoTracker CMXRos was quantified in two ways, either by applying a threshold and measuring the singal-positive area (Method 1) or by measuring the average signal intensity across the entire picture and subtracting the blank (Method 2)
(B) Cell number in each image was quantified by counting the DAPI-stained nuclei. The imageJ watershed algorithm was used to separate overlapping nuclei.
(C) Comparison of MitoTracker quantification methods 1 and 2; method 1 yielded more pronounced differences between the samples.
(D) Lung MVECs contained some dynabeads from the purification protocol. These beads were fluorescent in the same range as MitoTracker Red CMXRos and were thus manually removed from the images

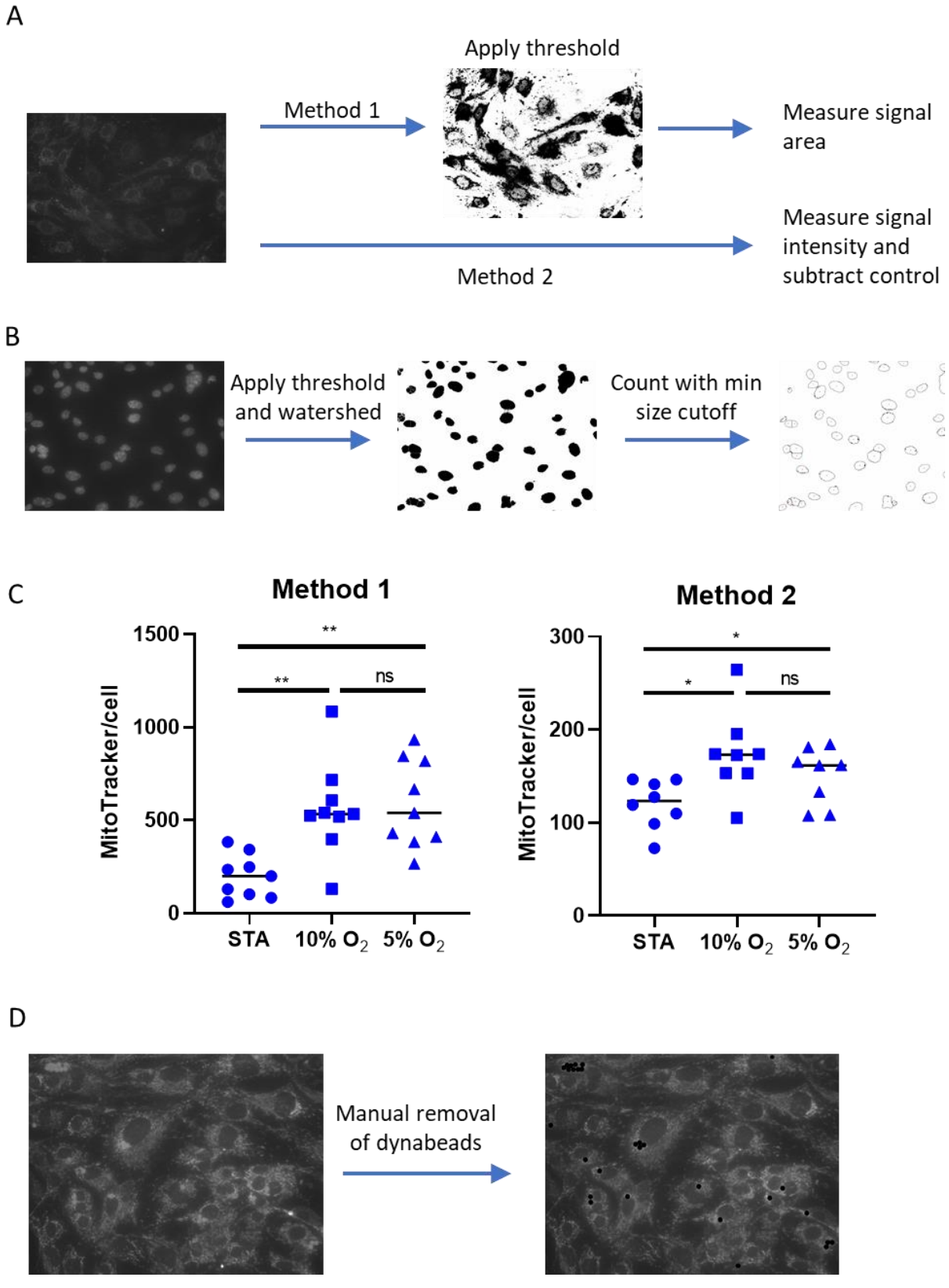
A
Apply threshold
Method 1
Measure signal area
Measure signal intensity and subtract control
Method 2
B
Apply threshold and watershed
Count with min size cutoff
C
Method 1
Method 2
MitoTracker/cell
1500
1000
500
0
300
200
100
**
ns
*
STA
10% O2
5% O2
D
Manual removal of dynabeads

Figure 4-9

Chapter 5: General discussion

5.1 Main Findings

5.1.1. Endothelial HIF shapes the lung pre-metastatic niche

This thesis has outlined the importance of oxygen levels in shaping endothelial cell physiology and in particular their ability to respond to a subsequent stimulus. Chapter 2 used a combination of *in vivo* and *ex vivo* approaches to show how hypoxic pre-incubations of differing lengths can modulate metastatic success to the lung. Acute exposure resulted in preferential stabilization of HIF-1α in overall lung tissue, as well as specifically within EC. This coincided with increased EC death and permeability, as well as increased secretion of CCL2 by EC and thus recruitment of pro-metastatic CCR2+ macrophages to the lung. This resulted in increased rates of metastasis compared to mice who were not subjected to hypoxia pre-conditioning prior to tumour cell injection. Upon prolonged hypoxia, HIF-1α levels subsided and HIF-2α was preferentially stabilized, leading to the re-establishment of a functional EC barrier and a metastatic burden comparable to mice who were not exposed to hypoxia. The importance of endothelial HIF within these processes was verified through lung endothelial-specific knockouts of each HIF isoform. Overall, this showed that hypoxic preconditioning alters the state of the lung microvasculature, which can increase metastatic burden by modulating the organ microenvironment.

5.1.2. Hyperoxia compromises the MVEC hypoxia response

Growing primary MVECs at different oxygen levels (STA, 10% O_2 – physiological for lung MVECs, or 5% O_2 – physiological for brain MVECs) had profound effects on MVEC gene expression and function (i.e. wound-closure). In particular, HIF levels were elevated considerably in physiological oxygen levels, compared to STA, showing that HIF is present at steady-state levels, prior to a hypoxic challenge, and as a result, these cells differed considerably in their response to a subsequent hypoxia exposure (1% O_2). MVECs previously cultured at STA showed little stabilisation of HIF-1α and HIF-2α, and consequently a very mild change in mRNA levels of hypoxia response genes. Under these conditions, brain MVECs in particular were unable to adapt to hypoxia, showing high rates of cell death and failing to upregulate VEGF, a crucial component of EC hypoxia response. If the same cells were grown under physiological oxygen levels, when exposed to hypoxia they instead displayed improved viability and increased stabilisation of HIF and hypoxia response genes.

Additionally, brain and lung MVECs also showed some intrinsic differences which occurred independently of oxygen availability. Most notably, brain MVECs expressed considerably less VEGF than their lung counterparts and their hypoxia response yielded higher levels of HIF-2α stabilisation. Lung MVECs on the other hand contained higher levels of HIF-1α, both at baseline and after 4h at 1% O_2.

5.1.3. Oxygen levels determine the metabolic preference in MVEC in an organ-specific manner

In chapter 4, the effects of oxygen levels on the metabolism of MVECs were investigated. Not surprisingly, both brain and lung MVEC had increased glycolytic activity if grown at lower O_2. However, lung MVECs displayed even higher basal glycolytic rates when maintained at lower oxygen levels, while brain MVECs retained more mitochondrial spare capacity. Interestingly, this correlated with an increased expression of ETC complex II in brain MVECs grown at 5% or 10%, compared to STA, which was not seen in lung MVECs. Hypoxia exposure for 24 h further exacerbated this difference in mitochondrial spare capacity as well as complex II expression.

Real time metabolic adaptation to hypoxia was also profoundly shaped by baseline oxygen level. MVECs grown at STA barely showed an upregulation of glycolysis in response to hypoxia, and this inability was even more severe in brain than in lung MVECs. The largest hypoxia-induced increase in glycolysis was observed when each cell population was grown at their physiological oxygen level: 5% for brain MVEC and 10% for lung MVEC. Thus, oxygen levels shaped both MVEC baseline metabolic preference, as well as their hypoxia-induced metabolic shift in an organ-specific manner.

These data show that priming endothelial cells through altered oxygen availability can significantly affect their response to a subsequent stimulus. One can also infer that endothelial heterogeneity is to a relevant extent intrinsic, since both MVEC populations were at their most plastic if grown at their own physiological oxygen levels, which is different in brain (5% O_2) and lung (10% O_2). This was further highlighted by brain (but not lung) MVECs displaying mitochondrial spare capacity at 5% and even 1% O_2, but not if primed in hyperoxia. Furthermore, the two populations differentially stabilised HIF isoforms and produced strikingly different amounts of VEGF, providing further evidence for their intrinsic difference. While there have been previous comparative studies on organ-specific EC heterogeneity

(Nolan *et al.*, 2013; Marcu *et al.*, 2018), all cells are usually cultured at the same oxygen level; in most cases this is either STA or 5% O_2. The data presented here shows that this likely introduces a confounding variable if the cell populations that are being compared are used to different oxygen levels *in vivo*.

The following sections will discuss the applications and relevance of these findings, by analysing scenarios during which humans are exposed to either hypoxia or hyperoxia, and if any consequences on endothelial health or metastatic progression have been investigated.

5.2 Human exposure to hypoxia

As highlighted above (Section 1.2), hypoxia can occur as a result of a wide variety of environmental, behavioural, physiological, or pathological reasons, such as altitude, smoking, exercise, anaemia, or chronic obstructive pulmonary disease. The HIF system has evolved to allow organisms to seamlessly adjust to changes in oxygen supply on several levels, ranging from systemic stimuli to modifications at the cellular level, for example as a result of altered metabolic needs. However, depending on the time and severity of the hypoxic exposure, these systems may be stretched beyond their physiological range, with potentially harmful side effects such as the increase in metastasis described in chapter 2. The following paragraphs will discuss two such examples and their implications on endothelial health.

Travelling at high altitude is an example of continuous hypoxia, i.e. a single uninterrupted stimulus. Dry ambient air contains 21% O_2 and has a pressure of 760 mmHg at sea level; therefore, the partial pressure of oxygen within this gas mixture is 160 mmHg. With increasing altitude atmospheric pressure decreases, and since the relative proportion of O_2 stays constant, this leads to a concurrent reduction in oxygen partial pressure. As a result, oxygen saturation within arterial blood decreases from 98% at sea level to below 80% at 6000 m. Mountaineers travelling at this altitude are thus exposed to considerable levels of hypoxia. As shown in a rat model, this leads to increased stabilisation of HIF-1α and consequently increased expression of its target iNOS (Zhang *et al.*, 2015). Importantly, iNOS has been identified in Chapter 2 of this thesis (Reiterer *et al.*, 2019) as well as in previous work (Branco-Price *et al.*, 2012) as a key mediator of HIF-1α's pro-metastatic effect. In humans, increased HIF-1α activity at high altitude has been inferred from the increased expression of its target genes, such as EPO (Abbrecht and Littell, 1972; Eckardt *et al.*, 1989). There is currently no data on the

effects of acute hypobaric hypoxia on metastatic progression but given the data presented in this thesis, this may warrant further investigation. Importantly, unlike in the experimental setup described in Chapter 2, altitude-induced hypoxia usually occurs gradually, as the climbers ascend; this may alter the patterns of HIF stabilisation.

Chronic mild hypoxia on the other hand may actually be beneficial, as indicated by a study comparing cancer mortality in Caucasians living at low or high altitude within the US (Hart, 2011). Indeed, this seems to be a general trend for humans living at high altitude (Thiersch and Swenson, 2018), irrespective of their racial background. This is in line with the data presented in Chapter 2, although endothelial integrity is only one of a wide variety of factors determining metastatic efficiency, and therefore it is unclear if or how the two effects could be related.

Intermittent hypoxia (IH) on the other hand is a combination of several acute hypoxic episodes, separated by periods of re-oxygenation. As such, its HIF profile is an exacerbated version of what is seen during a single acute exposure. The protein levels and transcriptional activity of HIF-1α increase progressively with each cycle (Yuan *et al.*, 2005), whereas HIF-2α protein expression is decreased and remains lowered for several hour even after IH has ceased (Nanduri *et al.*, 2009). IH is usually a result of obstructive sleep apnoea (OSA), a disorder which affects up to 25% of the adult population and is often severely underdiagnosed (Young *et al.*, 1993). It is characterised by the partial or complete obstruction of the upper airways during sleep (Budhiraja *et al.*, 2007), usually related to obesity. As such, its high prevalence is a relatively recent phenomenon and natural selection for an efficient countermeasure has not yet occurred. Therefore, it has been argued that IH invokes a particularly maladaptive response (Prabhakar and Semenza, 2012).

While the negative effects of OSA on the macrovasculature have been studied extensively (Budhiraja *et al.*, 2007; Atkeson and Jelic, 2008), its effects on the microvasculature are less well known (Hoyos *et al.*, 2015). Increased HIF-1α levels within the lung have been reported as a result of OSA (Nanduri *et al.*, 2009; Prabhakar *et al.*, 2010) but it is still unclear if this also affects endothelial cells, with some studies reporting HIF-1α stabilisation in EC following intermittent hypoxia, while others do not observe this (Polotsky *et al.*, 2010; Minoves *et al.*, 2017).

It has also been established that OSA increases cancer patient mortality (Nieto *et al.*, 2012; Campos-Rodriguez *et al.*, 2013) as well as lung metastasis in a murine melanoma model

(Almendros *et al.*, 2013). However, in this study the effects of intermittent hypoxia were only assessed in relation to cancer cells, and not the endothelium. Given the data presented in chapter 2 of this thesis, and the exacerbated stabilisation of HIF-1α compared to HIF-2α during intermittent hypoxia, the endothelium is likely facilitating this increased metastatic spread to the lung. Therefore, investigating the impact of EC dysfunction on tumour progression within OSA patients is likely relevant.

In summary, both scenarios considered above can lead to acute systemic hypoxia. Considering the data presented in Chapter 2, this may have a pro-metastatic influence on the lung microvasculature. However, any cancer research in these areas, if at all present, has so far not implicated the endothelium, making this a promising area for further studies.

5.3 Human exposure to hyperoxia

This thesis focused on oxygen as the agent for endothelial cell priming. Chapters 3 and 4 highlighted how hyperoxia alters EC physiology and metabolism, leaving the cells unable to react properly to a subsequent hypoxic stimulus. Under physiological conditions, ECs *in vivo* would never be exposed to such high levels of oxygen. However, modern technology has changed this and there are indeed several situations where ECs can be exposed to hyperoxia for prolonged periods of time. The following paragraphs will discuss these, focusing in particular on reports about side effects implicating or affecting endothelial cells.

5.3.1 Hyperbaric oxygen treatment

During hyperbaric oxygen treatment (HOT), patients breathe 100% O_2 at higher than atmospheric pressure. As a result, oxygen partial pressure can be as much as 15 times higher than in standard air (>2000 mmHg). This treatment leads to severe hyperoxia throughout the body. In a rat model, partial oxygen pressures as high as 450 mmHg were measured in the brain, more than 13 times higher than in control animals (Thom, 1989). Treatments usually last 1-2 h and are administered up to three times daily (Thom, 2011). HOT is mainly used to treat pathologies involving wound healing, such as refractory diabetic lower extremity wounds and delayed radiation injuries. In both cases, it has been reputed that using HOT as an adjunct to traditional wound care markedly improves outcome (Goldman, 2009). The therapeutic effect of HOT mainly derives from an increase in circulating stem cells, which promote vasculogenesis within the affected tissues; this occurs as a results of a hyperoxia-induced

increase in eNOS activity within the bone marrow (Thom *et al.*, 2006, 2010; Yang *et al.*, 2007). Furthermore, hyperoxia also stimulates growth factor production by these stem cells, further supporting the wound healing process. Paradoxically, this response is mediated by HIF, since the high levels of ROS created by hyperoxia override the PHD-VHL system, as described in section 1.2.3 (Sheikh *et al.*, 2000; Milovanova *et al.*, 2009). Side effects of HOT can appear either as a consequence of the overall increase in pressure or because of hyperoxia.

Nowadays, hyperoxic side effects of HOT are discussed mostly in the context of acute CNS toxicity, which manifests itself as a seizure during treatment. Its prevalence is low, affecting less than 0.03% of patients (Banham, 2011), and it does not appear to result in lasting damage. Indeed, most patients who experience a hyperoxia-induced seizure continue their hyperbaric treatment. Conversely, early research on the effects of hyperoxia on animals discovered serious detrimental effects on lung integrity, and notably on the viability of the endothelium. In rats exposed to pure oxygen at 1 atm for 72 h, half of all pulmonary MVECs had died by the end of the treatment (Kistler *et al.*, 1967). Primates seem to be slightly less affected by this than rodents, as monkeys showed less severe effects after the same treatment. However, after 12 days of pure oxygen exposure, even in monkeys total endothelial cell volume in the lung capillaries was decreased to one third (Kapanci *et al.*, 1969). The onset of this acute endothelial toxicity was found to occur after 12-16 h at 1 atm of pure oxygen but as early as 3-6 h at 2 atm. The duration and intensity of modern HOT treatment has thus been designed such that immediate toxicity towards the lung endothelium is generally avoided (Thorsen *et al.*, 1998). HOT also does not lead to increased metastasis (Poff *et al.*, 2015; Stępień *et al.*, 2016). Indeed, it has been found to limit tumour growth (Sletta *et al.*, 2017), especially when applied in conjunction with radiotherapy (Chen *et al.*, 2015), presumably because it reduces hypoxia within the primary tumour and the associated resistance to therapy (described in section 1.3.1). However, given the data presented in this thesis, questions should be raised with regards to changes in the plasticity of endothelial cells following HOT, even in the absence of immediate cell death. In fact, the data presented here may even provide an underestimation of the true detrimental effects of hyperoxia, since all experiments relied on MVECs from “adolescent” mice (6-8 weeks) and animal studies show that resistance to hyperoxia decreases with age (Clark and Lambertsen, 1971). Indeed, the choice to not use mice older than 8 weeks was made because we observed that their endothelial cells are less proliferative and responsive *in vitro*.

5.3.2 Perioperative hyperoxia

According to WHO guidelines, "adult patients undergoing general anaesthesia with endotracheal intubation for surgical procedures should receive 80% fraction of inspired oxygen intraoperatively and, if feasible, in the immediate postoperative period for 2–6 h" (Allegranzi *et al.*, 2016). The rationale is that molecular oxygen is required for oxidative killing of bacteria by neutrophils, which is the primary defence against surgical wound contamination. Indeed, initial data found surgical wound infection risk to be inversely correlated to tissue oxygenation (Hopf *et al.*, 1997). However, more recent meta analyses of several studies with thousands of patients have called these benefits into question (Volk *et al.*, 2017; Mattishent *et al.*, 2019), and suggest the use of 30% oxygen instead. These studies describe possible adverse effects of hyperoxia on patients but they focus mostly on the exacerbation and associated increases in mortality of a pre-existing pathology, such as myocardial infarction, chronic obstructive pulmonary disease, stroke, or traumatic brain injury (Wijesinghe *et al.*, 2009; Damiani *et al.*, 2014; Helmerhorst *et al.*, 2015). The hyperoxia-induced decrease in endothelial plasticity described in this thesis may not result in such immediate and pronounced negative effects. However, given that the immediate benefits of perioperative hyperoxia have been called into question, these data should at least provide pause for thought. To investigate the possibility of hyperoxia-induced damage during surgery, one could measure recovery from a surgical procedure which relies heavily on EC function. Liver regeneration following a partial hepatectomy, or lung alveolarization following unilateral pneumonectomy for example are guided by angiocrine stimuli from liver and lung ECs, respectively (Ding *et al.*, 2010, 2011). If perioperative hyperoxia does indeed lead to loss of EC plasticity, then this would likely be reflected in the healing rates from these procedures, as well as in long term effects if functional reprogramming occurs.

5.3.3 Oxygen exposure during diving

Hyperoxia during scuba diving is an inevitable side effect of the increased ambient pressure under water, which rises by 1 atm for each 10 m of depth. Importantly, the partial pressure of oxygen within the breathing mixture rises by the same factor. For example, compressed dry air (21% O_2) at surface level has an oxygen partial pressure of 160 mmHg but 580 mmHg at a depth of 30 m, which is equal to 76% O_2 at ambient pressure. As with HOT, hyperoxia during diving can also lead to acute CNS toxicity; this is observed if oxygen partial

pressure exceeds 160 kPa (1200 mmHg), which occurs at 66 m with dry air. An in vitro study using bovine aortic endothelial cells found that 160 kPa of O_2 resulted in severe mitochondrial damage due to excessive amounts of ROS, and thus increased rates of cell death (Wang *et al.*, 2015). However, damage to the endothelium can occur at much lower oxygen levels. A single session with 60% O_2 (simulating a dive at 28 m) for 80 min resulted in severely diminished arterial EC function, as measured by their ability to induce vessel dilation in response to shear stress (Brubakk *et al.*, 2005). Furthermore, it has been proposed that endothelial dysfunction is the underlying cause of decompression sickness (Madden and Laden, 2009), a disorder that occurs when divers ascend too quickly.

While endothelial health has been considered in all of the cases listed above, this is usually restricted to the lung microvasculature and in some cases also arterial ECs. The impact of hyperoxia on other microvascular beds is rarely discussed, if at all. However, according to the data presented in this thesis, it stands to reason that lung MVECs are actually better equipped to handle hyperoxic stress than their brain counterparts. In a rare study assessing the effect of hyperoxia on the brain vasculature, it was found that hyperbaric oxygen during diving reduces glucose delivery to the brain because of decreased glucose uptake by brain MVECs (Wilson and Matschinsky, 2019), in line with what was observed here (Fig. 4-5C). Similarly, an *in vitro* study using human skin MVECs found that 50% O_2 reduced cell proliferation, while 95% O_2 markedly induced cell death (Attaye *et al.*, 2017). Therefore, the effects of hyperoxia on systemic capillary beds certainly merit further investigation, in particular with regards to individuals who are exposed to both hyperoxic and hypoxic stimuli, such as prescribing HOT to a patient suffering from sleep apnoea.

5.4 Further work

The data presented in this thesis gives rise to a series of further questions.

Firstly, questions that can be answered by the *in vitro* setup used in this thesis:

1. Is the loss of plasticity experienced by MVECs grown at STA permanent or can this be reversed by moving the cells to physiological O_2? If it is reversible, how long does this take?
2. How long do MVECs need to be exposed to STA (or even more severe hyperoxia to model the scenarios discussed above) before they lose plasticity? Does the duration and the severity of the insult affect their ability to recover?

3. What is the mechanism behind the lack of plasticity exhibited by MVECs at STA? Possible hypotheses include epigenetic modifications by oxygen sensitive enzymes such as the Tet family, which have been shown to induce epigenetic asymmetry within embryonic stem cells based on oxygen availability (Burr *et al.*, 2018). Alternatively, hyperoxia-induced mitochondrial damage may play a role, as this has been shown to occur in pulmonary ECs (Ma *et al.*, 2018). This could also explain why brain MVECs are more severely affected, since they rely more strongly on mitochondrial metabolism at physioxia.

Secondly, questions about the *in vivo* implications of this work:

1. The acute consequences of hyperoxic toxicity have been assessed mostly with regards to the lung endothelium. What are the consequences on other vascular beds *in vivo*? Do they experience similar, or, as perhaps suggested by these data, even more severe changes in physiology and plasticity?
2. What are the long-term *in vivo* consequences of hyperoxia-induced loss of EC-plasticity? Is the angiocrine function of EC affected? As elaborated above, this could be investigated by measuring the recovery following partial hepatectomy or unilateral pneumonectomy. However, given the vast role of ECs in the control of organ function outlined in Chapter 1, loss of EC plasticity would likely have an effect on a wide variety of pathologies, such as cardiovascular disease or metabolic syndrome.
3. Do ECs play a role in the increased lung metastasis induced by intermittent hypoxia? This is strongly suggested by the stabilisation of HIF-1α over HIF-2α and could be easily investigated by repeating the experiments of Chapter 2 with an intermittent stimulus prior to tumour injection.

Thirdly, questions about the roles of HIF isoforms in lung compared to brain microvasculature, since the relative abundance of HIF-1α and HIF-2α in the two MVEC populations suggests that HIF-2α may be of greater importance for brain MVEC physiology and/or their hypoxia response.

1. The importance of each HIF isoform in these two microvasculatures could be analysed by repeating experiments from Chapters 3 and 4 using HIF-knockout cells. *In vitro* knockouts of HIF can be created from MVECs of double-floxed mice, as shown in Chapter 2.
2. *In vivo* knockouts in the brain microvasculature could be achieved by expressing the Cre-recombinase under a general endothelial-specific promoter such as Tie2. However,

any observed phenotype would not necessarily be due brain MVEC-specific effects, since the entire microvasculature would be affected. Efforts have been made to develop a BBB endothelial Cre-line but issues of specificity and efficiency still remain (Meng *et al.*, 2007; Ridder *et al.*, 2011; Crouthamel *et al.*, 2012; Assmann *et al.*, 2016).

In summary, this thesis has shown how endothelial cell priming by altering oxygen availability can affect the cells' plasticity and their ability to respond to a subsequent stimulus in a tissue-specific manner. Such priming may occur as a side effect of several pathologies, treatments, or activities. Endothelial cells play a central role in human health and disease; therefore, understanding these processes will be key in developing therapies or precautionary measures against endothelial damage, as well as approaches to improve tissue regeneration.

Appendix A – Coordinates of the cytokine array panel

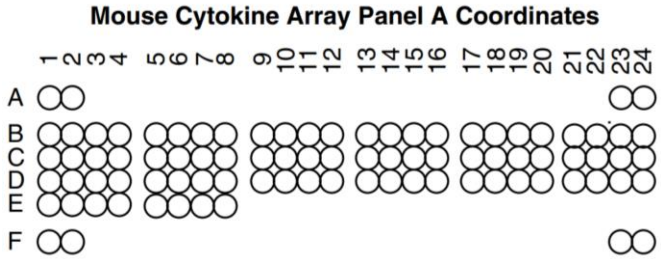

Coordinate	Target/Control	Coordinate	Target/Control
A1, A2	Reference Spot	C17, C18	IL-16
A23, A24	Reference Spot	C19, C20	IL-17
B1, B2	BLC	C21, C22	IL-23
B3, B4	C5/C5a	C23, C24	IL-27
B5, B6	G-CSF	D1, D2	CXCL10
B7, B8	I-309	D3, D4	CXCL11
B9, B10	Eotaxin	D5, D6	CXCL1
B11, B12	sICAM-1	D7, D8	M-CSF
B13, B14	IFN-γ	D9, D10	CCL2
B15, B16	IL-1α	D11, D12	CCL12
B17, B18	IL-1β	D13, D14	CXCL9
B19, B20	IL-1γ	D15, D16	CCL3
B21, B22	IL-1ra	D17, D18	CCL4
B23, B24	IL-2	D19, D20	CXCL2
C1, C2	IL-3	D21, D22	CCL5
C3, C4	IL-4	D23, D24	CXCL12
C5, C6	IL-5	E1, E2	CCL17
C7, C8	IL-6	E3, E4	TIMP-1
C9, C10	IL-7	E5, E6	TNF-α
C11, C12	IL-10	E7, E8	Reference Spot
C13, C14	IL-13	F1, F2	TREM-1
C15, C16	IL-12 p70	F23, F24	PBS (Negative Control)

Bibliography

Abbott, N. J. (2002) 'Astrocyte-endothelial interactions and blood-brain barrier permeability', *Journal of Anatomy*, pp. 629–638. doi: 10.1046/j.1469-7580.2002.00064.x.

Abbrecht, P. H. and Littell, J. K. (1972) 'Plasma erythropoietin in men and mice during acclimatization to different altitudes.', *Journal of applied physiology*, 32(1), pp. 54–58. doi: 10.1152/jappl.1972.32.1.54.

Agilent Learning Center (2019) *How to run an assay*.

Aird, W. C. (2007a) 'Phenotypic heterogeneity of the endothelium: I. Structure, function, and mechanisms', *Circulation Research*, pp. 158–173. doi: 10.1161/01.RES.0000255691.76142.4a.

Aird, W. C. (2007b) 'Phenotypic heterogeneity of the endothelium: II. Representative vascular beds', *Circulation Research*, 100(2), pp. 174–190. doi: 10.1161/01.RES.0000255690.03436.ae.

Aird, W. C. (2012) 'Endothelial cell heterogeneity', *Cold Spring Harbor Perspectives in Medicine*. Cold Spring Harbor Laboratory Press, 2(1). doi: 10.1101/cshperspect.a006429.

Allegranzi, B. *et al.* (2016) 'New WHO recommendations on intraoperative and postoperative measures for surgical site infection prevention: an evidence-based global perspective', *The Lancet Infectious Diseases*. Lancet Publishing Group, pp. e288–e303. doi: 10.1016/S1473-3099(16)30402-9.

Almendros, I. *et al.* (2013) 'Intermittent hypoxia increases melanoma metastasis to the lung in a mouse model of sleep apnea', *Respiratory Physiology and Neurobiology*, 186(3), pp. 303–307. doi: 10.1016/j.resp.2013.03.001.

Almendros, I. *et al.* (2014) 'Intermittent hypoxia-induced changes in tumor-associated macrophages and tumor malignancy in a mouse model of sleep apnea', *American Journal of Respiratory and Critical Care Medicine*, 189(5), pp. 593–601. doi: 10.1164/rccm.201310-1830OC.

Ampofo, E. *et al.* (2010) 'Phosphorylation of the von Hippel-Lindau protein (VHL) by protein kinase CK2 reduces its protein stability and affects p53 and HIF-1α mediated transcription', *International Journal of Biochemistry and Cell Biology*, 42(10), pp. 1729–1735. doi: 10.1016/j.biocel.2010.07.008.

An, H. J. *et al.* (2006) 'Activation of Ras up-regulates pro-apoptotic BNIP3 in nitric oxide-induced cell death', *Journal of Biological Chemistry*, 281(45), pp. 33939–33948. doi:

10.1074/jbc.M605819200.

Andreu-Agulló, C. *et al.* (2009) 'Vascular niche factor PEDF modulates notch-dependent stemness in the adult subependymal zone', *Nature Neuroscience*, 12(12), pp. 1514–1523. doi: 10.1038/nn.2437.

Appelhoffl, R. J. *et al.* (2004) 'Differential function of the prolyl hydroxylases PHD1, PHD2, and PHD3 in the regulation of hypoxia-inducible factor', *Journal of Biological Chemistry*, 279(37), pp. 38458–38465. doi: 10.1074/jbc.M406026200.

Aprelikova, O. *et al.* (2004) 'Regulation of HIF prolyl hydroxylases by hypoxia-inducible factors', *Journal of Cellular Biochemistry*, 92(3), pp. 491–501. doi: 10.1002/jcb.20067.

Assmann, J. C., Körbelin, J. and Schwaninger, M. (2016) 'Genetic manipulation of brain endothelial cells in vivo', *Biochimica et Biophysica Acta - Molecular Basis of Disease*. Elsevier, 1862(3), pp. 381–394. doi: 10.1016/j.bbadis.2015.10.006.

Astuti, D. *et al.* (2001) 'Gene mutations in the succinate dehydrogenase subunit SDHB cause susceptibility to familial pheochromocytoma and to familial paraganglioma', *American Journal of Human Genetics*, 69(1), pp. 49–54. doi: 10.1086/321282.

Atkeson, A. and Jelic, S. (2008) 'Mechanisms of endothelial dysfunction in obstructive sleep apnea', *Vascular Health and Risk Management*, pp. 1327–1335. doi: 10.2147/vhrm.s4078.

Atkins *et al.* (2007) 'Open discussion', *Clinical Cancer Research*. American Association for Cancer Research (AACR), 13(2 II), pp. 680s-684s. doi: 10.1158/1078-0432.CCR-06-1865.

Attaye, I. *et al.* (2017) 'The effects of hyperoxia on microvascular endothelial cell proliferation and production of vaso-active substances', *Intensive Care Medicine Experimental*. Springer Science and Business Media LLC, 5(1). doi: 10.1186/s40635-017-0135-4.

Augustin, H. G. and Koh, G. Y. (2017) 'Organotypic vasculature: From descriptive heterogeneity to functional pathophysiology', *Science*. American Association for the Advancement of Science. doi: 10.1126/science.aal2379.

Banerjee, D. *et al.* (2015) 'Notch suppresses angiogenesis and progression of hepatic metastases', *Cancer Research*. American Association for Cancer Research Inc., 75(8), pp. 1592–1602. doi: 10.1158/0008-5472.CAN-14-1493.

Banham, N. D. G. (2011) 'Oxygen toxicity seizures: 20 years' experience from a single hyperbaric unit', *Diving and Hyperbaric Medicine*, 41(4), pp. 202–210. Available at: http://www.ncbi.nlm.nih.gov/pubmed/22183697 (Accessed: 29 November 2019).

Barbacena, P., Carvalho, J. R. and Franco, C. A. (2016) 'Endothelial cell dynamics in vascular

remodelling', *Clinical Hemorheology and Microcirculation*. IOS Press, 64(4), pp. 557–563. doi: 10.3233/CH-168006.

Barteczek, P. *et al.* (2017) 'Neuronal HIF-1α and HIF-2α deficiency improves neuronal survival and sensorimotor function in the early acute phase after ischemic stroke', *Journal of Cerebral Blood Flow and Metabolism*, 37(1), pp. 291–306. doi: 10.1177/0271678X15624933.

Bartoszewski, R. *et al.* (2019) 'Primary endothelial-specific regulation of hypoxiainducible factor (HIF)-1 and HIF-2 and their target gene expression profiles during hypoxia', *FASEB Journal*, 33(7), p. fj.201802650RR. doi: 10.1096/fj.201802650RR.

Baysal, B. E. *et al.* (2000) 'Mutations in SDHD, a mitochondrial complex II gene, in hereditary paraganglioma', *Science*, 287(5454), pp. 848–851. doi: 10.1126/science.287.5454.848.

Bazzoni, G. and Dejana, E. (2004) 'Endothelial cell-to-cell junctions: Molecular organization and role in vascular homeostasis', *Physiological Reviews*, pp. 869–901. doi: 10.1152/physrev.00035.2003.

Beck, I. *et al.* (1991) 'Enhancer element at the 3'-flanking region controls transcriptional response to hypoxia in the human erythropoietin gene', *Journal of Biological Chemistry*, 266(24), pp. 15563–15566. Available at: http://www.ncbi.nlm.nih.gov/pubmed/1874713 (Accessed: 16 November 2019).

Bellot, G. *et al.* (2009) 'Hypoxia-Induced Autophagy Is Mediated through Hypoxia-Inducible Factor Induction of BNIP3 and BNIP3L via Their BH3 Domains', *Molecular and Cellular Biology*. American Society for Microbiology, 29(10), pp. 2570–2581. doi: 10.1128/mcb.00166-09.

Bendayan, M. (2002) 'Morphological and cytochemical aspects of capillary permeability', *Microscopy Research and Technique*, 57(5), pp. 327–349. doi: 10.1002/jemt.10088.

Biernacki, K. *et al.* (2004) 'Regulation of Cellular and Molecular Trafficking across Human Brain Endothelial Cells by Th1- and Th2-Polarized Lymphocytes', *Journal of Neuropathology and Experimental Neurology*. American Association of Neuropathologists Inc., 63(3), pp. 223–232. doi: 10.1093/jnen/63.3.223.

Blouin, A., Bolender, R. P. and Weibel, E. R. (1977) 'Distribution of organelles and membranes between hepatocytes and nonhepatocytes in the rat liver parenchyma. A stereological study', *Journal of Cell Biology*, 72(2), pp. 441–455. doi: 10.1083/jcb.72.2.441.

De Bock, K. *et al.* (2013) 'Role of PFKFB3-driven glycolysis in vessel sprouting', *Cell*. Cell Press, 154(3), pp. 651–663. doi: 10.1016/j.cell.2013.06.037.

Braet, F. and Wisse, E. (2002) 'Structural and functional aspects of liver sinusoidal endothelial

cell fenestrae: A review', *Comparative Hepatology*. doi: 10.1186/1476-5926-1-1.

Branco-Price, C. *et al.* (2012) 'Endothelial cell HIF-1α and HIF-2α differentially regulate metastatic success', *Cancer Cell*. Cell Press, 21(1), pp. 52–65. doi: 10.1016/j.ccr.2011.11.017.

Branco-Price, C., Evans, C. E. and Johnson, R. S. (2013) 'Endothelial hypoxic metabolism in carcinogenesis and dissemination: HIF-A isoforms are a NO metastatic phenomenon', *Oncotarget*, 4. doi: 10.18632/oncotarget.1461.

Le Bras, A. *et al.* (2007) 'HIF-2α specifically activates the VE-cadherin promoter independently of hypoxia and in synergy with Ets-1 through two essential ETS-binding sites', *Oncogene*, 26(53), pp. 7480–7489. doi: 10.1038/sj.onc.1210566.

Brubakk, A. O. *et al.* (2005) 'A single air dive reduces arterial endothelial function in man', *Journal of Physiology*, 566(3), pp. 901–906. doi: 10.1113/jphysiol.2005.089862.

Bruick, R. K. and McKnight, S. L. (2001) 'A conserved family of prolyl-4-hydroxylases that modify HIF', *Science*, 294(5545), pp. 1337–1340. doi: 10.1126/science.1066373.

Bryant, A. J. *et al.* (2016) 'Endothelial hif signaling regulates pulmonary fibrosis-associated pulmonary hypertension', *American Journal of Physiology - Lung Cellular and Molecular Physiology*, 310(3), pp. L249–L262. doi: 10.1152/ajplung.00258.2015.

Budhiraja, R., Parthasarathy, S. and Quan, S. F. (2007) 'Endothelial dysfunction in obstructive sleep apnea', *Journal of Clinical Sleep Medicine*, pp. 409–415. doi: 10.1164/ajrccm-conference.2011.183.1_meetingabstracts.a2205.

Burnstock, G. and Ralevic, V. (1994) 'New insights into the local regulation of blood flow by perivascular nerves and endothelium', *British Journal of Plastic Surgery*, 47(8), pp. 527–543. doi: 10.1016/0007-1226(94)90136-8.

Burr, S. *et al.* (2018) 'Oxygen gradients can determine epigenetic asymmetry and cellular differentiation viadifferential regulation of Tet activity in embryonic stem cells', *Nucleic Acids Research*. Oxford University Press, 46(3). doi: 10.1093/nar/gkx1197.

Butler, J. M., Kobayashi, H. and Rafii, S. (2010) *Instructive role of the vascular niche in promoting tumour growth and tissue repair by angiocrine factors, Nature Reviews Cancer*. doi: 10.1038/nrc2791.

Campochiaro, P. A. (2013) 'Ocular neovascularization.', *Journal of molecular medicine (Berlin, Germany)*, pp. 311–321. doi: 10.1007/s00109-013-0993-5.

Campos-Rodriguez, F. *et al.* (2013) 'Association between obstructive sleep apnea and cancer incidence in a large multicenter spanish cohort', *American Journal of Respiratory and Critical Care Medicine*, 187(1), pp. 99–105. doi: 10.1164/rccm.201209-1671OC.

Cantelmo, A. R. *et al.* (2016) 'Inhibition of the Glycolytic Activator PFKFB3 in Endothelium Induces Tumor Vessel Normalization, Impairs Metastasis, and Improves Chemotherapy', *Cancer Cell*, 30(6), pp. 968–985. doi: 10.1016/j.ccell.2016.10.006.

Cao, Z. *et al.* (2017) 'Molecular Checkpoint Decisions Made by Subverted Vascular Niche Transform Indolent Tumor Cells into Chemoresistant Cancer Stem Cells', *Cancer Cell*, 31(1), pp. 110–126. doi: 10.1016/j.ccell.2016.11.010.

Carmeliet, P. *et al.* (1998) 'Role of HIF-1α in hypoxiamediated apoptosis, cell proliferation and tumour angiogenesis', *Nature*, 394(6692), pp. 485–490. doi: 10.1038/28867.

Carmeliet, P. and Jain, R. K. (2000) 'Angiogenesis in cancer and other diseases', *Nature*, pp. 249–257. doi: 10.1038/35025220.

Carmeliet, P. and Jain, R. K. (2011a) 'Molecular mechanisms and clinical applications of angiogenesis', *Nature*, pp. 298–307. doi: 10.1038/nature10144.

Carmeliet, P. and Jain, R. K. (2011b) 'Principles and mechanisms of vessel normalization for cancer and other angiogenic diseases', *Nature Reviews Drug Discovery*, pp. 417–427. doi: 10.1038/nrd3455.

Carroll, V. A. and Ashcroft, M. (2006) 'Role of hypoxia-inducible factor (HIF)-1α versus HIF-2α in the regulation of HIF target genes in response to hypoxia, insulin-like growth factor-I, or loss of von Hippel-Lindau function: Implications for targeting the HIF pathway', *Cancer Research*, 66(12), pp. 6264–6270. doi: 10.1158/0008-5472.CAN-05-2519.

Cater, D. B. *et al.* (1961) 'Changes of oxygen tension in brain and somatic tissues induced by vasodilator and vasoconstrictor drugs', *Proceedings of the Royal Society of London. Series B. Biological Sciences*, 155(958), pp. 136–157. doi: 10.1098/rspb.1961.0061.

Chambers, A. F., Groom, A. C. and MacDonald, I. C. (2002) 'Dissemination and growth of cancer cells in metastatic sites', *Nature Reviews Cancer*, pp. 563–572. doi: 10.1038/nrc865.

Chang, C. H. *et al.* (2015) 'Metabolic Competition in the Tumor Microenvironment Is a Driver of Cancer Progression', *Cell*. Cell Press, 162(6), pp. 1229–1241. doi: 10.1016/j.cell.2015.08.016.

Chazotte, B. (2011) 'Labeling mitochondria with mitotracker dyes', *Cold Spring Harbor Protocols*, 6(8), pp. 990–992. doi: 10.1101/pdb.prot5648.

Chen, C. *et al.* (2018) 'Physioxia: A more effective approach for culturing human adipose-derived stem cells for cell transplantation', *Stem Cell Research and Therapy*. BioMed Central Ltd., 9(1). doi: 10.1186/s13287-018-0891-4.

Chen, J. R. *et al.* (2015) 'Radiotherapy after hyperbaric oxygenation in malignant gliomas', *Current Medical Research and Opinion*. Taylor and Francis Ltd, pp. 1977–1984. doi: 10.1185/03007995.2015.1082988.

Chen, L. *et al.* (2013) 'Toll-like receptor 4 has an essential role in early skin wound healing', *Journal of Investigative Dermatology*. Nature Publishing Group, 133(1), pp. 258–267. doi: 10.1038/jid.2012.267.

Chen, R. *et al.* (2011) 'Regulation of transcription of hypoxia-inducible factor-1α (HIF-1α) by heat shock factors HSF2 and HSF4', *Oncogene*, 30(22), pp. 2570–2580. doi: 10.1038/onc.2010.623.

Chi, J. T. *et al.* (2003) 'Endothelial cell diversity revealed by global expression profiling', *Proceedings of the National Academy of Sciences of the United States of America*, 100(19), pp. 10623–10628. doi: 10.1073/pnas.1434429100.

Christofk, H. R. *et al.* (2008) 'Pyruvate kinase M2 is a phosphotyrosine-binding protein', *Nature*. Nature Publishing Group, 452(7184), pp. 181–186. doi: 10.1038/nature06667.

Cines, D. B. *et al.* (1998) 'Endothelial cells in physiology and in the pathophysiology of vascular disorders', *Blood*, pp. 3527–3561. doi: 10.1182/blood.V91.10.3527.3527_3527_3561.

Clarenbach, C. F., Thurnheer, R. and Kohler, M. (2012) 'Vascular dysfunction in chronic obstructive pulmonary disease: Current evidence and perspectives', *Expert Review of Respiratory Medicine*, pp. 37–43. doi: 10.1586/ers.11.82.

Clark, J. M. and Lambertsen, C. J. (1971) 'Pulmonary oxygen toxicity: a review.', *Pharmacological Reviews*, pp. 37–133.

Cockman, M. E. *et al.* (2000) 'Hypoxia inducible factor-α binding and ubiquitylation by the von Hippel-Lindau tumor suppressor protein', *Journal of Biological Chemistry*, 275(33), pp. 25733–25741. doi: 10.1074/jbc.M002740200.

Coisne, C. *et al.* (2005) 'Mouse syngenic in vitro blood-brain barrier model: A new tool to examine inflammatory events in cerebral endothelium', *Laboratory Investigation*. Nature Publishing Group, 85(6), pp. 734–746. doi: 10.1038/labinvest.3700281.

Conn, E. M. *et al.* (2009) 'Comparative analysis of metastasis variants derived from human prostate carcinoma cells: Roles in intravasation of VEGF-mediated angiogenesis and uPA-mediated invasion', *American Journal of Pathology*. Elsevier Inc., 175(4), pp. 1638–1652. doi: 10.2353/ajpath.2009.090384.

Coppiello, G. *et al.* (2015) 'Meox2/Tcf15 heterodimers program the heart capillary endothelium for cardiac fatty acid uptake', *Circulation*, 131(9), pp. 815–826. doi:

10.1161/CIRCULATIONAHA.114.013721.

Corada, M. *et al.* (1999) 'Vascular endothelial-cadherin is an important determinant of microvascular integrity in vivo', *Proceedings of the National Academy of Sciences of the United States of America*, 96(17), pp. 9815–9820. doi: 10.1073/pnas.96.17.9815.

Cordon-Cardo, C. *et al.* (1989) 'Multidrug-resistance gene (P-glycoprotein) is expressed by endothelial cells at blood-brain barrier sites', *Proceedings of the National Academy of Sciences of the United States of America*, 86(2), pp. 695–698. doi: 10.1073/pnas.86.2.695.

Coupland, L. A., Chong, B. H. and Parish, C. R. (2012) 'Platelets and P-selectin control tumor cell metastasis in an organ-specific manner and independently of NK cells', *Cancer Research*, 72(18), pp. 4662–4671. doi: 10.1158/0008-5472.CAN-11-4010.

Cowburn, A. S. *et al.* (2016) 'HIF2α-Arginase axis is essential for the development of pulmonary hypertension', *Proceedings of the National Academy of Sciences of the United States of America*. National Academy of Sciences, 113(31), pp. 8801–8806. doi: 10.1073/pnas.1602978113.

Cowburn, A. S. *et al.* (2017) 'Cardiovascular adaptation to hypoxia and the role of peripheral resistance', *eLife*. eLife Sciences Publications Ltd, 6. doi: 10.7554/eLife.28755.

Crouch, E. E. *et al.* (2015) 'Regional and stage-specific effects of prospectively purified vascular cells on the adult V-SVZ neural stem cell lineage', *Journal of Neuroscience*. Society for Neuroscience, 35(11), pp. 4528–4539. doi: 10.1523/JNEUROSCI.1188-14.2015.

Crouthamel, M. H., Kelly, E. J. and Ho, R. J. Y. (2012) 'Development and characterization of transgenic mouse models for conditional gene knockout in the blood-brain and blood-CSF barriers', *Transgenic Research*, 21(1), pp. 113–130. doi: 10.1007/s11248-011-9512-z.

Cucullo, L. *et al.* (2011) 'The role of shear stress in Blood-Brain Barrier endothelial physiology', *BMC Neuroscience*. BioMed Central, 12(1), p. 40. doi: 10.1186/1471-2202-12-40.

Culic, O., Gruwel, M. L. H. and Schrader, J. (1997) 'Energy turnover of vascular endothelial cells', *American Journal of Physiology - Cell Physiology*, 273(1 42-1), pp. C205–C213. doi: 10.1152/ajpcell.1997.273.1.c205.

Dai, G. *et al.* (2004) 'Distinct endothelial phenotypes evoked by arterial waveforms derived from atherosclerosis-susceptible and -resistant regions of human vasculature', *Proceedings of the National Academy of Sciences of the United States of America*,

101(41), pp. 14871–14876. doi: 10.1073/pnas.0406073101.

Daijo, H. *et al.* (2016) 'Cigarette smoke reversibly activates hypoxia-inducible factor 1 in a reactive oxygen species-dependent manner', *Scientific Reports*, 6. doi: 10.1038/srep34424.

Damiani, E. *et al.* (2014) 'Arterial hyperoxia and mortality in critically ill patients: A systematic review and meta-analysis', *Critical Care*. BioMed Central Ltd., 18(1). doi: 10.1186/s13054-014-0711-x.

Daneman, R. and Prat, A. (2015) 'The blood–brain barrier', *Cold Spring Harbor Perspectives in Biology*. Cold Spring Harbor Laboratory Press, 7(1), pp. a020412--24. doi: 10.1101/cshperspect.a020412.

Davies, P. F. *et al.* (2014) 'Emerging topic: Flow-related epigenetic regulation of endothelial phenotype through DNA methylation', *Vascular Pharmacology*. Elsevier Inc., pp. 88–93. doi: 10.1016/j.vph.2014.05.007.

Delgado, A. C. *et al.* (2014) 'Endothelial NT-3 Delivered by Vasculature and CSF Promotes Quiescence of Subependymal Neural Stem Cells through Nitric Oxide Induction', *Neuron*. Cell Press, 83(3), pp. 572–585. doi: 10.1016/j.neuron.2014.06.015.

Deryugina, E. I. and Kiosses, W. B. (2017) 'Intratumoral Cancer Cell Intravasation Can Occur Independent of Invasion into the Adjacent Stroma', *Cell Reports*. Elsevier B.V., 19(3), pp. 601–616. doi: 10.1016/j.celrep.2017.03.064.

Diebold, I. *et al.* (2015) 'BMPR2 preserves mitochondrial function and DNA during reoxygenation to promote endothelial cell survival and reverse pulmonary hypertension', *Cell Metabolism*. Cell Press, 21(4), pp. 596–608. doi: 10.1016/j.cmet.2015.03.010.

Ding, B. Sen *et al.* (2010) 'Inductive angiocrine signals from sinusoidal endothelium are required for liver regeneration', *Nature*, 468(7321), pp. 310–315. doi: 10.1038/nature09493.

Ding, B. Sen *et al.* (2011) 'Endothelial-derived angiocrine signals induce and sustain regenerative lung alveolarization', *Cell*, 147(3), pp. 539–553. doi: 10.1016/j.cell.2011.10.003.

Ding, B. Sen *et al.* (2015) 'Endothelial MMP14 is required for endothelial-dependent growth support of human airway basal cells', *Journal of Cell Science*. Company of Biologists Ltd, 128(15), pp. 2983–2988. doi: 10.1242/jcs.168179.

Dings, J. *et al.* (1998) 'Clinical experience with 118 brain tissue oxygen partial pressure catheter probes', *Neurosurgery*, 43(5), pp. 1082–1094. doi: 10.1097/00006123-

199811000-00045.

Doddaballapur, A. *et al.* (2015) ‘Laminar shear stress inhibits endothelial cell metabolism via KLF2-mediated repression of PFKFB3’, *Arteriosclerosis, Thrombosis, and Vascular Biology*, 35(1), pp. 137–145. doi: 10.1161/ATVBAHA.114.304277.

Doe, M. R. *et al.* (2012) ‘Myc posttranscriptionally induces HIF1 protein and target gene expression in normal and cancer cells’, *Cancer Research*, 72(4), pp. 949–957. doi: 10.1158/0008-5472.CAN-11-2371.

Doll, D. N. *et al.* (2015) ‘Mitochondrial Crisis in Cerebrovascular Endothelial Cells Opens the Blood-Brain Barrier’, *Stroke*. Lippincott Williams & WilkinsHagerstown, MD, 46(6), pp. 1681–1689. doi: 10.1161/STROKEAHA.115.009099.

Dranka, B. P., Hill, B. G. and Darley-Usmar, V. M. (2010) ‘Mitochondrial reserve capacity in endothelial cells: The impact of nitric oxide and reactive oxygen species’, *Free Radical Biology and Medicine*, 48(7), pp. 905–914. doi: 10.1016/j.freeradbiomed.2010.01.015.

Draoui, N. and Feron, O. (2011) ‘Lactate shuttles at a glance: From physiological paradigms to anti-cancer treatments’, *DMM Disease Models and Mechanisms*, pp. 727–732. doi: 10.1242/dmm.007724.

Draoui, N., De Zeeuw, P. and Carmeliet, P. (2017) ‘Angiogenesis revisited from a metabolic perspective: Role and therapeutic implications of endothelial cell metabolism’, *Open Biology*. Royal Society Publishing, 7(12). doi: 10.1098/rsob.170219.

Duan, C. (2016) ‘Hypoxia-inducible factor 3 biology: Complexities and emerging themes’, *American Journal of Physiology - Cell Physiology*, 310(4), pp. C260–C269. doi: 10.1152/ajpcell.00315.2015.

Duelli, R. and Kuschinsky, W. (2001) ‘Brain glucose transporters: Relationship to local energy demand’, *News in Physiological Sciences*, 16(2), pp. 71–76. doi: 10.1152/physiologyonline.2001.16.2.71.

Eckardt, K. U. *et al.* (1989) ‘Rate of erythropoietin formation in humans in response to acute hypobaric hypoxia’, *Journal of Applied Physiology*, 66(4), pp. 1785–1788. doi: 10.1152/jappl.1989.66.4.1785.

Ehrismann, D. *et al.* (2007) ‘Studies on the activity of the hypoxia-inducible-factor hydroxylases using an oxygen consumption assay’, *Biochemical Journal*, 401(1), pp. 227–234. doi: 10.1042/BJ20061151.

Elefantova, K. *et al.* (2018) ‘Detection of the mitochondrial membrane potential by the cationic dye JC-1 in l1210 cells with massive overexpression of the plasma membrane ABCB1 drug transporter’, *International Journal of Molecular Sciences*. MDPI AG, 19(7). doi:

10.3390/ijms19071985.

Ema, M. *et al.* (1997) 'A novel bHLH-PAS factor with close sequence similarity to hypoxia-inducible factor 1α regulates the VEGF expression and is potentially involved in lung and vascular development', *Proceedings of the National Academy of Sciences of the United States of America*. National Academy of Sciences, 94(9), pp. 4273–4278. doi: 10.1073/pnas.94.9.4273.

Engelhardt, S. *et al.* (2014) 'Hypoxia selectively disrupts brain microvascular endothelial tight junction complexes through a hypoxia-inducible factor-1 (HIF-1) dependent mechanism', *Journal of Cellular Physiology*, 229(8), pp. 1096–1105. doi: 10.1002/jcp.24544.

Epstein, A. C. R. *et al.* (2001) 'C. elegans EGL-9 and mammalian homologs define a family of dioxygenases that regulate HIF by prolyl hydroxylation', *Cell*. Cell Press, 107(1), pp. 43–54. doi: 10.1016/S0092-8674(01)00507-4.

Estrella, V. *et al.* (2013) 'Acidity generated by the tumor microenvironment drives local invasion', *Cancer Research*, 73(5), pp. 1524–1535. doi: 10.1158/0008-5472.CAN-12-2796.

Evans, C. E. *et al.* (2016) 'Diverse roles of cell-specific hypoxia-inducible factor 1 in cancer-Associated hypercoagulation', *Blood*. American Society of Hematology, 127(10), pp. 1355–1360. doi: 10.1182/blood-2015-09-671982.

Evans, C. E. *et al.* (2017) 'Modelling pulmonary microthrombosis coupled to metastasis: Distinct effects of thrombogenesis on tumorigenesis', *Biology Open*, 6(5), pp. 688–697. doi: 10.1242/bio.024653.

Eytan, G. D. *et al.* (1997) 'Efficiency of P-glycoprotein-mediated exclusion of rhodamine dyes from multidrug-resistant cells is determined by their passive transmembrane movement rate', *European Journal of Biochemistry*, 248(1), pp. 104–112. doi: 10.1111/j.1432-1033.1997.00104.x.

Fan, Y. *et al.* (2014) 'Profilin-1 phosphorylation directs angiocrine expression and glioblastoma progression through HIF-1α accumulation', *Nature Cell Biology*. Nature Publishing Group, 16(5), pp. 445–456. doi: 10.1038/ncb2954.

Farber, H. W. and Loscalzo, J. (2004) 'Mechanisms of disease: Pulmonary arterial hypertension', *New England Journal of Medicine*, 351(16), pp. 1655–1665. doi: 10.1056/NEJMra035488.

Feng, J. *et al.* (2007) 'Vascular bed-specific endothelium-dependent vasomomotor relaxation in the hagfish, Myxine glutinosa', *American Journal of Physiology - Regulatory*

Integrative and Comparative Physiology, 293(2). doi: 10.1152/ajpregu.00080.2007.

Ferguson, D. C. J. *et al.* (2018) 'Altered cellular redox homeostasis and redox responses under standard oxygen cell culture conditions versus physioxia', *Free Radical Biology and Medicine*. Elsevier Inc., 126, pp. 322–333. doi: 10.1016/j.freeradbiomed.2018.08.025.

Ferrara, N., Gerber, H. P. and LeCouter, J. (2003) 'The biology of VEGF and its receptors', *Nature Medicine*, pp. 669–676. doi: 10.1038/nm0603-669.

Fidler, I. J. (1970) 'Metastasis: Quantitative analysis of distribution and fate of tumor emboli labeled with 125l-5-lodo-2'-deoxyuridine', *Journal of the National Cancer Institute*, 45(4), pp. 773–782. doi: 10.1093/jnci/45.4.773.

Flamme, I. *et al.* (1997) 'HRF, a putative basic helix-loop-helix-PAS-domain transcription factor is closely related to hypoxia-inducible factor-lot and developmentally expressed in blood vessels', *Mechanisms of Development*, 63(1), pp. 51–60. doi: 10.1016/S0925-4773(97)00674-6.

Franco, C. A. and Gerhardt, H. (2017) 'Morph or Move? How Distinct Endothelial Cell Responses to Blood Flow Shape Vascular Networks', *Developmental Cell*. Cell Press, pp. 574–576. doi: 10.1016/j.devcel.2017.06.008.

Gaillard, P. J. *et al.* (2000) 'Astrocytes increase the functional expression of P-glycoprotein in an in vitro model of the blood-brain barrier', *Pharmaceutical Research*, 17(10), pp. 1198–1205. doi: 10.1023/A:1026406528530.

Gandhi, S. and Chandna, S. (2017) 'Radiation-induced inflammatory cascade and its reverberating crosstalks as potential cause of post-radiotherapy second malignancies', *Cancer and Metastasis Reviews*, 36(2), pp. 375–393. doi: 10.1007/s10555-017-9669-x.

Gavard, J. (2014) 'Endothelial permeability and VE-cadherin: A wacky comradeship', *Cell Adhesion and Migration*. Taylor and Francis Inc., pp. 158–164. doi: 10.4161/cam.29026.

Gerri, C. *et al.* (2018) 'Hif-1a and Hif-2a regulate hemogenic endothelium and hematopoietic stem cell formation in zebrafish', *Blood*. American Society of Hematology, 131(9), pp. 963–973. doi: 10.1182/blood-2017-07-797795.

Giannotta, M., Trani, M. and Dejana, E. (2013) 'VE-cadherin and endothelial adherens junctions: Active guardians of vascular integrity', *Developmental Cell*, pp. 441–454. doi: 10.1016/j.devcel.2013.08.020.

Giatromanolaki, A. *et al.* (2003) 'Hypoxia-inducible factors 1α and 2α are related to vascular endothelial growth factor expression and a poorer prognosis in nodular malignant melanomas of the skin', *Melanoma Research*, 13(5), pp. 493–501. doi:

10.1097/00008390-200310000-00008.

Gilkes, D. M., Chaturvedi, P., *et al.* (2013) 'Collagen prolyl hydroxylases are essential for breast cancer metastasis', *Cancer Research*, 73(11), pp. 3285–3296. doi: 10.1158/0008-5472.CAN-12-3963.

Gilkes, D. M., Bajpai, S., Chaturvedi, P., *et al.* (2013) 'Hypoxia-inducible f0actor 1 (HIF-1) promotes extracellular matrix remodeling under hypoxic conditions by inducing P4HA1, P4HA2, and PLOD2 expression in fibroblasts', *Journal of Biological Chemistry*, 288(15), pp. 10819–10829. doi: 10.1074/jbc.M112.442939.

Gilkes, D. M., Bajpai, S., Wong, C. C., *et al.* (2013) 'Procollagen lysyl hydroxylase 2 is essential for hypoxia-induced breast cancer metastasis', *Molecular Cancer Research*, 11(5), pp. 456–466. doi: 10.1158/1541-7786.MCR-12-0629.

Gilmore, A. P. (2005) 'Anoikis', *Cell Death & Differentiation*, 12(S2), pp. 1473–1477. doi: 10.1038/sj.cdd.4401723.

Gimbrone, M. A. and García-Cardeña, G. (2016) 'Endothelial Cell Dysfunction and the Pathobiology of Atherosclerosis', *Circulation Research*. Lippincott Williams and Wilkins, 118(4), pp. 620–636. doi: 10.1161/CIRCRESAHA.115.306301.

Goldman, R. J. (2009) 'Hyperbaric Oxygen Therapy for Wound Healing and Limb Salvage: A Systematic Review', *PM and R*, pp. 471–489. doi: 10.1016/j.pmrj.2009.03.012.

Gómez-Gaviro, M. V. *et al.* (2012) 'Betacellulin promotes cell proliferation in the neural stem cell niche and stimulates neurogenesis', *Proceedings of the National Academy of Sciences of the United States of America*, 109(4), pp. 1317–1322. doi: 10.1073/pnas.1016199109.

Gong, H. *et al.* (2015) 'HIF2α signaling inhibits adherens junctional disruption in acute lung injury', *Journal of Clinical Investigation*, 125(2), pp. 652–664. doi: 10.1172/JCI77701.

Gras, E. *et al.* (2016) 'Endothelin-1 mediates intermittent hypoxia-induced inflammatory vascular remodeling through HIF-1 activation', *Journal of Applied Physiology*, 120(4), pp. 437–443. doi: 10.1152/japplphysiol.00641.2015.

Greijer, A. E. and Van Der Wall, E. (2004) 'The role of hypoxia inducible factor 1 (HIF-1) in hypoxia induced apoptosis', *Journal of Clinical Pathology*, 57(10), pp. 1009–1014. doi: 10.1136/jcp.2003.015032.

Gruber, M. *et al.* (2007) 'Acute postnatal ablation of Hif-2α results in anemia', *Proceedings of the National Academy of Sciences of the United States of America*, 104(7), pp. 2301–2306. doi: 10.1073/pnas.0608382104.

Gu, Y. Z. *et al.* (1998) 'Molecular characterization and chromosomal localization of a third α-

class hypoxia inducible factor subunit, HIF3α', *Gene Expression*, 7(3), pp. 205–213.

Le Guelte, A. and Gavard, J. (2011) 'Role of endothelial cell-cell junctions in endothelial permeability', *Methods in Molecular Biology*, 763, pp. 265–279. doi: 10.1007/978-1-61779-191-8_18.

Gupta, G. P. *et al.* (2007) 'Mediators of vascular remodelling co-opted for sequential steps in lung metastasis', *Nature*, 446(7137), pp. 765–770. doi: 10.1038/nature05760.

Haddad, J. J. and Harb, H. L. (2005) 'Cytokines and the regulation of hypoxia-inducible factor (HIF)-1α', *International Immunopharmacology*, 5(3), pp. 461–483. doi: 10.1016/j.intimp.2004.11.009.

Hagen, T. *et al.* (2003) 'Redistribution of Intracellular Oxygen in Hypoxia by Nitric Oxide: Effect on HIF1α', *Science*, 302(5652), pp. 1975–1978. doi: 10.1126/science.1088805.

Hamm, A. *et al.* (2013) 'PHD2 regulates arteriogenic macrophages through TIE2 signalling', *EMBO Molecular Medicine*, 5(6), pp. 843–857. doi: 10.1002/emmm.201302695.

Han, J. *et al.* (2015) 'Vascular Endothelial Growth Factor Receptor 3 Controls Neural Stem Cell Activation in Mice and Humans', *Cell Reports*. Elsevier, 10(7), pp. 1158–1172. doi: 10.1016/j.celrep.2015.01.049.

Hao, J. (2015) 'HIF-1 is a critical target of pancreatic cancer', *OncoImmunology*. Taylor and Francis Inc., 4(9), pp. 1–3. doi: 10.1080/2162402X.2015.1026535.

Hara, S. *et al.* (2001) 'Expression and characterization of hypoxia-inducible factor (HIF)-3α in human kidney: Suppression of HIF-mediated gene expression by HIF-3α', *Biochemical and Biophysical Research Communications*. Academic Press Inc., 287(4), pp. 808–813. doi: 10.1006/bbrc.2001.5659.

Harney, A. S. *et al.* (2015) 'Real-time imaging reveals local, transient vascular permeability, and tumor cell intravasation stimulated by TIE2hi macrophage–derived VEGFA', *Cancer Discovery*. American Association for Cancer Research Inc., 5(9), pp. 932–943. doi: 10.1158/2159-8290.CD-15-0012.

Harrison, L. and Blackwell, K. (2004) 'Hypoxia and anemia: factors in decreased sensitivity to radiation therapy and chemotherapy?', *Oncologist*, 9. doi: 10.1634/theoncologist.9-90005-31.

Hart, J. (2011) 'Cancer mortality for a single race in low versus high elevation counties in the U.S', *Dose-Response*, 9(3), pp. 348–355. doi: 10.2203/dose-response.10-014.Hart.

Heiden, M. G. Vander, Cantley, L. C. and Thompson, C. B. (2009) 'Understanding the warburg effect: The metabolic requirements of cell proliferation', *Science*, pp. 1029–1033. doi: 10.1126/science.1160809.

Helczynska, K. *et al.* (2008) 'Hypoxia-inducible factor-2α correlates to distant recurrence and poor outcome in invasive breast cancer', *Cancer Research*, 68(22), pp. 9212–9220. doi: 10.1158/0008-5472.CAN-08-1135.

Helmerhorst, H. J. F. *et al.* (2015) 'Association between arterial hyperoxia and outcome in subsets of critical illness: A systematic review, meta-analysis, and meta-regression of cohort studies', *Critical Care Medicine*. Lippincott Williams and Wilkins, 43(7), pp. 1508–1519. doi: 10.1097/CCM.0000000000000998.

Henn, A., Darou, S. and Yerden, R. (2019) 'Full-time physioxic culture conditions promote MSC proliferation more than hypoxic preconditioning', *Cytotherapy*. Elsevier BV, 21(5), pp. S73–S74. doi: 10.1016/j.jcyt.2019.03.470.

Herriges, M. and Morrisey, E. E. (2014) 'Lung development: Orchestrating the generation and regeneration of a complex organ', *Development (Cambridge)*, pp. 502–513. doi: 10.1242/dev.098186.

Hirsilä, M. *et al.* (2003) 'Characterization of the human prolyl 4-hydroxylases that modify the hypoxia-inducible factor', *Journal of Biological Chemistry*, 278(33), pp. 30772–30780. doi: 10.1074/jbc.M304982200.

Hogenesch, J. B. *et al.* (1997) 'Characterization of a subset of the basic-helix-loop-helix-PAS superfamily that interacts with components of the dioxin signaling pathway', *Journal of Biological Chemistry*, 272(13), pp. 8581–8593. doi: 10.1074/jbc.272.13.8581.

Hopf, H. W. *et al.* (1997) 'Wound tissue oxygen tension predicts the risk of wound infection in surgical patients', *Archives of Surgery*. American Medical Association, 132(9), pp. 997–1005. doi: 10.1001/archsurg.1997.01430330063010.

Hoyos, C. M. *et al.* (2015) 'Does obstructive sleep apnea cause endothelial dysfunction? A critical review of the literature', *Sleep Medicine Reviews*. W.B. Saunders Ltd, pp. 15–26. doi: 10.1016/j.smrv.2014.06.003.

Huang, D. *et al.* (2001) 'Absence of monocyte chemoattractant protein 1 in mice leads to decreased local macrophage recruitment and antigen-specific T helper cell type 1 immune response in experimental autoimmune encephalomyelitis', *Journal of Experimental Medicine*, 193(6), pp. 713–725. doi: 10.1084/jem.193.6.713.

Huang, Y. *et al.* (2009) 'Pulmonary vascular destabilization in the premetastatic phase facilitates lung metastasis', *Cancer Research*, 69(19), pp. 7529–7537. doi: 10.1158/0008-5472.CAN-08-4382.

Huang, Y. *et al.* (2012) 'Normal glucose uptake in the brain and heart requires an endothelial cell-specific HIF-1α-dependent function', *Proceedings of the National Academy of*

Sciences of the United States of America, 109(43), pp. 17478–17483. doi: 10.1073/pnas.1209281109.

Huang, Y. *et al.* (2013) 'Hypoxia Inducible Factor 3α Plays a Critical Role in Alveolarization and Distal Epithelial Cell Differentiation during Mouse Lung Development', *PLoS ONE*. Edited by O. Eickelberg, 8(2), p. e57695. doi: 10.1371/journal.pone.0057695.

Hur, E. *et al.* (2001) 'Mitogen-activated protein kinase kinase inhibitor PD98059 blocks the trans-activation but not the stabilization or DNA binding ability of Hypoxia-inducible factor-1α', *Molecular Pharmacology*. American Society for Pharmacology and Experimental Therapy, 59(5), pp. 1216–1224. doi: 10.1124/mol.59.5.1216.

Iommarini, L. *et al.* (2017) 'Non-canonical mechanisms regulating hypoxia-inducible factor 1 alpha in cancer', *Frontiers in Oncology*. Frontiers Media S.A. doi: 10.3389/fonc.2017.00286.

Ivan, M. *et al.* (2001) 'HIFα targeted for VHL-mediated destruction by proline hydroxylation: Implications for O2 sensing', *Science*. American Association for the Advancement of Science, 292(5516), pp. 464–468. doi: 10.1126/science.1059817.

Jaakkola, P. *et al.* (2001) 'Targeting of HIF-α to the von Hippel-Lindau ubiquitylation complex by O 2 -regulated prolyl hydroxylation', *Science*. American Association for the Advancement of Science, 292(5516), pp. 468–472. doi: 10.1126/science.1059796.

Janota, C., Lemere, C. A. and Brito, M. A. (2016) 'Dissecting the Contribution of Vascular Alterations and Aging to Alzheimer's Disease', *Molecular Neurobiology*. Humana Press Inc., pp. 3793–3811. doi: 10.1007/s12035-015-9319-7.

Jenvey, C. J. and Stabel, J. R. (2017) 'Autofluorescence and Nonspecific Immunofluorescent Labeling in Frozen Bovine Intestinal Tissue Sections: Solutions for Multicolor Immunofluorescence Experiments', *Journal of Histochemistry and Cytochemistry*. Histochemical Society Inc., 65(9), pp. 531–541. doi: 10.1369/0022155417724425.

Jiang, Y.-Z. *et al.* (2013) 'Transcriptional and Functional Adaptations of Human Endothelial Cells to Physiological Chronic Low Oxygen1', *Biology of Reproduction*. Oxford University Press (OUP), 88(5). doi: 10.1095/biolreprod.113.108225.

Jing, S. W. *et al.* (2012) 'HIF-1α contributes to hypoxia-induced invasion and metastasis of esophageal carcinoma via inibiting E-cadherin and promoting MMP-2 expression', *Acta Medica Okayama*, 66(5), pp. 399–407. doi: 10.18926/AMO/48964.

Kalsi, K. K. *et al.* (2017) 'Mechanisms for the control of local tissue blood flow during thermal interventions: influence of temperature-dependent ATP release from human blood and endothelial cells', *Experimental Physiology*. Blackwell Publishing Ltd, 102(2), pp.

228–244. doi: 10.1113/EP085910.

Kapanci, Y. *et al.* (1969) 'Pathogenesis and reversibility of the pulmonary lesions of oxygen toxicity in monkeys. II. Ultrastructural and morphometric studies.', *Laboratory Investigation*, 20(1), pp. 101–118.

Kapitsinou, P. P. *et al.* (2014) 'Endothelial HIF-2 mediates protection and recovery from ischemic kidney injury', *Journal of Clinical Investigation*, 124(6), pp. 2396–2409. doi: 10.1172/JCI69073.

Keith, B., Johnson, R. S. and Simon, M. C. (2011) 'HIF1alpha and HIF2alpha: sibling rivalry in hypoxic tumour growth and progression', *Nat. Rev. Cancer*, 12. doi: 10.1038/nrc3183.

Kim, J. H. *et al.* (2013) 'Reactive oxygen species-responsive miR-210 regulates proliferation and migration of adipose-derived stem cells via PTPN2', *Cell Death and Disease*, 4(4). doi: 10.1038/cddis.2013.117.

Kim, J. J. *et al.* (2015) 'WSB1 promotes tumor metastasis by inducing pVHL degradation', *Genes and Development*. Cold Spring Harbor Laboratory Press, 29(21), pp. 2244–2257. doi: 10.1101/gad.268128.115.

Kim, J. W. *et al.* (2006) 'HIF-1-mediated expression of pyruvate dehydrogenase kinase: A metabolic switch required for cellular adaptation to hypoxia', *Cell Metabolism*, 3(3), pp. 177–185. doi: 10.1016/j.cmet.2006.02.002.

Kim, Y.-Y. and Lee, S. M. (2007) 'Treatment and Prevention of High Altitude Illness and Mountain Sickness', *Journal of the Korean Medical Association*. Korean Medical Association (KAMJE), 50(11), p. 1005. doi: 10.5124/jkma.2007.50.11.1005.

Kistler, G. S., Caldwell, P. R. and Weibel, E. R. (1967) 'Development of fine structural damage to alveolar and capillary lining cells in oxygen-poisoned rat lungs.', *The Journal of cell biology*, 32(3), pp. 605–628. doi: 10.1083/jcb.32.3.605.

Kitamura, T., Qian, B. Z., Soong, D., *et al.* (2015) 'CCL2-induced chemokine cascade promotes breast cancer metastasis by enhancing retention of metastasis-associated macrophages', *Journal of Experimental Medicine*, 212(7), pp. 1043–1059. doi: 10.1084/jem.20141836.

Kitamura, T. and Pollard, J. W. (2015) 'Therapeutic potential of chemokine signal inhibition for metastatic breast cancer', *Pharmacological Research*, 100, pp. 266–270. doi: 10.1016/j.phrs.2015.08.004.

Kitamura, T., Qian, B. Z. and Pollard, J. W. (2015) 'Immune cell promotion of metastasis', *Nature Reviews Immunology*. Nature Publishing Group, pp. 73–86. doi:

10.1038/nri3789.

Kobayashi, S. *et al.* (2015) 'Hypoxia-inducible factor-3α promotes angiogenic activity of pulmonary endothelial cells by repressing the expression of the VE-cadherin gene', *Genes to Cells*, 20(3), pp. 224–241. doi: 10.1111/gtc.12215.

Koh, M. Y., Darnay, B. G. and Powis, G. (2008) 'Hypoxia-Associated Factor, a Novel E3-Ubiquitin Ligase, Binds and Ubiquitinates Hypoxia-Inducible Factor 1 , Leading to Its Oxygen-Independent Degradation', *Molecular and Cellular Biology*, 28(23), pp. 7081–7095. doi: 10.1128/mcb.00773-08.

Koh, M. Y. and Powis, G. (2012) 'Passing the baton: The HIF switch', *Trends in Biochemical Sciences*, 37(9), pp. 364–372. doi: 10.1016/j.tibs.2012.06.004.

Koivunen, P. *et al.* (2004) 'Catalytic Properties of the Asparaginyl Hydroxylase (FIH) in the Oxygen Sensing Pathway Are Distinct from Those of Its Prolyl 4-Hydroxylases', *Journal of Biological Chemistry*, 279(11), pp. 9899–9904. doi: 10.1074/jbc.M312254200.

Koshikawa, N. *et al.* (2009) 'Reactive oxygen species-generating mitochondrial DNA mutation up-regulates hypoxia-inducible factor-1α gene transcription via phosphatidylinositol 3-kinase-Akt/protein kinase C/histone deacetylase pathway', *Journal of Biological Chemistry*, 284(48), pp. 33185–33194. doi: 10.1074/jbc.M109.054221.

Kostallari, E. and Shah, V. H. (2016) 'Angiocrine signaling in the hepatic sinusoids in health and disease', *American Journal of Physiology - Gastrointestinal and Liver Physiology*. American Physiological Society, 311(2), pp. G246–G251. doi: 10.1152/ajpgi.00118.2016.

Koziel, A. *et al.* (2012) 'The influence of high glucose on the aerobic metabolism of endothelial EA.hy926 cells', *Pflugers Archiv European Journal of Physiology*, 464(6), pp. 657–669. doi: 10.1007/s00424-012-1156-1.

Krishnamachary, B. *et al.* (2006) 'Hypoxia-inducible factor-1-dependent repression of E-cadherin in von Hippel-Lindau tumor suppressor-null renal cell carcinoma mediated by TCF3, ZFHX1A, and ZFHX1B', *Cancer Research*, 66(5), pp. 2725–2731. doi: 10.1158/0008-5472.CAN-05-3719.

Krock, B. L., Skuli, N. and Simon, M. C. (2011) 'Hypoxia-Induced Angiogenesis: Good and Evil', *Genes and Cancer*, 2(12), pp. 1117–1133. doi: 10.1177/1947601911423654.

Krotova, K. *et al.* (2010) 'Hypoxic upregulation of arginase II in human lung endothelial cells', *American Journal of Physiology - Cell Physiology*, 299(6). doi: 10.1152/ajpcell.00068.2010.

Krützfeldt, A. *et al.* (1990) 'Metabolism of exogenous substrates by coronary endothelial cells in culture', *Journal of Molecular and Cellular Cardiology*, 22(12), pp. 1393–1404. doi: 10.1016/0022-2828(90)90984-A.

Kumar, H. and Choi, D. K. (2015) 'Hypoxia Inducible Factor Pathway and Physiological Adaptation: A Cell Survival Pathway?', *Mediators of Inflammation*, 2015, pp. 1–11. doi: 10.1155/2015/584758.

Labelle, M. and Hynes, R. O. (2012) 'The initial hours of metastasis: The importance of cooperative host-tumor cell interactions during hematogenous dissemination', *Cancer Discovery*, 2(12), pp. 1091–1099. doi: 10.1158/2159-8290.CD-12-0329.

Lacorre, D. A. *et al.* (2004) 'Plasticity of endothelial cells: Rapid dedifferentiation of freshly isolated high endothelial venule endothelial cells outside the lymphoid tissue microenvironment', *Blood*, 103(11), pp. 4164–4172. doi: 10.1182/blood-2003-10-3537.

Lambert, C. M. *et al.* (2010) 'HIF-1 inhibition decreases systemic vascular remodelling diseases by promoting apoptosis through a hexokinase 2-dependent mechanism', *Cardiovascular Research*, 88(1), pp. 196–204. doi: 10.1093/cvr/cvq152.

Lando, D., Peet, D. J., Whelan, D. A., *et al.* (2002) 'Asparagine hydroxylation of the HIF transactivation domain: A hypoxic switch', *Science*, 295(5556), pp. 858–861. doi: 10.1126/science.1068592.

Lando, D., Peet, D. J., Gorman, J. J., *et al.* (2002) 'FIH-1 is an asparaginyl hydroxylase enzyme that regulates the transcriptional activity of hypoxia-inducible factor', *Genes and Development*, 16(12), pp. 1466–1471. doi: 10.1101/gad.991402.

Laoui, D. *et al.* (2014) 'Tumor hypoxia does not drive differentiation of tumor-associated macrophages but rather fine-tunes the M2-like macrophage population', *Cancer Research*, 74(1), pp. 24–30. doi: 10.1158/0008-5472.CAN-13-1196.

Laughner, E. *et al.* (2001) 'HER2 (neu) Signaling Increases the Rate of Hypoxia-Inducible Factor 1 (HIF-1) Synthesis: Novel Mechanism for HIF-1-Mediated Vascular Endothelial Growth Factor Expression', *Molecular and Cellular Biology*. American Society for Microbiology, 21(12), pp. 3995–4004. doi: 10.1128/mcb.21.12.3995-4004.2001.

Lee, E. *et al.* (2002) 'Two transactivation domains of hypoxia-inducible factor-1α regulated by the MEK-1/p42/p44 MARK pathway', *Molecules and Cells*, 14(1), pp. 9–15. Available at: http://www.ncbi.nlm.nih.gov/pubmed/12243358 (Accessed: 24 November 2019).

Lee, J. Y., McMurtry, S. A. and Stevens, T. (2017) 'Single cell cloning generates lung

endothelial colonies with conserved growth, angiogenic, and bioenergetic characteristics', *Pulmonary Circulation*, 7(4), pp. 777–792. doi: 10.1177/2045893217731295.

Lee, S. H. *et al.* (2009) 'HIF-1 is induced via EGFR activation and mediates resistance to anoikis-like cell death under lipid rafts/caveolae-disrupting stress', *Carcinogenesis*, 30(12), pp. 1997–2004. doi: 10.1093/carcin/bgp233.

Leventhal, C. *et al.* (1999) 'Endothelial trophic support of neuronal production and recruitment from the adult mammalian subependyma', *Molecular and Cellular Neurosciences*, 13(6), pp. 450–464. doi: 10.1006/mcne.1999.0762.

Lewis, C. E., Harney, A. S. and Pollard, J. W. (2016) 'Erratum: The Multifaceted Role of Perivascular Macrophages in Tumors (Cancer Cell (2016) 30(1) (18–25) (S1535610816302227) (10.1016/j.ccell.2016.05.017))', *Cancer Cell*, 30(2), p. 365. doi: 10.1016/j.ccell.2016.07.009.

Li, A. E. *et al.* (1999) 'A role for reactive oxygen species in endothelial cell anoikis', *Circulation Research*, 85(4), pp. 304–310. doi: 10.1161/01.RES.85.4.304.

Li, N. *et al.* (2016) 'Hypoxia inducible factor 1 (HIF-1) recruits macrophage to activate pancreatic stellate cells in ancreatic ductal adenocarcinoma', *International Journal of Molecular Sciences*, 17(6). doi: 10.3390/ijms17060799.

Li, X. and Carmeliet, P. (2018) 'Targeting angiogenic metabolism in disease', *Science*. American Association for the Advancement of Science, pp. 1335–1336. doi: 10.1126/science.aar5557.

Liu, J. F., Tsao, Y. T. and Hou, C. H. (2015) 'Amphiregulin enhances intercellular adhesion molecule-1 expression and promotes tumor metastasis in human osteosarcoma', *Oncotarget*, 6. doi: 10.18632/oncotarget.5679.

Liu, K. E. and Frazier, W. A. (2015) 'Phosphorylation of the BNIP3 C-terminus inhibits mitochondrial damage and cell death without blocking autophagy', *PLoS ONE*. Public Library of Science, 10(6). doi: 10.1371/journal.pone.0129667.

Lorenzo, A. *et al.* (2011) 'Endothelial reticulon-4B (Nogo-B) regulates ICAM-1-mediated leukocyte transmigration and acute inflammation', *Blood*, 117. doi: 10.1182/blood-2010-04-281956.

Luo, W. *et al.* (2010) 'Hsp70 and CHIP selectively mediate ubiquitination and degradation of hypoxia-inducible factor (HIF)-1α but not HIF-2α', *Journal of Biological Chemistry*, 285(6), pp. 3651–3663. doi: 10.1074/jbc.M109.068577.

Ma, C. *et al.* (2018) 'Hyperoxia causes mitochondrial fragmentation in pulmonary endothelial

cells by increasing expression of pro-fission proteins', *Arteriosclerosis, Thrombosis, and Vascular Biology*. Lippincott Williams and Wilkins, 38(3), pp. 622–635. doi: 10.1161/ATVBAHA.117.310605.

Madden, L. A. and Laden, G. (2009) 'Gas bubbles may not be the underlying cause of decompression illness - The at-depth endothelial dysfunction hypothesis', *Medical Hypotheses*, 72(4), pp. 389–392. doi: 10.1016/j.mehy.2008.11.022.

Mahon, P. C., Hirota, K. and Semenza, G. L. (2001) 'FIH-1: A novel protein that interacts with HIF-1α and VHL to mediate repression of HIF-1 transcriptional activity', *Genes and Development*, 15(20), pp. 2675–2686. doi: 10.1101/gad.924501.

Makino, Y. *et al.* (2001) 'Inhibitory PAS domain protein is a negative regulator of hypoxia-inducible gene expression', *Nature*, 414(6863), pp. 550–554. doi: 10.1038/35107085.

Marcu, R. *et al.* (2018) 'Human Organ-Specific Endothelial Cell Heterogeneity', *iScience*. Elsevier, 4, pp. 20–35. doi: 10.1016/j.isci.2018.05.003.

Marques-Santos, L. F. *et al.* (2003) 'Mitotracker Green is a P-Glycoprotein Substrate', *Bioscience Reports*, 23(4), pp. 199–212. doi: 10.1023/B:BIRE.0000007693.33521.18.

Mata-Greenwood, E., Goyal, D. and Goyal, R. (2017) 'Comparative and experimental studies on the genes altered by chronic hypoxia in human brain microendothelial cells', *Frontiers in Physiology*. Frontiers Media S.A., 8(MAY). doi: 10.3389/fphys.2017.00365.

Mattishent, K. *et al.* (2019) 'Safety of 80% vs 30–35% fraction of inspired oxygen in patients undergoing surgery: a systematic review and meta-analysis', *British Journal of Anaesthesia*. Elsevier Ltd, pp. 311–324. doi: 10.1016/j.bja.2018.11.026.

Maxwell, P. H. *et al.* (1999) 'The tumour suppressor protein VHL targets hypoxia-inducible factors for oxygen-dependent proteolysis', *Nature*, 399(6733), pp. 271–275. doi: 10.1038/20459.

Maynard, M. A. *et al.* (2005) 'Human HIF-3α4 is a dominant-negative regulator of HIF-1 and is down-regulated in renal cell carcinoma', *FASEB Journal*, 19(11), pp. 1396–1406. doi: 10.1096/fj.05-3788com.

Maynard, M. A. *et al.* (2007) 'Dominant-negative HIF-3α4 suppresses VHL-null renal cell carcinoma progression', *Cell Cycle*. Taylor and Francis Inc., 6(22), pp. 2810–2816. doi: 10.4161/cc.6.22.4947.

McKeown, S. R. (2014) 'Defining normoxia, physoxia and hypoxia in tumours - Implications for treatment response', *British Journal of Radiology*. British Institute of Radiology. doi: 10.1259/bjr.20130676.

Meng, F. *et al.* (2007) 'Surfactant protein A promoter directs the expression of Cre recombinase in brain microvascular endothelial cells of transgenic mice', *Matrix Biology*, 26(1), pp. 54–57. doi: 10.1016/j.matbio.2006.09.003.

Mergenthaler, P. *et al.* (2013) 'Sugar for the brain: The role of glucose in physiological and pathological brain function', *Trends in Neurosciences*. NIH Public Access, 36(10), pp. 587–597. doi: 10.1016/j.tins.2013.07.001.

Metallo, C. M., Walther, J. L. and Stephanopoulos, G. (2009) 'Evaluation of 13C isotopic tracers for metabolic flux analysis in mammalian cells', *Journal of Biotechnology*, 144(3), pp. 167–174. doi: 10.1016/j.jbiotec.2009.07.010.

Metzen, E. *et al.* (2003) 'Nitric oxide impairs normoxic degradation of HIF-1α by inhibition of prolyl hydroxylases', *Molecular Biology of the Cell*, 14(8), pp. 3470–3481. doi: 10.1091/mbc.E02-12-0791.

Michiels, C. (2003) 'Endothelial cell functions', *Journal of Cellular Physiology*, pp. 430–443. doi: 10.1002/jcp.10333.

Miller, G. W. *et al.* (2010) 'A short-breath-hold technique for lung pO2 mapping with 3He MRI', *Magnetic Resonance in Medicine*. John Wiley & Sons, Ltd, 63(1), pp. 127–136. doi: 10.1002/mrm.22181.

Milovanova, T. N. *et al.* (2009) 'Hyperbaric oxygen stimulates vasculogenic stem cell growth and differentiation in vivo', *Journal of Applied Physiology*, 106(2), pp. 711–728. doi: 10.1152/japplphysiol.91054.2008.

Minoves, M. *et al.* (2017) 'An innovative intermittent hypoxia model for cell cultures allowing fast PO2 oscillations with minimal gas consumption', *American Journal of Physiology - Cell Physiology*, 313(4), pp. C460–C468. doi: 10.1152/ajpcell.00098.2017.

Montero-Balaguer, M. *et al.* (2009) 'Stable vascular connections and remodeling require full expression of VE-cadherin in zebrafish embryos', *PLoS ONE*. Edited by P. Callaerts, 4(6), p. e5772. doi: 10.1371/journal.pone.0005772.

Mookerjee, S. A. *et al.* (2017) 'Quantifying intracellular rates of glycolytic and oxidative ATP production and consumption using extracellular flux measurements', *Journal of Biological Chemistry*. American Society for Biochemistry and Molecular Biology Inc., 292(17), pp. 7189–7207. doi: 10.1074/jbc.M116.774471.

Muñoz-Nájar, U. M. *et al.* (2006) 'Hypoxia stimulates breast carcinoma cell invasion through MT1-MMP and MMP-2 activation', *Oncogene*, 25(16), pp. 2379–2392. doi: 10.1038/sj.onc.1209273.

Nakajima, E. C. and Van Houten, B. (2013) 'Metabolic symbiosis in cancer: Refocusing the

Warburg lens', *Molecular Carcinogenesis*, 52(5), pp. 329–337. doi: 10.1002/mc.21863.

Nanduri, J. *et al.* (2009) 'Intermittent hypoxia degrades HIF-2α via calpains resulting in oxidative stress: Implications for recurrent apnea-induced morbidities', *Proceedings of the National Academy of Sciences of the United States of America*, 106(4), pp. 1199–1204. doi: 10.1073/pnas.0811018106.

Nanduri, J. *et al.* (2015) 'Hypoxia-inducible factors and hypertension: lessons from sleep apnea syndrome', *Journal of Molecular Medicine*. Springer Verlag, pp. 473–480. doi: 10.1007/s00109-015-1274-2.

Neely, J. R. *et al.* (1972) 'The effects of increased heart work on the tricarboxylate cycle and its interactions with glycolysis in the perfused rat heart.', *The Biochemical journal*, 128(1), pp. 147–159. doi: 10.1042/bj1280147.

Newby, D., Marks, L. and Lyall, F. (2005) 'Dissolved oxygen concentration in culture medium: Assumptions and pitfalls', *Placenta*. W.B. Saunders, 26(4), pp. 353–357. doi: 10.1016/j.placenta.2004.07.002.

Nguyen, H. M. *et al.* (2016) 'Reduction in cardiolipin decreases mitochondrial spare respiratory capacity and increases glucose transport into and across human brain cerebral microvascular endothelial cells', *Journal of Neurochemistry*, 139(1), pp. 68–80. doi: 10.1111/jnc.13753.

Niemann, S. and Muller, U. (2000) 'Mutations in SDHC cause autosomal dominant paraganglioma, type 3', *Nature Genetics*, 26(3), pp. 268–270. doi: 10.1038/81551.

Nieto, F. J. *et al.* (2012) 'Sleep-disordered breathing and cancer mortality: Results from the Wisconsin Sleep Cohort Study', *American Journal of Respiratory and Critical Care Medicine*, 186(2), pp. 190–194. doi: 10.1164/rccm.201201-0130OC.

Nitta, T. *et al.* (2003) 'Size-selective loosening of the blood-brain barrier in claudin-5-deficient mice', *Journal of Cell Biology*, 161(3), pp. 653–660. doi: 10.1083/jcb.200302070.

Niu, G. *et al.* (2008) 'Signal transducer and activator of transcription 3 is required for hypoxia-inducible factor-1α RNA expression in both tumor cells and tumor-associated myeloid cells', *Molecular Cancer Research*, 6(7), pp. 1099–1105. doi: 10.1158/1541-7786.MCR-07-2177.

Nolan, D. J. *et al.* (2013) 'Molecular Signatures of Tissue-Specific Microvascular Endothelial Cell Heterogeneity in Organ Maintenance and Regeneration', *Developmental Cell*. Cell Press, 26(2), pp. 204–219. doi: 10.1016/j.devcel.2013.06.017.

Nytko, K. J. *et al.* (2011) 'Vitamin C is dispensable for oxygen sensing in vivo', *Blood*, 117(20), pp. 5485–5493. doi: 10.1182/blood-2010-09-307637.

Oldendorf, W. H., Cornford, M. E. and Brown, W. J. (1977) 'The large apparent work capability of the blood-brain barrier: A study of the mitochondrial content of capillary endothelial cells in brain and other tissues of the rat', *Annals of Neurology*. John Wiley & Sons, Ltd, 1(5), pp. 409–417. doi: 10.1002/ana.410010502.

Olson, A. L. and Pessin, J. E. (1996) 'Structure, Function, and Regulation of the Mammalian Facilitative Glucose Transporter Gene Family', *Annual Review of Nutrition*, 16(1), pp. 235–256. doi: 10.1146/annurev.nu.16.070196.001315.

OpenSTAX CNX (2015) *OpenSTAX, Biology - Oxidative Phosphorylation*.

Ottone, C. *et al.* (2014) 'Direct cell-cell contact with the vascular niche maintains quiescent neural stem cells', *Nature Cell Biology*. Nature Publishing Group, 16(11), pp. 1045–1056. doi: 10.1038/ncb3045.

Pagé, E. L. *et al.* (2002) 'Induction of hypoxia-inducible factor-1α by transcriptional and translational mechanisms', *Journal of Biological Chemistry*, 277(50), pp. 48403–48409. doi: 10.1074/jbc.M209114200.

Paget, S. (1889) 'the Distribution of Secondary Growths in Cancer of the Breast.', *The Lancet*, 133(3421), pp. 571–573. doi: 10.1016/S0140-6736(00)49915-0.

Park, S. O. *et al.* (2008) 'ALK5- and TGFBR2-independent role of ALK1 in the pathogenesis of hereditary hemorrhagic telangiectasia type 2', *Blood*, 111(2), pp. 633–642. doi: 10.1182/blood-2007-08-107359.

Pasquier, J. *et al.* (2018) 'Surgical peritoneal stress creates a pro-metastatic niche promoting resistance to apoptosis via IL-8 11 Medical and Health Sciences 1112 Oncology and Carcinogenesis 11 Medical and Health Sciences 1103 Clinical Sciences', *Journal of Translational Medicine*, 16(1), p. 271. doi: 10.1186/s12967-018-1643-z.

Patanaphan, V., Salazar, O. M. and Risco, R. (1988) 'Breast cancer: Metastatic patterns and their prognosis', *Southern Medical Journal*, 81(9), pp. 1109–1112. doi: 10.1097/00007611-198809000-00011.

Paulin, R. and Michelakis, E. D. (2014) 'The metabolic theory of pulmonary arterial hypertension', *Circulation Research*, 115(1), pp. 148–164. doi: 10.1161/CIRCRESAHA.115.301130.

Dela Paz, N. G. and D'Amore, P. A. (2009) 'Arterial versus venous endothelial cells', *Cell and Tissue Research*, pp. 5–16. doi: 10.1007/s00441-008-0706-5.

Peinado, H. *et al.* (2017) 'Pre-metastatic niches: Organ-specific homes for metastases', *Nature Reviews Cancer*. Nature Publishing Group, pp. 302–317. doi: 10.1038/nrc.2017.6.

Peyssonnaux, C. *et al.* (2007) 'Regulation of iron homeostasis by the hypoxia-inducible

transcription factors (HIFs)', *Journal of Clinical Investigation*, 117(7), pp. 1926–1932. doi: 10.1172/JCI31370.

Pfleger, J., He, M. and Abdellatif, M. (2015) 'Mitochondrial complex II is a source of the reserve respiratory capacity that is regulated by metabolic sensors and promotes cell survival', *Cell Death and Disease*. Nature Publishing Group, 6(7). doi: 10.1038/cddis.2015.202.

Pihlajaniemi, T., Myllylä, R. and Kivirikko, K. I. (1991) 'Prolyl 4-hydroxylase and its role in collagen synthesis', *Journal of Hepatology*, 13(SUPPL. 3), p. S2. doi: 10.1016/0168-8278(91)90002-S.

Poff, A. M. *et al.* (2015) 'Non-toxic metabolic management of metastatic cancer in VM mice: Novel combination of ketogenic diet, ketone supplementation, and hyperbaric oxygen therapy', *PLoS ONE*. Public Library of Science, 10(6). doi: 10.1371/journal.pone.0127407.

Polotsky, V. Y. *et al.* (2010) 'Intermittent and sustained hypoxia induce a similar gene expression profile in human aortic endothelial cells', *Physiological Genomics*, 41(3), pp. 306–314. doi: 10.1152/physiolgenomics.00091.2009.

Prabhakar, N. R., Kumar, G. K. and Nanduri, J. (2010) 'Intermittent hypoxia augments acute hypoxic sensing via HIF-mediated ROS', *Respir. Physiol. Neurobiol.*, 174. doi: 10.1016/j.resp.2010.08.022.

Prabhakar, N. R. and Semenza, G. L. (2012) 'Adaptive and maladaptive cardiorespiratory responses to continuous and intermittent hypoxia mediated by hypoxia-inducible factors 1 and 2', *Physiological Reviews*, 92(3), pp. 967–1003. doi: 10.1152/physrev.00030.2011.

Pugh, C. W. *et al.* (1991) 'Functional analysis of an oxygen-regulated transcriptional enhancer typing 3′ to the mouse erythropoietin gene', *Proceedings of the National Academy of Sciences of the United States of America*. National Academy of Sciences, 88(23), pp. 10553–10557. doi: 10.1073/pnas.88.23.10553.

Puisségur, M. P. *et al.* (2011) 'MiR-210 is overexpressed in late stages of lung cancer and mediates mitochondrial alterations associated with modulation of HIF-1 activity', *Cell Death and Differentiation*, 18(3), pp. 465–478. doi: 10.1038/cdd.2010.119.

Qi, W. X. *et al.* (2013) 'Incidence and risk of hypertension with vandetanib in cancer patients: A systematic review and meta-analysis of clinical trials', *British Journal of Clinical Pharmacology*, 75(4), pp. 919–930. doi: 10.1111/j.1365-2125.2012.04417.x.

Qian, B. Z. *et al.* (2011) 'CCL2 recruits inflammatory monocytes to facilitate breast-tumour

metastasis', *Nature*, 475(7355), pp. 222–225. doi: 10.1038/nature10138.

Qian, B. Z. *et al.* (2015) 'FLT1 signaling in metastasis-associated macrophages activates an inflammatory signature that promotes breast cancer metastasis', *Journal of Experimental Medicine*, 212(9), pp. 1433–1448. doi: 10.1084/jem.20141555.

Rafii, S. *et al.* (2015) 'Platelet-derived SDF-1 primes the pulmonary capillary vascular niche to drive lung alveolar regeneration', *Nature Cell Biology*. Nature Publishing Group, 17(2), pp. 123–136. doi: 10.1038/ncb3096.

Rafii, S., Butler, J. M. and Ding, B. Sen (2016) 'Angiocrine functions of organ-specific endothelial cells', *Nature*. Nature Publishing Group, pp. 316–325. doi: 10.1038/nature17040.

Rahimi, N. (2006) 'VEGFR-1 and VEGFR-2: Two non-identical twins with a unique physiognomy', *Frontiers in Bioscience*, pp. 818–829. doi: 10.2741/1839.

Ramasamy, S. K. (2017) 'Structure and Functions of Blood Vessels and Vascular Niches in Bone', *Stem Cells International*. Hindawi Limited. doi: 10.1155/2017/5046953.

Rankin, E. B., Nam, J. M. and Giaccia, A. J. (2016) 'Hypoxia: Signaling the Metastatic Cascade', *Trends in cancer*, 2. doi: 10.1016/j.trecan.2016.05.006.

Reissmann, K. R. (2016) 'Reissmann KR. Studies on the mechanism of erythropoietic stimulation in parabiotic rats during hypoxia', *Blood*, 127(5), p. 519. doi: 10.1182/blood-2015-12-686386.

Reiterer, M. *et al.* (2019) 'Acute and chronic hypoxia differentially predispose lungs for metastases', *Scientific Reports*. Springer Science and Business Media LLC, 9(1). doi: 10.1038/s41598-019-46763-y.

Reiterer, M. and Branco, C. M. (2019) 'Endothelial cells and organ function: applications and implications of understanding unique and reciprocal remodelling', *The FEBS Journal*, p. febs.15143. doi: 10.1111/febs.15143.

Reymond, N., D'Água, B. B. and Ridley, A. J. (2013) 'Crossing the endothelial barrier during metastasis', *Nature Reviews Cancer*, pp. 858–870. doi: 10.1038/nrc3628.

Ribatti, D. *et al.* (2002) 'Endothelial cell heterogeneity and organ specificity', *Journal of Hematotherapy and Stem Cell Research*, pp. 81–90. doi: 10.1089/152581602753448559.

Richard, D. E. *et al.* (1999) 'p42/p44 mitogen-activated protein kinases phosphorylate hypoxia-reducible factor (HIF-1α) and enhance the transcriptional activity of HIF-1', *Journal of Biological Chemistry*, 274(46), pp. 32631–32637. doi: 10.1074/jbc.274.46.32631.

Ridder, D. A. *et al.* (2011) 'TAK1 in brain endothelial cells mediates fever and lethargy',

Journal of Experimental Medicine, 208(13), pp. 2615–2623. doi: 10.1084/jem.20110398.

Rohan, T. E. *et al.* (2014) 'Tumor microenvironment of metastasis and risk of distant metastasis of breast cancer', *Journal of the National Cancer Institute*. Oxford University Press, 106(8). doi: 10.1093/jnci/dju136.

Rohlenova, K. *et al.* (2018) 'Endothelial Cell Metabolism in Health and Disease', *Trends in Cell Biology*. Elsevier Ltd, pp. 224–236. doi: 10.1016/j.tcb.2017.10.010.

Rose, S., Misharin, A. and Perlman, H. (2012) 'A novel Ly6C/Ly6G-based strategy to analyze the mouse splenic myeloid compartment', *Cytometry. Part A: the journal of the International Society for Analytical Cytology*, 81. doi: 10.1002/cyto.a.22012.

Ruck, T. *et al.* (2014) 'Isolation of primary murine brain microvascular endothelial cells', *Journal of Visualized Experiments*, (93), p. e52204. doi: 10.3791/52204.

Ryan, H. E., Lo, J. and Johnson, R. S. (1998) 'HIF-1α is required for solid tumor formation and embryonic vascularization', *EMBO Journal*, 17(11), pp. 3005–3015. doi: 10.1093/emboj/17.11.3005.

Sakamoto, S. *et al.* (2002) 'Involvement of kupffer cells in the interaction between neutrophils and sinusoidal endothelial cells in rats', *Shock*. BioMedical Press, 18(2), pp. 152–157. doi: 10.1097/00024382-200208000-00011.

Sakao, S. *et al.* (2005) 'Initial apoptosis is followed by increased proliferation of apoptosis-resistant endothelial cells', *FASEB Journal*, 19(9), pp. 1178–1180. doi: 10.1096/fj.04-3261fje.

Sang, N. *et al.* (2003) 'MAPK signaling up-regulates the activity of hypoxia-inducible factors by its effects on p300', *Journal of Biological Chemistry*, 278(16), pp. 14013–14019. doi: 10.1074/jbc.M209702200.

Sansbury, B. E. *et al.* (2011) 'Bioenergetic function in cardiovascular cells: The importance of the reserve capacity and its biological regulation', in *Chemico-Biological Interactions*, pp. 288–295. doi: 10.1016/j.cbi.2010.12.002.

Dos Santos, A. C. *et al.* (2005) 'CCL2 and CCL5 mediate leukocyte adhesion in experimental autoimmune encephalomyelitis - An intravital microscopy study', *Journal of Neuroimmunology*. Elsevier, 162(1–2), pp. 122–129. doi: 10.1016/j.jneuroim.2005.01.020.

Dos Santos, W. L. C. *et al.* (1996) 'Control of lymphocyte adhesion to brain and aortic endothelium: ICAM-1, VCAM-1 and negative charge', *Journal of Neuroimmunology*. Elsevier B.V., 66(1–2), pp. 125–134. doi: 10.1016/0165-5728(96)00037-9.

Scharf, J. G., Unterman, T. G. and Kietzmann, T. (2005) 'Oxygen-dependent modulation of insulin-like growth factor binding protein biosynthesis in primary cultures of rat hepatocytes', *Endocrinology*, 146(12), pp. 5433–5443. doi: 10.1210/en.2005-0948.

Schindelin, J. *et al.* (2012) 'Fiji: An open-source platform for biological-image analysis', *Nature Methods*, 9(7), pp. 676–682. doi: 10.1038/nmeth.2019.

Schoch, H. J. (2002) 'Hypoxia-induced vascular endothelial growth factor expression causes vascular leakage in the brain', *Brain*. Oxford University Press (OUP), 125(11), pp. 2549–2557. doi: 10.1093/brain/awf257.

Schönenberger, M. J. and Kovacs, W. J. (2015) 'Hypoxia signaling pathways: Modulators of oxygen-related organelles', *Frontiers in Cell and Developmental Biology*. Frontiers Media S.A. doi: 10.3389/fcell.2015.00042.

Selak, M. A. *et al.* (2005) 'Succinate links TCA cycle dysfunction to oncogenesis by inhibiting HIF-α prolyl hydroxylase', *Cancer Cell*, 7(1), pp. 77–85. doi: 10.1016/j.ccr.2004.11.022.

Semenza, G. L. (2011) 'Regulation of metabolism by hypoxia-inducible factor 1', *Cold Spring Harbor Symposia on Quantitative Biology*, 76, pp. 347–353. doi: 10.1101/sqb.2011.76.010678.

Semenza, G. L. (2012) 'Hypoxia-inducible factors in physiology and medicine', *Cell*, pp. 399–408. doi: 10.1016/j.cell.2012.01.021.

Semenza, G. L. and Wang, G. L. (1992) 'A nuclear factor induced by hypoxia via de novo protein synthesis binds to the human erythropoietin gene enhancer at a site required for transcriptional activation.', *Molecular and Cellular Biology*. American Society for Microbiology, 12(12), pp. 5447–5454. doi: 10.1128/mcb.12.12.5447.

Senger, D. R. *et al.* (1983) 'Tumor cells secrete a vascular permeability factor that promotes accumulation of ascites fluid', *Science*, 219(4587), pp. 983–985. doi: 10.1126/science.6823562.

Shah, Y. M. *et al.* (2009) 'Intestinal Hypoxia-Inducible Transcription Factors Are Essential for Iron Absorption following Iron Deficiency', *Cell Metabolism*, 9(2), pp. 152–164. doi: 10.1016/j.cmet.2008.12.012.

Sheikh, A. Y. *et al.* (2000) 'Effect of hyperoxia on vascular endothelial growth factor levels in a wound model', *Archives of Surgery*. American Medical Association, 135(11), pp. 1293–1297. doi: 10.1001/archsurg.135.11.1293.

Shimoda, L. A. and Semenza, G. L. (2011) 'HIF and the lung: role of hypoxia-inducible factors in pulmonary development and disease', *American journal of respiratory and critical*

care medicine, 183. doi: 10.1164/rccm.201009-1393PP.

Shyh-Chang, N., Daley, G. Q. and Cantley, L. C. (2013) 'Stem cell metabolism in tissue development and aging', *Development (Cambridge)*, pp. 2535–2547. doi: 10.1242/dev.091777.

Sim, J. *et al.* (2018) 'The Factor Inhibiting HIF Asparaginyl Hydroxylase Regulates Oxidative Metabolism and Accelerates Metabolic Adaptation to Hypoxia', *Cell Metabolism*. Cell Press, 27(4), pp. 898-913.e7. doi: 10.1016/j.cmet.2018.02.020.

Simionescu, M., Gafencu, A. and Antohe, F. (2002) 'Transcytosis of plasma macromolecules in endothelial cells: A cell biological survey', *Microscopy Research and Technique*. Wiley-Liss Inc., 57(5), pp. 269–288. doi: 10.1002/jemt.10086.

Skuli, N. *et al.* (2009) 'Endothelial deletion of hypoxia-inducible factor-2α (HIF-2α) alters vascular function and tumor angiogenesis', *Blood*, 114(2), pp. 469–477. doi: 10.1182/blood-2008-12-193581.

Sletta, K. Y. *et al.* (2017) 'Oxygen-dependent regulation of tumor growth and metastasis in human breast cancer xenografts', *PLoS ONE*. Edited by A. Ahmad, 12(8), p. e0183254. doi: 10.1371/journal.pone.0183254.

Smith, H. A. and Kang, Y. (2013) 'Acute infection induces a metastatic niche: A double menace for cancer patients', *Clinical Cancer Research*, 19(17), pp. 4547–4549. doi: 10.1158/1078-0432.CCR-13-1524.

Smith, R. H., Guilbeau, E. J. and Reneau, D. D. (1977) 'The oxygen tension field within a discrete volume of cerebral cortex', *Microvascular Research*, 13(2), pp. 233–240. doi: 10.1016/0026-2862(77)90088-7.

Sone, H., Deo, B. K. and Kumagai, A. K. (2000) 'Enhancement of glucose transport by vascular endothelial growth factor in retinal endothelial cells', *Investigative Ophthalmology and Visual Science*, 41(7), pp. 1876–1884.

Stępień, K., Ostrowski, R. P. and Matyja, E. (2016) 'Hyperbaric oxygen as an adjunctive therapy in treatment of malignancies, including brain tumours', *Medical Oncology*. Humana Press Inc. doi: 10.1007/s12032-016-0814-0.

Strilic, B. and Offermanns, S. (2017) 'Intravascular Survival and Extravasation of Tumor Cells', *Cancer Cell*, 32(3), pp. 282–293. doi: 10.1016/j.ccell.2017.07.001.

Subileau, E. A. *et al.* (2009) 'Expression of chemokines and their receptors by human brain endothelium: Implications for multiple sclerosis', *Journal of Neuropathology and Experimental Neurology*, 68(3), pp. 227–240. doi: 10.1097/NEN.0b013e318197eca7.

Sumbayev, V. V. *et al.* (2003) 'HIF-1α protein as a target for S-nitrosation', *FEBS Letters*,

535(1–3), pp. 106–112. doi: 10.1016/S0014-5793(02)03887-5.

Sun, X. *et al.* (2017) 'CCL2-driven inflammation increases mammary gland stromal density and cancer susceptibility in a transgenic mouse model', *Breast Cancer Research*, 19(1). doi: 10.1186/s13058-016-0796-z.

Sun, Y. *et al.* (2011) 'Sudan black B reduces autofluorescence in murine renal tissue', *Archives of Pathology and Laboratory Medicine*, 135(10), pp. 1335–1342. doi: 10.5858/arpa.2010-0549-OA.

Sure, V. N. *et al.* (2018) 'A novel high-throughput assay for respiration in isolated brain microvessels reveals impaired mitochondrial function in the aged mice', *GeroScience*. Springer International Publishing, 40(4), pp. 365–375. doi: 10.1007/s11357-018-0037-8.

Sutendra, G. and Michelakis, E. D. (2014) 'The metabolic basis of pulmonary arterial hypertension', *Cell Metabolism*. Cell Press, pp. 558–573. doi: 10.1016/j.cmet.2014.01.004.

Taha, C. *et al.* (1999) 'Opposite translational control of GLUT1 and GLUT4 glucose transporter mRNAs in response insulin. Role of mammalian target of rapamycin, protein kinase B, and phosphatidylinositol 3-kinase in GLUT1 mRNA translation', *Journal of Biological Chemistry*, 274(46), pp. 33085–33091. doi: 10.1074/jbc.274.46.33085.

Takata, K. *et al.* (1990) 'Erythrocyte/HEPG2-type glucose transporter is concentrated in cells of blood-tissue barriers', *Biochemical and Biophysical Research Communications*, 173(1), pp. 67–73. doi: 10.1016/S0006-291X(05)81022-8.

Takata, K., Hirano, H. and Kasahara, M. (1997) 'Transport of glucose across the blood-tissue barriers', *International Review of Cytology*, 172, pp. 1–53. doi: 10.1016/s0074-7696(08)62357-8.

Takeda, N. *et al.* (2010) 'Differential activation and antagonistic function of HIF-α isoforms in macrophages are essential for NO homeostasis', *Genes and Development*, 24(5), pp. 491–501. doi: 10.1101/gad.1881410.

Talks, K. L. *et al.* (2000) 'The expression and distribution of the hypoxia-inducible factors HIF-1α and HIF-2α in normal human tissues, cancers, and tumor-associated macrophages', *American Journal of Pathology*. American Society for Investigative Pathology Inc., 157(2), pp. 411–421. doi: 10.1016/S0002-9440(10)64554-3.

Tan, S. Y. S. and Krasnow, M. A. (2016) 'Developmental origin of lung macrophage diversity', *Development (Cambridge)*, 143(8), pp. 1318–1327. doi: 10.1242/dev.129122.

Tang, H. *et al.* (2018) 'Endothelial HIF-2α contributes to severe pulmonary hypertension due to endothelial-to-mesenchymal transition', *American Journal of Physiology - Lung Cellular and Molecular Physiology*. American Physiological Society, 314(2), pp. L256–L275. doi: 10.1152/ajplung.00096.2017.

Tang, N. *et al.* (2004) 'Loss of HIF-1α in endothelial cells disrupts a hypoxia-driven VEGF autocrine loop necessary for tumorigenesis', *Cancer Cell*, 6(5), pp. 485–495. doi: 10.1016/j.ccr.2004.09.026.

Tanner, L. B. *et al.* (2018) 'Four Key Steps Control Glycolytic Flux in Mammalian Cells', *Cell Systems*, 7(1), pp. 49-62.e8. doi: 10.1016/j.cels.2018.06.003.

Tarhonskaya, H. *et al.* (2015) 'Kinetic investigations of the role of factor inhibiting hypoxia-inducible factor (FIH) as an oxygen sensor', *Journal of Biological Chemistry*. American Society for Biochemistry and Molecular Biology Inc., 290(32), pp. 19726–19742. doi: 10.1074/jbc.M115.653014.

Teslaa, T. and Teitell, M. A. (2014) 'Techniques to monitor glycolysis', in *Methods in Enzymology*. Academic Press Inc., pp. 91–114. doi: 10.1016/B978-0-12-416618-9.00005-4.

Theodorou, K. and Boon, R. A. (2018) 'Endothelial cell metabolism in atherosclerosis', *Frontiers in Cell and Developmental Biology*, 6(AUG), pp. 3–58. doi: 10.3389/fcell.2018.00082.

Thiebaut, F. *et al.* (1989) 'Immunohistochemical localization in normal tissues of different epitopes in the multidrug transport protein P170: evidence for localization in brain capillaries and crossreactivity of one antibody with a muscle protein', *Journal of Histochemistry and Cytochemistry*, 37(2), pp. 159–164. doi: 10.1177/37.2.2463300.

Thiersch, M. and Swenson, E. R. (2018) 'High Altitude and Cancer Mortality', *High Altitude Medicine and Biology*, 19(2), pp. 116–123. doi: 10.1089/ham.2017.0061.

Thom, S., Bhopale, V. and Milovanova, T. (2010) '[abstract] NITRIC OXIDE SYNTHASE ACTIVATION AND CD34+ STEM CELL MOBILIZATION BY HYPERBARIC OXYGEN IN DIABETIC PATIENTS'.

Thom, S. R. (1989) 'Analytic Reviews: Hyperbaric Oxygen Therapy', *Journal of Intensive Care Medicine*, 4(2), pp. 58–74. doi: 10.1177/088506668900400204.

Thom, S. R. *et al.* (2006) 'Stem cell mobilization by hyperbaric oxygen', *American Journal of Physiology - Heart and Circulatory Physiology*, 290(4). doi: 10.1152/ajpheart.00888.2005.

Thom, S. R. (2011) 'Hyperbaric oxygen: Its mechanisms and efficacy', *Plastic and*

Reconstructive Surgery, 127(SUPPL. 1 S). doi: 10.1097/PRS.0b013e3181fbe2bf.

Thomas, J. D., Dias, L. M. and Johannes, G. J. (2008) 'Translational repression during chronic hypoxia is dependent on glucose levels', *Rna*, 14(4), pp. 771–781. doi: 10.1261/rna.857308.

Thorsen, E., Aanderud, L. and Aasen, T. B. (1998) 'Effects of a standard hyperbaric oxygen treatment protocol on pulmonary function', *European Respiratory Journal*, 12(6), pp. 1442–1445. doi: 10.1183/09031936.98.12061442.

Tian, H., McKnight, S. L. and Russell, D. W. (1997) 'Endothelial PAS domain protein 1 (EPAS1), a transcription factor selectively expressed in endothelial cells', *Genes and Development*. Cold Spring Harbor Laboratory Press, 11(1), pp. 72–82. doi: 10.1101/gad.11.1.72.

Tien, Y. W. *et al.* (2001) 'Tumor angiogenesis and its possible role in intravasation of colorectal epithelial cells', *Clinical Cancer Research*, 7(6), pp. 1627–1632. Available at: http://www.ncbi.nlm.nih.gov/pubmed/11410499 (Accessed: 5 December 2019).

Timpano, S. and Uniacke, J. (2016) 'Human cells cultured under physiological oxygen utilize two cap-binding proteins to recruit distinct mRNAs for translation', *Journal of Biological Chemistry*. American Society for Biochemistry and Molecular Biology Inc., 291(20), pp. 10772–10782. doi: 10.1074/jbc.M116.717363.

Toschi, A. *et al.* (2008) 'Differential dependence of hypoxia-inducible factors 1α and 2α on mTORC1 and mTORC2', *Journal of Biological Chemistry*, 283(50), pp. 34495–34499. doi: 10.1074/jbc.C800170200.

Trollmann, R. *et al.* (2014) 'Pharmacologic stabilization of hypoxia-inducible transcription factors protects developing mouse brain from hypoxia-induced apoptotic cell death', *Neuroscience*, 278. doi: 10.1016/j.neuroscience.2014.08.019.

Tsukurov, O. I. *et al.* (2000) 'The response of adult human saphenous vein endothelial cells to combined pressurized pulsatile flow and cyclic strain, in vitro', *Annals of Vascular Surgery*. Springer New York, 14(3), pp. 260–267. doi: 10.1007/s100169910044.

Tsuzuki, Y. *et al.* (2000) 'Vascular endothelial growth factor (VEGF) modulation by targeting hypoxia-inducible factor-1α → hypoxia response element → VEGF cascade differentially regulates vascular response and growth rate in tumors', *Cancer Research*, 60(22), pp. 6248–6252.

Uchida, T. *et al.* (2004) 'Prolonged hypoxia differentially regulates hypoxia-inducible factor (HIF)-1α and HIF-2α expression in lung epithelial cells: Implication of natural antisense HIF-1α', *Journal of Biological Chemistry*, 279(15), pp. 14871–14878. doi:

10.1074/jbc.M400461200.

Ullah, M. S., Davies, A. J. and Halestrap, A. P. (2006) 'The plasma membrane lactate transporter MCT4, but not MCT1, is up-regulated by hypoxia through a HIF-1α-dependent mechanism', *Journal of Biological Chemistry*, 281(14), pp. 9030–9037. doi: 10.1074/jbc.M511397200.

Varela, L. *et al.* (2017) 'Endothelial HIF-1α enables hypothalamic glucose uptake to drive POMC neurons', *Diabetes*. American Diabetes Association Inc., 66(6), pp. 1511–1520. doi: 10.2337/db16-1106.

Verdegem, D. *et al.* (2014) 'Endothelial cell metabolism: Parallels and divergences with cancer cell metabolism', *Cancer and Metabolism*, 2(1), p. 19. doi: 10.1186/2049-3002-2-19.

Volk, T., Peters, J. and Sessler, D. I. (2017) 'The WHO recommendation for 80% perioperative oxygen is poorly justified', *Anaesthesist*. Springer Verlag, pp. 227–229. doi: 10.1007/s00101-017-0286-4.

Wacker, B. K., Perfater, J. L. and Gidday, J. M. (2012) 'Hypoxic preconditioning induces stroke tolerance in mice via a cascading HIF, sphingosine kinase, and CCL2 signaling pathway', *Journal of Neurochemistry*, 123(6), pp. 954–962. doi: 10.1111/jnc.12047.

Wadley, A. J., Veldhuijzen Van Zanten, J. J. C. S. and Aldred, S. (2013) 'The interactions of oxidative stress and inflammation with vascular dysfunction in ageing: The vascular health triad', *Age*, 35(3), pp. 705–718. doi: 10.1007/s11357-012-9402-1.

Wahl, M. L., Owen, C. S. and Grant, D. S. (2002) 'Angiostatin induces intracellular acidosis and anoikis in endothelial cells at a tumor-like low pH', *Endothelium: Journal of Endothelial Cell Research*, 9(3), pp. 205–216. doi: 10.1080/10623320213633.

Wallez, Y. and Huber, P. (2008) 'Endothelial adherens and tight junctions in vascular homeostasis, inflammation and angiogenesis', *Biochimica et Biophysica Acta - Biomembranes*, pp. 794–809. doi: 10.1016/j.bbamem.2007.09.003.

Wang, G. L. *et al.* (1995) 'Hypoxia-inducible factor 1 is a basic-helix-loop-helix-PAS heterodimer regulated by cellular O2 tension', *Proceedings of the National Academy of Sciences of the United States of America*, 92(12), pp. 5510–5514. doi: 10.1073/pnas.92.12.5510.

Wang, G. L. and Semenza, G. L. (1995) 'Purification and characterization of hypoxia-inducible factor', *Journal of Biological Chemistry*. American Society for Biochemistry and Molecular Biology Inc., 270(3), pp. 1230–1237. doi: 10.1074/jbc.270.3.1230.

Wang, M. *et al.* (2018) 'Thrombotic Regulation From the Endothelial Cell Perspectives', *Arteriosclerosis, thrombosis, and vascular biology*. NLM (Medline), pp. e90–e95. doi:

10.1161/ATVBAHA.118.310367.

Wang, Q. *et al.* (2015) 'Reactive oxygen species, mitochondria, and endothelial cell death during in vitro simulated dives', *Medicine and Science in Sports and Exercise*. Lippincott Williams and Wilkins, 47(7), pp. 1362–1371. doi: 10.1249/MSS.0000000000000563.

Wang, Y. *et al.* (2010) 'HIF-1α and HIF-2α correlate with migration and invasion in gastric cancer', *Cancer Biology and Therapy*, 10(4), pp. 376–382. doi: 10.4161/cbt.10.4.12441.

Warburg, O., Wind, F. and Negelein, E. (1927) 'The metabolism of tumors in the body', *Journal of General Physiology*, 8(6), pp. 519–530. doi: 10.1085/jgp.8.6.519.

Ward, P. S. and Thompson, C. B. (2012) 'Metabolic Reprogramming: A Cancer Hallmark Even Warburg Did Not Anticipate', *Cancer Cell*, pp. 297–308. doi: 10.1016/j.ccr.2012.02.014.

Watson, E. C., Grant, Z. L. and Coultas, L. (2017) 'Endothelial cell apoptosis in angiogenesis and vessel regression', *Cellular and Molecular Life Sciences*. Birkhauser Verlag AG, pp. 4387–4403. doi: 10.1007/s00018-017-2577-y.

Watson, P. M. D. *et al.* (2013a) 'Modelling the endothelial blood-CNS barriers: A method for the production of robust in vitro models of the rat blood-brain barrier and blood-spinal cord barrier', *BMC Neuroscience*. BioMed Central, 14, p. 59. doi: 10.1186/1471-2202-14-59.

Watson, P. M. D. *et al.* (2013b) 'Modelling the endothelial blood-CNS barriers: A method for the production of robust in vitro models of the rat blood-brain barrier and blood-spinal cord barrier', *BMC Neuroscience*. BioMed Central, 14(1), p. 59. doi: 10.1186/1471-2202-14-59.

Weidemann, A. and Johnson, R. S. (2008) 'Biology of HIF-1α', *Cell Death and Differentiation*, 15(4), pp. 621–627. doi: 10.1038/cdd.2008.12.

Weir, E. K. and Anand, S. (1995) 'The mechanism of acute hypoxic pulmonary vasoconstriction: The tale of two channels', *FASEB Journal*, pp. 183–189. doi: 10.1096/fasebj.9.2.7781921.

Weis, S. *et al.* (2004) 'Endothelial barrier disruption by VEGF-mediated Src activity potentiates tumor cell extravasation and metastasis', *Journal of Cell Biology*, 167(2), pp. 223–229. doi: 10.1083/jcb.200408130.

Welser-Alves, J. V., Boroujerdi, A. and Milner, R. (2014) 'Isolation and culture of primary mouse brain endothelial cells', in *Methods in Molecular Biology*, pp. 345–356. doi:

10.1007/978-1-4939-0320-7_28.

Wenes, M. *et al.* (2016) 'Macrophage Metabolism Controls Tumor Blood Vessel Morphogenesis and Metastasis', *Cell Metabolism*. Cell Press, 24(5), pp. 701–715. doi: 10.1016/j.cmet.2016.09.008.

Wenger, R. *et al.* (2015) 'Frequently asked questions in hypoxia research', *Hypoxia*. Dove Press, 3, p. 35. doi: 10.2147/hp.s92198.

Wieland, E. *et al.* (2017) 'Endothelial Notch1 Activity Facilitates Metastasis', *Cancer Cell*, 31(3), pp. 355–367. doi: 10.1016/j.ccell.2017.01.007.

Wiesener, M. S. *et al.* (2003) 'Widespread hypoxia-inducible expression of HIF-2alpha in distinct cell populations of different organs.', *The FASEB journal : official publication of the Federation of American Societies for Experimental Biology*, 17(2), pp. 271–273. doi: 10.1096/fj.02-0445fje.

Wijesinghe, M. *et al.* (2009) 'Routine use of oxygen in the treatment of myocardial infarction: Systematic review', *Heart*, pp. 198–202. doi: 10.1136/hrt.2008.148742.

Wild, J. M. *et al.* (2005) '3D volume-localized pO2 measurement in the human lung with 3He MRI', *Magnetic Resonance in Medicine*. John Wiley & Sons, Ltd, 53(5), pp. 1055–1064. doi: 10.1002/mrm.20423.

Wilson, D. F. and Matschinsky, F. M. (2019) 'Hyperbaric oxygen toxicity in brain: A case of hyperoxia induced hypoglycemic brain syndrome', *Medical Hypotheses*. Churchill Livingstone, 132. doi: 10.1016/j.mehy.2019.109375.

Wohlfeil, S. A. *et al.* (2019) 'Hepatic endothelial notch activation protects against liver metastasis by regulating endothelial-tumor cell adhesion independent of angiocrine signaling', *Cancer Research*. American Association for Cancer Research Inc., 79(3), pp. 598–610. doi: 10.1158/0008-5472.CAN-18-1752.

Woik, N. and Kroll, J. (2015) 'Regulation of lung development and regeneration by the vascular system', *Cellular and Molecular Life Sciences*. Birkhauser Verlag AG, pp. 2709–2718. doi: 10.1007/s00018-015-1907-1.

Wong, B. W. *et al.* (2017) 'Endothelial cell metabolism in health and disease: impact of hypoxia', *The EMBO journal*, 36. doi: 10.15252/embj.201696150.

Wu, D. *et al.* (2017) 'HIF-1α is required for disturbed flow-induced metabolic reprogramming in human and porcine vascular endothelium', *eLife*, 6. doi: 10.7554/eLife.25217.

Wüst, R. C. I., Helmes, M. and Stienen, G. J. M. (2015) 'Rapid changes in NADH and flavin autofluorescence in rat cardiac trabeculae reveal large mitochondrial complex II reserve capacity', *Journal of Physiology*. Blackwell Publishing Ltd, 593(8), pp. 1829–1840.

doi: 10.1113/jphysiol.2014.286153.

Xu, W. *et al.* (2011) 'Oncometabolite 2-hydroxyglutarate is a competitive inhibitor of α-ketoglutarate-dependent dioxygenases', *Cancer Cell*, 19(1), pp. 17–30. doi: 10.1016/j.ccr.2010.12.014.

Yadava, N. and Nicholls, D. G. (2007) 'Spare respiratory capacity rather than oxidative stress regulates glutamate excitotoxicity after partial respiratory inhibition of mitochondrial complex I with rotenone', *Journal of Neuroscience*, 27(27), pp. 7310–7317. doi: 10.1523/JNEUROSCI.0212-07.2007.

Yamamoto, H. *et al.* (2016) 'Autocrine VEGF isoforms differentially regulate endothelial cell behavior', *Frontiers in Cell and Developmental Biology*. Frontiers, 4(SEP), p. 99. doi: 10.3389/fcell.2016.00099.

Yamamura, T. *et al.* (2001) 'Morphologic analysis of microvessels in colorectal tumors with respect to the formation of liver metastases', *Journal of Surgical Oncology*, 78(4), pp. 259–264. doi: 10.1002/jso.1164.

Yan, H. *et al.* (2009) 'IDH1 and IDH2 mutations in gliomas', *New England Journal of Medicine*, 360(8), pp. 765–773. doi: 10.1056/NEJMoa0808710.

Yan, J., Zhang, Z. and Shi, H. (2012) 'HIF-1 is involved in high glucose-induced paracellular permeability of brain endothelial cells', *Cellular and Molecular Life Sciences*, 69(1), pp. 115–128. doi: 10.1007/s00018-011-0731-5.

Yang, B. *et al.* (2007) 'STEM CELL MOBILIZATION IN DIABETICS-RESPONSES TO HYPERBARIC OXYGEN THERAPY.'

Yang, Q. *et al.* (2018) 'PRKAA1/AMPKα1-driven glycolysis in endothelial cells exposed to disturbed flow protects against atherosclerosis', *Nature Communications*. Nature Publishing Group, 9(1). doi: 10.1038/s41467-018-07132-x.

Yano, K. *et al.* (2007) 'Phenotypic heterogeneity is an evolutionarily conserved feature of the endothelium', *Blood*, 109(2), pp. 613–615. doi: 10.1182/blood-2006-05-026401.

Yau, J. W., Teoh, H. and Verma, S. (2015) 'Endothelial cell control of thrombosis', *BMC Cardiovascular Disorders*. BioMed Central Ltd. doi: 10.1186/s12872-015-0124-z.

Yetkin-Arik, B. *et al.* (2019) 'Endothelial tip cells in vitro are less glycolytic and have a more flexible response to metabolic stress than non-tip cells', *Scientific Reports*. Nature Publishing Group, 9(1). doi: 10.1038/s41598-019-46503-2.

Yi, W. *et al.* (2012) 'Phosphofructokinase 1 glycosylation regulates cell growth and metabolism', *Science*. American Association for the Advancement of Science, 337(6097), pp. 975–980. doi: 10.1126/science.1222278.

Young, T. *et al.* (1993) 'The Occurrence of Sleep-Disordered Breathing among Middle-Aged Adults', *New England Journal of Medicine*, 328(17), pp. 1230–1235. doi: 10.1056/NEJM199304293281704.

Yu, J. *et al.* (2005) 'Endothelial nitric oxide synthase is critical for ischemic remodeling, mural cell recruitment, and blood flow reserve', *Proceedings of the National Academy of Sciences of the United States of America*, 102(31), pp. 10999–11004. doi: 10.1073/pnas.0501444102.

Yu, L. and Hales, C. A. (2011) 'Long-term exposure to hypoxia inhibits tumor progression of lung cancer in rats and mice', *BMC Cancer*, 11(1), p. 331. doi: 10.1186/1471-2407-11-331.

Yuan, G. *et al.* (2005) 'Ca2+/calmodulin kinase-dependent activation of hypoxia inducible factor 1 transcriptional activity in cells subjected to intermittent hypoxia', *Journal of Biological Chemistry*, 280(6), pp. 4321–4328. doi: 10.1074/jbc.M407706200.

Yuan, G. *et al.* (2008) 'Induction of HIF-1α expression by intermittent hypoxia: Involvement of NADPH oxidase, Ca2+ signaling, prolyl hydroxylases, and mTOR', *Journal of Cellular Physiology*, 217(3), pp. 674–685. doi: 10.1002/jcp.21537.

Zamora, R. *et al.* (2001) 'Nitric Oxide Suppresses the Expression of Bcl-2 Binding Protein BNIP3 in Hepatocytes', *Journal of Biological Chemistry*, 276(50), pp. 46887–46895. doi: 10.1074/jbc.M101865200.

Zhang, F. *et al.* (2015) 'High altitude increases the expression of hypoxia-inducible factor 1a and inducible nitric oxide synthase with intest-inal mucosal barrier failure in rats', *International Journal of Clinical and Experimental Pathology*, 8(5), pp. 5189–5195. Available at: http://www.ncbi.nlm.nih.gov/pubmed/26191216 (Accessed: 11 December 2019).

Zhang, H. *et al.* (2008) 'Mitochondrial autophagy is an HIF-1-dependent adaptive metabolic response to hypoxia', *Journal of Biological Chemistry*, 283(16), pp. 10892–10903. doi: 10.1074/jbc.M800102200.

Zhang, H. *et al.* (2012) 'HIF-1-dependent expression of angiopoietin-like 4 and L1CAM mediates vascular metastasis of hypoxic breast cancer cells to the lungs', *Oncogene*, 31(14), pp. 1757–1770. doi: 10.1038/onc.2011.365.

Zhang, J. and Ney, P. A. (2009) 'Role of BNIP3 and NIX in cell death, autophagy, and mitophagy', *Cell Death and Differentiation*, pp. 939–946. doi: 10.1038/cdd.2009.16.

Zhang, J. Z., Behrooz, A. and Ismail-Beigi, F. (1999) 'Regulation of glucose transport by hypoxia', *American Journal of Kidney Diseases*. W.B. Saunders, 34(1), pp. 189–202.

doi: 10.1016/S0272-6386(99)70131-9.

Zhang, P. *et al.* (2014) 'Hypoxia-Inducible Factor 3 Is an Oxygen-Dependent Transcription Activator and Regulates a Distinct Transcriptional Response to Hypoxia', *Cell Reports*. Elsevier, 6(6), pp. 1110–1121. doi: 10.1016/j.celrep.2014.02.011.

Zhang, S. *et al.* (2017) 'HIF-2α and Oct4 have synergistic effects on survival and myocardial repair of very small embryonic-like mesenchymal stem cells in infarcted hearts', *Cell Death and Disease*, 8(1). doi: 10.1038/cddis.2016.480.

Zhitomirsky, B., Farber, H. and Assaraf, Y. G. (2018) 'LysoTracker and MitoTracker Red are transport substrates of P-glycoprotein: implications for anticancer drug design evading multidrug resistance', *Journal of Cellular and Molecular Medicine*, 22(4), pp. 2131–2141. doi: 10.1111/jcmm.13485.

Zhong, H. *et al.* (1999) 'Overexpression of hypoxia-inducible factor 1α in common human cancers and their metastases', *Cancer Research*, 59(22), pp. 5830–5835.